

STRUCTURE DETERMINATION OF ALKALI METAL ENOLATES AND PHENOLATES
USING THE METHOD OF CONTINUOUS VARIATION

A Dissertation

Presented to the Faculty of the Graduate School

Of Cornell University

In Partial Fulfillment of the Requirements for the Degree of

Doctor of Philosophy

by

Laura Leigh Tomasevich

May 2014

© Laura Leigh Tomasevich

STRUCTURE DETERMINATION OF ALKALI METAL ENOLATES AND PHENOLATES
USING THE METHOD OF CONTINUOUS VARIATION

Laura Leigh Tomasevich, Ph. D.

Cornell University 2014

Enolate alkylation is a robust method for forming carbon-carbon bonds and has been used extensively for many decades. Despite their prevalence, the characterization of enolate aggregates has not been thoroughly explored, though prior research has shown that they form highly ordered and symmetrical aggregates in solution. Scalar coupling in NMR is often used to determine the solution structure, but this method fails when the metal is bonded to quadrupolar oxygen. Structurally diverse enolates, counterions, and ligands require a flexible method for characterization. The method of continuous variation (MCV) in conjunction with ^6Li , ^{19}F , and ^1H NMR spectroscopies was used to gain structural insight into the aggregation state and stability of lithium and sodium enolates and phenolates in a range of solvents.

BIOGRAPHICAL SKETCH

Laura Leigh Tomasevich was born Pittsburgh, Pennsylvania to John and Karin Tomasevich in 1986. While growing up in the suburbs of Pittsburgh she enjoyed participating in a variety of sports, mostly soccer and track. After graduating from Norwin High School in 2004 she stayed local and attended Washington and Jefferson College where she investigated novel heterocyclic rearrangements. She received a bachelor's degree in chemistry with minors in psychology and religious studies in 2008. She began her doctoral studies at Cornell University in 2008 under the guidance of Professor David B. Collum, studying the solution structures of enolates and phenolates. In 2010 she married fellow chemist and cat-lover Mike Leonard, who resides in Pittsburgh with his two cats. After spending their entire relationship living apart, Laura and Mike are looking forward to finally spending some time together.

For John Tomasevich

ACKNOWLEDGMENTS

This work is dedicated to my dad, John Tomasevich, who passed away earlier this year. Even though you didn't get to see me graduate, I know you were proud of me. I can only hope that I will go through life with the same passion and perfection that you had for your life and work. Thank you for teaching me everything I know about home repair (especially plumbing and wiring which has been useful on multiple occasions), for teaching me soccer and then driving me all across the eastern US for soccer games, for teaching me to drive your (monstrous) truck, for being both mother and father to me, and especially for encouraging me to pursue my dream to be a chemist, even though you didn't know what a chemist does (anything!). You are my inspiration and my motivation, and I will always love you. I will always be your little girl and I hope we will meet again one day.

To my wonderful husband Mike, thank you for always being loving and supportive. From the day I met you until now, I am a better person because of you. Remember, there's no "C" on the periodic table, the chicken dance is better with a few beers, cats will always think chicken "leftovers" are meant for them, never forget what the "6" represents in Motel 6, kiddieland rides are only fair game if you have kids, offsides does not mean the player is facing away from you, and apparently coffee is the sweet nectar of the devil. I love you and look forward to spending the rest of my life with you.

My previous group members Tim, Emily, Allison, Lekha, Josie, Ananda, Alex, Hari, Shannon, Suzanna, Onella, Joe, Angela and current group members, Ma, Jun, Joo, Evan, Mike, Jackie, Russell, Naomi, Yolanda, Janis, and Kyle have

been invaluable to me and I couldn't have asked for a better group of people. I'll never forget any of you, and I hope our paths cross again and again throughout our lives. The eclectic mix of people that the Collum group always seems to be has offered me more than I could have ever fathomed. I found the love and acceptance I had been searching for over waffles at group meeting, stacks of NMR spectra, rainy BBQs, midnight chats, 8 hour proposal edits, all-you-can-eat chicken wings, LDA fires, drunken parties, hallway cart races, Matlab error codes, pulled pork sandwiches, chemical barcode scanning, pumpkin carving, Mnova crashes, ice skating/falling, broken glassware, 42,651 feet of muddy race, wiking trips, least-squares fits, bike rides, doctor visits, A exam preps, swimming and rafting, smoking glove boxes, police calls, freezer meltdowns, the Nines pizza, yellow &@% bases, NYC trips--I could write a whole book on these memories alone! I wish you all the best of the luck in the future—you are all great scientists and I know you will all find success with whatever you pursue. I'd like to thank my committee members, Bruce Ganem and Will Dichtel as well as Brian Crane for the help and support during my graduate career.

Cornell Chemistry is composed of an amazing group of people and it's impossible to give everyone the thanks they deserve, but here is my attempt in no particular order: Ivan, you are a great NMR spectroscopist, a great soccer goalie, and you pretty much saved my graduate career in June 2010 by seeing that tetramer I missed in the haystack. Thanks for always listening to me and offering advice, Pat. Denise and Josh, the stockroom is a better place because of you both—enjoy your retirement Denise, and I wish you the best of luck Josh as the size of your family doubles. To Tony, Dave, Larry, and Jason, thanks for keeping everything running smoothly and always saying hi. I've always

appreciated the chats, Chuck, Gary, and Kenny, and even more so appreciate the work you do. Tom, thanks for picking me for orgo lab and also always being a bright spot in my day, and Kyle, your parties are truly epic.

To my friends, you are the reason I keep going each day. Amanda, I never thought 13+ years ago when you asked me to be your running partner we'd be a few months away from going through 2 weddings together. I wish you all the happiness in the world as you begin your new life with Scott. Prachi, life just dished you out a raw deal, but I know you will make it through—you are an incredible person and I know you won't ever give up (and thank you for listening to my endless trivial complaints and being an excellent host and camping buddy). Laura #1, I hope we're able to get together more frequently in the future, and thanks for taking time from med school to go for a boat ride on a hot August day. I wish you the best of luck in whatever you choose to pursue, Paul, and may the Prius (or Rav4) see you through many miles of adventures. Darren, my liver will never be the same after you introduced me to Captain and ginger ale, but it sure is tasty. To my Cornell friends, you have made the last 5 years truly special. Sonia, Sean, Hoang, and Jimmy, thanks for trekking all the way to my wedding, for being great friends, and I loved all the BBQs. Eugenia, I really miss all the crazy long runs and our wicycling trip is one of my favorite memories from Ithaca. Thanks for being a great friend, Josh, for listening to my A exam talk at least 50 times, and for always hooking me up with Amazon stuff within 2 days. I hope to see you in Pittsburgh, Allikat, where maybe we can have a beer somewhere other than a women's restroom. It's been great catching up with you Nick, and thanks for all the synthesis advice my second year. Thanks for all the chats and debates, Kyle, and I hope you're able to finish your degree

soon. Daniel, from early morning gym trips to late night skype chats, you've been a great friend and I wish you the best of luck as a doctor. Skippy and Gremmie, you taught me what unconditional love is, and I couldn't have ever asked for better B&Ws.

Last but not least, I'd like to thank Dave for being an advisor, debate partner, and part-time psychoanalyst. Your office seems to continually result in a warp in the space-time continuum, which is both unnerving and yet oddly pleasing. Two hours later, I usually find the range of topics covered to be reminiscent of a drunkard's walk—random, but with a predictable outcome. I have never decided if we are polar opposites or a disconcerting level of similar. Either way, you have taught me the meaning of persistence, the masonry skills of a wall-builder, the acquiescence of broken walls, and the realization of what matters in life. You described your dad as the Rock of Gibraltar—the voids left by others were filled by him. Freudian theories aside, your greatest impact as an advisor is not limited to commentary on organolithiums. You know exactly the type of students attracted to your group, and I hope when needed, you always choose to be that rock.

TABLE OF CONTENTS

Biographical Sketch	iii
Acknowledgments	v
Table of Contents	ix
List of Figures	x
List of Tables	xx
Chapter I: Structure Determination Using the Method of Continuous Variation: Lithium Phenolates Solvated by Protic and Dipolar Aprotic Ligands	1
Appendix I: Supporting Information for Chapter I	
A. Combinations of phenolates with various solvents: Job plots	31
B. Solvent Swaps	73
References and Footnotes I	90
Chapter II: Method of Continuous Variation: Characterization of Alkali Metal Enolates Using ^1H and ^{19}F NMR Spectroscopies	99
Appendix II: Supporting Information for Chapter II	
A. Lithium Phenolates: Job Plots using ^{19}F NMR	127
B. Lithium Salts of 1-Naphthol and 4-Fluorophenol: Job Plots using ^{19}F NMR	131
C. Lithium Enolates: Job Plots using ^{19}F and ^1H NMR	140
D. Sodium Enolates and Phenolates: Job Plots using ^{19}F and ^1H NMR	147
E. NaICA NMR Characterization and Additional Preparations	156
F. Comparing Lithium and Non-Lithium Ensembles with Underlying Math	161
G. Matlab Files for a Singly-Tagged Tetramer Ensemble	167
References and Footnotes II	174

LIST OF FIGURES

Figure I.1	⁶ Li NMR spectra recorded as approximate 1:1 mixtures of lithium phenolates in toluene cosolvent	9
Figure I.2	⁶ Li NMR spectra of 2 and 1 in solutions 0.50M isobutylamine / toluene.	11
Figure I.3	Job plot showing the relative integrations of dimeric homo- and heteroaggregates versus measured mole fractions.	12
Figure I.4	Job plot showing the relative integrations of trimeric homo- and heteroaggregates versus measured mole fractions.	12
Figure I.5	Job plot showing the relative integrations of tetrameric homo- and heteroaggregates versus measured mole fractions.	13
Figure I.6	⁶ Li NMR spectrum of 0.50 M DMSO / toluene solutions containing approximate 1:1 mixtures of 3 and 4 .	13
Figure I.7	Expected ⁶ Li NMR when replacing solvent S by S'.	14
Figure I.8	¹⁹ F NMR spectra of a 1:1 mixture of 2 and 1 in toluene containing 0.50 M DMSO recorded at -80 °C.	19
Figure AI.1	⁶ Li NMR stack plot of 1 and 2 in TMEDA / toluene.	31
Figure AI.2	Job plot of 1 and 2 in TMEDA / toluene.	31
Figure AI.3	⁶ Li NMR stack plot of 3 and 4 in TMEDA / toluene.	32
Figure AI.4	Job plot of 3 and 4 in TMEDA / toluene.	32
Figure AI.5	⁶ Li NMR stack plot of 1 and 2 in diethyl ether / toluene.	33
Figure AI.6	Job plot of 1 and 2 in diethyl ether / toluene.	33
Figure AI.7	⁶ Li NMR stack plot of 1 and 2 in neat diethyl ether.	34
Figure AI.8	Job plot of 1 and 2 in neat diethyl ether.	34
Figure AI.9	⁶ Li NMR stack plot of 3 and 4 in diethyl ether / toluene.	35

Figure AI.10	Job plot of 3 and 4 in diethyl ether / toluene.	35
Figure AI.11	⁶ Li NMR stack plot of 1 and 2 in acetonitrile / toluene.	36
Figure AI.12	⁶ Li NMR stack plot of 3 and 4 in acetonitrile / toluene.	37
Figure AI.13	Job plot of 3 and 4 in acetonitrile / toluene.	37
Figure AI.14	⁶ Li NMR stack plot of 1 and 2 in pyridine / toluene.	38
Figure AI.15	Job plot of 1 and 2 in pyridine / toluene.	38
Figure AI.16	⁶ Li NMR stack plot of 2 and 9 in pyridine / toluene.	39
Figure AI.17	Job plot of 2 and 9 in pyridine / toluene.	39
Figure AI.18	⁶ Li NMR stack plot of 3 and 4 in pyridine / toluene.	40
Figure AI.19	Job plot of 3 and 4 in pyridine / toluene.	40
Figure AI.20	⁶ Li NMR stack plot of 1 and 2 in dimethylacetamide / toluene.	41
Figure AI.21	Job plot of 1 and 2 in dimethylacetamide / toluene.	41
Figure AI.22	⁶ Li NMR stack plot of 3 and 4 in dimethylacetamide / toluene.	42
Figure AI.23	Job plot of 3 and 4 in dimethylacetamide / toluene.	42
Figure AI.24	⁶ Li NMR stack plot of 1 and 2 in dimethylformamide / toluene.	43
Figure AI.25	Job plot of 1 and 2 in dimethylformamide / toluene.	43
Figure AI.26	⁶ Li NMR stack plot of 1 and 2 in dimethylsulfoxide / toluene.	44
Figure AI.27	Job plot of 1 and 2 in dimethylsulfoxide / toluene.	44
Figure AI.28	¹⁹ F NMR stack plot of 1 and 2 in dimethylsulfoxide / toluene.	45
Figure AI.29	⁶ Li NMR stack plot of 3 and 4 in dimethylsulfoxide / toluene.	46
Figure AI.30	Job plot of 3 and 4 in dimethylsulfoxide / toluene.	46

Figure AI.31	^6Li NMR stack plot of 1 and 2 in DMPU/toluene.	47
Figure AI.32	Job plot of 1 and 2 in DMPU/toluene.	47
Figure AI.33	^6Li NMR stack plot of 3 and 4 in DMPU/toluene.	48
Figure AI.34	^6Li NMR stack plot of 1 and 2 in <i>N</i> -methylpyrrolidone/toluene.	49
Figure AI.35	Job plot of 1 and 2 in <i>N</i> -methylpyrrolidone/toluene.	49
Figure AI.36	^6Li NMR stack plot of 3 and 4 in <i>N</i> -methylpyrrolidone/toluene.	50
Figure AI.37	Job plot of 3 and 4 in <i>N</i> -methylpyrrolidone/toluene.	50
Figure AI.38	^6Li NMR stack plot of 1 and 2 in <i>n</i> -propylamine/toluene.	51
Figure AI.39	Job plot of 1 and 2 in <i>n</i> -propylamine/toluene.	51
Figure AI.40	^6Li NMR stack plot of 3 and 4 in <i>n</i> -propylamine/toluene.	52
Figure AI.41	Job plot of 3 and 4 in <i>n</i> -propylamine/toluene.	52
Figure AI.42	^6Li NMR stack plot of 1 and 2 in piperidine/toluene.	53
Figure AI.43	Job plot of 1 and 2 in piperidine/toluene.	53
Figure AI.44	^{19}F NMR stack plot of 1 and 2 in piperidine/toluene.	54
Figure AI.45	^6Li NMR stack plot of 2 and 9 in piperidine/toluene.	55
Figure AI.46	Job plot of 2 and 9 in piperidine/toluene.	55
Figure AI.47	^6Li NMR stack plot of 3 and 4 in piperidine/toluene.	56
Figure AI.48	Job plot of 3 and 4 in piperidine/toluene.	56
Figure AI.49	^6Li NMR stack plot of 1 and 2 in pyrrolidine/toluene.	57
Figure AI.50	Job plot of 1 and 2 in pyrrolidine/toluene.	57
Figure AI.51	^6Li NMR stack plot of 3 and 4 in pyrrolidine/toluene.	58
Figure AI.52	Job plot of 3 and 4 in pyrrolidine/toluene.	58

Figure AI.53	^6Li NMR stack plot of 1 and 2 in <i>i</i> -butylamine / toluene.	59
Figure AI.54	Job plot of 1 and 2 in <i>i</i> -butylamine / toluene.	59
Figure AI.55	^6Li NMR stack plot of 3 and 4 in <i>i</i> -butylamine / toluene.	60
Figure AI.56	Job plot of 3 and 4 in <i>i</i> -butylamine / toluene.	60
Figure AI.57	^6Li NMR stack plot of 1 and 2 in <i>sec</i> -butylamine / toluene.	61
Figure AI.58	Job plot of 1 and 2 in <i>sec</i> -butylamine / toluene.	61
Figure AI.59	^6Li NMR stack plot of 1 and 2 in <i>t</i> -butylamine / toluene.	62
Figure AI.60	Job plot of 1 and 2 in <i>t</i> -butylamine / toluene.	62
Figure AI.61	^6Li NMR stack plot of 2 and 9 in Diisopropylamine / toluene.	63
Figure AI.62	Job plot of 2 and 9 in Diisopropylamine / toluene.	63
Figure AI.63	^6Li NMR stack plot of 1 and 2 in Diisopropylamine / toluene.	64
Figure AI.64	^6Li NMR stack plot of 3 and 4 in Diisopropylamine / toluene.	65
Figure AI.65	Job plot of 3 and 4 in Diisopropylamine / toluene.	65
Figure AI.66	^6Li NMR stack plot of 1 and 2 in diethylamine / toluene.	66
Figure AI.67	Job plot of 1 and 2 in diethylamine / toluene.	66
Figure AI.68	^6Li NMR stack plot of 3 and 4 in diethylamine / toluene.	67
Figure AI.69	Job plot of 3 and 4 in diethylamine / toluene.	67
Figure AI.70	^6Li NMR stack plot of 1 and 2 in <i>n</i> -dipropylamine / toluene.	68
Figure AI.71	Job plot of 1 and 2 in <i>n</i> -dipropylamine / toluene.	68

Figure AI.72	^6Li NMR stack plot of 3 and 4 in <i>n</i> -dipropylamine/ toluene.	69
Figure AI.73	Job plot of 3 and 4 in <i>n</i> -dipropylamine/ toluene.	69
Figure AI.74	^6Li NMR stack plot of 1 and 2 in <i>t</i> -butanol/ toluene.	70
Figure AI.75	Job plot of 1 and 2 in <i>t</i> -butanol/ toluene.	70
Figure AI.76	^6Li NMR stack plot of 1 and 2 in <i>sec</i> -butanol/ toluene.	71
Figure AI.77	Job plot of 1 and 2 in <i>sec</i> -butanol/ toluene.	71
Figure AI.78	^6Li NMR stack plot of 1 and 2 in <i>n</i> -butanol/ toluene.	72
Figure AI.79	^6Li NMR stack plot of 1 and 2 in <i>n</i> -butanol/ ether.	73
Figure AI.80	Solvent swap on 0.1M [^6Li] 1 with pyridine and diethylamine.	73
Figure AI.81	Solvent swap on 0.1M [^6Li] 2 with diethylamine and TMEDA.	74
Figure AI.82	Solvent swap on 0.1M [^6Li] 1 with diethylacetamide and TMEDA.	75
Figure AI.83	Solvent swap on 0.1M [^6Li] 1 with diethylformamide and TMEDA.	76
Figure AI.84	Solvent swap on 0.1M [^6Li] 1 with N-methyl pyrrolidone and TMEDA.	77
Figure AI.85	Solvent swap on 0.1M [^6Li] 1 with N-methyl pyrrolidone and TMEDA.	78
Figure AI.86	Solvent swap on 0.1M [^6Li] 1 with N-methyl pyrrolidone and pyridine.	79
Figure AI.87	Solvent swap on 0.1M [^6Li] 1 with N-methyl pyrrolidone and pyridine.	80
Figure AI.88	Solvent swap on 0.1M [^6Li] 1 with pyridine and diethylether.	81
Figure AI.89	Solvent swap on 0.1M [^6Li] 1 in diethylether with and increasing pyridine.	82
Figure AI.90	Solvent swap on 0.1M [^6Li] 1 with 1 equiv pyridine with increasing diethylether.	83

Figure AI.91	Solvent swap on 0.1M [⁶ Li] 1 with pyridine and TMEDA.	84
Figure AI.92	Solvent swap on 0.1M [⁶ Li] 1 with pyridine and TMEDA.	85
Figure AI.93	Solvent swap on 0.1M [⁶ Li] 1 with pyridine and TMEDA.	86
Figure AI.94	Solvent swap on 0.1M [⁶ Li] 1 with pyridine and <i>n</i> -propylamine.	87
Figure AI.95	Solvent swap on 0.1M [⁶ Li] 1 with pyridine and pyrrolidine.	88
Figure AI.96	Solvent swap on 0.1M [⁶ Li] 1 with pyridine and <i>t</i> -butanol.	89
Figure II.1	¹⁹ F NMR spectra of a 1:1 mixture of 2 and 3 0.50 M THF/toluene.	108
Figure II.2	¹⁹ F NMR spectra of mixtures of 2 and 3 in 0.50 M THF/toluene	109
Figure II.3	Job plot of 2 and 3 in THF/toluene.	110
Figure II.4	¹⁹ F NMR spectra of 1 and 3 in 0.50 M propylamine/toluene at -80 °C.	112
Figure II.5	Job plot of 1 and 3 in propylamine/toluene.	112
Figure II.6	¹ H NMR spectra of 10 and 16 in 0.50 M TMEDA/toluene- <i>d</i> ₈ at -80 °C.	113
Figure II.7	Job plot of 10 and 16 in TMEDA/toluene.	114
Figure II.8	¹ H NMR spectra of 15 in ligand/toluene- <i>d</i> ₈ solution. The ligands are as follows: (a) 0.50 M TMEDA, (b) 0.50 M THF, and (c) 0.50 M THF with addition of 0.50 M TMEDA subsequent to enolization.	117
Figure AII.1	¹⁹ F NMR spectra of 0.10 M solutions of 3 and 4 in 0.50 M TMEDA/toluene.	127
Figure AII.2	Job plot of 3 and 4 in TMEDA/toluene.	127

Figure AII.3	^{19}F NMR spectra of 0.10 M solutions of 3 and 5 in 0.50 M TMEDA/toluene.	128
Figure AII.4	Job plot of 3 and 5 in TMEDA/toluene.	128
Figure AII.5	^{19}F NMR spectra of 0.10 M solutions of 2 and 3 in 0.50 M TMEDA/toluene.	129
Figure AII.6	Job plot of 2 and 3 in TMEDA/toluene.	129
Figure AII.7	^{19}F NMR spectra of 0.10 M solutions of 2 and 3 in 0.50 M THF/toluene.	130
Figure AII.8	Job plot of 2 and 3 in THF/toluene.	130
Figure AII.9	^{19}F NMR spectra of 0.10 M solutions of 3 and 1 in 0.50 M NMP/toluene.	131
Figure AII.10	Job plot of 3 and 1 in NMP/toluene.	131
Figure AII.11	^{19}F NMR spectra of 0.10 M solutions of 3 and 1 in 0.50 M DMF/toluene.	132
Figure AII.12	Job plot of 3 and 1 in DMF/toluene.	132
Figure AII.13	^{19}F NMR spectra of 0.10 M solutions of 3 and 1 in 0.50 M DMSO/toluene.	133
Figure AII.14	Job plot of 3 and 1 in DMSO/toluene.	133
Figure AII.15	^{19}F NMR spectra of 0.10 M solutions of 3 and 1 in 0.50 M DMPU/toluene.	134
Figure AII.16	Job plot of 3 and 1 in DMPU/toluene.	134
Figure AII.17	^{19}F NMR spectra of 0.10 M solutions of 3 and 1 in 0.50 M <i>n</i> -PrNH ₂ /toluene.	135
Figure AII.18	Job plot of 3 and 1 in <i>n</i> -PrNH ₂ /toluene.	135
Figure AII.19	^{19}F NMR spectra of 0.10 M solutions of 3 and 1 in 0.50 M Et ₂ NH/toluene.	136
Figure AII.20	Job plot of 3 and 1 in Et ₂ NH/toluene.	136
Figure AII.21	^{19}F NMR spectra of 0.10 M solutions of 3 and 1 in 0.50 M <i>n</i> -Pr ₂ NH /toluene.	137

Figure AII.22	^{19}F NMR spectra of 0.10 M solutions of 3 and 1 in 0.50 M piperidine/toluene.	138
Figure AII.23	Job plot of 3 and 1 in piperidine/toluene.	138
Figure AII.24	^{19}F NMR spectra of 0.10 M solutions of 3 and 1 in 0.50 M <i>t</i> -BuOH/toluene.	139
Figure AII.25	Job plot of 3 and 1 in <i>t</i> -BuOH/toluene.	139
Figure AII.26	^1H NMR spectra of 0.10 M solutions of 8 and 6 in 0.50 M THF/toluene.	140
Figure AII.27	^1H NMR spectra of 0.10 M solutions of 8 and 6 in 0.50 M TMEDA/toluene.	141
Figure AII.28	Job plot of 8 and 6 in TMEDA/toluene.	141
Figure AII.29	^{19}F NMR spectra of 0.10 M solutions of 8 and 6 in 0.50 M TMEDA/toluene.	142
Figure AII.30	Job plot of 8 and 6 in TMEDA/toluene.	142
Figure AII.31	^1H NMR spectra of 0.10 M solutions of 8 and 7 in 0.50 M THF/toluene.	143
Figure AII.32	Job plot of 8 and 7 in THF/toluene.	143
Figure AII.33	^1H NMR spectra of 0.10 M solutions of 8 and 7 in 0.50 M TMEDA/toluene.	144
Figure AII.34	Job plot of 8 and 7 in TMEDA/toluene.	144
Figure AII.35	^{19}F NMR spectra of 0.10 M solutions of 8 and 7 in 0.50 M TMEDA/toluene.	145
Figure AII.36	Job plot of 8 and 7 in TMEDA/toluene.	145
Figure AII.37	^1H NMR spectra of 0.10 M solutions of 7 and 9 in 0.50 M TMEDA/toluene.	146
Figure AII.38	Job plot of 7 and 9 in TMEDA/toluene.	146
Figure AII.39	^1H NMR spectra of 0.10 M solutions of 10 and 16 in 0.50 M TMEDA/toluene.	147
Figure AII.40	Job plot of 10 and 16 in TMEDA/toluene.	147

Figure AII.41	¹ H NMR spectra of 0.10 M solutions of 11 and 13 in 0.50 M TMEDA/toluene.	148
Figure AII.42	Job plot of 11 and 13 in TMEDA/toluene.	148
Figure AII.43	¹ H NMR spectra of 0.10 M solutions of 12 and 15 in 0.50 M TMEDA/toluene.	149
Figure AII.44	Job plot of 12 and 15 in TMEDA/toluene.	149
Figure AII.45	¹ H NMR spectra of 0.10 M solutions of 14 and 13 in 0.50 M TMEDA/toluene.	150
Figure AII.46	Job plot of 14 and 13 in TMEDA/toluene.	150
Figure AII.47	¹ H NMR spectra of 0.10 M solutions of 11 and 10 in 0.50 M THF/toluene.	151
Figure AII.48	¹ H NMR spectra of 0.10 M solutions of 11 and 12 in 0.50 M THF/toluene.	152
Figure AII.49	¹ H NMR spectra of 0.10 M solutions of 11 and 13 in 0.50 M THF/toluene.	153
Figure AII.50	¹ H NMR spectra of 0.10 M solutions of 11 and 14 in 0.50 M THF/toluene.	154
Figure AII.51	Job plot of 11 and 14 in THF/toluene.	154
Figure AII.52	¹ H NMR spectra of 0.10 M solutions of 17 and 18 in 0.50 M THF/toluene.	155
Figure AII.53	¹ H NMR spectrum of NaICA.	156
Figure AII.54	¹³ C NMR spectrum of NaICA.	157
Figure AII.55	COSY NMR spectrum of NaICA.	158
Figure AII.56	HSQCAD NMR spectrum of NaICA.	159
Figure AII.57	ROESY NMR spectrum of NaICA.	160
Figure AII.58	A 1 : 1 mixture of A and B, with roughly the expected NMR ratios of 1 : 4 : 6 : 4 : 1.	162
Figure AII.59	Monomer through hexamer statistical Job plots.	163

Figure AII.60	A 1 : 1 mixture of A and B, with a distinct A envelope and B envelope.	164
Figure AII.61	Job plot correcting for the number of fluorines in a Substrate.	164
Figure AII.62	Tetramer ensembles for a singly-tagged substrate, resulting in the detection of 4 NMR peaks.	165
Figure AII.63	Monomer through hexamer singly-tagged Job plots.	166

LIST OF TABLES

Table I.1	Solvent-dependent aggregation states and ^6Li NMR chemical shifts for homoaggregates of 1-4 .	5
Table II.1	Characterization of lithium phenolates and enolates in solution using ^{19}F and ^1H NMR spectroscopies.	115
Table II.2	Sodium enolate tetramers characterized using ^1H NMR spectroscopy in conjunction with MCV.	116
Table AII.1	The statistical ensemble ratios and the statistical singly-tagged NMR ratios for a 1 : 1 tetrameric mixture.	165

CHAPTER I

Structure Determination Using the Method of Continuous Variation: Lithium Phenolates Solvated by Protic and Dipolar Aprotic Ligands

Structure Determination Using the Method of Continuous Variation:
Lithium Phenolates Solvated by Protic and Dipolar Aprotic Ligands*

Abstract

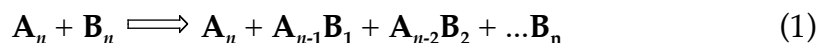
The method of continuous variation (MCV) in conjunction with ^6Li NMR spectroscopy was used to characterize four lithium phenolates solvated by a range of solvents including *N,N,N',N'*-tetramethylethylenediamine, Et_2O , pyridine, protic amines, alcohols, and highly dipolar aprotic solvents. Dimers, trimers, and tetramers were observed, depending on the precise lithium phenolate-solvent combinations. Competition experiments (solvent swaps) provide insights into relative solvation energies propensities toward mixed solvation.

Introduction

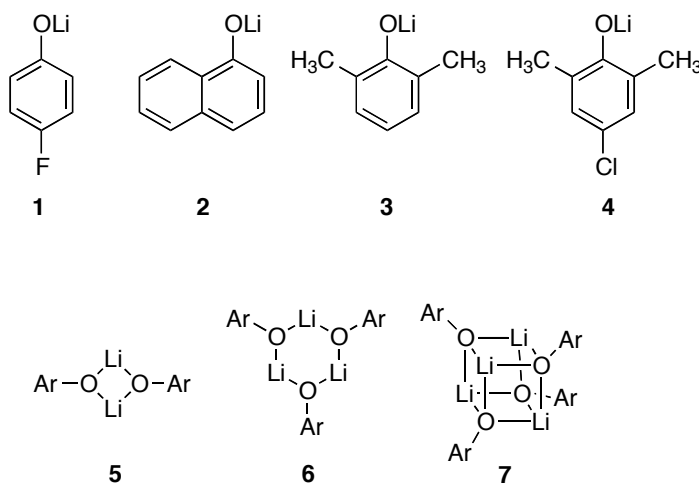
As part of a collaboration to study β -amino ester enolates used by Sanofi-Aventis to prepare the antithrombotic drug otamixaban,^{1,2} we were forced to find a general solution to the problem of characterizing lithium enolates in tetrahydrofuran (THF) solution.³ The lack of measurable Li-O scalar coupling precluded the most powerful and general NMR spectroscopic strategies used to characterize analogous Li-C and Li-N lithium salts.⁴ Despite scattered reports of solution structural studies of lithium enolates and related O-lithiated species,⁵⁻¹¹ none of the methods manifested the right combination of reliability and generality to characterize a variety of lithium enolates in a range of solvents and

* Reproduced with permission from Tomasevich, L. L. and Collum, D. B. *J. Org. Chem.* **2013**, *78*, 7498. Copyright 2013 American Chemical Society.

temperatures. We turned to the method of continuous variation (MCV)¹²⁻¹⁴ and a strategy founded on studies by Weingarten,¹⁵ Chabanel,¹⁶ Maddaluno,¹⁷ Gunther,¹⁸ and Gagne¹⁹ in which the aggregation number (n) of enolates A_n and B_n can be extracted from characteristic ensembles (eq 1). Using ^6Li NMR spectroscopy with the aid of parametric fitting we have characterized more than 100 lithium enolate-solvent combinations to date.^{20,21}



Taking a cue from early studies by Jackman and coworkers,⁶ we occasionally turn to lithium phenolates as enolate models.²¹ In the current study, we exploited the low basicity of lithium phenolates (**1-4**) to study protic and dipolar aprotic solvents that would not necessarily be compatible with more reactive lithium enolates. Lithium phenolates **1-4** manifest low, intermediate, and high steric demand and have been shown in previous studies to provide ensembles that are well-resolved in ^6Li spectra.²¹ The solvent-dependent formation of dimers, trimers, and tetramers (**5-7**) reveals relationships of solvation and aggregation that may seem counterintuitive.



Results

The assigned aggregation states with 5.0 equivalents per lithium of each solvent in toluene cosolvent are summarized in Table I.1. The table headings indicate the pairings (1-2 and 3-4) used to make the structural assignments as dimer 5, trimer 6, or tetramer 7. We occasionally used lithium phenolate 8 or lithium naphtholate 9 as pairing partners to confirm or further probe a structural assignment. The sections below delineate how we determined the solvent-dependent aggregation states and obtained insight into the relative binding efficacies of the solvents. Representative data are presented. The preponderance of spectra and affiliated Job plots are archived in supporting information.

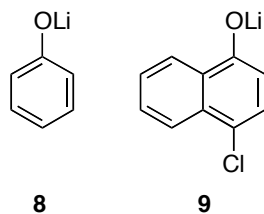
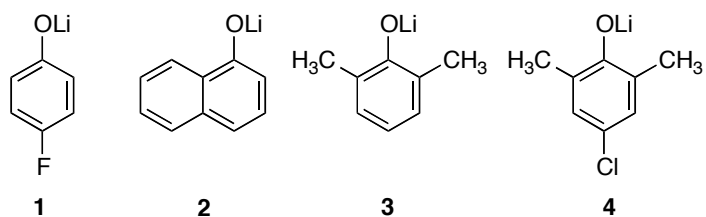


Table I.1. Solvent-dependent aggregation states and ^6Li NMR chemical shifts for homoaggregates of 1-4 at -60 to -110 °C (see supporting information). Assignments are based on pairings of 1-2 and 3-4.



Entry	Solvent ²²	Aggregate (δ ppm)			
1	TMEDA	dimer (0.01)	dimer (0.23)	dimer (0.03)	dimer (-0.20)
2	Et ₂ O	tetramer (0.21)	tetramer (1.35)	trimer (1.06)	trimer (0.69)
3	MeCN	tetramer (0.42)	tetramer (1.50)	tetramer (0.92)	tetramer (0.55)
4	pyridine	tetramer (2.00)	tetramer (3.10)	dimer (2.15)	dimer (1.94)
5	DMA	tetramer (1.17)	tetramer (2.02)	tetramer (1.33)	tetramer (1.04)
6	DMF	tetramer (1.24)	tetramer (2.16)	-- ^a	-- ^a
7	DMSO	tetramer (0.60)	tetramer (1.62)	tetramer (1.28) trimer (0.82)	tetramer (0.53) trimer (0.53)
8	DMPU	tetramer (0.87)	tetramer (1.93)	-- ^b (0.92)	-- ^b (0.70)
9	NMP	tetramer (1.13)	tetramer (2.03)	tetramer (1.47)	tetramer (1.16)
10	PrNH ₂	tetramer (0.87)	tetramer (2.07)	dimer (0.49)	dimer (0.25)
11	piperidine	tetramer ^b (0.75)	trimer ^c (1.80)	dimer ^d (0.36)	dimer (0.08)

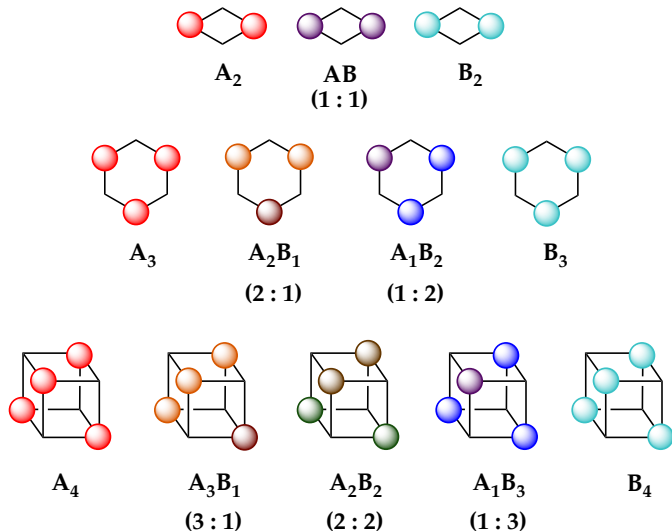
12	pyrrolidine	tetramer (0.70)	tetramer (1.96)	dimer ^d (0.59)	dimer (0.32)
13	<i>i</i> -BuNH ₂	tetramer (0.91)	tetramer (2.22)	dimer (0.71)	dimer (0.44)
14	<i>s</i> -BuNH ₂	tetramer (0.87)	tetramer (2.09)	-- ^b (0.13)	-- ^b (-0.22)
15	<i>t</i> -BuNH ₂	tetramer (0.78)	tetramer (1.96)	-- ^b (1.08)	-- ^b (0.88)
16	(<i>i</i> -Pr) ₂ NH	-- ^e (1.07)	trimer ^c (1.28)	dimer (1.07)	dimer (0.84)
17	Et ₂ NH	tetramer (0.55)	tetramer (1.79)	trimer (0.82)	trimer (0.42)
18	<i>n</i> -Pr ₂ NH	tetramer (0.49)	tetramer (1.78)	trimer (0.81)	trimer (0.42)
19	<i>t</i> -BuOH	tetramer (0.50)	tetramer (1.56)	-- ^b --	-- ^b --
20	<i>n</i> -BuOH	tetramer (0.90) ^g	tetramer (2.05) ^g	-- ^f --	-- ^f --
21	<i>s</i> -BuOH	tetramer (0.64)	tetramer (1.73)	-- ^b (0.13)	-- ^b (-0.23)

^aInsoluble. ^bCould not be resolved. ^cWith 4-chloro-1-naphthol. ^dAppears to be only tetrameric by ⁶Li NMR spectroscopy, whereas ¹⁹F NMR spectroscopy shows both the trimer and tetramer. ^eA major peak was left unassigned. ^fFails to mix aggregate with **2** and **8**. ^gTemperature routinely at -80 °C; for exceptions see supporting information. ^hResolves only with Et₂O as cosolvent.

MCV. Lithium phenolates **1-4** were characterized using the Method of Continuous Variation^{13,14} (MCV).¹² The output is often called a Job plot in which a physical property (*P*) is plotted against the mole fraction of **A** or **B** (X_A or X_B) in mixtures in which the total concentrations of **A** and **B** remain constant. In its simplest and most prevalent uses, MCV identifies the stoichiometry of a single complex (or aggregate) such as **AB** from the association of **A** and **B**. The stoichiometry of the complex is ascertained from the mole fraction corresponding to the maximum in the curve. In relatively rare instances, parametric fits are used to determine the equilibrium constant for complexation.¹⁴

MCV can be extended to an ensemble of $\mathbf{A}_m\mathbf{B}_n$ aggregates (eq 1) by monitoring the concentrations of all species versus X_A or X_B .^{3,20,21} Chart 1 summarizes the number of spectroscopically distinct aggregates expected for cyclic dimers, cyclic trimers, and cubic tetramers derived from $\mathbf{A}_n/\mathbf{B}_n$ mixtures. Magnetically inequivalent ^6Li nuclei within each aggregate are denoted with colored spheres. The number of aggregates within the ensembles and the affiliated spectral complexity increase markedly with aggregate size. An ensemble of tetramers, for example, contains five aggregates displaying up to a total of eight discrete resonances.

Chart 1. Dimer, trimer, and tetramer mixtures showing magnetically inequivalent lithium sites.



^6Li NMR Spectroscopy. Ensembles of homo- and heteroaggregates²³ derived from binary mixtures of lithium phenolates were prepared using [^6Li] lithium hexamethyldisilazide [^6Li]LiHMDS.²⁴ (The hexamethyldisilazane byproduct has no measurable Lewis basicity.^{4d}) Resolution is optimal when the chemical shift separation of the homoaggregates is large, a factor that contributed to our choice of lithium phenolates 1-4. Figure I.1a and I.1b offer examples of spectra for ensembles of cyclic dimers and tetramers, respectively. The line widths and resolution were optimized by adjusting the probe temperature, although the origins of the temperature dependencies were not always obvious. The stoichiometries apparent from the number of aggregates and their spectral symmetries are labeled and color coded.

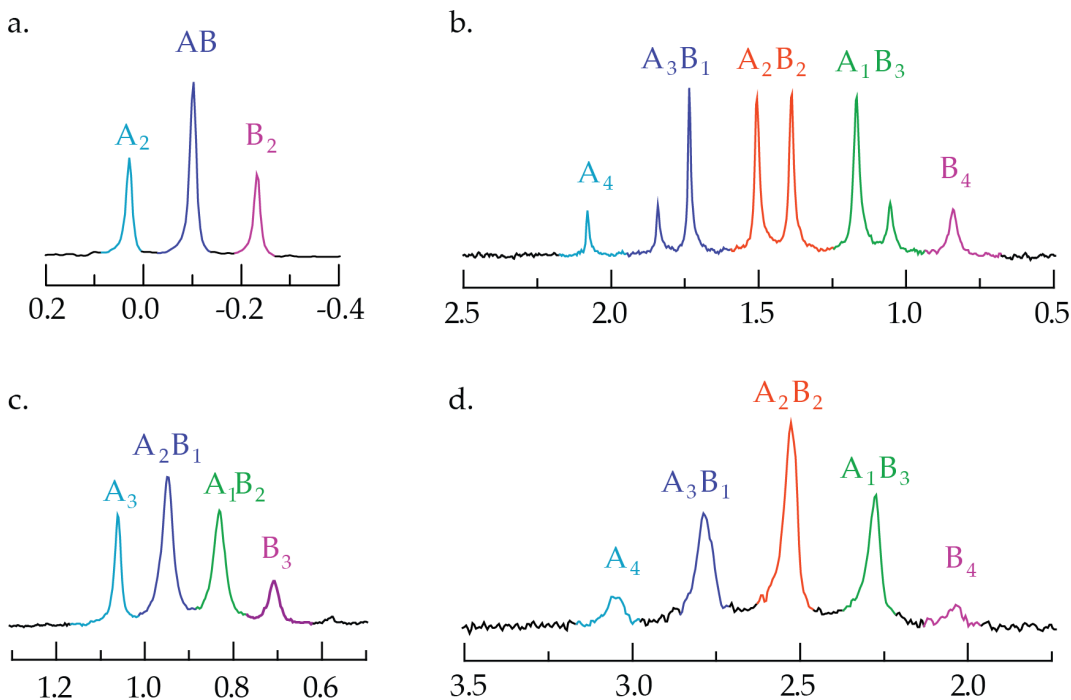


Figure I.1. ^6Li NMR spectra recorded as approximate 1:1 mixtures of lithium phenolates in toluene cosolvent: (a) dimers of $[\text{}^6\text{Li}]\mathbf{3}$ (**A**) and $[\text{}^6\text{Li}]\mathbf{4}$ (**B**) in 0.50 M TMEDA ($-80\text{ }^\circ\text{C}$); (b) tetramers of $[\text{}^6\text{Li}]\mathbf{2}$ (**A**) and $[\text{}^6\text{Li}]\mathbf{1}$ (**B**) in 0.50 M propylamine with slow intraaggregate exchange ($-80\text{ }^\circ\text{C}$); (c) trimers of $[\text{}^6\text{Li}]\mathbf{3}$ (**A**) and $[\text{}^6\text{Li}]\mathbf{4}$ (**B**) in 0.50 M Et_2O with rapid intraaggregate exchange ($-80\text{ }^\circ\text{C}$); and (d) tetramers of $[\text{}^6\text{Li}]\mathbf{2}$ (**A**) and $[\text{}^6\text{Li}]\mathbf{1}$ (**B**) in 0.50 M pyridine in ether cosolvent with rapid intraaggregate exchange ($22\text{ }^\circ\text{C}$).

For a number of lithium phenolate-solvent combinations we found that certain proportions of two lithium phenolates result in a loss of resolution owing to inexplicably enhanced interaggregate exchange. We occasionally observed the aggregates in the limit of rapid *intraaggregate* yet slow *interaggregate* exchange.²⁵ Under these conditions, each stoichiometry appears as a single resonance.²¹ In the case of lithium phenolate trimers, for example, fast *intraaggregate* exchange was the only viable option (Figure I.1c). Figure I.1d shows a tetramer similar to that in Figure I.1b but in the limit of rapid *intraaggregate* exchange. Both limiting perspectives have merit: the symmetries are highly characteristic in the slow

exchange limit, whereas the spectra are simpler and often more tractable in complex systems such as hexamers in the fast intraaggregate exchange limit.³

Job Plots and Parametric Fits. We monitored the homo- and heteroaggregates for various proportions of two lithium phenolates at a constant total lithium phenolate concentration (Figure I.2). Plotting the *relative* integrations of the homo- and heteroaggregates versus *measured* mole fraction of the lithium phenolate subunits (X_A or X_B) afforded Job plots for dimers, trimers, and tetramers shown emblematically in Figures I.3-I.5. We always use the so-called measured mole fraction—the mole fraction within only the ensemble of interest—rather than the overall mole fraction of lithium phenolates added to the samples because it eliminates the distorting effects of impurities and enables concurrent analysis of several ensembles (Figure I.6). The curves represent parametric fits using methods detailed elsewhere.^{3,20a} Although the fitting protocols measure deviation from statistical, the aggregate distributions almost always approximate statistical. Deviations from statistical, especially a resistance to form ensembles, constitute evidence of two different aggregation states. Figure I.6 displays an unusual circumstance in which intraaggregate exchange is slow for the tetramer ensemble and fast for the trimer ensemble.

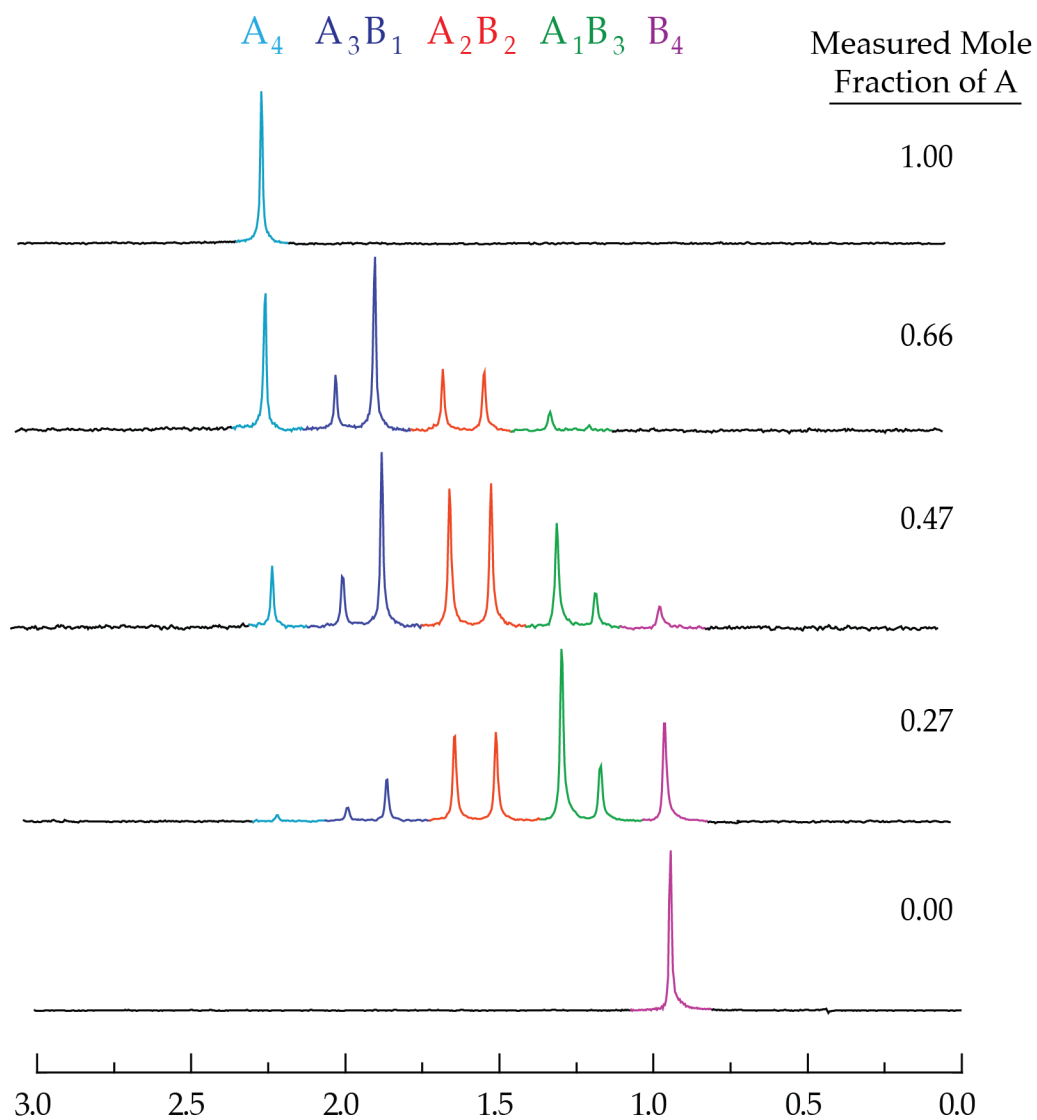


Figure I.2. ^6Li NMR spectra recorded of $[\text{}^6\text{Li}]_2$ (**A**) and $[\text{}^6\text{Li}]_1$ (**B**) in solutions 0.50 M isobutylamine in toluene at $-80\text{ }^\circ\text{C}$.

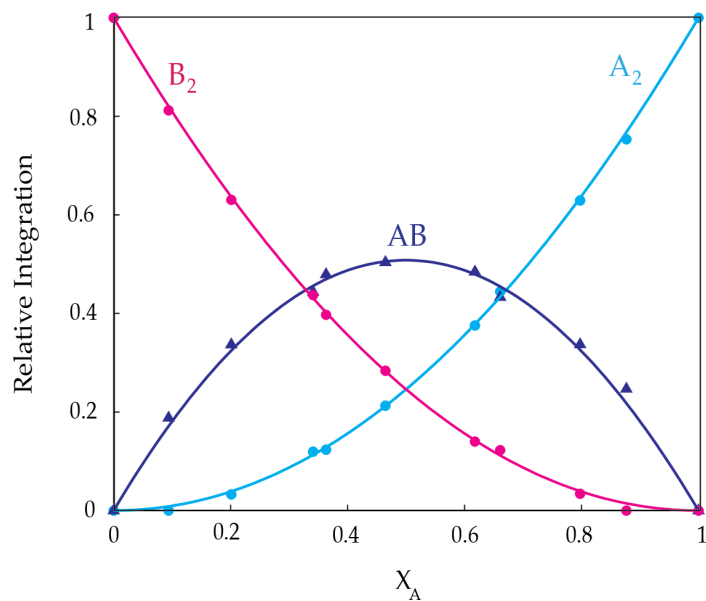


Figure I.3. Job plot showing the relative integrations of dimeric homo- and heteroaggregates versus measured mole fractions of **3** (X_A) for 0.10 M mixtures of phenolates [^6Li]**3** (**A**) and [^6Li]**4** (**B**) in 0.50 M pyridine/toluene at $-80\text{ }^\circ\text{C}$.

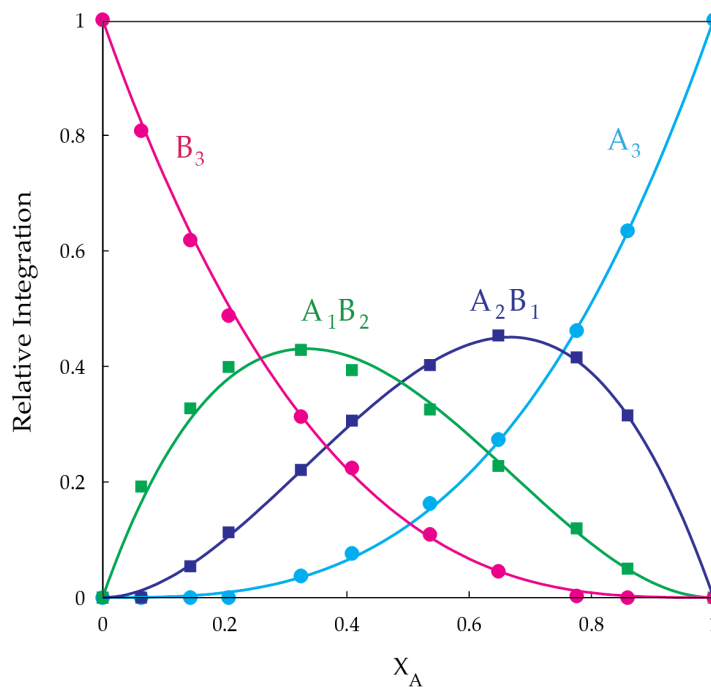


Figure I.4. Job plot showing the relative integrations of trimeric homo- and heteroaggregates versus measured mole fractions of **3** (X_A) for 0.10 M mixtures of phenolates [^6Li]**3** (**A**) and [^6Li]**4** (**B**) in 0.50 M diethyl ether/toluene at $-90\text{ }^\circ\text{C}$.

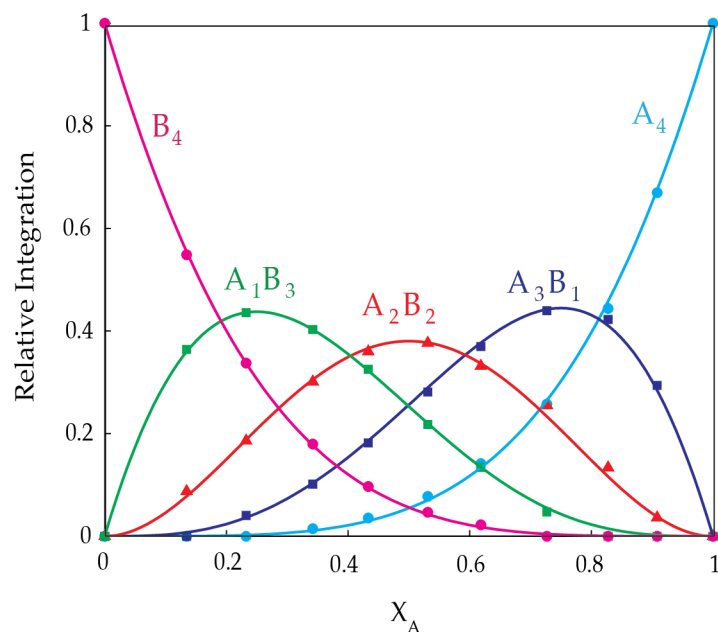


Figure I.5. Job plot showing the relative integrations of tetrameric homo- and heteroaggregates versus measured mole fractions of **2** (X_A) for 0.10 M mixtures of phenolates [^6Li]**2** (**A**) and [^6Li]**1** (**B**) in 0.50 M isobutylamine/toluene at -80°C .

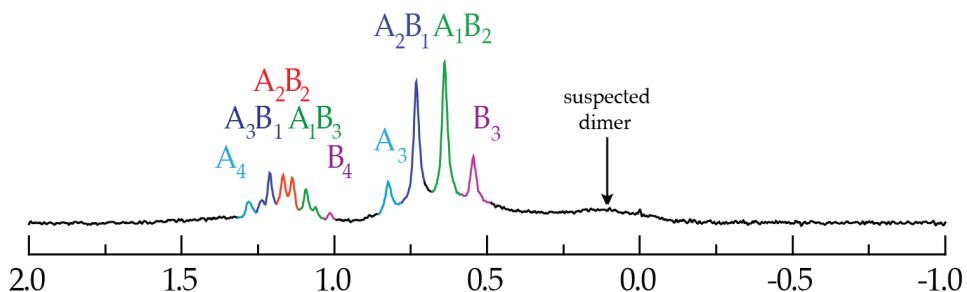


Figure I.6. ^6Li NMR spectrum of 0.50 M dimethylsulfoxide (DMSO)/toluene solutions containing approximate 1:1 mixtures of [^6Li]**3** and [^6Li]**4** recorded at -90°C showing trimeric and tetrameric ensembles of homo- and heteroaggregates. The tetramer is at the limit of slow intraaggregate exchange whereas the trimer is undergoing rapid intraaggregate exchange. An ensemble appears upon warming to -50°C and shows characteristics of dimers.

Solvent Swapping and Relative Binding Constants. We have developed a number of strategies for probing aggregate structure and solvation under the rubric of “solvent swapping.”^{20a,21} Solvent swaps are multipurpose and can take

several of the forms described below. They provide insights into lithium phenolate solvation albeit with occasional complications.

A solvent swap requires a measurable ^6Li chemical shift difference for a single lithium phenolate solvated by two solvents. It is based on rapid solvent-solvent exchange (ligand substitution)²⁶ and much slower aggregate-aggregate exchange. Several behaviors can be observed by recording incrementally replacing one solvent by a second or by holding one solvent concentration fixed and varying the other (Figure I.7).

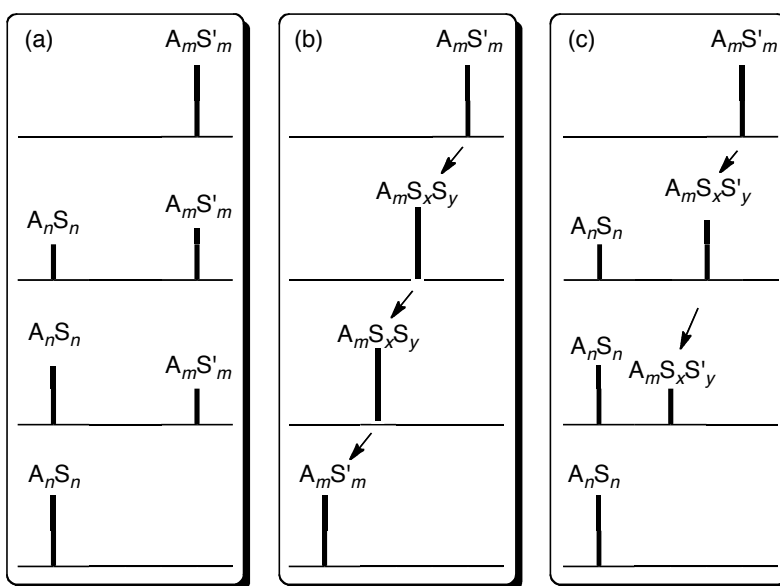
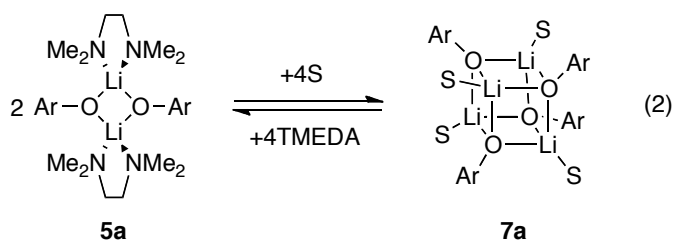


Figure I.7. Expected ^6Li NMR when replacing solvent S by S' : (a) elicits only a change in aggregation state (A_n for A_m), (b) causes solvent substitution on a common aggregate (A_m), or (c) causes an aggregation state change (A_n for A_m) and concurrent partial exchange of solvent on A_m to form a mixed solvate.

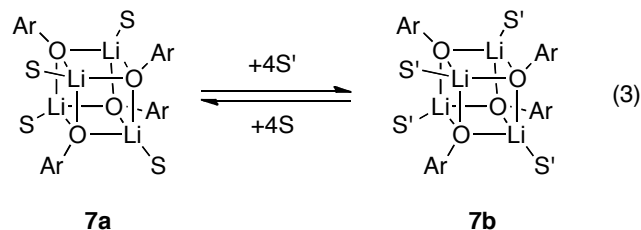
Results from the solvent swapping experiments illustrated in Figure I.7a-c are as follows:

(a) If the observable aggregates in the two solvents are different—dimer versus tetramer, for example—incremental solvent swap in conjunction with *slow* aggregate-aggregate exchange causes one to disappear and the other to appear

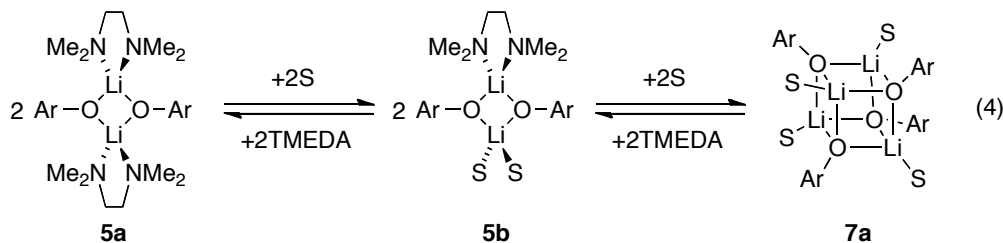
(Figure I.7a). The coexistence of both forms in slow exchange confirms differential aggregation. With a TMEDA-solvated dimer as a benchmark (eq 2), the relative binding constants of other solvents to the lithium phenolate tetramer can be measured²⁷ provided that mixed-solvated dimers or mixed-solvated tetramers do not intervene (*vide infra*).²⁸⁻³⁰



(b) If the two observable forms in the two coordinating solvents differ only in ligating solvent, incremental solvent swap in conjunction with *rapid solvent exchange* will cause the resonances to exchange via time-averaging (Figure I.7b).²⁶ The solvent-concentration-dependent shift confirms the common aggregation state and provides qualitative insights into relative binding affinities. This experiment works particularly well with pyridine as one of the solvents owing to the marked (>1.0 ppm) downfield shift of pyridine solvates.^{6b,31-33} Quantitation is precluded by the unknown additive effects on the chemical shift by intervening mixed solvates—three $A_4S_mS'_{4-m}$ tetramer-based mixed solvates, for example. Nevertheless, the magnitude of the shift gives a qualitative sense of the relative capacity to solvate the tetramer.



(c) The useful dimer-tetramer competition in eq 2 occasionally shows evidence of mixed solvates.^{34,35} The example in Figure I.7c is characteristic of the occasional intervention of a mixed solvated dimer (eq 4). Strongly coordinating monodentate ligands can displace one chelated TMEDA ligand from the dimer.²⁸ Although TMEDA does not appear well suited to solvate tetramers, we nonetheless found evidence that η^1 -TMEDA solvated tetramers³⁶ can intervene even in cooperation with strongly coordinating monodentate ligands (*vide infra*).



The results described below derived from combinations of the solvent swapping strategies. In most cases the strategy will be self-evident; all data are archived in supporting information. Our initial goal to quantitatively measure solvation of lithium phenolates was thwarted by sporadic technical problems and intervening mixed solvation. Consequently, the discussion is largely about qualitative effects (and selective examples at that) but they are revealing nonetheless.

Aprotic Solvents. Mixtures of **1** and **2** in Et₂O show exclusively tetramers. Solutions of lithium phenolate **1** in neat Et₂O with as little as 2.0 equiv of TMEDA (see eq 2) contain exclusively TMEDA-solvated dimer **5a**. Although this outcome does not attest to the relative binding constants of Et₂O and TMEDA because of the unknowable energy of aggregation, ether is poorly coordinating³⁷ compared with other solvents (except the highly hindered *i*-Pr₂NH). By contrast, 5 equiv of TMEDA and 5 equiv of pyridine (eq 2; S = pyridine) afforded nearly equal parts dimer and tetramer. Both resonances are at approximately the same chemical shift as observed when the solvents are used separately, suggesting the absence of mixed solvation (see Figure I.7a). The dramatic downfield chemical shift imparted by pyridine is a highly characteristic and useful diagnostic probe.^{6b,31} Adding pyridine incrementally in neat Et₂O in an experiment akin to that represented by eq 3 (Figure I.7b) shows much stronger binding of pyridine than of Et₂O on a per-molar basis.

Incrementally increasing the pyridine concentration in pyridine-TMEDA solutions of naphtholate **2** yields the expected replacement of the TMEDA-solvated dimer with a pyridine-solvated tetramer. However, accompanying substantial downfield shifting of the dimer implicates mixed-solvated dimer **5b** (eq 4; S = pyridine).

Dipolar Aprotic Solvents. Highly dipolar solvents in toluene cosolvent (Table I.1, entries 5-9) display a strong tendency to form tetramers for all four lithium phenolates **1-4**, which is contrary to the often-cited belief that dipolar solvents promote deaggregation.³⁸ Addition of 1.0 equiv of the dipolar solvents to TMEDA-solvated dimer **5a** elicits quantitative conversion to the corresponding tetramers (eq 2), indicating that dipolar solvents bind more

strongly than do pyridine (as well as *n*-PrNH₂ and pyrrolidine; *vide infra*). Despite concerns that the dipolar ligands might catalyze facile exchanges, intraaggregate exchange is slow at low temperatures. Even the hindered 2,6-dimethylphenolates **3** and **4**, which display a penchant to deaggregate in THF²¹ afford tetramers when solvated by most of the highly dipolar ligands. Inexplicably high interaggregate exchange rates for *N,N'*-dimethyl-*N,N'*-trimethyleneurea (DMPU) precluded studies of **3** and **4**. Acetonitrile mimicked the carbonyl-based dipolar ligands in promoting tetramers, although high interaggregate exchange rates precluded detailed studies. Attempts to measure the relative binding constants of the dipolar ligands were largely unsuccessful.^{39,40}

Mixtures of the hindered 2,6-dimethylphenolates **3** and **4** solvated by DMSO are outliers, affording ensembles of dimers, trimers, and tetramers observed concurrently (Figure I.6.) DMSO-solvated mixtures of **1** and **2** also departed from the norm in that intraaggregate exchange rates depended markedly on the stoichiometry of the mixed tetramers. We turned to an alternative strategy to examine DMSO solvates.

Previous studies have shown that ¹⁹F NMR spectroscopy affords superior resolution in highly fluxional ensembles,²¹ but the spectral fingerprint of such ensembles is markedly different. Ensembles of **1** and **2** observed with ¹⁹F NMR spectroscopy, for example, are necessarily missing the NMR silent homonuclear tetramer of **2**. Moreover, the 1 : 3, 2 : 2, and 3 : 1 heterotetramers will each appear as a single resonance irrespective of the rate of intraaggregate exchange because of the NMR silent subunits of **2**. Mixtures of **1** and **2** in DMSO/toluene afford a well-resolved four-resonance tetramer ensemble as well as very low

concentrations of what appears to be the corresponding trimer ensemble (Figure I.8).

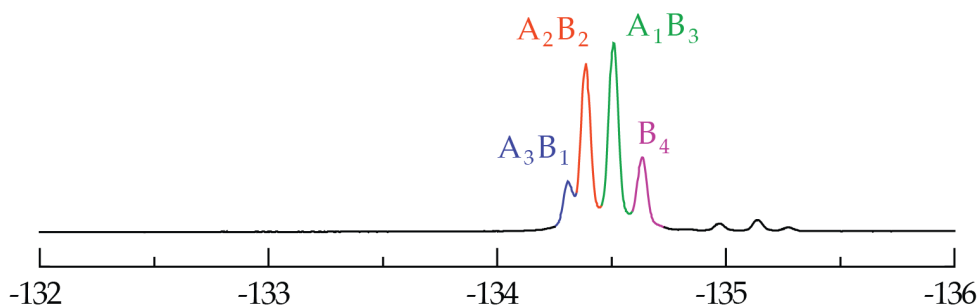


Figure I.8. ^{19}F NMR spectra of a 1:1 mixture of **2** (**A**) and **1** (**B**) in toluene containing 0.50 M DMSO recorded at $-80\text{ }^\circ\text{C}$. A_4 is absent because it is NMR silent.

Protic Amines. We examined mono- and dialkylamines spanning a range of steric demands. *n*-PrNH₂/toluene solutions of **1** and **2** afford tetramers consistent with anticipated⁴¹ strong coordination akin to that of dipolar ligands.⁴² Dipolar ligands and monoalkylamines, however, give different results with mixtures of hindered lithium phenolates **3** and **4**. Whereas dipolar ligands afford tetramers, *n*-PrNH₂/toluene solutions contain only dimers. One could imagine highly stabilized tetrasolvated dimers, yet we observed dimers with as little as 1.0 equiv of *i*-BuNH₂. This dimer preference may be general, but high exchange rates for *t*-BuNH₂ and *s*-BuNH₂ precluded analysis. Further studies are needed to make definitive statements.

Pyrrolidine, the least sterically demanding dialkylamine, showed a high penchant for forming tetramers of unhindered lithium phenolates **1** and **2**. Solvent-swapping experiments showed pyrrolidine has a surprisingly high binding affinity compared to that of even pyridine.⁴³ Et₂NH, by contrast, affords

tetramers but is a weaker ligand than pyridine. Piperidine produced conflicting results by affording a tetramer ensemble with mixtures of **1** and **2** and a trimer ensemble with mixtures of lithium naphtholates **2** and **9**, apparently resulting from divergent steric demands of unhindered phenolates **1** and **2**.

The capacity of **2** solvated by piperidine to participate in two ensembles with equal facility affording statistical distributions in both cases is the first instance of such promiscuity reported to date. In previous studies, the rule of thumb “like aggregates with like” has held true.^{20a,21} Hindered lithium phenolates **3** and **4** display an unexpected tendency to form trimers with unhindered dialkylamines.^{6,44-46}

The highly hindered *i*-Pr₂NH, a ligand of some interest in the context of enolates generated from lithium diisopropylamide,² affords trimers from lithium naphtholates **2** and **9**, showing similarity to the less hindered piperidine. Failure to form heteroaggregates between **1** and **2** suggested that unhindered lithium phenolate **1** does *not* form trimers and more hindered lithium naphtholate **2** does *not* form tetramers. Although lithium phenolate **1** showed solubility consistent with at least partial solvation by *i*-Pr₂NH, attempts to characterize the suspected tetramer fell short. Dimethylated lithium phenolates **3** and **4** afforded trimers for most dialkylamines yet afforded exclusively dimers with *i*-Pr₂NH.

Alcohols. Alcohols generally displayed technical problems associated with high exchange rates. Methanol and ethanol, for example, failed to provide tractable results altogether. By contrast, *t*-BuOH affords tetramers with unhindered lithium phenolates **1** and **2** and intractable mixtures with hindered lithium phenolates **3** and **4**. The less demanding *n*-butanol and *s*-BuOH also afford tetramers with **1** and **2**, although *n*-butanol shows an odd tendency to

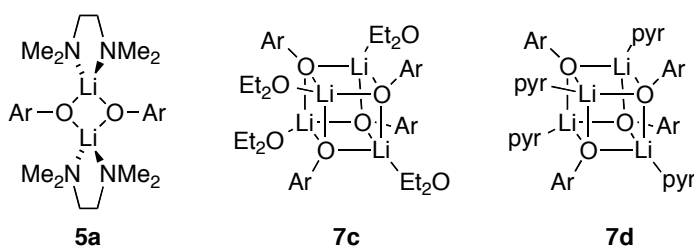
afford resolved tetramer ensembles only using Et₂O as cosolvent, which suggested a cooperative solvation effect. Solvent swaps competing the alcohols with TMEDA (eq 2) show the anticipated qualitative drop in binding with increasing steric demands: primary > secondary > tertiary.⁴⁵

Discussion

Lithium enolates, alkoxides, carboxylates, and phenolates are notoriously difficult to study in solution³⁻¹⁰ owing to the absence of the single most important NMR spectroscopic probe—scalar coupling. It was in this context that we turned to the Method of Continuous Variation (MCV).^{3,20,21} The underlying theme of this paper, however, is less about the role of MCV in determining aggregation states of lithium phenolates—a topic covered in previous studies²¹—and more about the merits of relatively nonbasic and stable lithium phenolates for the study of lithium ion solvation using solvents that are not easily examined with more reactive organolithiums. Lithium phenolates characterized by low steric demands (**1**), intermediate steric demands (**2**), and high steric demands (**3** and **4**) were used emblematically. The solvents are moderately polar (pyridine, Et₂O, and TMEDA; Table I.1, entries 1-3), highly dipolar (Table I.1, entries 5-9), and protic (amines and alcohols; entries 10-21). In addition to investigation of solvent-dependent aggregation states (Table I.1), solvent swapping experiments using binary solvent mixtures represented by eqs 2-4 shed light on relative binding energies, relationships of solvation and aggregation, and mixed solvation. Descriptions of metal ion solvation as a molecular phenomenon rather than a bulk medium effect are still so elusive that even incremental gains are notable.⁴⁷ Note that the results described herein are obtained at low ligand

concentrations (0.50 M); high concentrations often elicit rapid aggregate exchanges that may obscure affiliated deep-seated structural changes. Occasionally, an additional (lower) aggregate also appears.

Nonpolar solvents established a foundation for the study. Et₂O promotes tetramers and is poorly coordinating relative to most ligands. TMEDA dependably affords chelated dimers (**5a**), allowing for solvent comparisons through competition according to eq 2. Pyridine is comparable to THF²⁸ and readily promotes tetramers with the particular advantage of causing marked (≈ 1.0 ppm) downfield ⁶Li shifts used that are useful both diagnostically and to maximize resolution. These three solvents have routinely been used as benchmarks in investigations of the dipolar and protic solvents.



The dipolar ligands are all very strongly coordinating as shown by the especially facile conversion of TMEDA-solvated dimers to tetramers (eq 2). Despite failed efforts to quantitate their relative binding affinities, we confirmed that they act quite similarly to one another. The seemingly paradoxical tendency to afford tetramers despite a reputation for deaggregating lithium salts is consistent with previous studies showing that a lack of deaggregation⁴⁸ and even promotion of aggregation^{6d} are possible. DMSO is an outlier, showing a marked tendency to afford dimers, trimers, and tetramers *concurrently*. Overall, the

dipolar ligands remind us that simple maxims about solvation and aggregation must be viewed skeptically: metal ion and aggregate solvation are complex.

The protic amines provided the most widely varying results, possibly because of their enormous range of structural diversity and steric demands. At one extreme, monoalkylamines are comparable to the dipolar ligands, although we noted a greater penchant of the amines to support dimers. The least hindered dialkylamine, pyrrolidine, is also a strong ligand, exceeding pyridine in its capacity to bind. Previous studies of pyrrolidine⁴³ and pyrrolidine-based chelates³³ have shown similarly strong ligation. At the other extreme, diisopropylamine appears to bind, but it is a poorly coordinating ligand at best. This additional data in conjunction with other studies⁴³ showing poor coordination of *i*-Pr₂NH contrasts with provocative and still somewhat baffling evidence that *i*-Pr₂NH can influence the chemistry of lithium enolates *in neat THF solution*.⁴⁹ Dialkylamines also cause the unexpected appearance of lithium phenolate trimers. It would be a mistake, however, to underestimate the complexity of the steric contributions on a tetramer containing up to four ligands that could promote lower aggregates by default.

Our previous studies of LiHMDS solvated by R-X-R' ligands in which R and R' varied widely showed a remarkably linear correlation of binding constant with X = O and NH: the binding is independent of X.⁴³ One can see similar trends with lithium phenolates, although the correlation is unlikely to be as strong. We presume, for example, that serial solvation of the four sites of a tetramer is nonstatistical, especially for sterically demanding ligands.

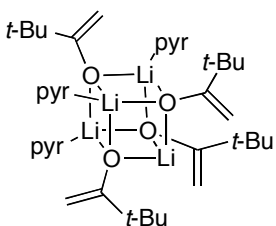
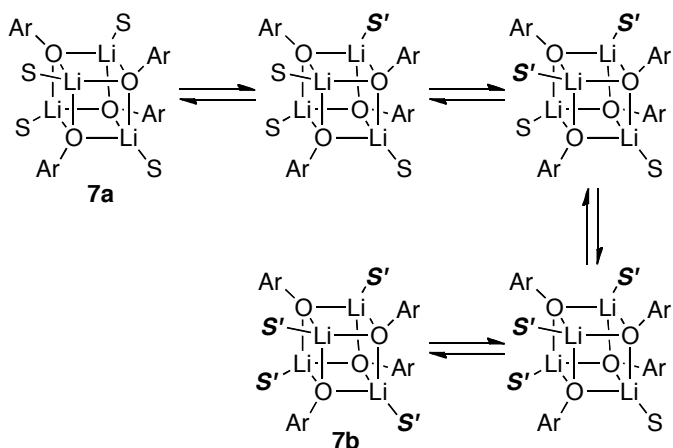
Studies of the alcohols were clearly the most disappointing given their prevalence in industrial scale reactions of alkali metal phenolates.⁵⁰ We observed

evidence that low concentrations of alcohols could support tetramers in solution, but studies of the most commonly used alcohols—methanol and ethanol—were precluded by high exchange rates. Although these high rates may simply reflect low steric demands, we cannot rule out a role of the alcoholic proton in the catalysis of inter- and intraaggregate exchanges.⁵¹ Somewhat more hindered cases such as *n*-BuOH and the highly hindered *t*-BuOH afford tetramers, but only the latter is well behaved. We reiterate that exchange rates may be blinding us to deaggregation at the high ligand concentrations often used in synthesis.^{6b}

Solvent swapping studies using binary mixtures of coordinating solvents provided glimpses of an elusive but fascinating phenomenon collectively referred to as correlated (cooperative)³⁴ solvation that has captivated our attention for some time.²⁸ This topic is important given the prevalence of solvent mixtures in organic chemistry. The extent to which the multiple ligands compete and cooperatively bind is relatively unexplored.²⁸⁻³⁰

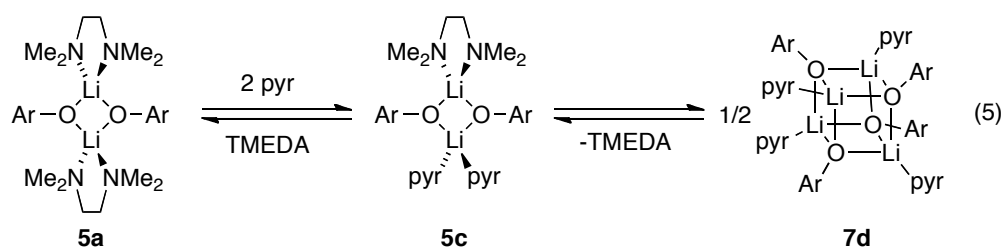
In routine cases such as incrementally swapping pyridine, it is possible that one homosolvated tetramer may be replaced by another (eq 3). The far more likely scenario, however, is that the marked changes in chemical shift result from an ensemble of mixed solvate tetramers (Chart 2). That is not to say, however, that they distribute statistically. Reich notes nonstatistical replacements of ethereal solvents by increments of hexamethylphosphoramide.^{10b} Jacobsen noted a surprising tendency of a hindered lithium pinacolate to favor trisolvate **8** with added pyridine.⁹

Chart 2

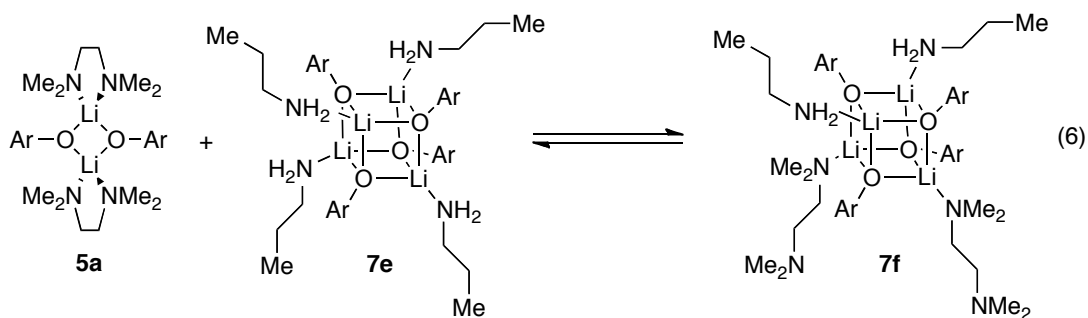


8

We qualitatively observed cooperative solvation on multiple occasions. Lithium naphtholate **2** in TMEDA/pyridine mixtures, for example, afforded the anticipated TMEDA-solvated dimer and pyridine-solvated tetramer, yet the dimer showed clear evidence of an intervening TMEDA/pyridine mixed-solvated dimer (eq 5). We saw no evidence that the corresponding tetramer contained any coordinated TMEDA. By contrast, lithium phenolate **1** in analogous TMEDA/pyridine mixtures showed the opposite: substantial solvent-dependent chemical shifts of the tetramer characteristic of mixed solvation occurs with no obvious changes in the dimer.



A more detailed investigation of mixed solvation is required to reveal intimate details. One possible strategy is foreshadowed by an experiment in which lithium phenolates are starved of solvent to force coordination of both solvents (eq 6). We expected lithium naphtholate **2** containing 0.50 equiv of *n*-PrNH₂ and 0.50 equiv of TMEDA—one solvent molecule per lithium—to provide a mixture of homosolvated dimer **5a** and tetramer **7a** (see eq 2) but only tetramer forms, suggesting cooperativity in tetramer **7f**. The η¹-bound TMEDA is inferred but well precedented.³⁶ If so, cooperativity—a nonstatistical preference for mixed solvation—is strongly indicated.



Conclusion

Our efforts to untangle organolithium chemistry often yield both insights into organolithium chemistry and tactical advances—expansion of our toolbox—that promise greater clarity in future studies. Several insights from the present study are noteworthy. Dipolar ligands promote aggregation, and DMSO offers evidence that it is an outlier compared with its carbonyl-based brethren. Protic

amines with widely varying steric demands show a large range of binding affinity, resulting in highly amine-dependent distributions of aggregates. The most interesting results came from binary solvent mixtures in which evidence of mixed solvates suggest cooperative solvation.

From a tactical perspective, some promising protocols emerged for studying the coordination chemistry (solvation) of enolates, phenolates, and related O-lithiated species. Studies of binary mixtures may be a fruitful direction for future studies. In particular, aggregate distributions under starved conditions in which both ligands in a binary mixture are forced to bind may reveal interesting insights into solvent-solvent (ligand-ligand) interactions within aggregates. We are using pyridine centrally in a number of projects owing to exceptional chemical shifts caused by coordination, which not only improve resolution but also confirm the very existence (or absence) of the pyridine-lithium contacts. Confirming the presence or absence of solvent-lithium contacts can be difficult. We have also documented another example in which ^{19}F NMR spectroscopy was used to resolve aggregate distributions that could not be resolved by ^6Li NMR spectroscopy,²¹ underscoring the potential importance of alternative nuclei in studies of salt aggregation and solvation using MCV.

Experimental Section

Reagents and Solvents. All phenols used are commercially available. TMEDA, Et_2O , and all amines were distilled from solutions containing sodium benzophenone ketyl. Toluene was distilled from blue solutions containing sodium benzophenone ketyl with approximately 1% tetraglyme to dissolve the

ketyl. Alcohols and all solvents containing carbonyls were distilled from 3 or 4 Å molecular sieves. [⁶Li]LiHMDS was prepared and recrystallized as described previously.²⁴ Air- and moisture-sensitive materials were manipulated under argon using standard glove box, vacuum line, and syringe techniques.

NMR Spectroscopy. Individual stock solutions of substrates and base were prepared at room temperature. An NMR tube under vacuum was flame dried on a Schlenk line and allowed to return to room temperature. It was then backfilled with argon and placed in a -78 °C dry ice/acetone bath. The appropriate amounts of [⁶Li]LiHMDS and phenol were added sequentially via syringe. The tube was sealed under partial vacuum, stored in a -86 °C freezer, and shaken prior to placement into the spectrometer. Each NMR sample contained 0.10 M total phenol and 0.11 M LiHMDS.

⁶Li NMR spectra were typically recorded at -80 °C (unless stated otherwise) on a 500 or 600 MHz spectrometer with the delay between scans set to >5 x T1 to ensure accurate integrations. Chemical shifts are reported relative to a 0.30 M ⁶LiCl/MeOH standard at the reported probe temperature. The resonances were integrated using the standard software accompanying the spectrometers. After weighted Fourier transform with 64,000 points and phasing, line broadening was set between 0 and 0.3, and a baseline correction was applied when appropriate. Deconvolution was performed in the absolute intensity mode, with application of a drift correction using default parameters for contributions from Lorentzian and Gaussian line shapes. The mathematics underlying the parametric fits have been described in detail.^{3,20a}

Acknowledgments. We thank the National Institutes of Health (GM077167) and Sanofi-Aventis for direct support of this work.

APPENDIX I

Dimer Job Plots in TMEDA

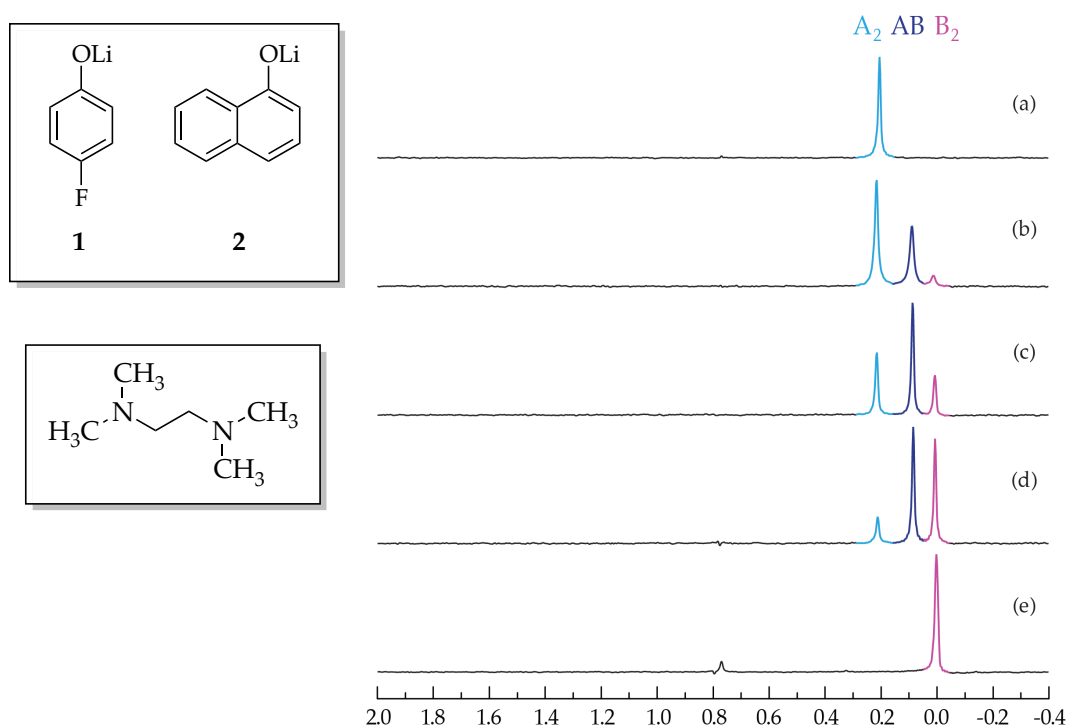


Figure AI.1. ^6Li NMR spectra of 0.10 M solutions of $[\text{}^6\text{Li}]\mathbf{2}$ (A) and $[\text{}^6\text{Li}]\mathbf{1}$ (B) in 0.50 M $(\text{CH}_3)_2\text{NCH}_2\text{CH}_2\text{N}(\text{CH}_3)_2$ /toluene at $-90\text{ }^\circ\text{C}$. The measured mole fractions of A in (a)-(e) are 1.00, 0.74, 0.56, 0.25, and 0.00, respectively.

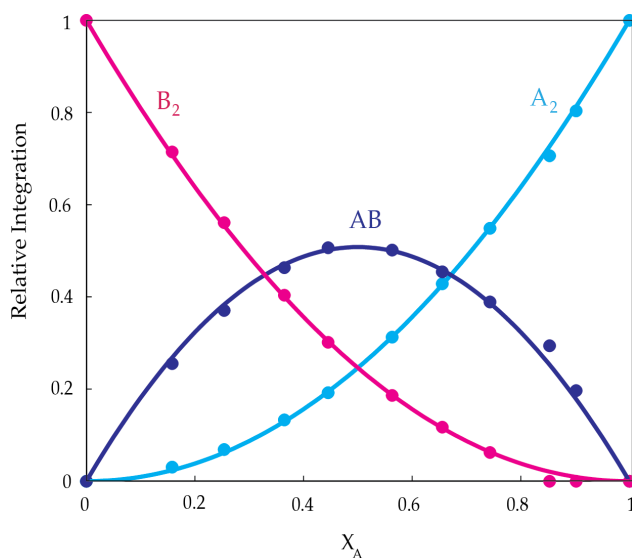


Figure AI.2. Job plot showing the relative integrations versus the measured mole fractions of 2 for 0.10 M mixtures of $[\text{}^6\text{Li}]\mathbf{2}$ (A) and $[\text{}^6\text{Li}]\mathbf{1}$ (B) in 0.50 M $(\text{CH}_3)_2\text{NCH}_2\text{CH}_2\text{N}(\text{CH}_3)_2$ /toluene at $-90\text{ }^\circ\text{C}$.

Dimer Job Plots in TMEDA

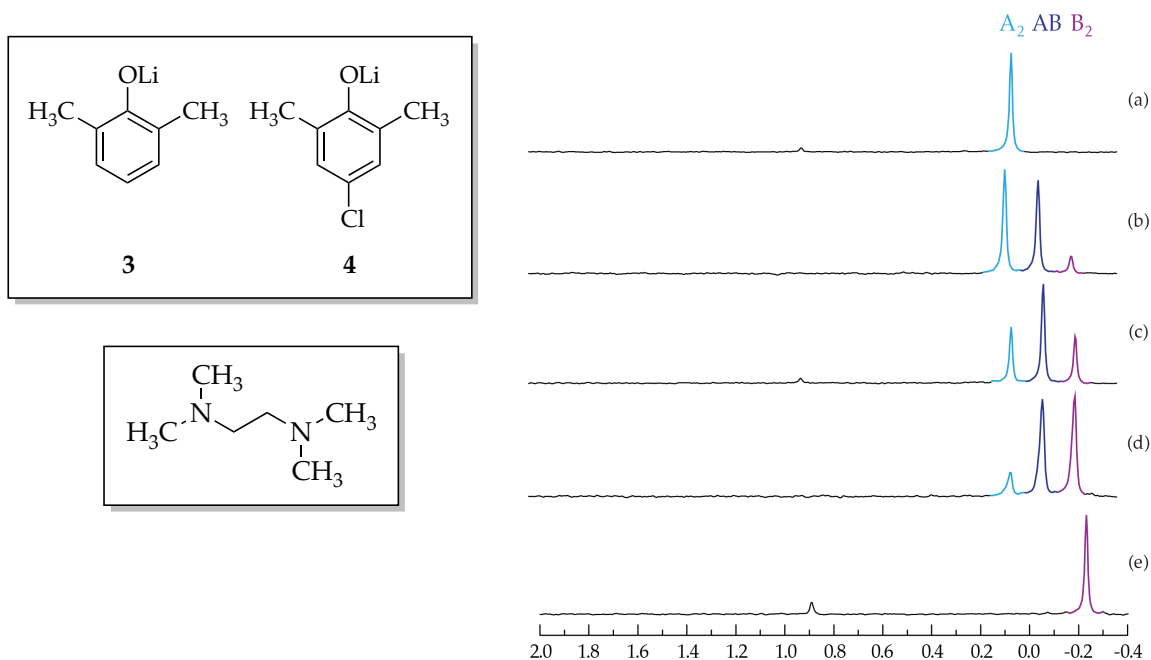


Figure AI.3. ^6Li NMR spectra of 0.10 M solutions of $[\text{}^6\text{Li}]\mathbf{3}$ (**A**) and $[\text{}^6\text{Li}]\mathbf{4}$ (**B**) in 0.50 M $(\text{CH}_3)_2\text{NCH}_2\text{CH}_2\text{N}(\text{CH}_3)_2$ /toluene at -80°C . The measured mole fractions of **A** in (a)-(e) are 1.00, 0.66, 0.48, 0.30, and 0.00, respectively.

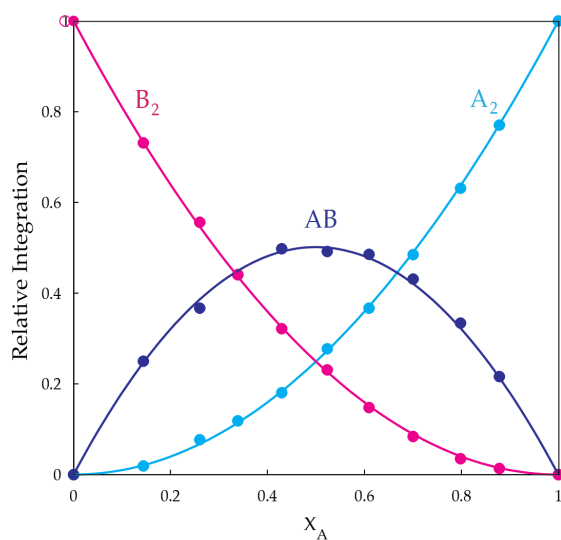


Figure AI.4. Job plot showing the relative integrations versus the measured mole fractions of **3** for 0.10 M mixtures of $[\text{}^6\text{Li}]\mathbf{3}$ (**A**) and $[\text{}^6\text{Li}]\mathbf{4}$ (**B**) in 0.50 M $(\text{CH}_3)_2\text{NCH}_2\text{CH}_2\text{N}(\text{CH}_3)_2$ /toluene at -80°C .

Tetramer Job Plots in Diethyl Ether

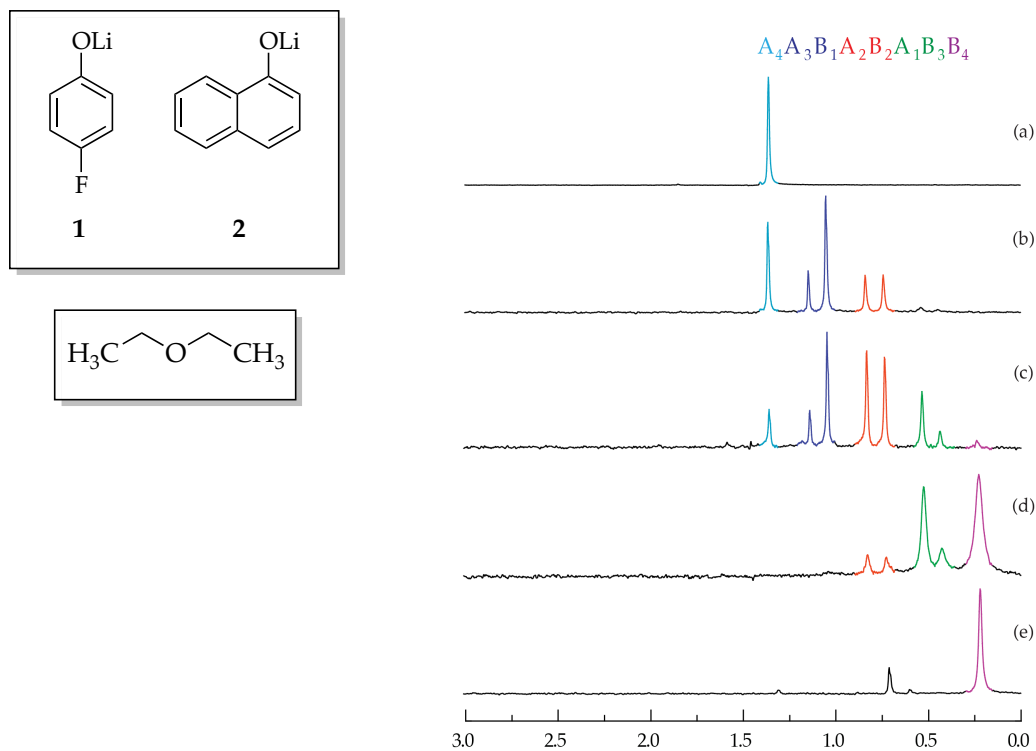


Figure AI.5. ^6Li NMR spectra of 0.10 M solutions of $[\text{}^6\text{Li}]\mathbf{2}$ (A) and $[\text{}^6\text{Li}]\mathbf{1}$ (B) in 0.50 M Et_2O /toluene at -90°C . The measured mole fractions of A in (a)-(e) are 1.00, 0.70, 0.43, 0.17, and 0.00, respectively.

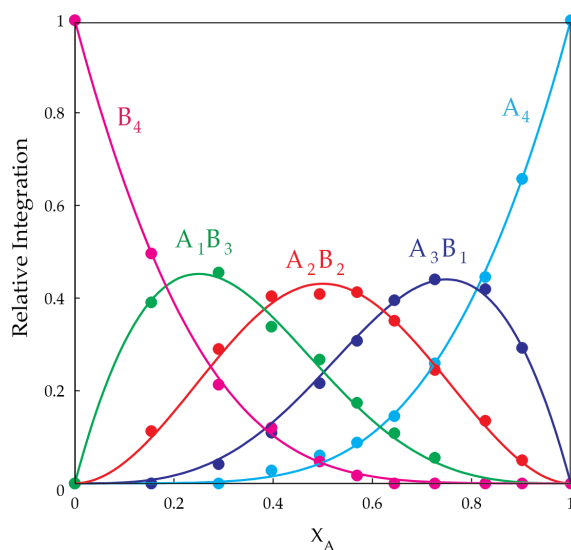


Figure AI.6. Job plot showing the relative integrations versus the measured mole fractions of $\mathbf{2}$ for 0.10 M mixtures of $[\text{}^6\text{Li}]\mathbf{2}$ (A) and $[\text{}^6\text{Li}]\mathbf{1}$ (B) in 0.50 M Et_2O /toluene at -90°C .

Tetramer Job Plots in Diethylether

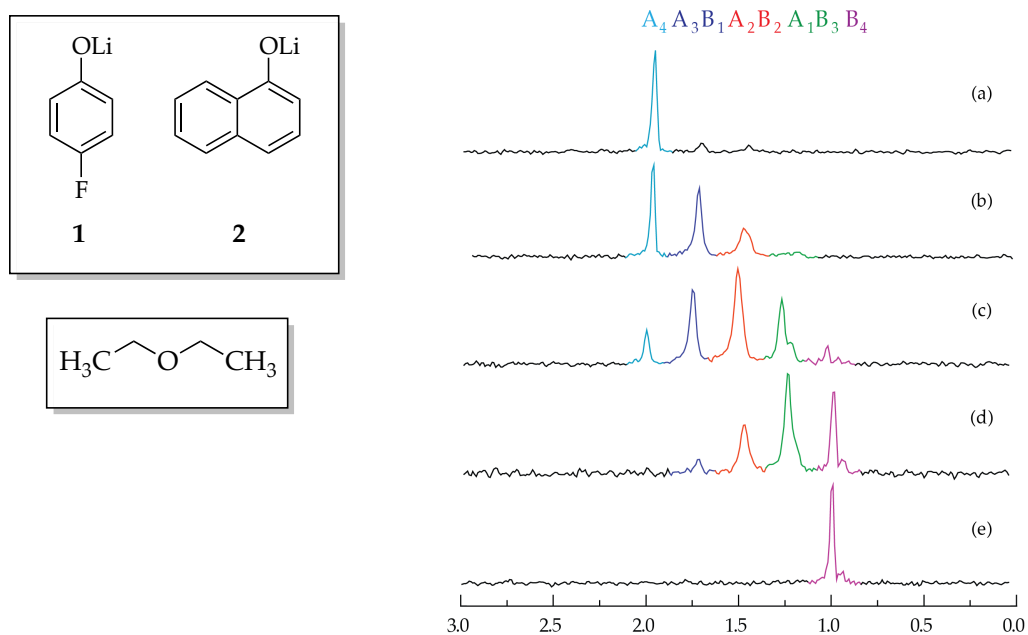


Figure AI.7. ^6Li NMR spectra of 0.10 M solutions of $[\text{}^6\text{Li}]\mathbf{2}$ (**A**) and $[\text{}^6\text{Li}]\mathbf{1}$ (**B**) in neat Et_2O at +22 °C. The measured mole fractions of **A** in (a)-(e) are 1.00, 0.72, 0.48, 0.25, and 0.00, respectively.

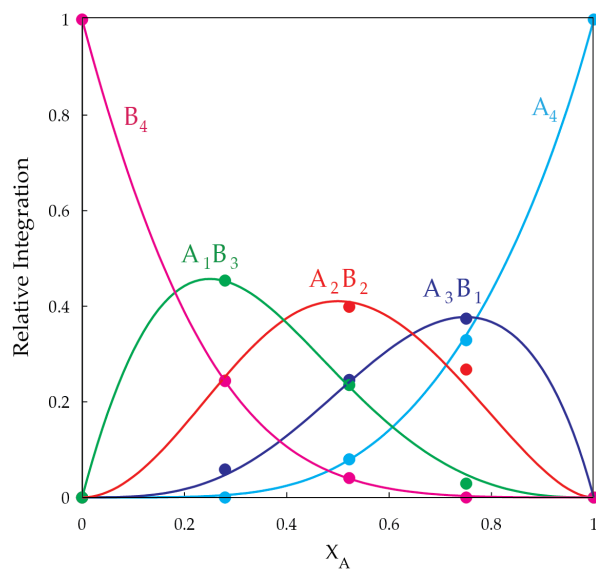


Figure AI.8. Job plot showing the relative integrations versus the measured mole fractions of **2** for 0.10 M mixtures of $[\text{}^6\text{Li}]\mathbf{2}$ (**A**) and $[\text{}^6\text{Li}]\mathbf{1}$ (**B**) in 0.50 M Et_2O /toluene at +22 °C.

Trimer Job Plots in Diethylether

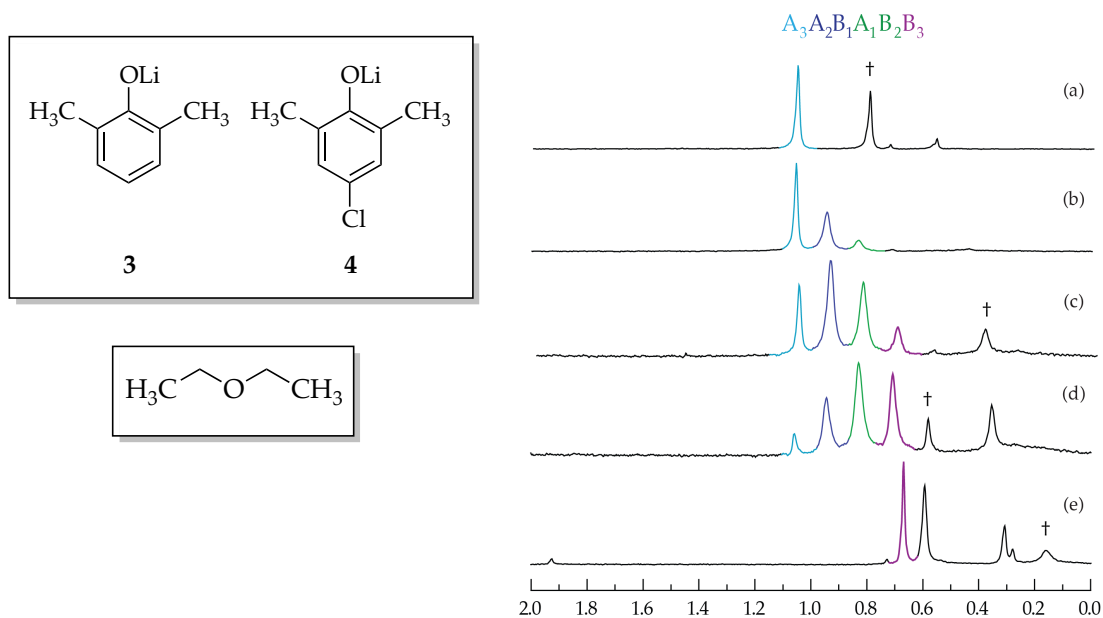


Figure AI.9. ^6Li NMR spectra of 0.10 M solutions of $[\text{}^6\text{Li}]\mathbf{3}$ (A) and $[\text{}^6\text{Li}]\mathbf{4}$ (B) in 0.50 M Et_2O /toluene at -90°C . The measured mole fractions of A in (a)-(e) are 1.00, 0.86, 0.54, 0.32, and 0.00, respectively. † indicates unknown aggregate.

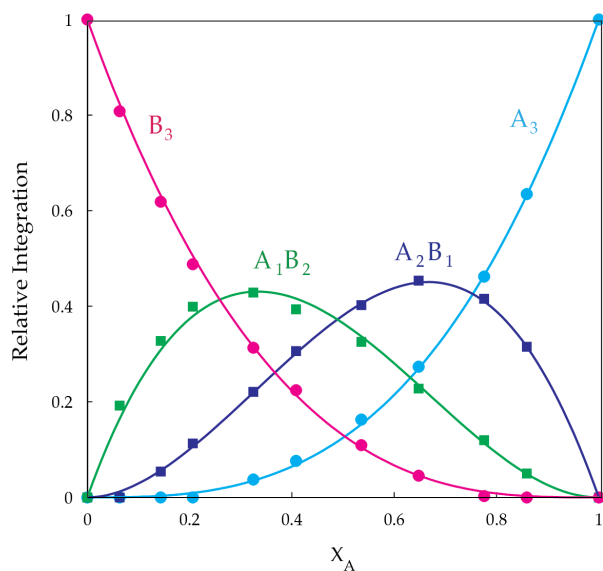


Figure AI.10. Job plot showing the relative integrations versus the measured mole fractions of $\mathbf{3}$ for 0.10 M mixtures of $[\text{}^6\text{Li}]\mathbf{3}$ (A) and $[\text{}^6\text{Li}]\mathbf{4}$ (B) in 0.50 M Et_2O /toluene at -90°C .

Tetramer Job Plots in Acetonitrile

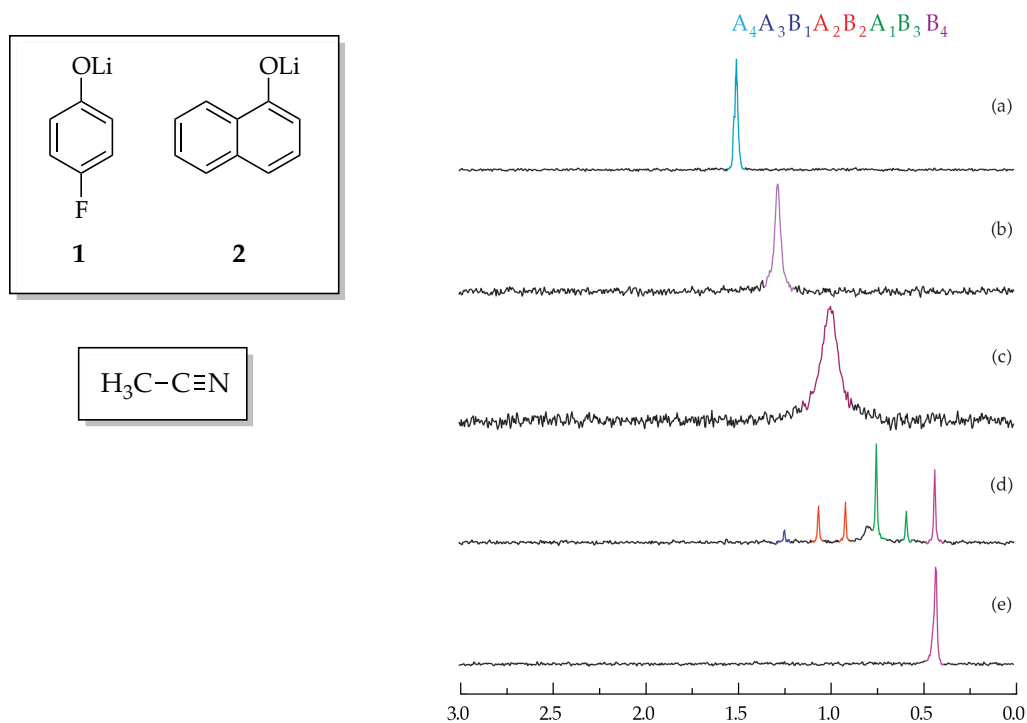


Figure AI.11. ${}^6\text{Li}$ NMR spectra of 0.10 M solutions of $[\text{}^6\text{Li}]_2$ (**A**) and $[\text{}^6\text{Li}]_1$ (**B**) in 0.50 M H_3CCN /toluene at $-80\text{ }^\circ\text{C}$. The mole fractions of **A** in (a)-(e) are roughly 1.00, 0.75, 0.50, 0.25, and 0.00, respectively. The intermolecular exchange rate is fast except for when the ratio of **1** to **2** is 3:1.

Tetramer Job Plots in Acetonitrile

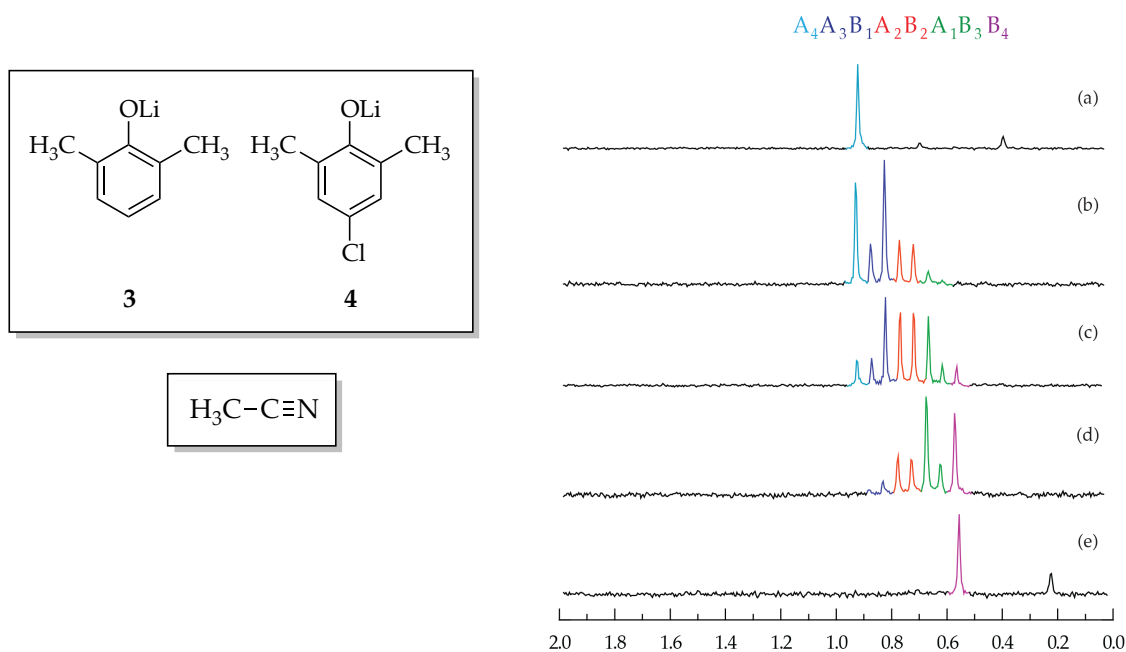


Figure AI.12. ^6Li NMR spectra of 0.10 M solutions of $[^6\text{Li}]3$ (**A**) and $[^6\text{Li}]4$ (**B**) in 0.50 M H_3CCN /toluene at $-80\text{ }^\circ\text{C}$. The measured mole fractions of **A** in (a)-(e) are 1.00, 0.71, 0.47, 0.27, and 0.00, respectively.

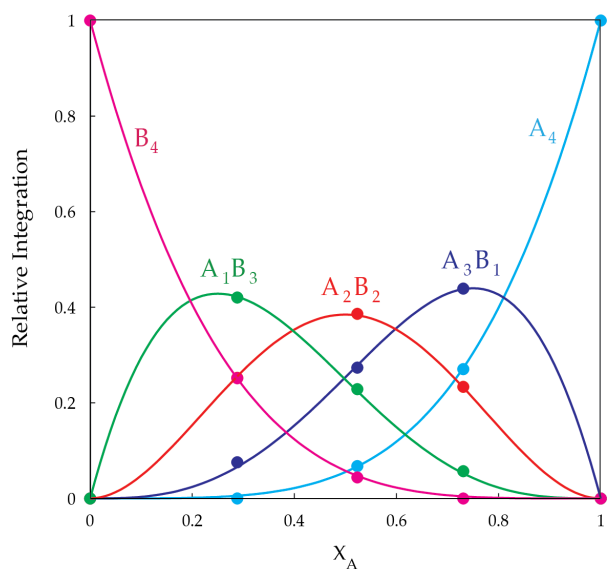


Figure AI.13. Job plot showing the relative integrations versus the measured mole fractions of **3** for 0.10 M mixtures of $[^6\text{Li}]3$ (**A**) and $[^6\text{Li}]4$ (**B**) in 0.50 M H_3CCN /toluene at $-80\text{ }^\circ\text{C}$.

Tetramer Job Plots in Pyridine

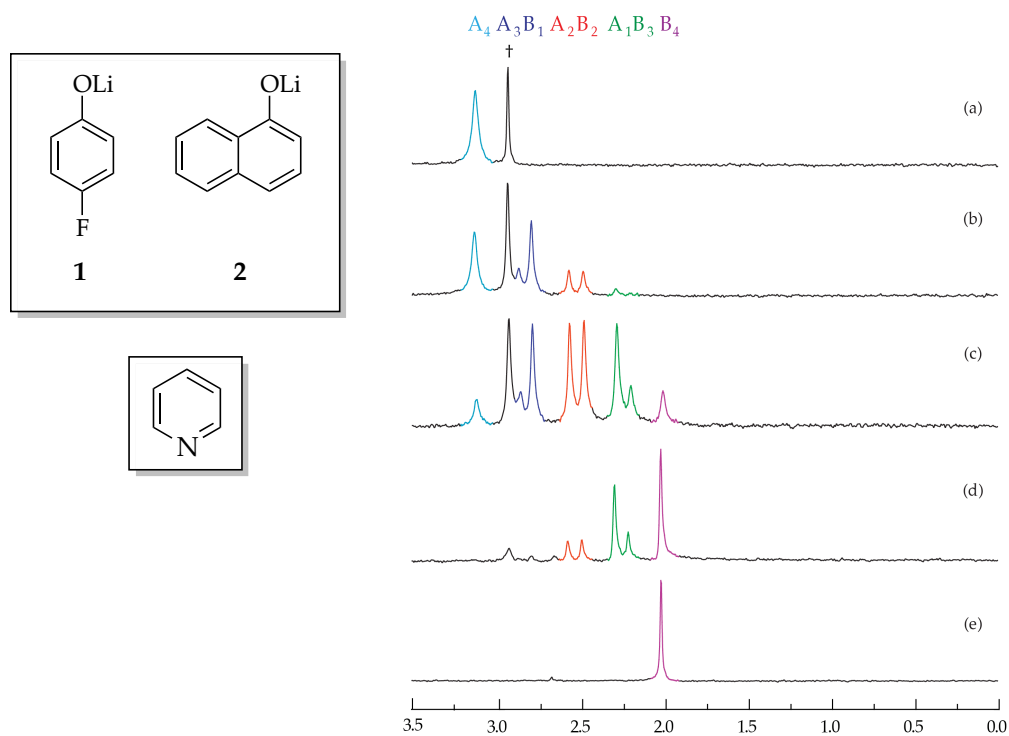


Figure AI.14. ^6Li NMR spectra of 0.10 M solutions of $[\text{}^6\text{Li}]\mathbf{2}$ (**A**) and $[\text{}^6\text{Li}]\mathbf{1}$ (**B**) in 0.50 M pyridine/toluene at $-80\text{ }^\circ\text{C}$. The measured mole fractions of **A** in (a)-(e) are 1.00, 0.80, 0.50, 0.13, and 0.00, respectively. † indicates unknown aggregate.

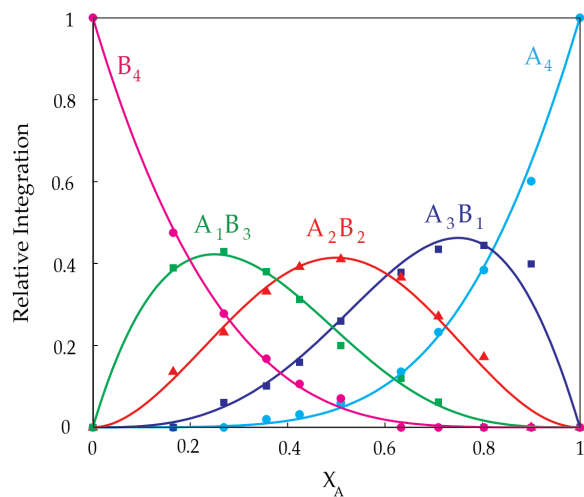


Figure AI.15. Job plot showing the relative integrations versus the measured mole fractions of **2** for 0.10 M mixtures of $[\text{}^6\text{Li}]\mathbf{2}$ (**A**) and $[\text{}^6\text{Li}]\mathbf{1}$ (**B**) in 0.50 M pyridine/toluene at $-80\text{ }^\circ\text{C}$.

Tetramer Job Plots in Pyridine

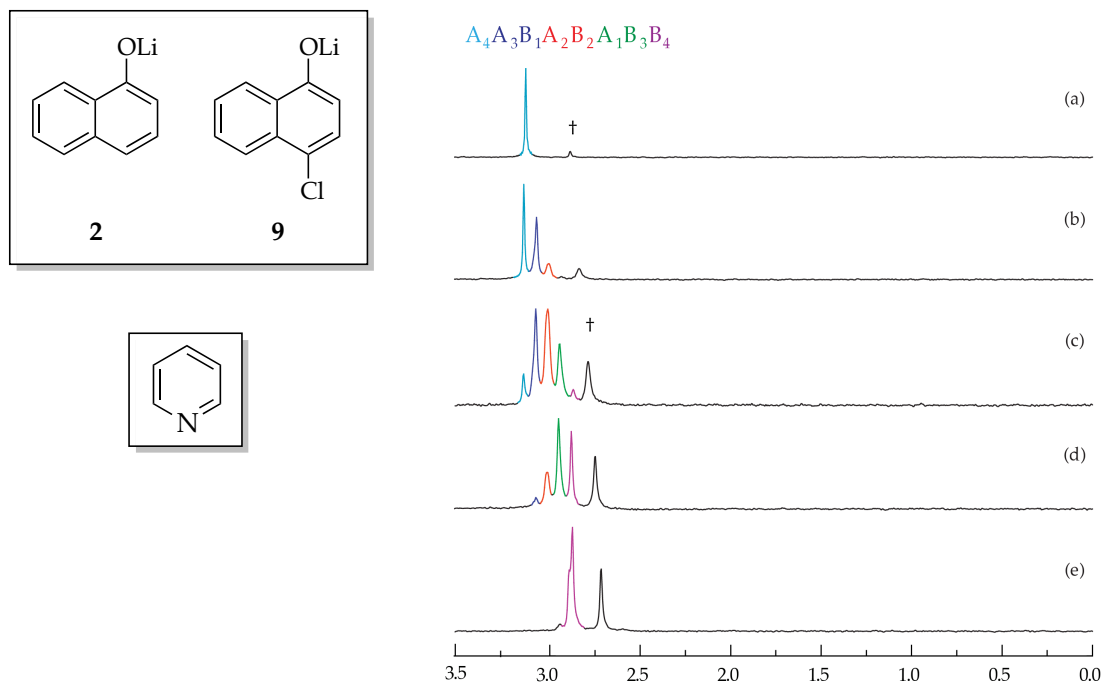


Figure AI.16. ^6Li NMR spectra of 0.10 M solutions of $[\text{}^6\text{Li}]2$ (A) and $[\text{}^6\text{Li}]1$ (B) in 0.50 M pyridine/toluene at $-80\text{ }^\circ\text{C}$. The measured mole fractions of A in (a)-(e) are 1.00, 0.63, 0.49, 0.29, and 0.00, respectively. † indicates unknown aggregate.

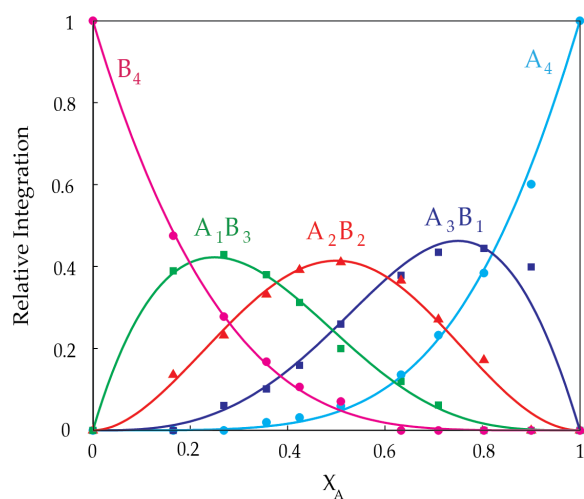


Figure AI.17. Job plot showing the relative integrations versus the measured mole fractions of 2 for 0.10 M mixtures of $[\text{}^6\text{Li}]2$ (A) and $[\text{}^6\text{Li}]1$ (B) in 0.50 M pyridine/toluene at $-80\text{ }^\circ\text{C}$.

Dimer Job Plots in Pyridine

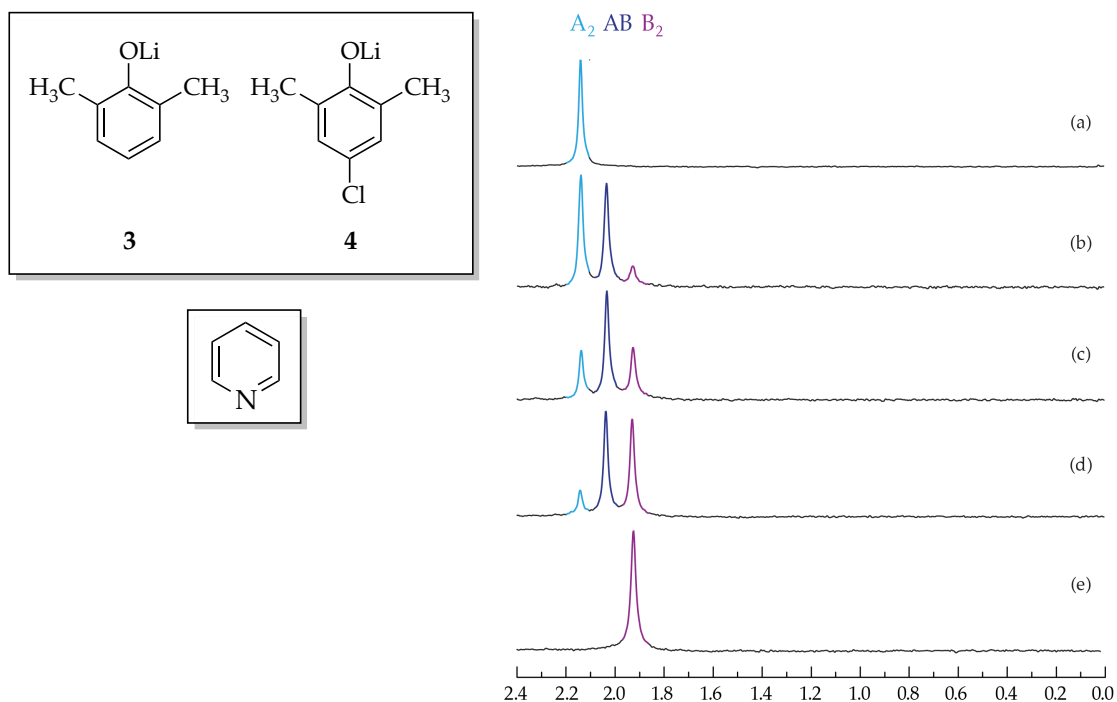


Figure AI.18. ^6Li NMR spectra of 0.10 M solutions of $[\text{}^6\text{Li}]\mathbf{3}$ (**A**) and $[\text{}^6\text{Li}]\mathbf{4}$ (**B**) in 0.50 M pyridine/toluene at -100°C . The measured mole fractions of **A** in (a)-(e) are 1.00, 0.66, 0.56, 0.33, and 0.00, respectively.

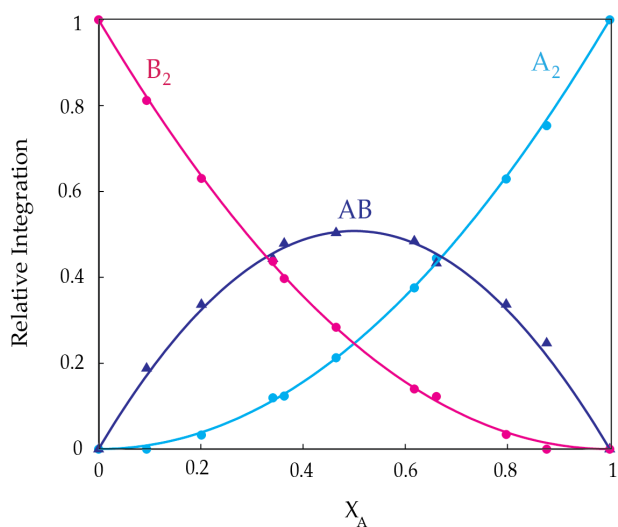


Figure AI.19. Job plot showing the relative integrations versus the measured mole fractions of **3** for 0.10 M mixtures of $[\text{}^6\text{Li}]\mathbf{3}$ (**A**) and $[\text{}^6\text{Li}]\mathbf{4}$ (**B**) in 0.50 M pyridine/toluene at -100°C .

Tetramer Job Plots in Dimethylacetamide

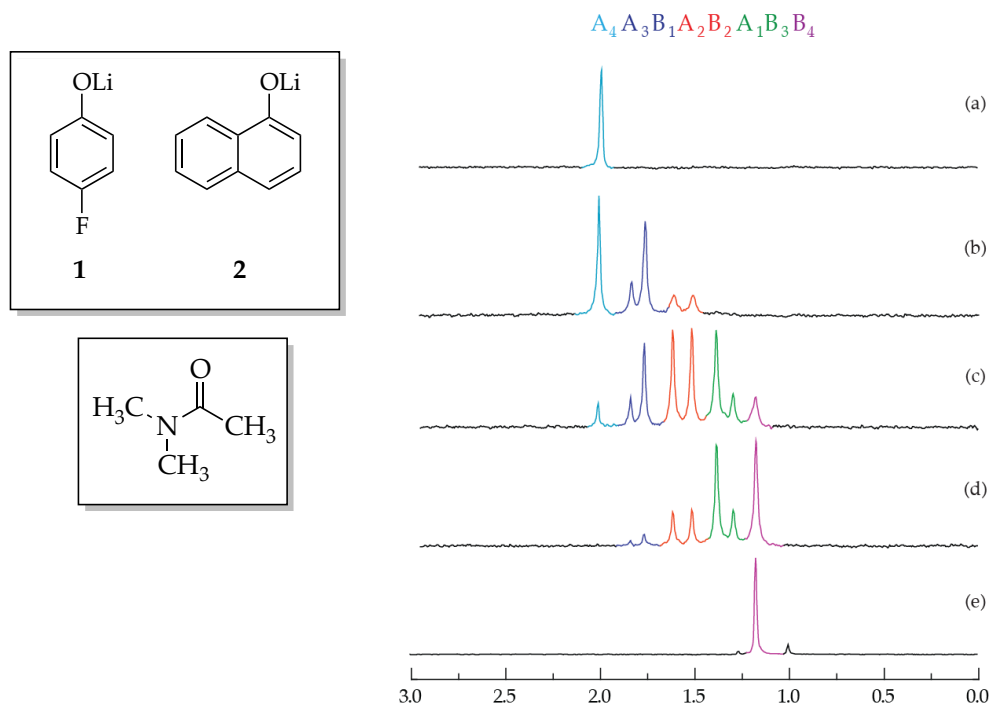


Figure AI.20. ^6Li NMR spectra of 0.10 M solutions of $[\text{}^6\text{Li}]2$ (**A**) and $[\text{}^6\text{Li}]1$ (**B**) in 0.50 M dimethylacetamide/toluene at $-80\text{ }^\circ\text{C}$. The measured mole fractions of **A** in (a)-(e) are 1.00, 0.64, 0.45, 0.25, and 0.00, respectively.

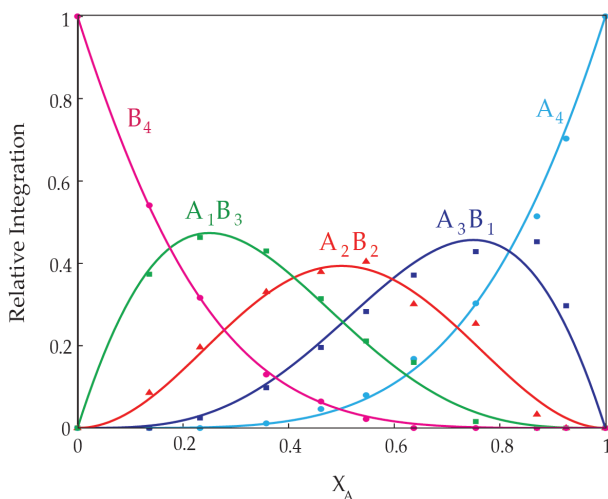


Figure AI.21. Job plot showing the relative integrations versus the measured mole fractions of **2** for 0.10 M mixtures of $[\text{}^6\text{Li}]2$ (**A**) and $[\text{}^6\text{Li}]1$ (**B**) in 0.50 M dimethylacetamide/toluene at $-80\text{ }^\circ\text{C}$.

Tetramer Job Plots in Dimethylacetamide

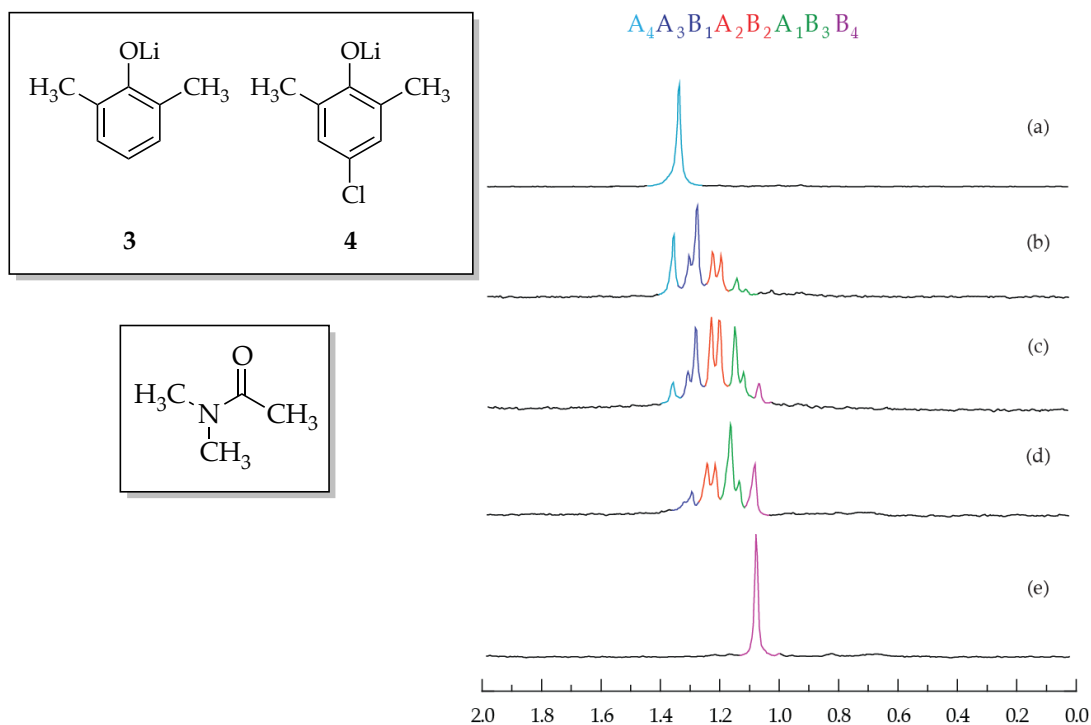


Figure AI.22. ^6Li NMR spectra of 0.10 M solutions of $[\text{}^6\text{Li}]\mathbf{3}$ (A) and $[\text{}^6\text{Li}]\mathbf{4}$ (B) in 0.50 M dimethylacetamide/toluene at $-80\text{ }^\circ\text{C}$. The measured mole fractions of A in (a)-(e) are 1.00, 0.61, 0.50, 0.29, and 0.00, respectively.

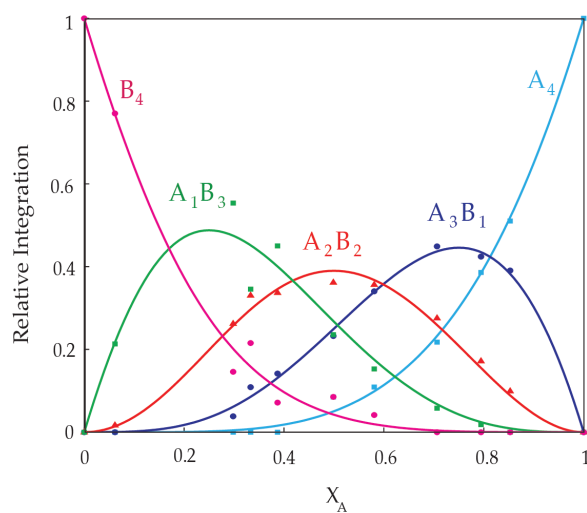


Figure AI.23. Job plot showing the relative integrations versus the measured mole fractions of $\mathbf{3}$ for 0.10 M mixtures of $[\text{}^6\text{Li}]\mathbf{3}$ (A) and $[\text{}^6\text{Li}]\mathbf{4}$ (B) in 0.50 M dimethylacetamide/toluene at $-80\text{ }^\circ\text{C}$.

Tetramer Job Plots in Dimethylformamide

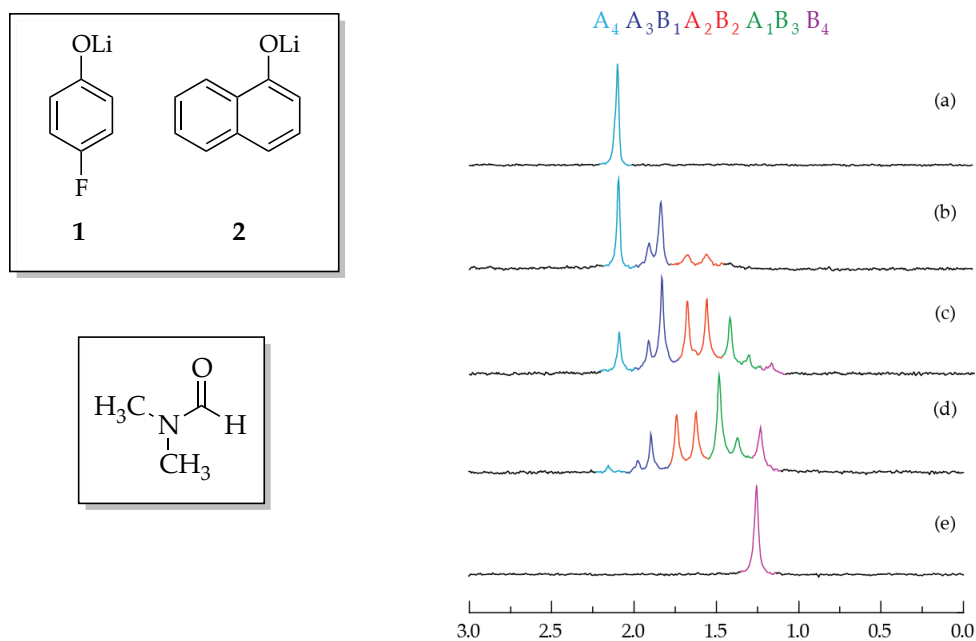


Figure AI.24. ^6Li NMR spectra of 0.10 M solutions of $[\text{}^6\text{Li}]2$ (**A**) and $[\text{}^6\text{Li}]1$ (**B**) in 0.50 M dimethylformamide/toluene at $-80\text{ }^\circ\text{C}$. The measured mole fractions of **A** in (a)-(e) are 1.00, 0.65, 0.44, 0.23, and 0.00, respectively.

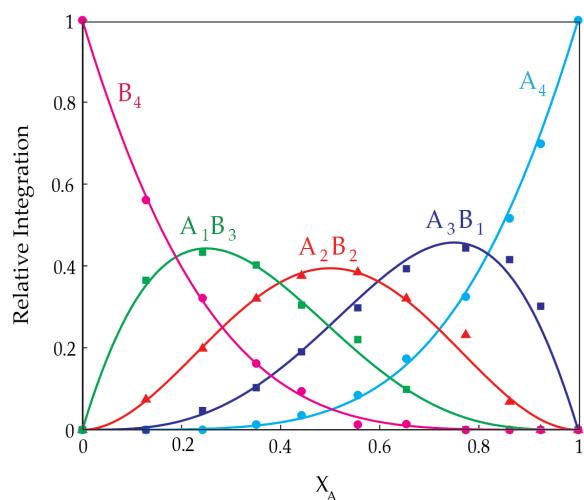


Figure AI.25. Job plot showing the relative integrations versus the measured mole fractions of **2** for 0.10 M mixtures of $[\text{}^6\text{Li}]2$ (**A**) and $[\text{}^6\text{Li}]1$ (**B**) in 0.50 M dimethylformamide/toluene at $-80\text{ }^\circ\text{C}$.

Tetramer Job Plots in Dimethylsulfoxide

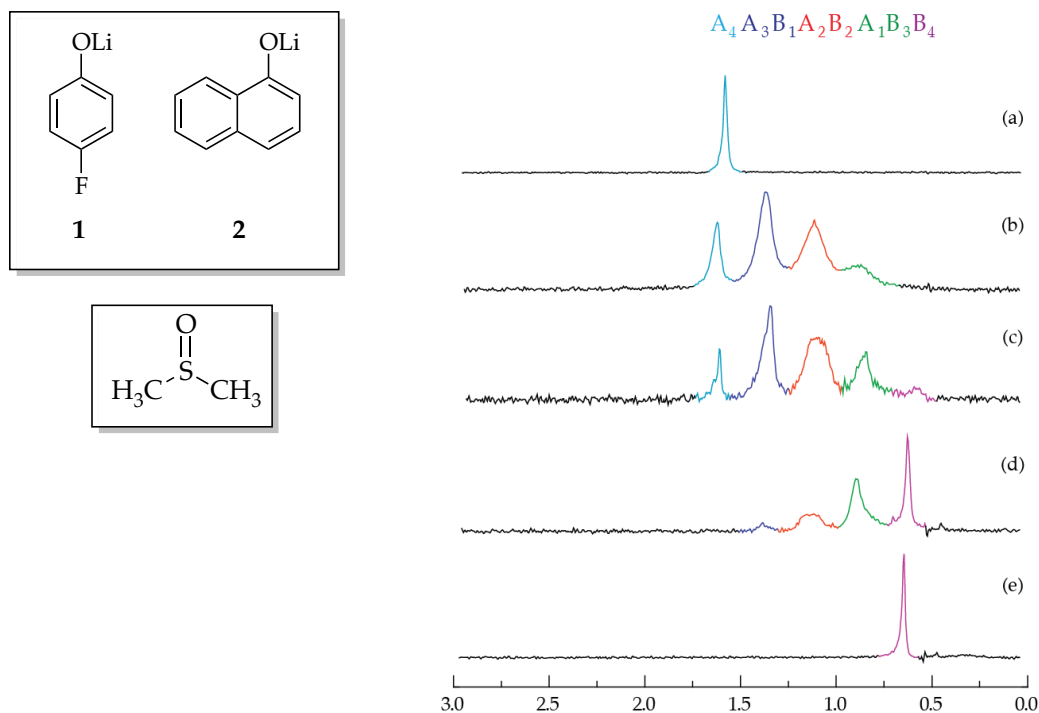


Figure AI.26. ^6Li NMR spectra of 0.10 M solutions of $[\text{}^6\text{Li}]2$ (**A**) and $[\text{}^6\text{Li}]1$ (**B**) in 0.50 M DMSO/toluene at $-80\text{ }^\circ\text{C}$. The measured mole fractions of **A** in (a)-(e) are 1.00, 0.76, 0.46, 0.37, and 0.00, respectively.

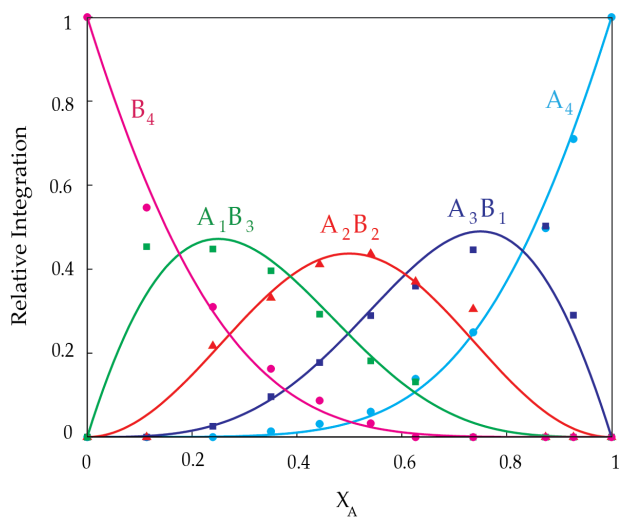


Figure AI.27. Job plot showing the relative integrations versus the measured mole fractions of **2** for 0.10 M mixtures of $[\text{}^6\text{Li}]2$ (**A**) and $[\text{}^6\text{Li}]1$ (**B**) in 0.50 M DMSO/toluene at $-80\text{ }^\circ\text{C}$.

^{19}F Spectra in Dimethylsulfoxide

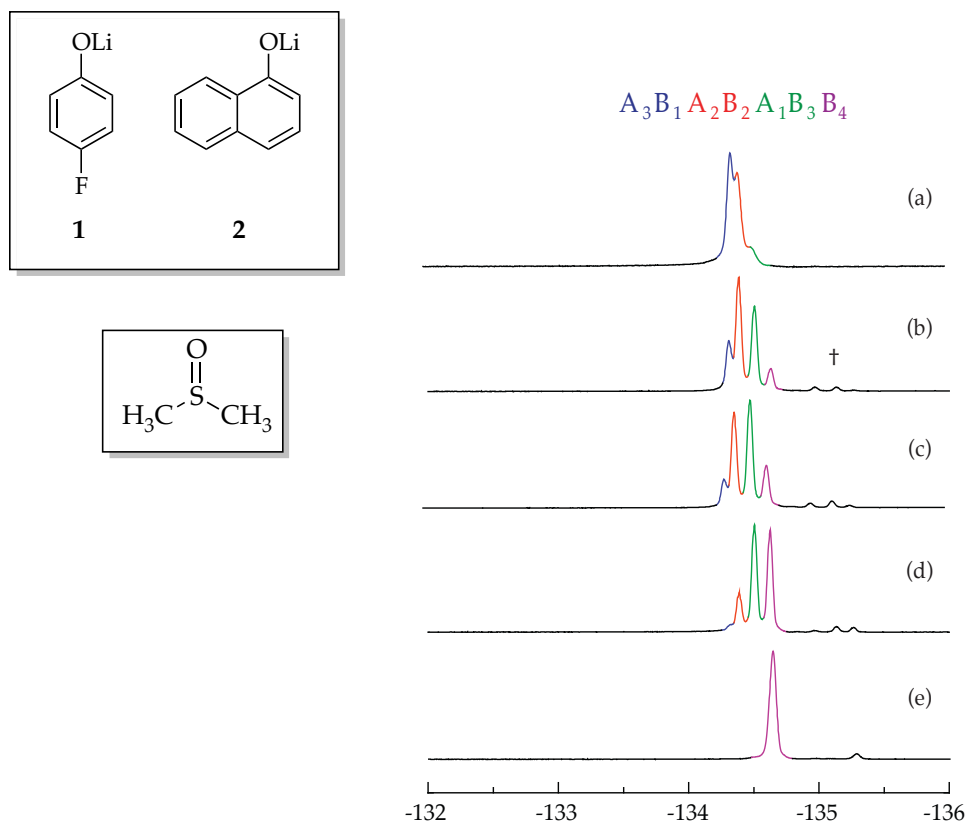


Figure AI.28. ^{19}F NMR spectra of 0.10 M solutions of $[\text{}^6\text{Li}]\mathbf{2}$ (**A**) and $[\text{}^6\text{Li}]\mathbf{1}$ (**B**) in 0.50 M dimethylsulfoxide/toluene at $-80\text{ }^\circ\text{C}$. The mole fractions of **A** in (a)-(e) are roughly 0.90, 0.70, 0.40, 0.20, and 0.00, respectively. The naphtholate homoaggregate is invisible by ^{19}F NMR, so the A_3B_1 is the last observable species. At high naphtholate mole fraction, resolution becomes difficult and the A_2B_2 aggregate becomes a minor shoulder on the A_3B_1 peak. † appears to be a minor trimer component.

Trimer Job Plots in Dimethylsulfoxide

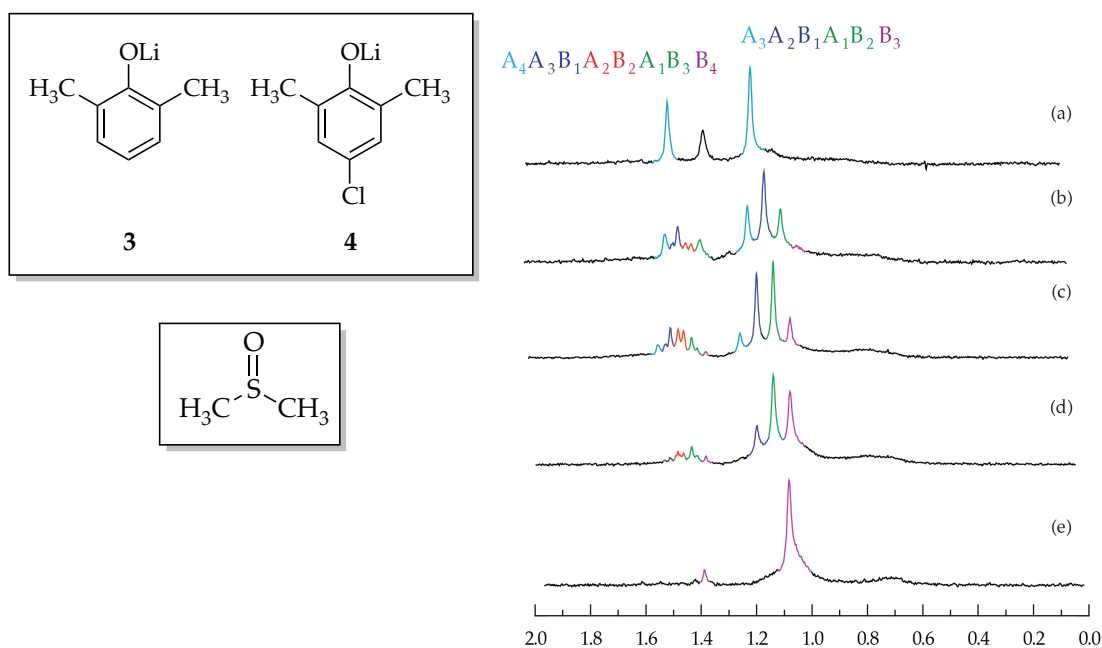


Figure AI.29. ^6Li NMR spectra of 0.10 M solutions of $[\text{}^6\text{Li}]\mathbf{3}$ (**A**) and $[\text{}^6\text{Li}]\mathbf{1}$ (**B**) in 0.50 M DMSO/toluene at $-80\text{ }^\circ\text{C}$. The measured mole fractions of **A** in (a)-(e) are 1.00, 0.69, 0.54, 0.32, and 0.00, respectively.

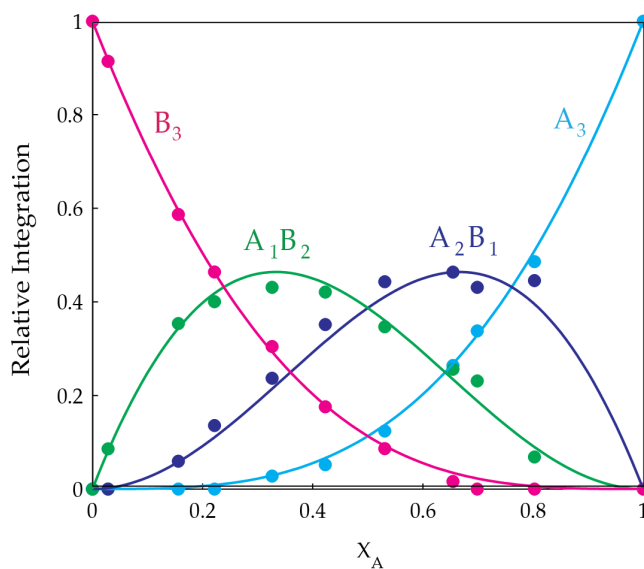


Figure AI.30. Job plot showing the relative integrations versus the measured mole fractions of **3** for 0.10 M mixtures of $[\text{}^6\text{Li}]\mathbf{3}$ (**A**) and $[\text{}^6\text{Li}]\mathbf{4}$ (**B**) in 0.50 M DMSO/toluene at $-80\text{ }^\circ\text{C}$.

Tetramer Job Plots in DMPU

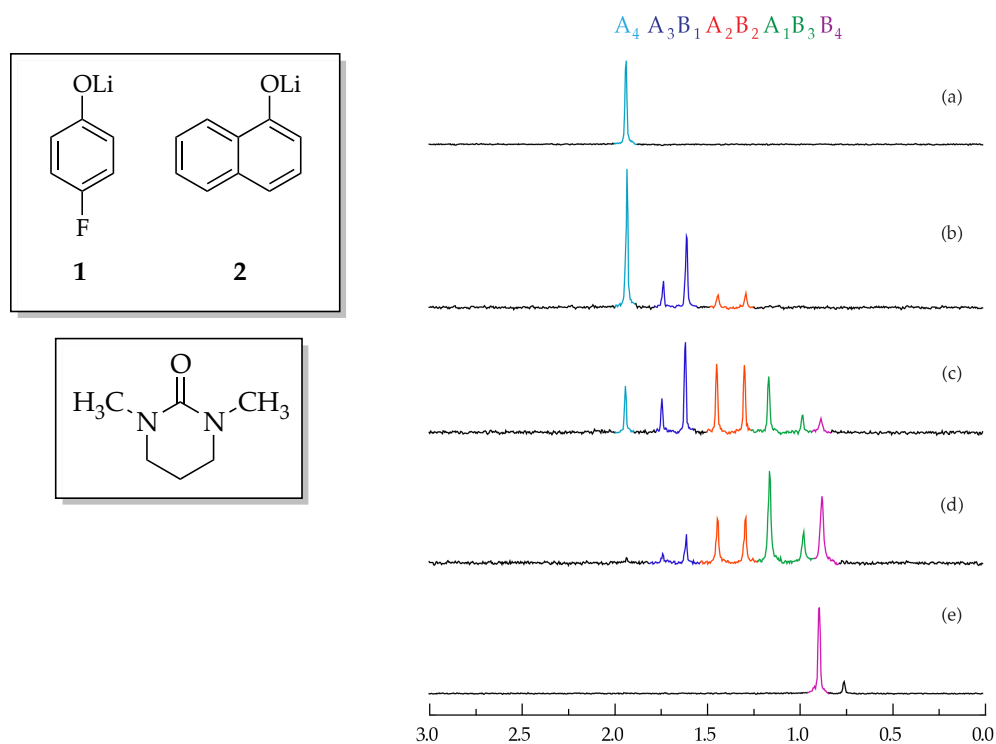


Figure AI.31. ^6Li NMR spectra of 0.10 M solutions of $[\text{}^6\text{Li}]2$ (**A**) and $[\text{}^6\text{Li}]1$ (**B**) in 0.50 M DMPU/toluene at $-80\text{ }^\circ\text{C}$. The measured mole fractions of **A** in (a)-(e) are 1.00, 0.70, 0.46, 0.15, and 0.00, respectively.

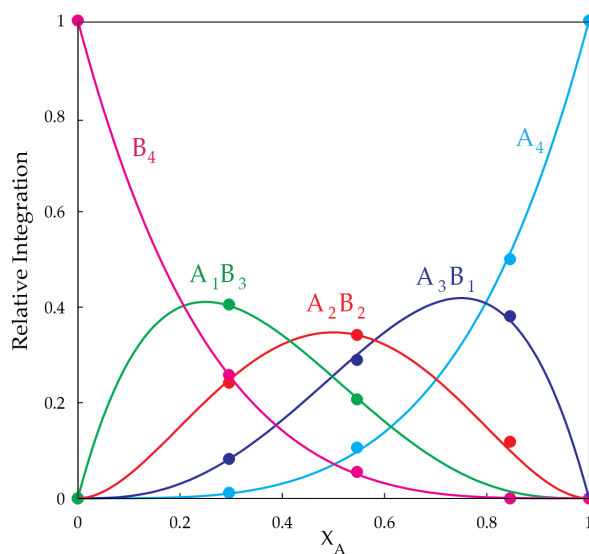


Figure AI.32. Job plot showing the relative integrations versus the measured mole fractions of **2** for 0.10 M mixtures of $[\text{}^6\text{Li}]2$ (**A**) and $[\text{}^6\text{Li}]1$ (**B**) in 0.50 M DMPU/toluene at $-80\text{ }^\circ\text{C}$.

Tetramer Job Plots in DMPU

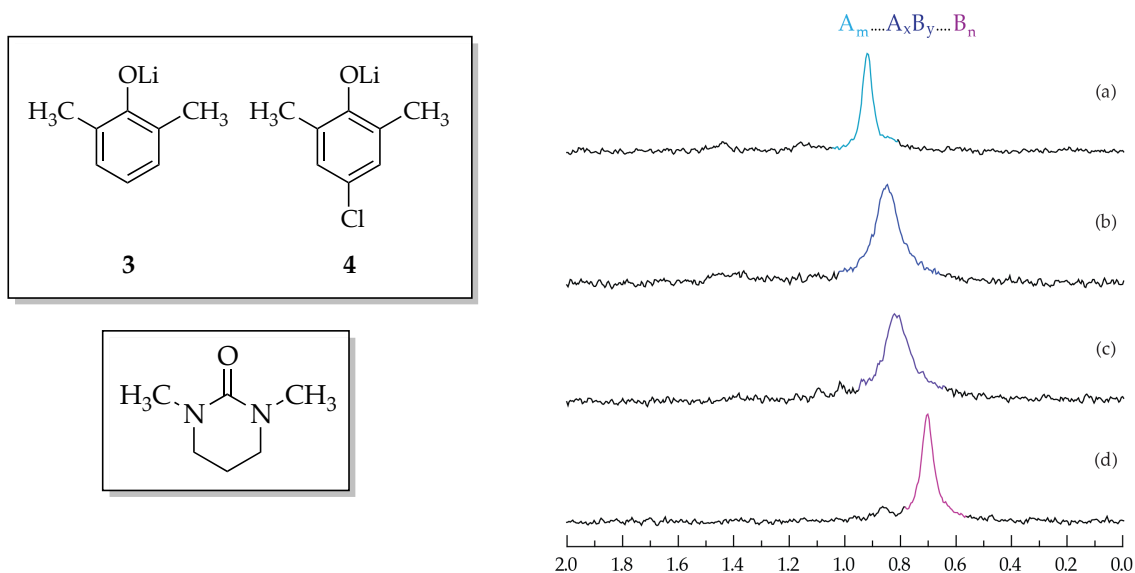


Figure AI.33. ^6Li NMR spectra of 0.10 M solutions of $[\text{}^6\text{Li}]\mathbf{3}$ (A) and $[\text{}^6\text{Li}]\mathbf{4}$ (B) in 0.50 M DMPU/toluene at -80°C . The measured mole fractions cannot be calculated, but tubes (a) and (d) are **3** and **4**, respectively, whereas tubes (b) and (c) are mixtures.

Tetramer Job Plots in *N*-Methylpyrrolidone

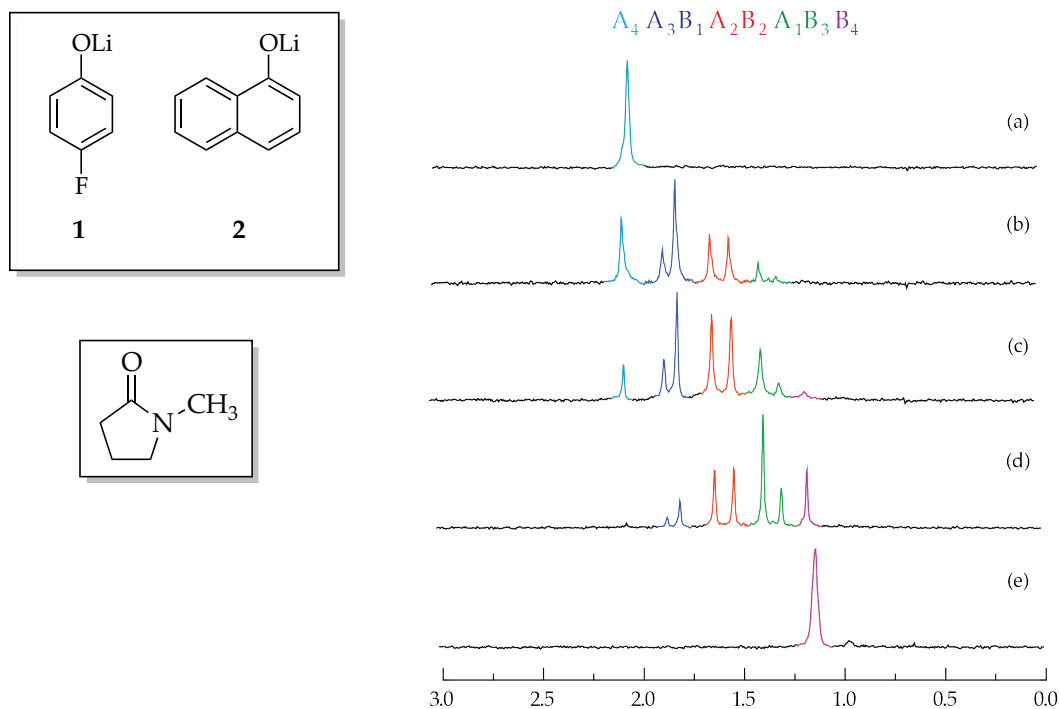


Figure AI.34. ^6Li NMR spectra of 0.10 M solutions of $[\text{}^6\text{Li}]2$ (**A**) and $[\text{}^6\text{Li}]1$ (**B**) in 0.50 M *N*-methylpyrrolidone/toluene at $-85\text{ }^\circ\text{C}$. The measured mole fractions of **A** in (a)-(e) are 1.00, 0.65, 0.44, 0.30, and 0.00, respectively.

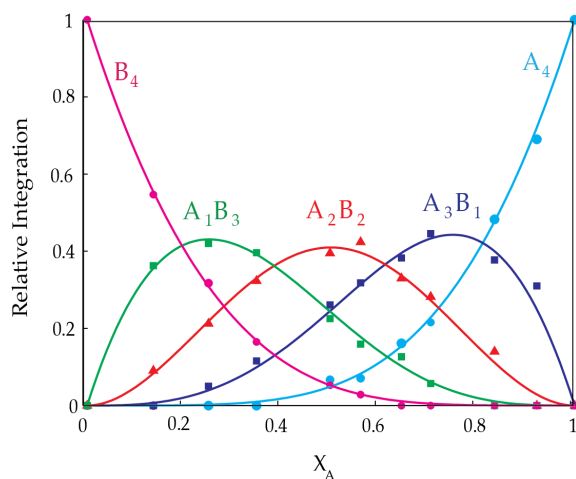


Figure AI.35. Job plot showing the relative integrations versus the measured mole fractions of **2** for 0.10 M mixtures of $[\text{}^6\text{Li}]2$ (**A**) and $[\text{}^6\text{Li}]1$ (**B**) in 0.50 M *N*-methylpyrrolidone/ toluene at $-85\text{ }^\circ\text{C}$.

Tetramer Job Plots in *N*-Methylpyrrolidone

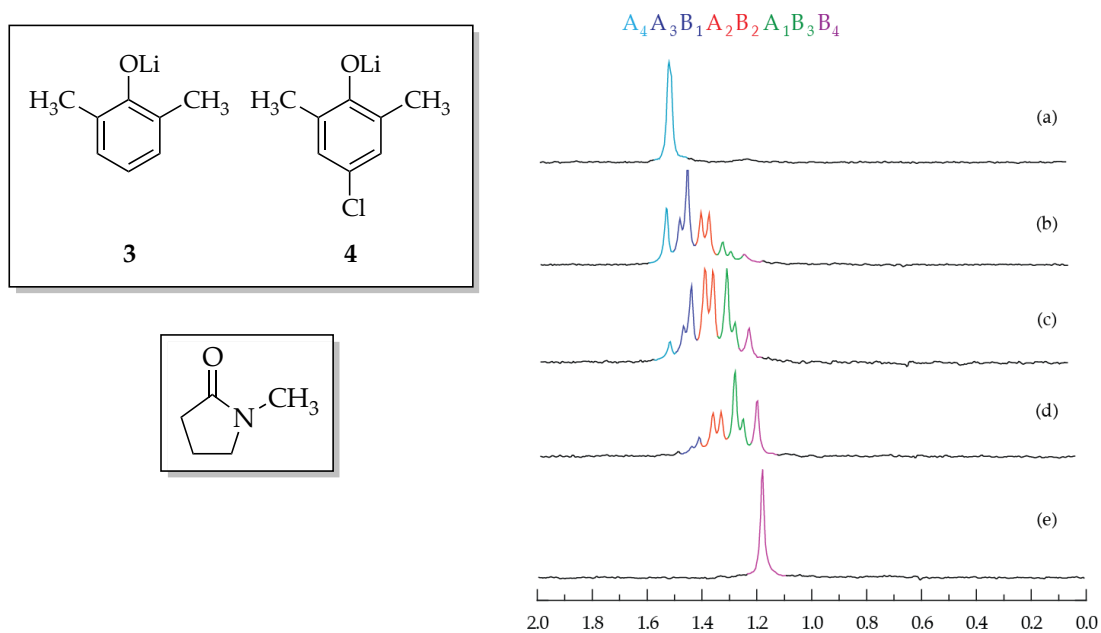


Figure AI.36. ^6Li NMR spectra of 0.10 M solutions of $[\text{}^6\text{Li}]\mathbf{3}$ (**A**) and $[\text{}^6\text{Li}]\mathbf{4}$ (**B**) in 0.50 M *N*-methylpyrrolidone/toluene at $-80\text{ }^\circ\text{C}$. The measured mole fractions of **A** in (a)-(e) are 1.00, 0.68, 0.53, 0.33, and 0.00, respectively.

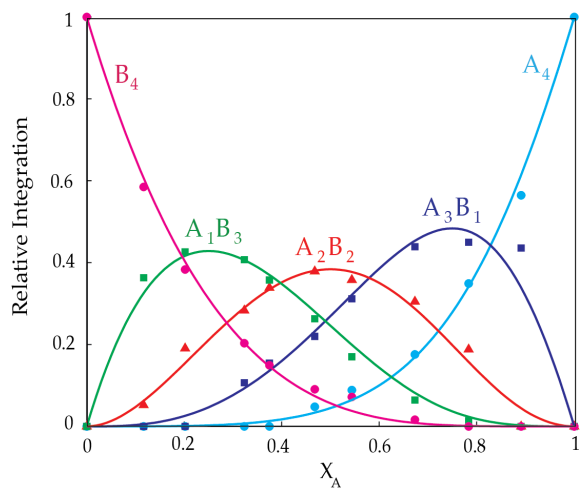


Figure AI.37. Job plot showing the relative integrations versus the measured mole fractions of **3** for 0.10 M mixtures of $[\text{}^6\text{Li}]\mathbf{3}$ (**A**) and $[\text{}^6\text{Li}]\mathbf{4}$ (**B**) in 0.50 M *N*-methylpyrrolidone/toluene at $-80\text{ }^\circ\text{C}$.

Tetramer Job Plots in *n*-Propylamine

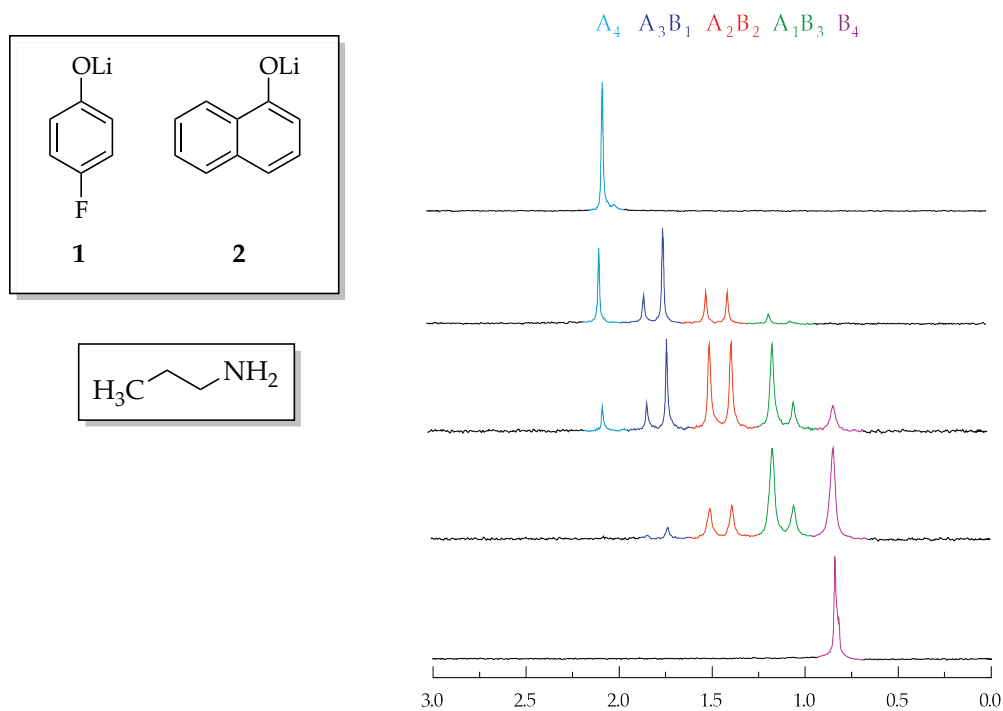


Figure AI.38. ${}^6\text{Li}$ NMR spectra of 0.10 M solutions of $[\text{}^6\text{Li}]_2$ (**A**) and $[\text{}^6\text{Li}]_1$ (**B**) in 0.50 M *n*-PrNH₂/toluene at -80 °C. The measured mole fractions of **A** in (a)-(e) are 1.00, 0.76, 0.56, 0.28, and 0.00, respectively.

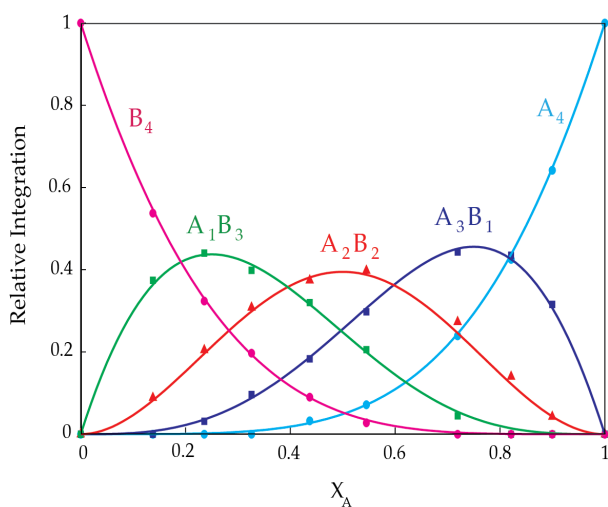


Figure AI.39. Job plot showing the relative integrations versus the measured mole fractions of **2** for 0.10 M mixtures of $[\text{}^6\text{Li}]_2$ (**A**) and $[\text{}^6\text{Li}]_1$ (**B**) in 0.50 M *n*-PrNH₂/toluene at -80 °C.

Dimer Job Plots in *n*-Propylamine

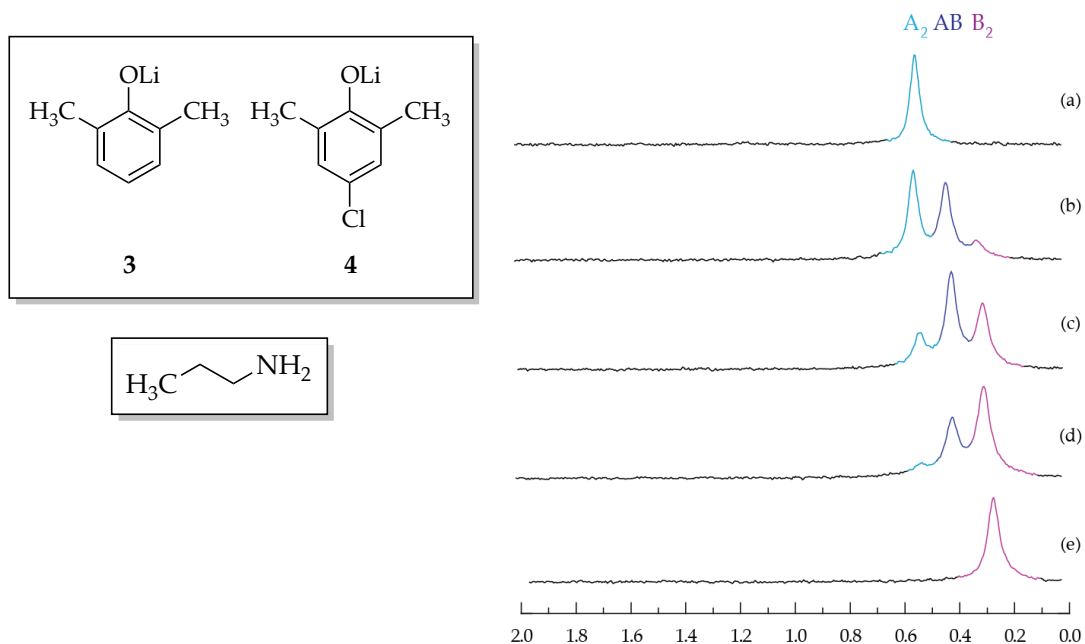


Figure AI.40. ${}^6\text{Li}$ NMR spectra of 0.10 M solutions of $[\text{}^6\text{Li}]\mathbf{3}$ (A) and $[\text{}^6\text{Li}]\mathbf{4}$ (B) in 0.50 M *n*-PrNH₂/toluene at -110 °C. The measured mole fractions of A in (a)-(e) are 1.00, 0.73, 0.58, 0.34, and 0.00, respectively.

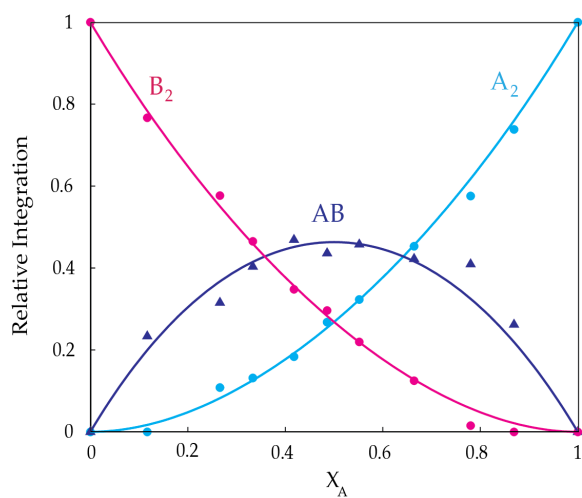


Figure AI.41. Job plot showing the relative integrations versus the measured mole fractions of $\mathbf{3}$ for 0.10 M mixtures of $[\text{}^6\text{Li}]\mathbf{3}$ (A) and $[\text{}^6\text{Li}]\mathbf{4}$ (B) in 0.50 M *n*-PrNH₂/toluene at -110 °C.

Tetramer Job Plots in Piperidine

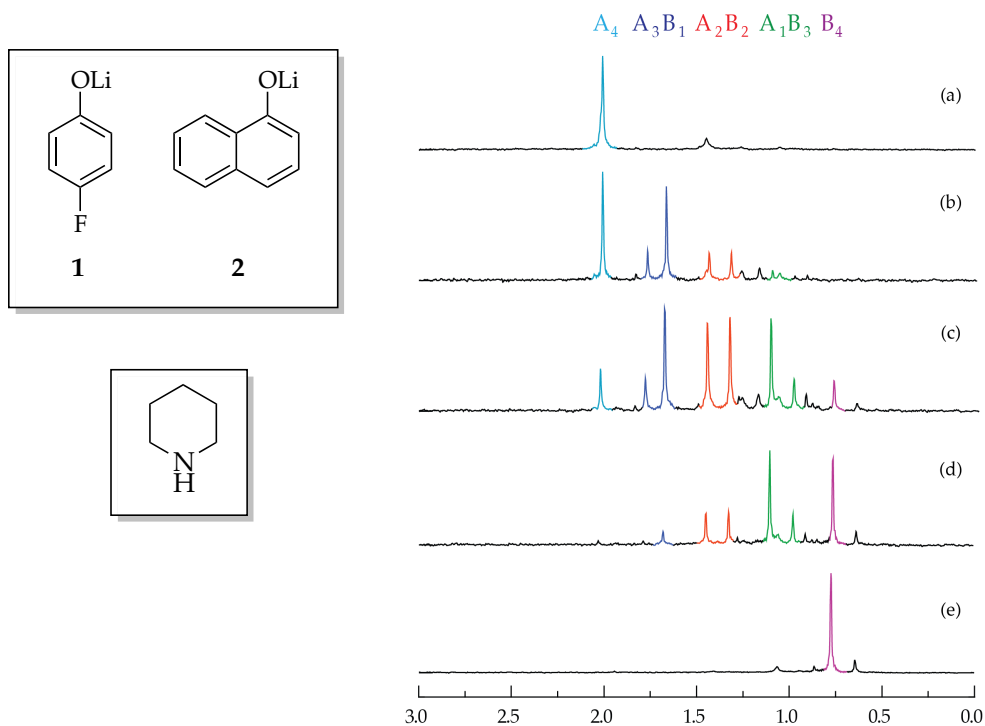


Figure AI.42. ^6Li NMR spectra of 0.10 M solutions of $[\text{}^6\text{Li}]2$ (**A**) and $[\text{}^6\text{Li}]1$ (**B**) in 0.50 M piperidine/toluene at $-60\text{ }^\circ\text{C}$. The measured mole fractions of **A** in (a)-(e) are 1.00, 0.74, 0.48, 0.21, and 0.00, respectively.

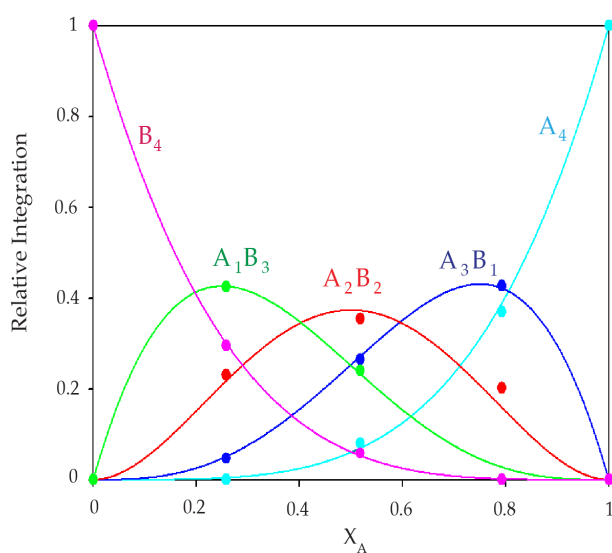


Figure AI.43. Job plot showing the relative integrations versus the measured mole fractions of **2** for 0.10 M mixtures of $[\text{}^6\text{Li}]2$ (**A**) and $[\text{}^6\text{Li}]1$ (**B**) in 0.50 M piperidine/toluene at $-60\text{ }^\circ\text{C}$.

^{19}F Spectra in Piperidine

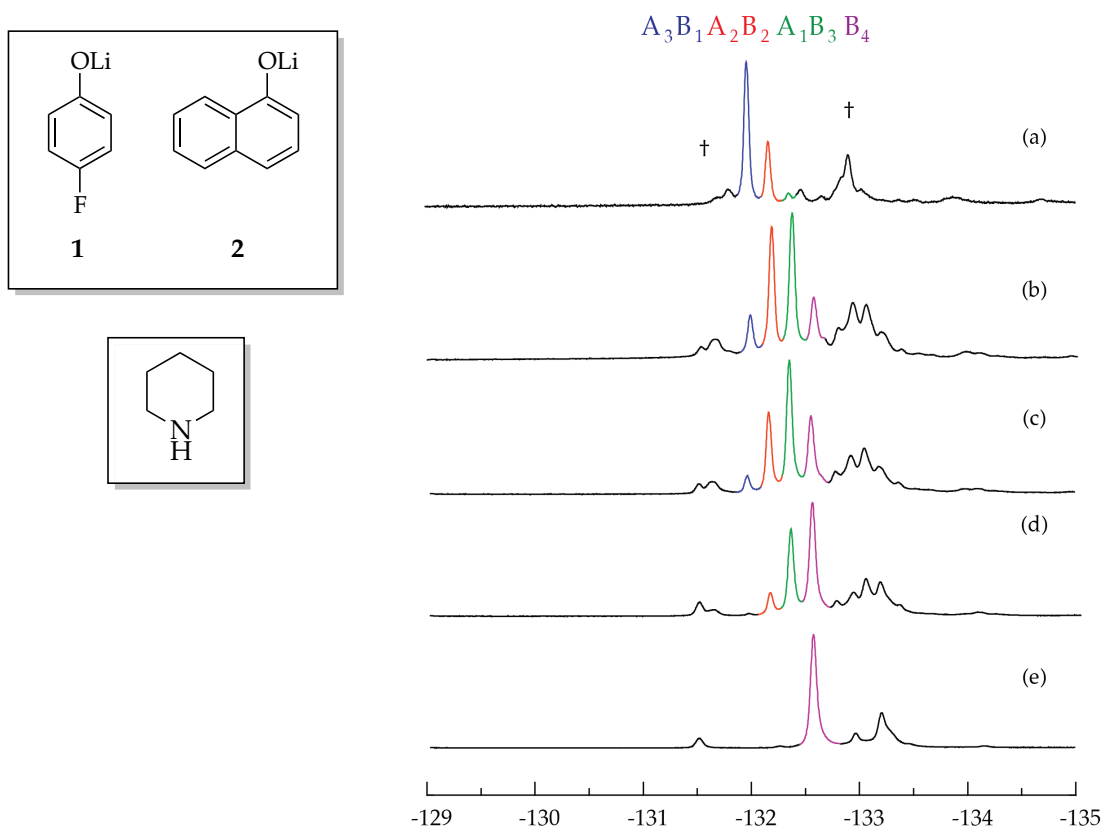


Figure AI.44. ^{19}F NMR spectra of 0.10 M solutions of $[^6\text{Li}]\mathbf{2}$ (**A**) and $[^6\text{Li}]\mathbf{1}$ (**B**) in 0.50 M piperidine/toluene at $-80\text{ }^\circ\text{C}$. The mole fractions of **A** in (a)-(e) are roughly 0.90, 0.60, 0.40, 0.20, and 0.00, respectively. The naphtholate homoaggregate is invisible by ^{19}F NMR, so the A_3B_1 is the last observable species. **1** has three additional resonances, which form the unidentifiable ensembles denoted by †.

Trimer Job Plots in Piperidine

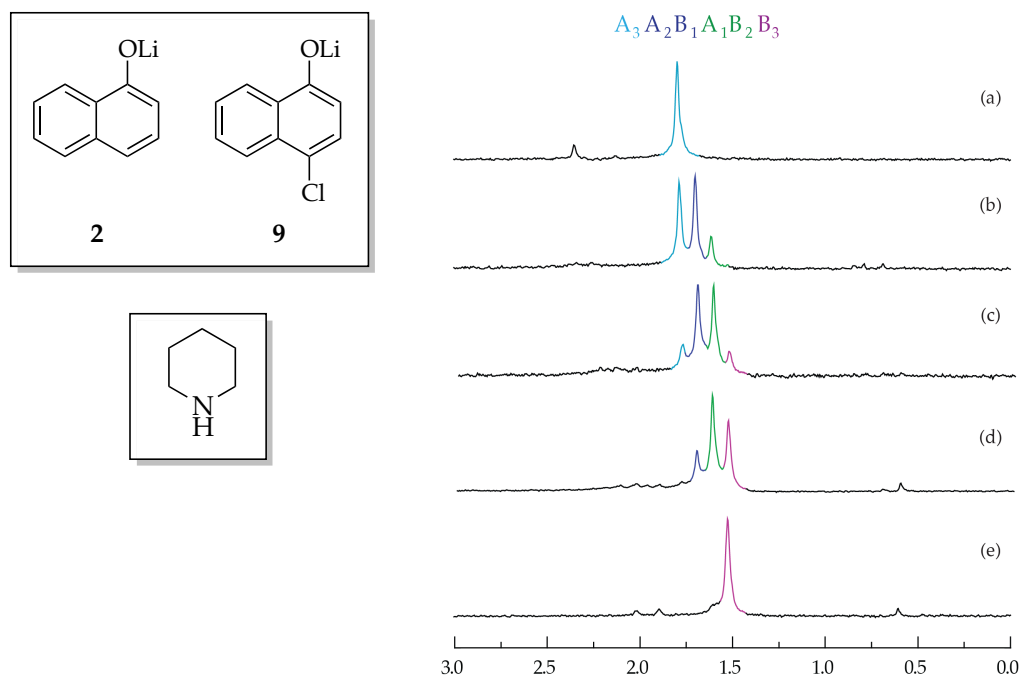


Figure AI.45. ^6Li NMR spectra of 0.10 M solutions of $[\text{}^6\text{Li}]\mathbf{2}$ (**A**) and $[\text{}^6\text{Li}]\mathbf{9}$ (**B**) in 0.50 M piperidine/toluene at $-90\text{ }^\circ\text{C}$. The measured mole fractions of **A** in (a)-(e) are 1.00, 0.64, 0.43, 0.24, and 0.00, respectively.

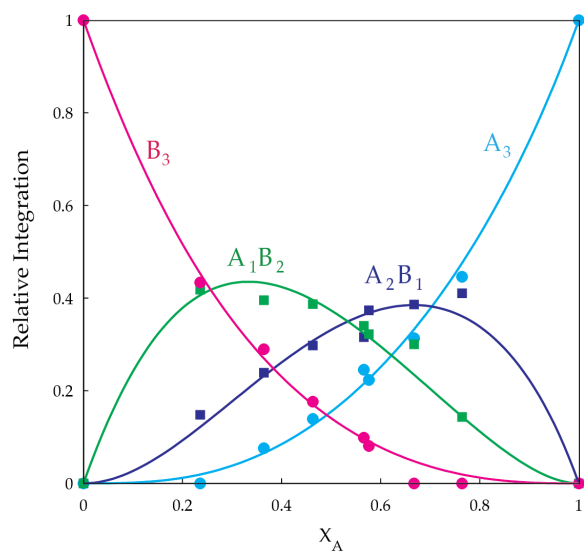


Figure AI.46. Job plot showing the relative integrations versus the measured mole fractions of **2** for 0.10 M mixtures of $[\text{}^6\text{Li}]\mathbf{2}$ (**A**) and $[\text{}^6\text{Li}]\mathbf{9}$ (**A**) in 0.50 M piperidine/toluene at $-90\text{ }^\circ\text{C}$.

Job Plots in Piperidine

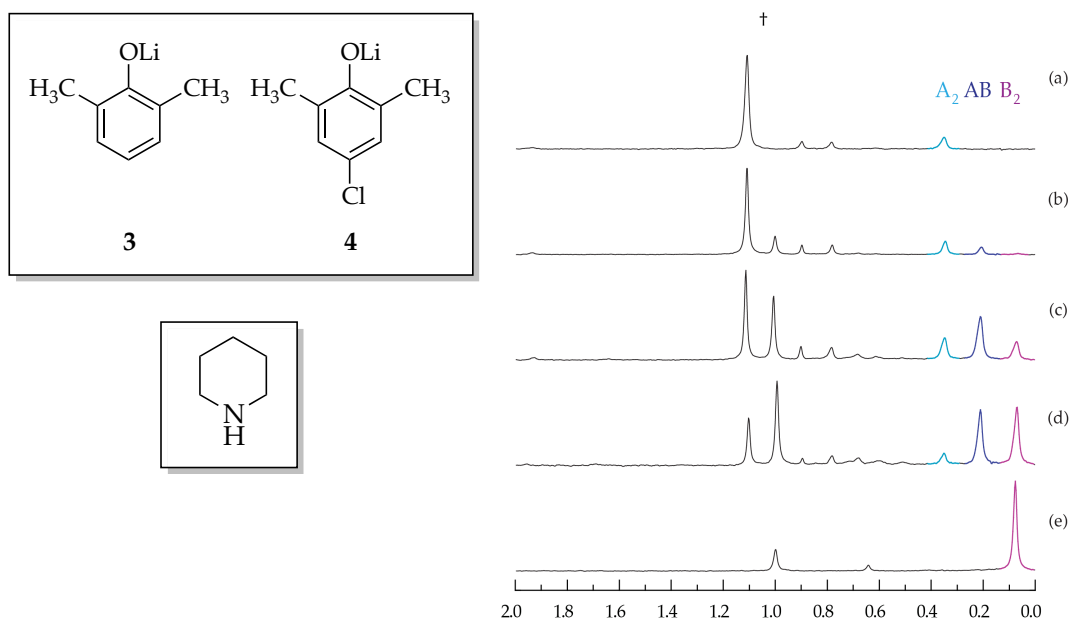


Figure AI.47. ^6Li NMR spectra of 0.10 M solutions of $[\text{}^6\text{Li}]\mathbf{2}$ (A) and $[\text{}^6\text{Li}]\mathbf{9}$ (B) in 0.50 M piperidine/toluene at $-90\text{ }^\circ\text{C}$. The measured mole fractions of A in (a)-(e) are 1.00, 0.78, 0.52, 0.33, and 0.00, respectively. † indicates unknown aggregate.

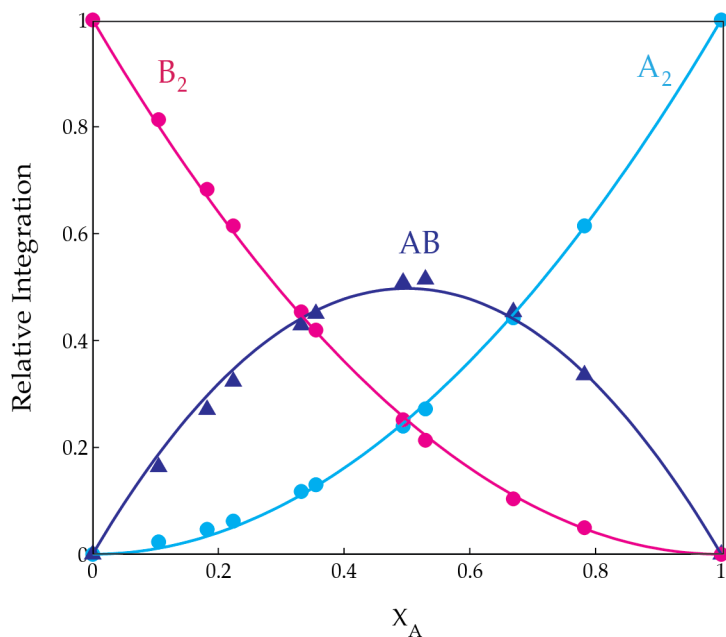


Figure AI.48. Job plot showing the relative integrations versus the measured mole fractions of $\mathbf{2}$ for 0.10 M mixtures of $[\text{}^6\text{Li}]\mathbf{2}$ (A) and $[\text{}^6\text{Li}]\mathbf{1}$ (B) in 0.50 M piperidine/toluene at $-90\text{ }^\circ\text{C}$.

Job Plots in Pyrrolidine

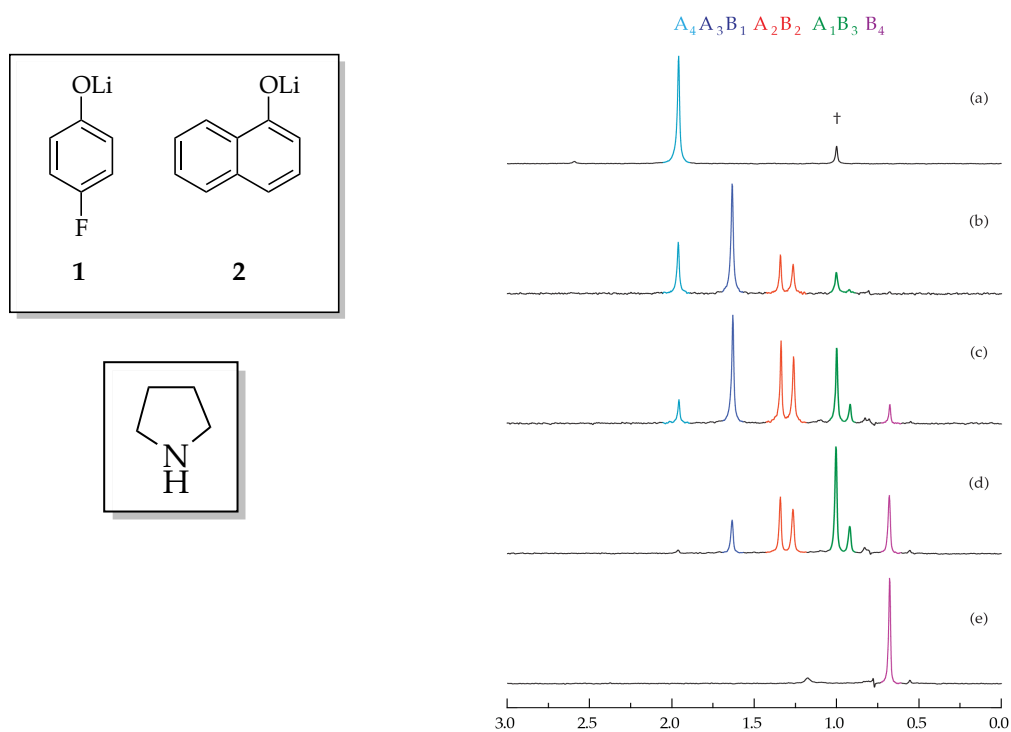


Figure AI.49. ${}^6\text{Li}$ NMR spectra of 0.10 M solutions of $[{}^6\text{Li}]2$ (A) and $[{}^6\text{Li}]9$ (B) in 0.50 M pyrrolidine/toluene at $-90\text{ }^\circ\text{C}$. The measured mole fractions of A in (a)-(e) are 1.00, 0.69, 0.52, 0.35, and 0.00, respectively. † indicates unknown aggregate.

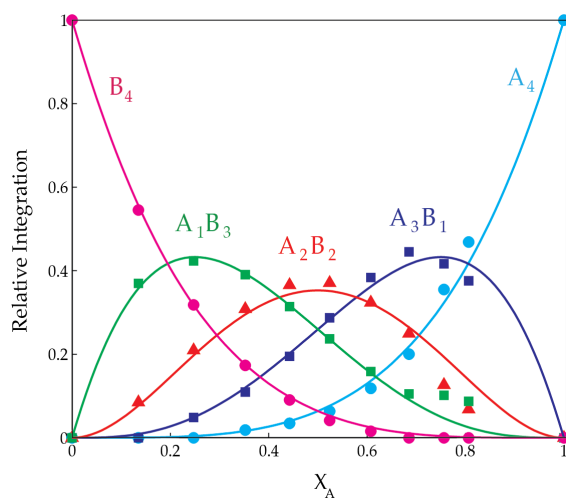


Figure AI.50. Job plot showing the relative integrations versus the measured mole fractions of 2 for 0.10 M mixtures of $[{}^6\text{Li}]2$ (A) and $[{}^6\text{Li}]1$ (B) in 0.50 M pyrrolidine/toluene at $-90\text{ }^\circ\text{C}$.

Job Plots in Pyrrolidine

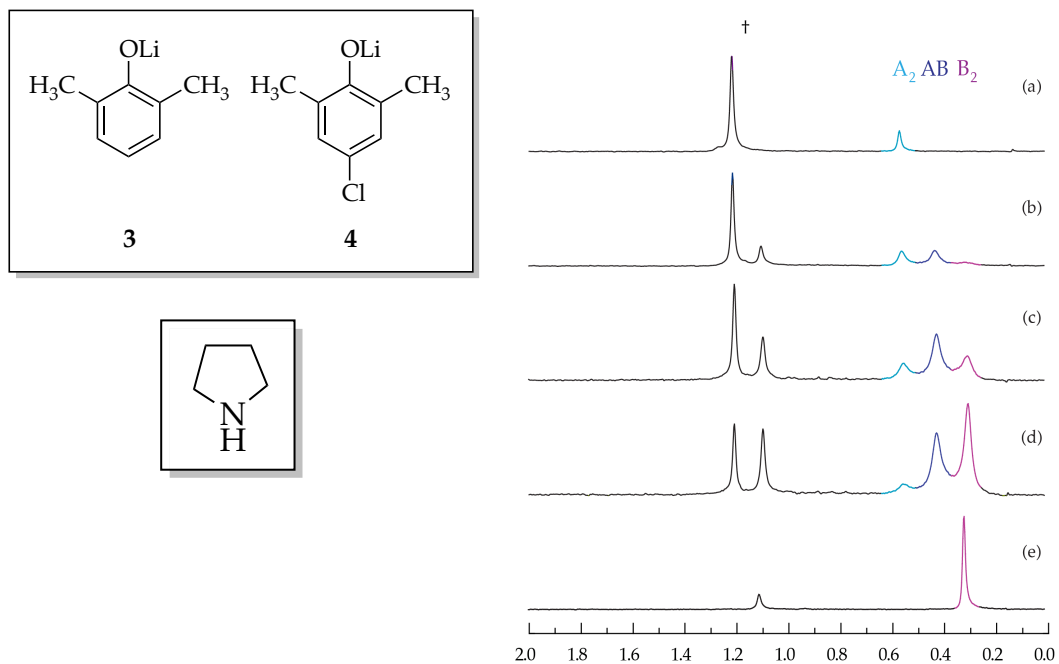


Figure AI.51. ^6Li NMR spectra of 0.10 M solutions of $[\text{}^6\text{Li}]\mathbf{2}$ (**A**) and $[\text{}^6\text{Li}]\mathbf{9}$ (**B**) in 0.50 M pyrrolidine/toluene at $-90\text{ }^\circ\text{C}$. The measured mole fractions of **A** in (a)-(e) are 1.00, 0.58, 0.45, 0.29, and 0.00, respectively. † indicates unknown aggregate.

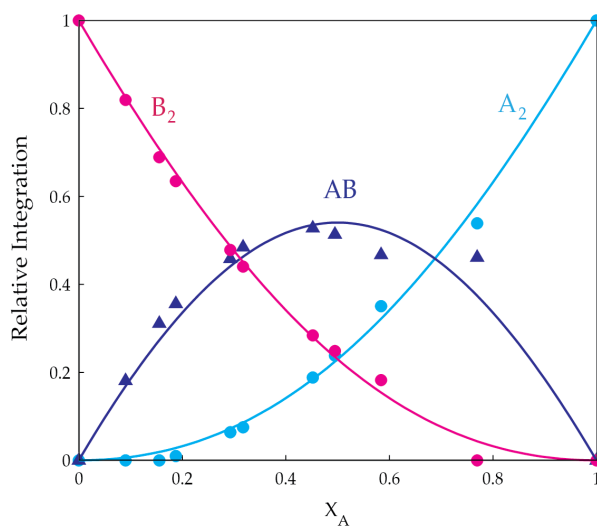


Figure AI.52. Job plot showing the relative integrations versus the measured mole fractions of **2** for 0.10 M mixtures of $[\text{}^6\text{Li}]\mathbf{2}$ (**A**) and $[\text{}^6\text{Li}]\mathbf{1}$ (**B**) in 0.50 M pyrrolidine/toluene at $-90\text{ }^\circ\text{C}$.

Tetramer Job Plots in *i*-Butylamine

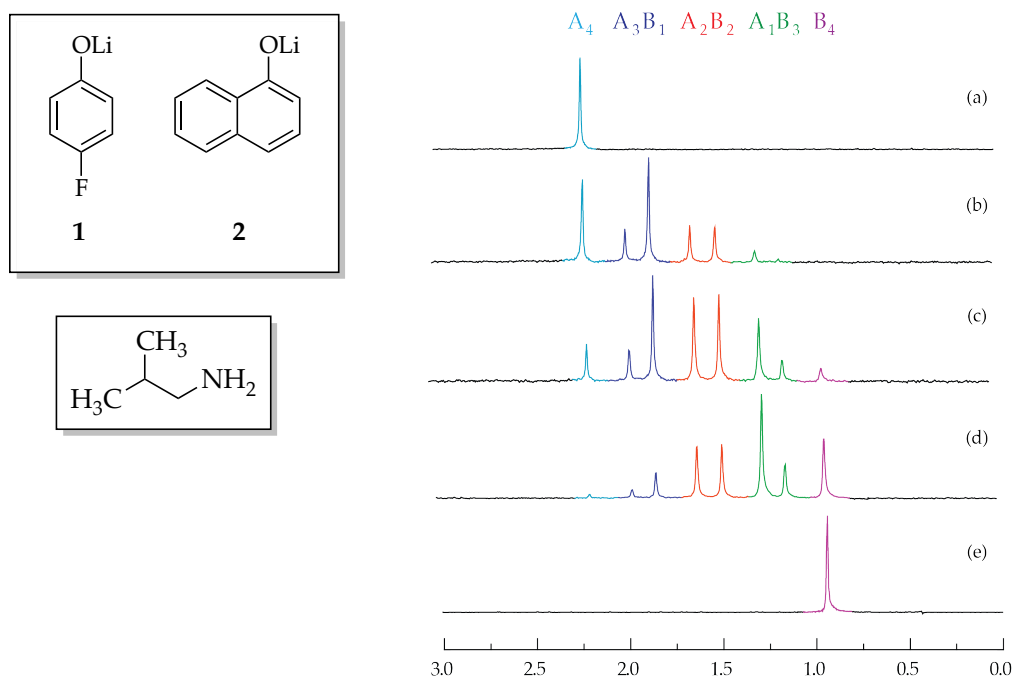


Figure AI.53. ^6Li NMR spectra of 0.10 M solutions of $[\text{}^6\text{Li}]2$ (A) and $[\text{}^6\text{Li}]1$ (B) in 0.50 M *i*-BuNH₂/toluene at -80 °C. The measured mole fractions of A in (a)-(e) are 1.00, 0.66, 0.53, 0.73, and 1.00, respectively.

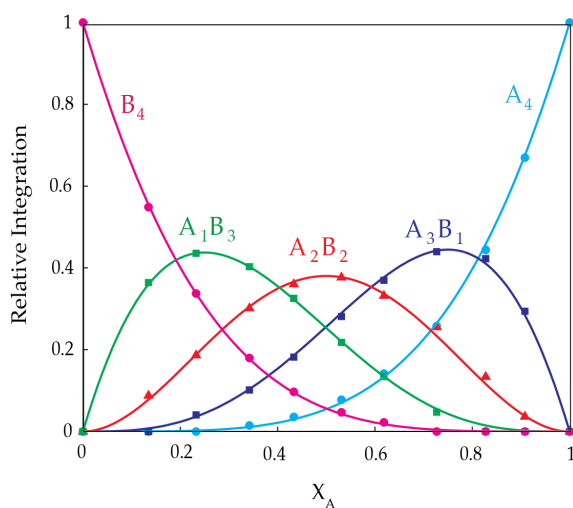


Figure AI.54. Job plot showing the relative integrations versus the measured mole fractions of 2 for 0.10 M mixtures of $[\text{}^6\text{Li}]2$ (A) and $[\text{}^6\text{Li}]1$ (B) in 0.50 M *i*-BuNH₂/toluene at -80 °C.

Dimer Job Plots in *i*-Butylamine

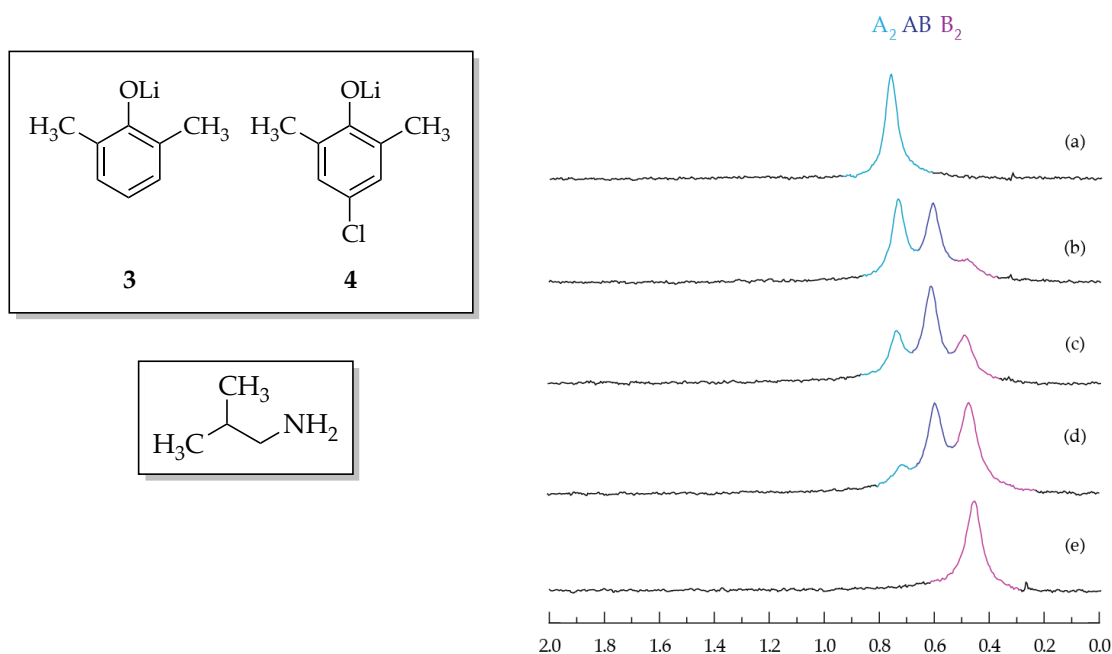


Figure AI.55. ^6Li NMR spectra of 0.10 M solutions of $[\text{}^6\text{Li}]\mathbf{3}$ (**A**) and $[\text{}^6\text{Li}]\mathbf{4}$ (**B**) in 0.50 M *i*-BuNH₂/toluene at -110 °C. The measured mole fractions of **A** in (a)-(e) are 1.00, 0.62, 0.48, 0.46, and 0.00, respectively.

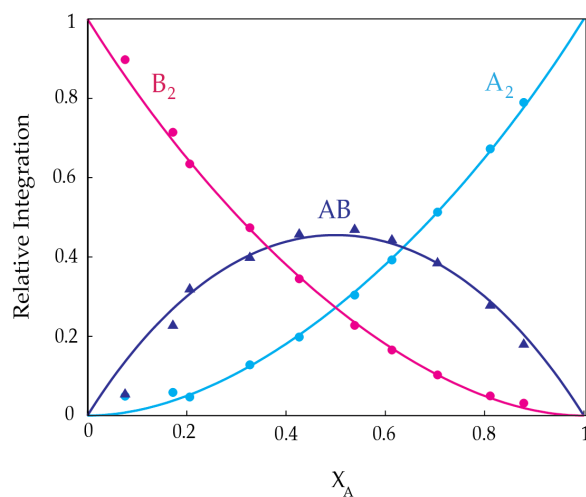


Figure AI.56. Job plot showing the relative integrations versus the measured mole fractions of **3** for 0.10 M mixtures of $[\text{}^6\text{Li}]\mathbf{3}$ (**A**) and $[\text{}^6\text{Li}]\mathbf{4}$ (**B**) in 0.50 M *i*-BuNH₂/toluene at -110 °C.

Tetramer Job Plots in *sec*-Butylamine

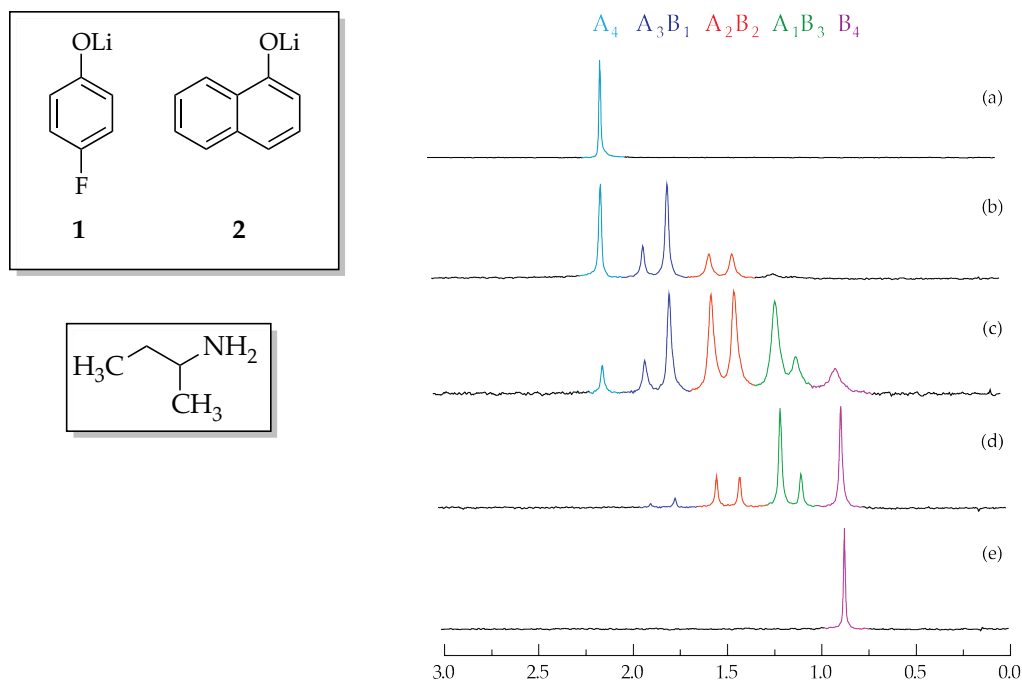


Figure AI.57. ^6Li NMR spectra of 0.10 M solutions of $[\text{}^6\text{Li}]2$ (**A**) and $[\text{}^6\text{Li}]1$ (**B**) in 0.50 M *sec*-BuNH₂/toluene at -60 °C. The measured mole fractions of **A** in (a)-(e) are 1.00, 0.76, 0.43, 0.28, and 1.00, respectively.

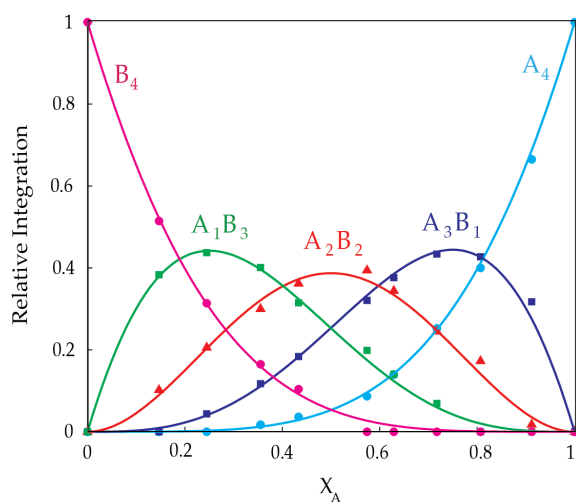


Figure AI.58. Job plot showing the relative integrations versus the measured mole fractions of **2** for 0.10 M mixtures of $[\text{}^6\text{Li}]2$ (**A**) and $[\text{}^6\text{Li}]1$ (**B**) in 0.50 M *sec*-BuNH₂/toluene at -60 °C.

Tetramer Job Plots in *t*-Butylamine

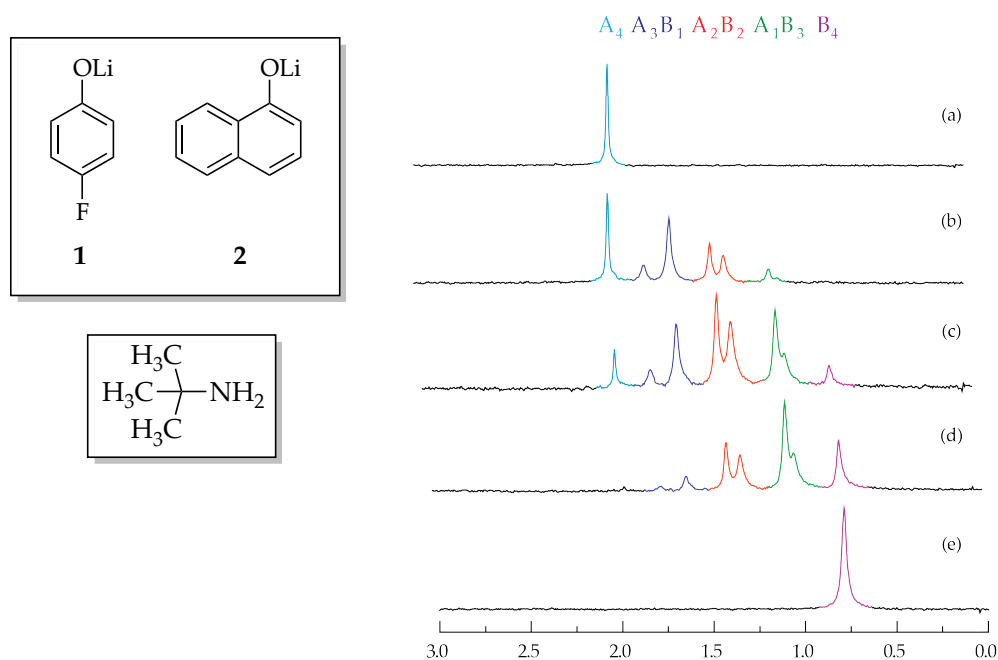


Figure AI.59. ^6Li NMR spectra of 0.10 M solutions of $[^6\text{Li}]2$ (A) and $[^6\text{Li}]1$ (B) in 0.50 M *t*-BuNH₂/toluene at -80 °C. The measured mole fractions of A in (a)-(e) are 1.00, 0.68, 0.53, 0.32, and 1.00, respectively.

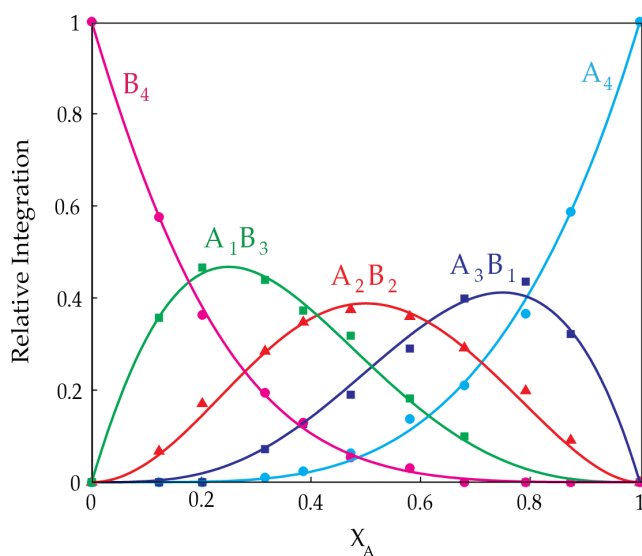


Figure AI.60. Job plot showing the relative integrations versus the measured mole fractions of 2 for 0.10 M mixtures of $[^6\text{Li}]2$ (A) and $[^6\text{Li}]1$ (B) in 0.50 M *t*-BuNH₂/toluene at -80 °C.

Trimer Job Plots in Diisopropylamine

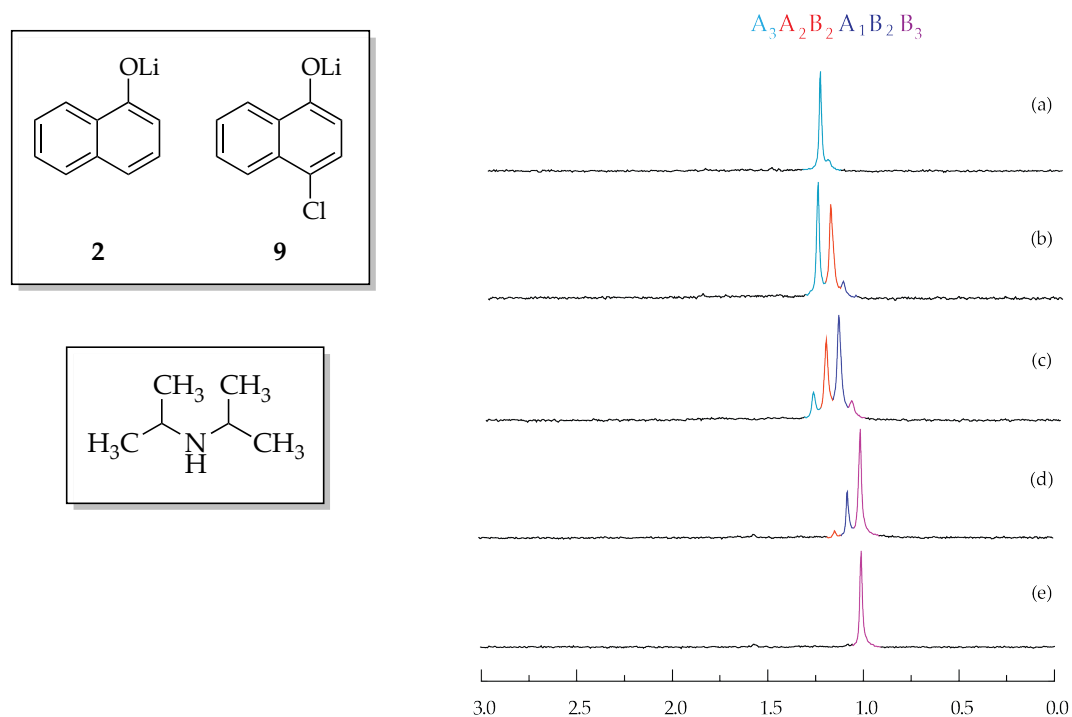


Figure AI.61. ^6Li NMR spectra of 0.10 M solutions of $[\text{}^6\text{Li}]\mathbf{2}$ (A) and $[\text{}^6\text{Li}]\mathbf{9}$ (B) in 1.0 M *i*-Pr₂NH/toluene at -60 °C. The measured mole fractions of A in (a)-(e) are 1.00, 0.89, 0.53, 0.23, and 0.00, respectively.

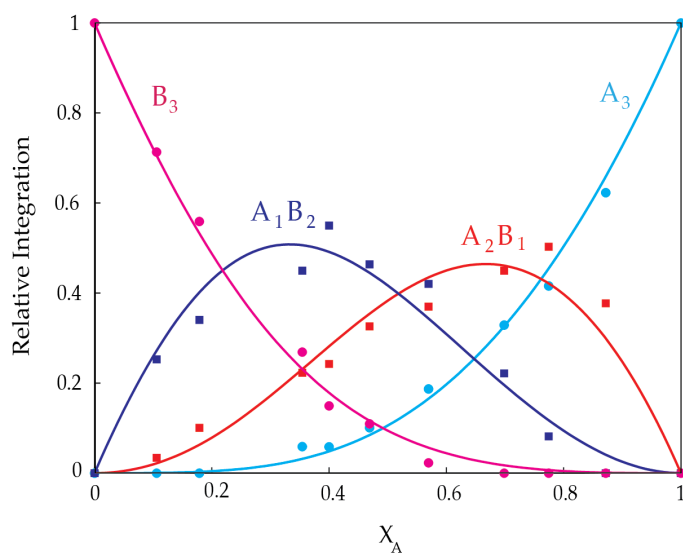


Figure AI.62. Job plot showing the relative integrations versus the measured mole fractions of $\mathbf{2}$ for 0.10 M mixtures of $[\text{}^6\text{Li}]\mathbf{2}$ (A) and $[\text{}^6\text{Li}]\mathbf{9}$ (B) in 1.0 M *i*-Pr₂NH/ toluene at -60 °C.

^6Li Spectra in Diisopropylamine

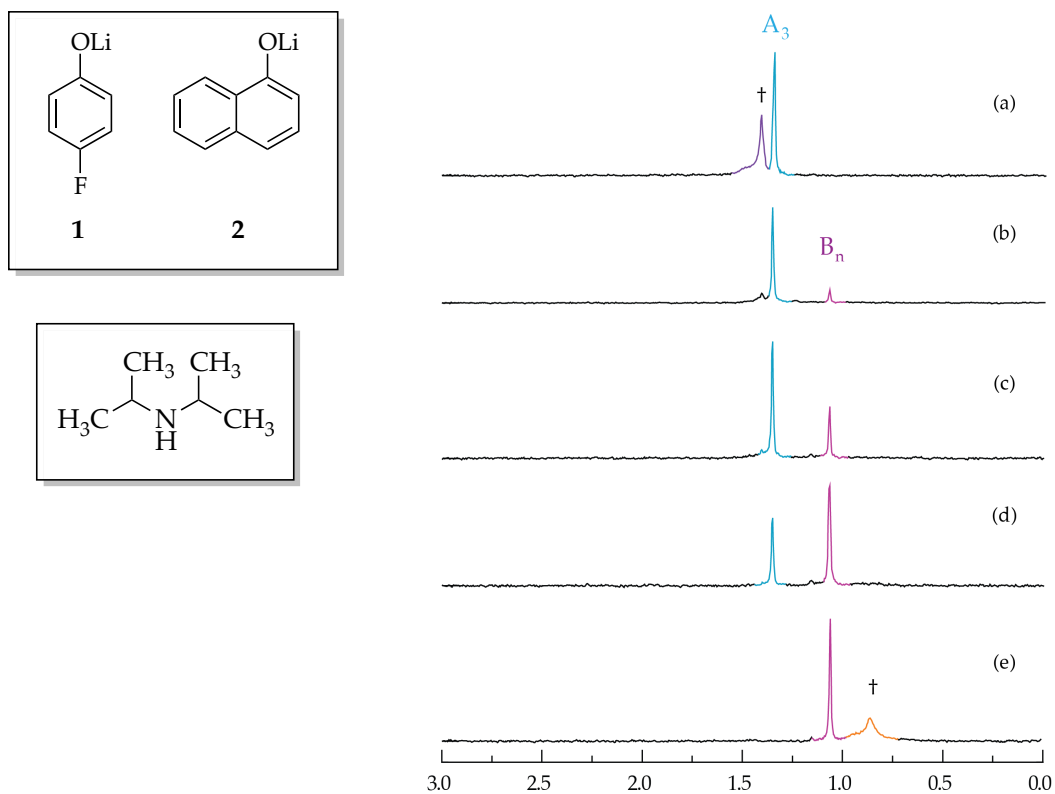


Figure AI.63. ^6Li NMR spectra of 0.10 M solutions of $[\text{}^6\text{Li}]_2$ (**A**) and $[\text{}^6\text{Li}]_1$ (**B**) in 1.0 M diisopropylamine/toluene at $-40\text{ }^\circ\text{C}$. The mole fractions of **2** in (a)-(e) are approximately 1.00, 0.75, 0.50, 0.25, 0.00, respectively. The absence of heteroaggregate formation indicates that **2** and **1** are not the same aggregation state. **2** was characterized as a trimer (previous page). \dagger indicates unknown aggregate.

Dimer Job Plots in Diisopropylamine

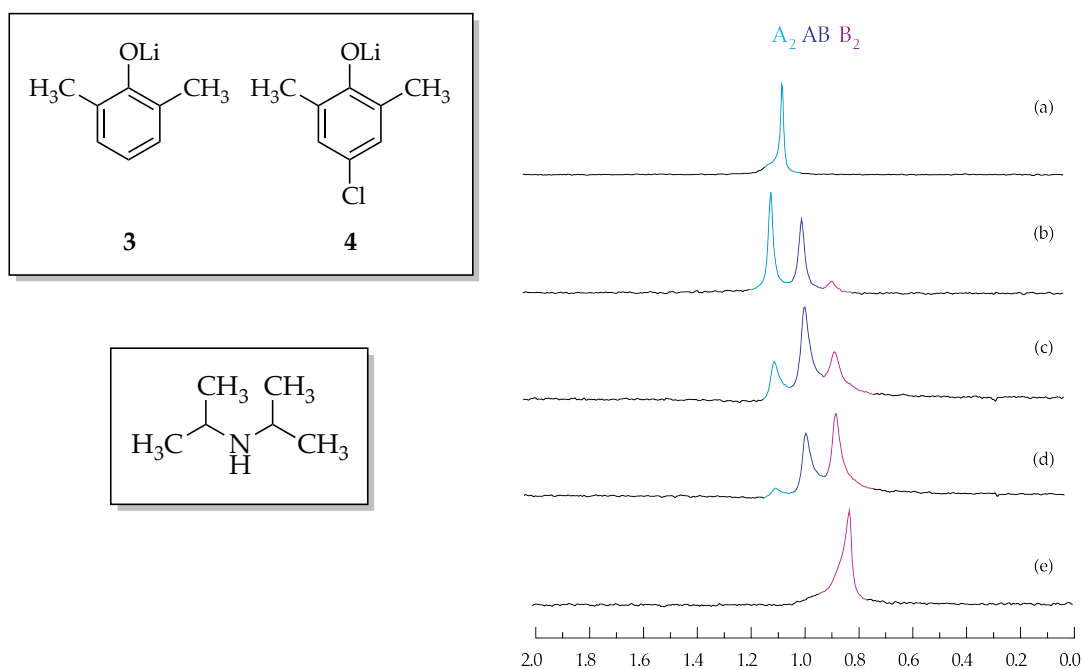


Figure AI.64. ^6Li NMR spectra of 0.10 M solutions of $[^6\text{Li}]\mathbf{3}$ (**A**) and $[^6\text{Li}]\mathbf{4}$ (**B**) in 1.0 M *i*-Pr₂NH/toluene at -80 °C. The measured mole fractions of **A** in (a)-(e) are 1.00, 0.73, 0.54, 0.31, and 0.00, respectively.

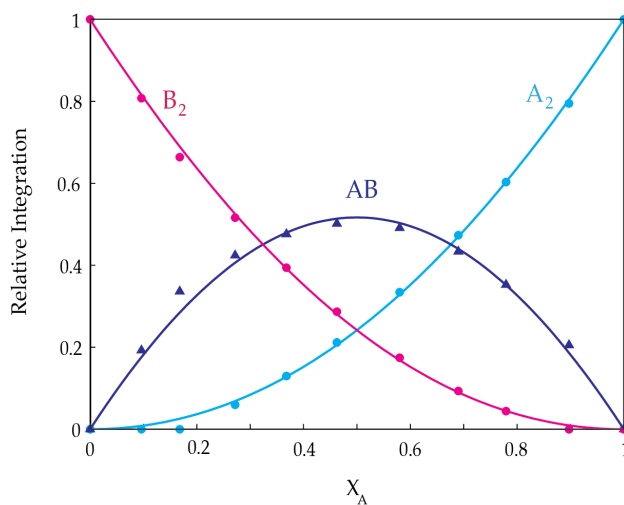


Figure AI.65. Job plot showing the relative integrations versus the measured mole fractions of **3** for 0.10 M mixtures of $[^6\text{Li}]\mathbf{3}$ (**A**) and $[^6\text{Li}]\mathbf{4}$ (**B**) in 1.0 M *i*-Pr₂NH/toluene at -80 °C.

Tetramer Job Plots in Diethylamine

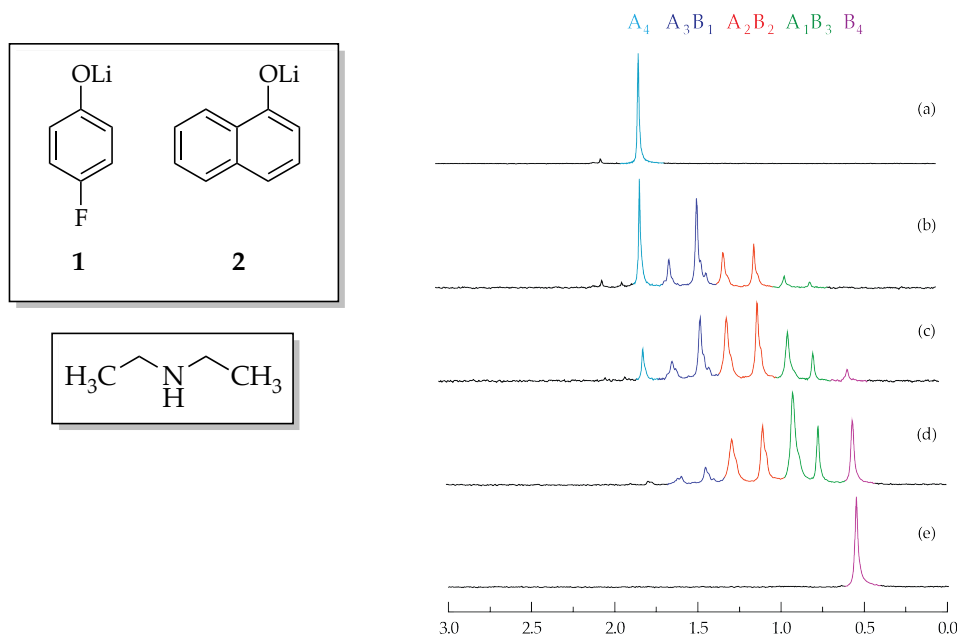


Figure AI.66. ^6Li NMR spectra of 0.10 M solutions of $[\text{}^6\text{Li}]2$ (**A**) and $[\text{}^6\text{Li}]1$ (**B**) in 0.50 M Et_2NH /toluene at $-60\text{ }^\circ\text{C}$. The measured mole fractions of **A** in (a)-(e) are 1.00, 0.65, 0.47, 0.29, and 0.00, respectively.

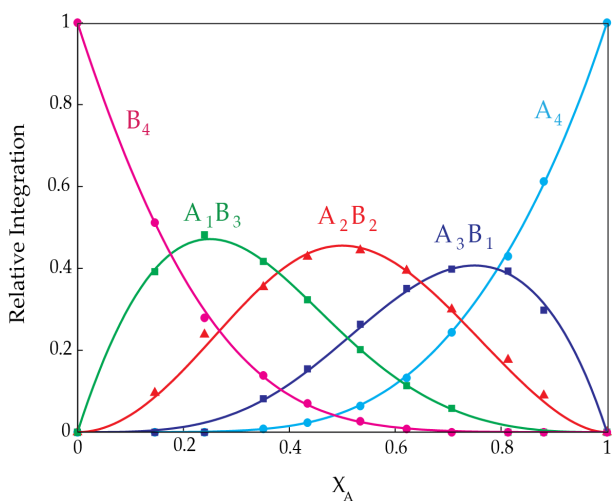


Figure AI.67. Job plot showing the relative integrations versus the measured mole fractions of **2** for 0.10 M mixtures of $[\text{}^6\text{Li}]2$ (**A**) and $[\text{}^6\text{Li}]1$ (**B**) in 0.50 M Et_2NH /toluene at $-60\text{ }^\circ\text{C}$.

Trimer Job Plots in Diethylamine

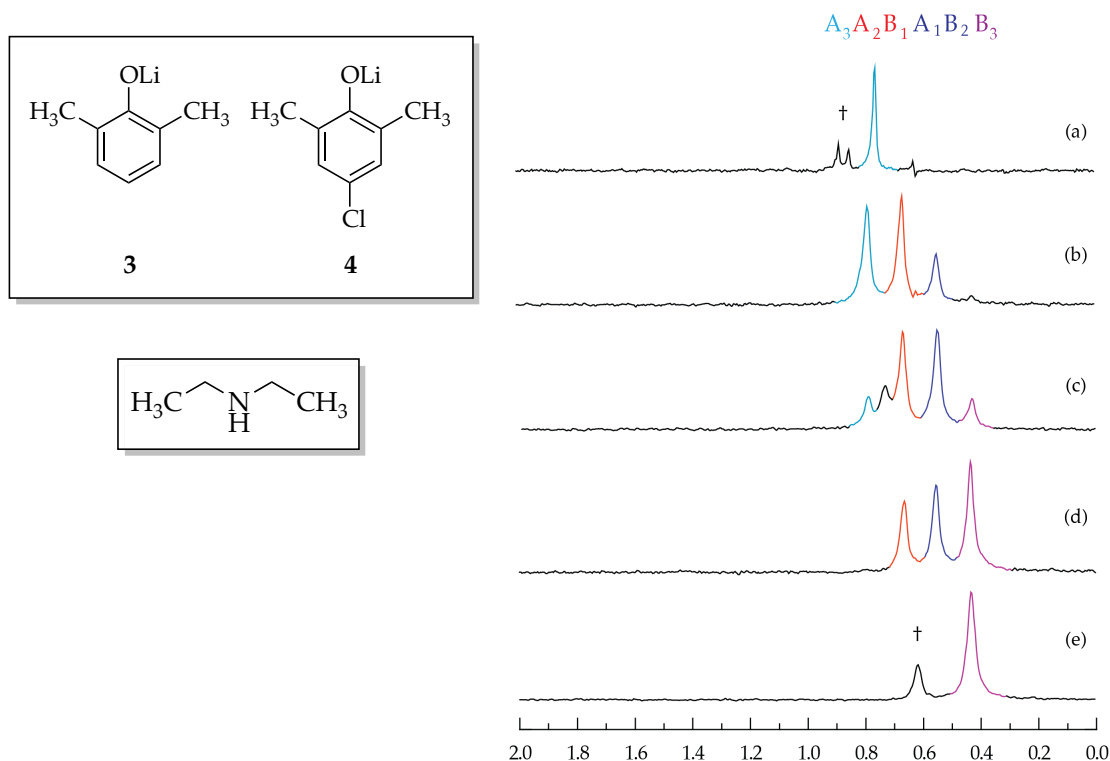


Figure AI.68. ^6Li NMR spectra of 0.10 M solutions of $[\text{}^6\text{Li}]\mathbf{3}$ (A) and $[\text{}^6\text{Li}]\mathbf{4}$ (B) in 0.50 M Et_2NH /toluene at $-80\text{ }^\circ\text{C}$. The measured mole fractions of A in (a)-(e) are 1.00, 0.69, 0.53, 0.31, and 0.00, respectively. \dagger indicates unknown aggregate.

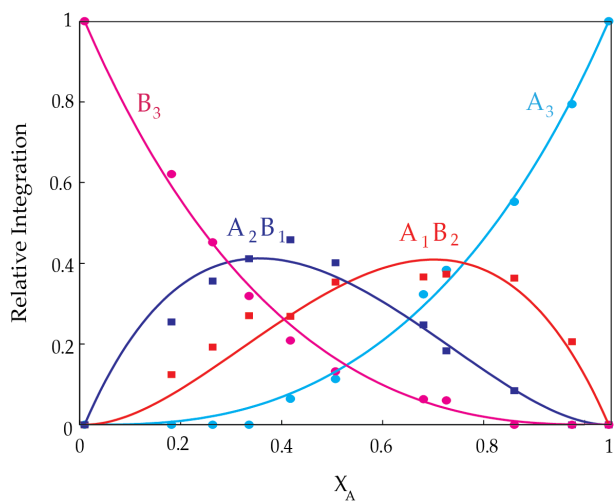


Figure AI.69. Job plot showing the relative integrations versus the measured mole fractions of $\mathbf{3}$ for 0.10 M mixtures of $[\text{}^6\text{Li}]\mathbf{3}$ (A) and $[\text{}^6\text{Li}]\mathbf{4}$ (B) in 0.50 M Et_2NH /toluene at $-80\text{ }^\circ\text{C}$.

Tetramer Job Plots in *n*-Dipropylamine

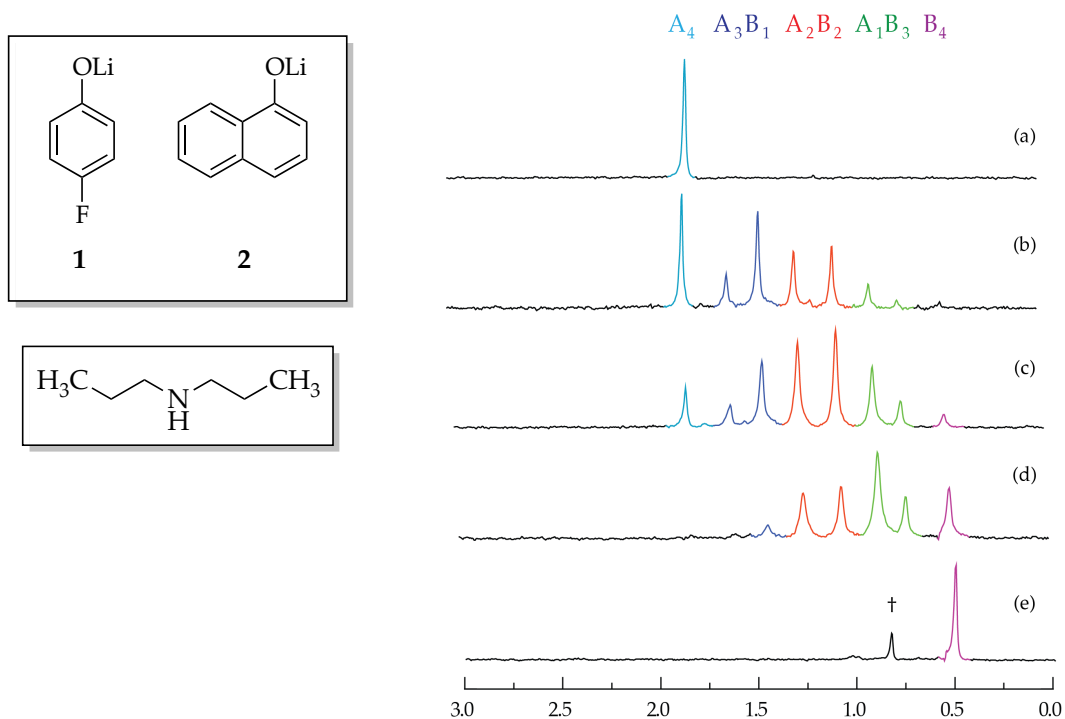


Figure AI.70. ^6Li NMR spectra of 0.10 M solutions of $[\text{}^6\text{Li}]2$ (A) and $[\text{}^6\text{Li}]1$ (B) in 0.50 M *n*-Pr₂NH/toluene at -80 °C. The measured mole fractions of A in (a)-(e) are 1.00, 0.68, 0.52, 0.31, and 0.00, respectively.

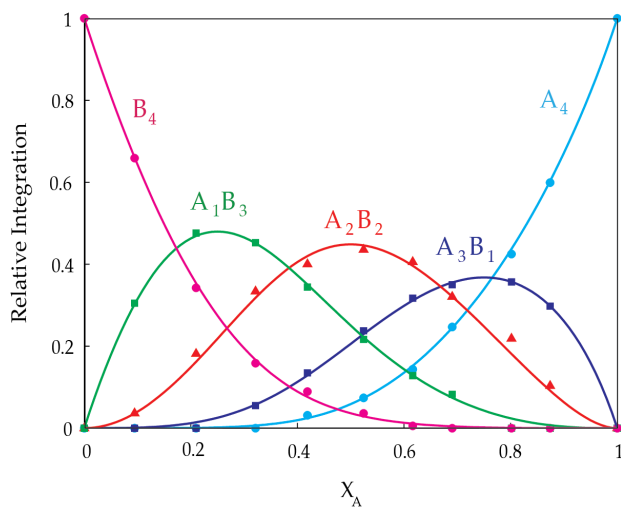


Figure AI.71. Job plot showing the relative integrations versus the measured mole fractions of 2 for 0.10 M mixtures of $[\text{}^6\text{Li}]2$ (A) and $[\text{}^6\text{Li}]1$ (B) in 0.50 M *n*-Pr₂NH/ toluene at -80 °C.

Trimer Job Plots in *n*-Dipropylamine

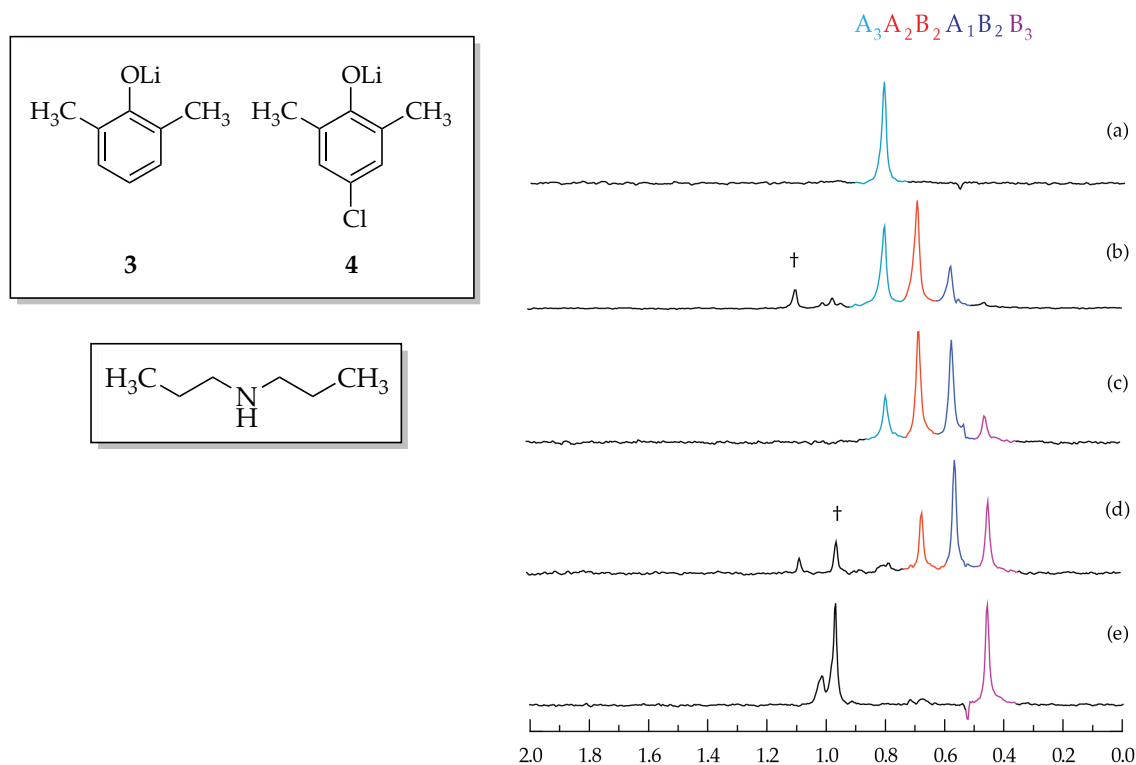


Figure AI.72. ^6Li NMR spectra of 0.10 M solutions of $[\text{}^6\text{Li}]\mathbf{3}$ (**A**) and $[\text{}^6\text{Li}]\mathbf{4}$ (**B**) in 0.50 M *n*-Pr₂NH/toluene at -80 °C. The measured mole fractions of **A** in (a)-(e) are 1.00, 0.62, 0.46, 0.27, and 0.00, respectively. † indicates unknown aggregate.

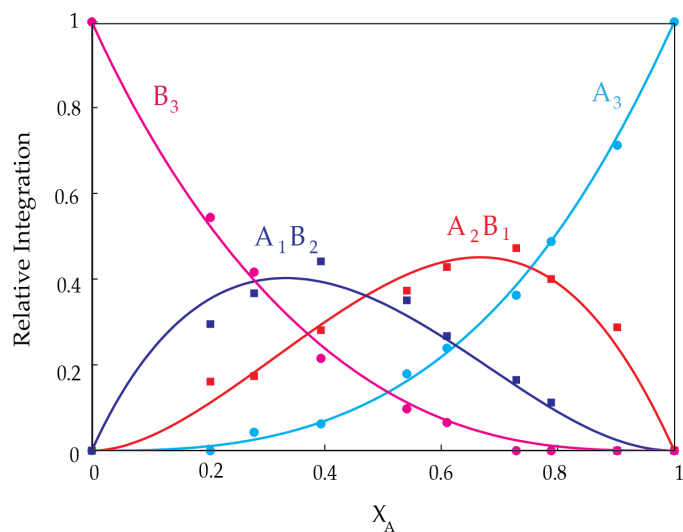


Figure AI.73. Job plot showing the relative integrations versus the measured mole fractions of **3** for 0.10 M mixtures of $[\text{}^6\text{Li}]\mathbf{3}$ (**A**) and $[\text{}^6\text{Li}]\mathbf{4}$ (**B**) in 0.50 M *n*-Pr₂NH/toluene at -80 °C.

Tetramer Job Plots in *t*-Butanol

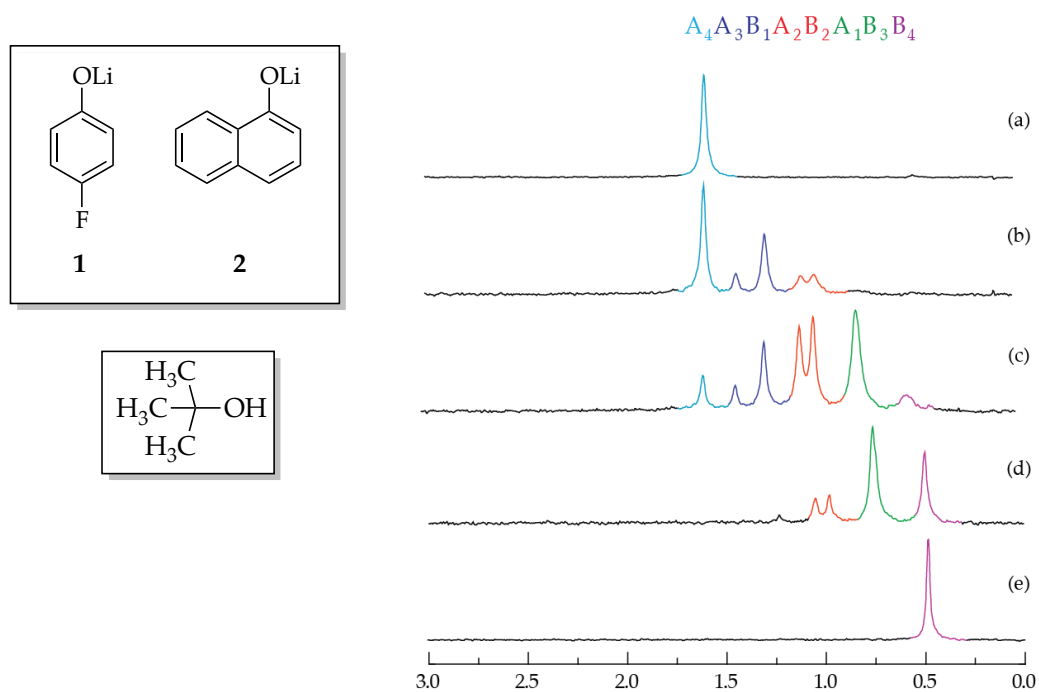


Figure AI.74. ${}^6\text{Li}$ NMR spectra of 0.10 M solutions of $[{}^6\text{Li}]2$ (**A**) and $[{}^6\text{Li}]1$ (**B**) in 0.50 M *t*-BuOH/toluene at $-95\text{ }^\circ\text{C}$. The measured mole fractions of **A** in (a)-(e) are 1.00, 0.75, 0.41, 0.21, and 0.00, respectively.

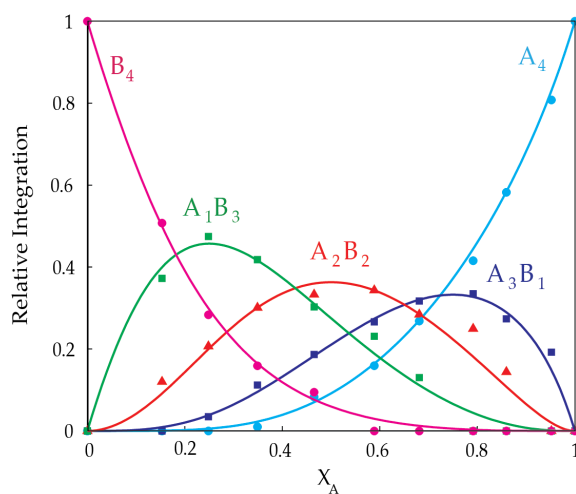


Figure AI.75. Job plot showing the relative integrations versus the measured mole fractions of **2** for 0.10 M mixtures of $[{}^6\text{Li}]2$ (**A**) and $[{}^6\text{Li}]1$ (**B**) in 0.50 M *t*-BuOH/toluene at $-95\text{ }^\circ\text{C}$.

Tetramer Job Plots in *sec*-Butanol

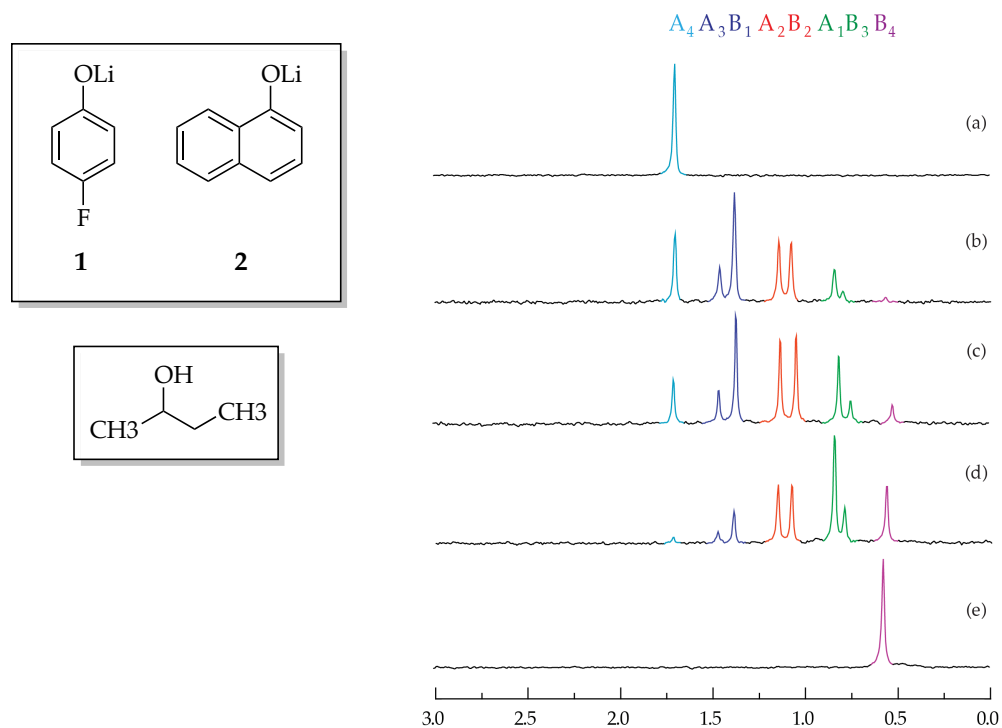


Figure AI.76. ^6Li NMR spectra of 0.10 M solutions of $[\text{}^6\text{Li}]\mathbf{2}$ (**A**) and $[\text{}^6\text{Li}]\mathbf{1}$ (**B**) in 0.50 M *sec*-BuOH/toluene at $-80\text{ }^\circ\text{C}$. The mole fractions of **A** in (a)-(e) are 1.00, 0.65, 0.46, 0.27, 0.00, respectively.

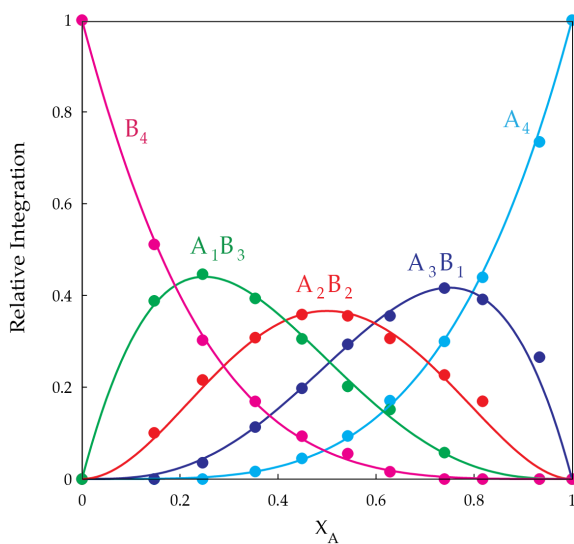


Figure AI.77. Job plot showing the relative integrations versus mole fractions of **2** for 0.10 M mixtures of $[\text{}^6\text{Li}]\mathbf{2}$ (**A**) and $[\text{}^6\text{Li}]\mathbf{1}$ (**B**) in 0.50 M *sec*-BuOH/toluene at $-80\text{ }^\circ\text{C}$.

^6Li Spectra in *n*-Butanol

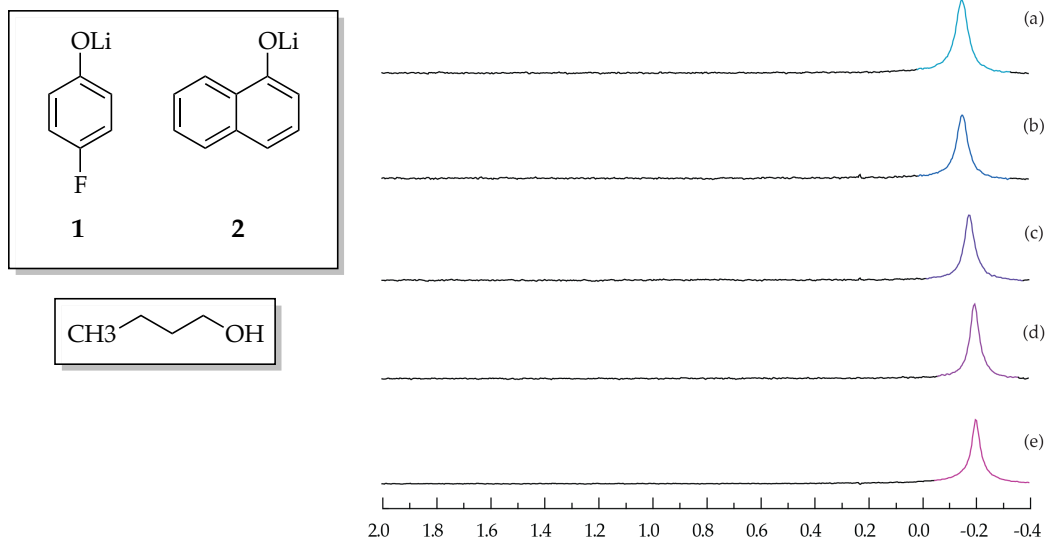


Figure AI.78. ^6Li NMR spectra of 0.10 M solutions of $[\text{}^6\text{Li}]\mathbf{2}$ (a) and $[\text{}^6\text{Li}]\mathbf{1}$ (e) in 0.50 M *n*-BuOH/toluene at $-110\text{ }^\circ\text{C}$. The measured mole fractions cannot be calculated, but the mole fraction of $\mathbf{2}$ in tubes (b), (c), and (d) are roughly 0.75, 0.50, and 0.25, respectively.

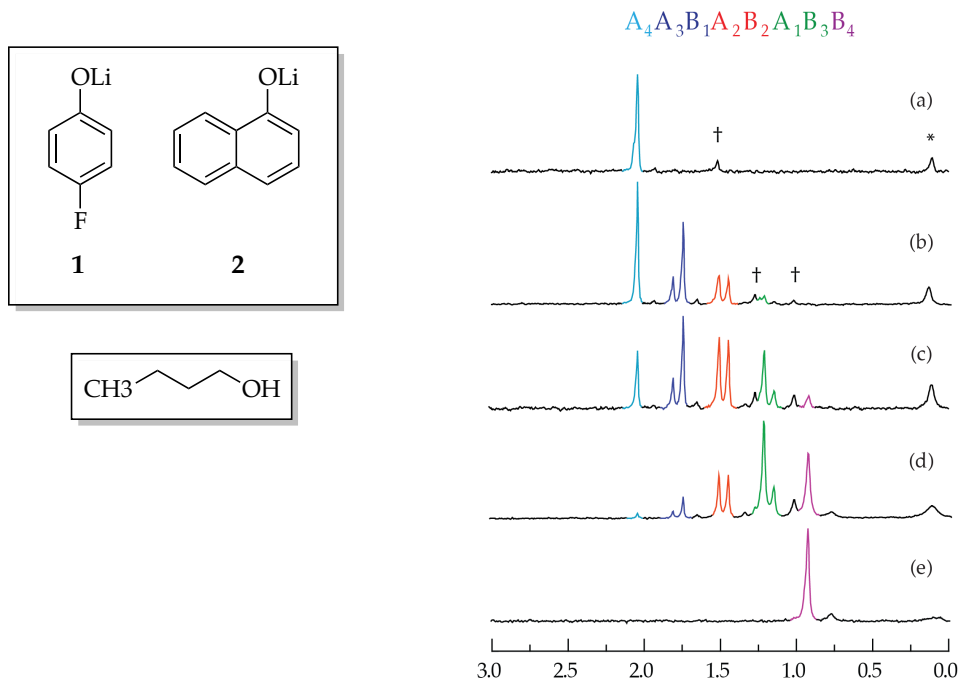


Figure AI.79. ^6Li NMR spectra of 0.10 M solutions of $[\text{}^6\text{Li}]\mathbf{2}$ (A) and $[\text{}^6\text{Li}]\mathbf{1}$ (B) in 0.50 M *n*-BuOH/ether at $-60\text{ }^\circ\text{C}$. The mole fractions of A in tubes (a)-(e) are roughly 1.00, 0.75, 0.50, 0.25, 0.00, respectively. The ether cosolvent provides the aggregate resolution, however, *n*-BuOH has been shown to bind to lithium preferentially over ether. † denotes unknown aggregate. * denotes $^6\text{LiHMDS}$.

Solvent Swap

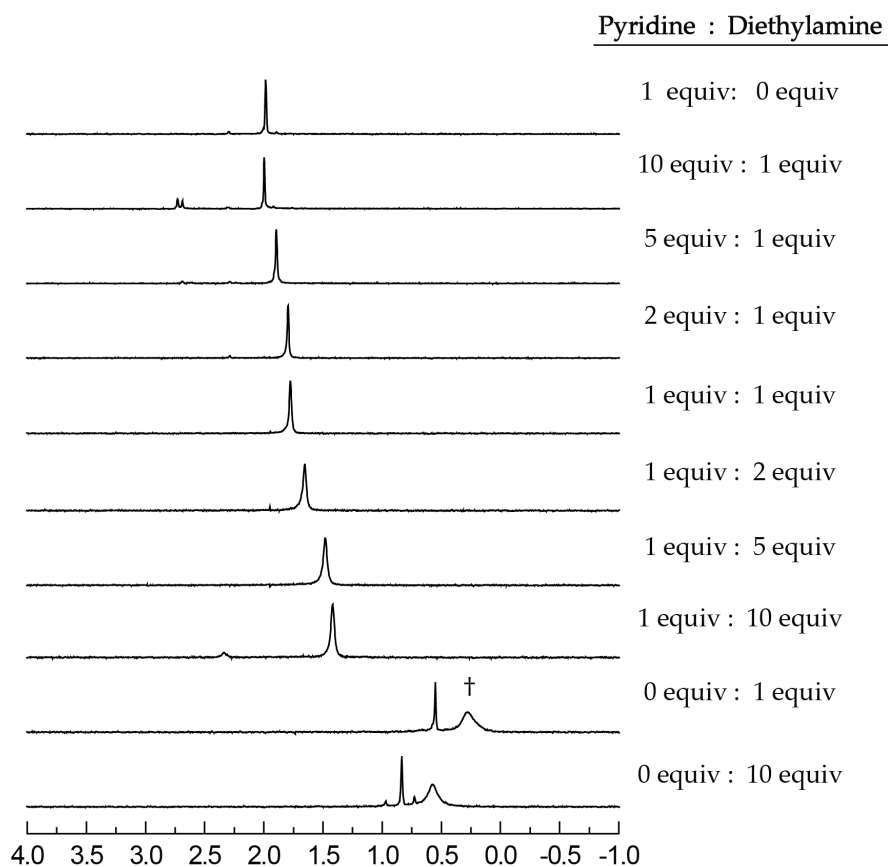


Figure AI.80. Solvent swap on 0.10 M of $[{}^6\text{Li}]\mathbf{1}$ in various pyridine and Et_2NH concentrations with toluene as cosolvent at $-80\text{ }^\circ\text{C}$. The chemical shift more closely resembles pyridine even at high Et_2NH concentrations. The peak migration, however, indicates that Et_2NH is also functioning as a ligand to the tetramer. The medium dependent chemical shift is clearly demonstrated going from 1.0 equiv to 10 equiv of Et_2NH . † denotes unknown aggregate.

Solvent Swap

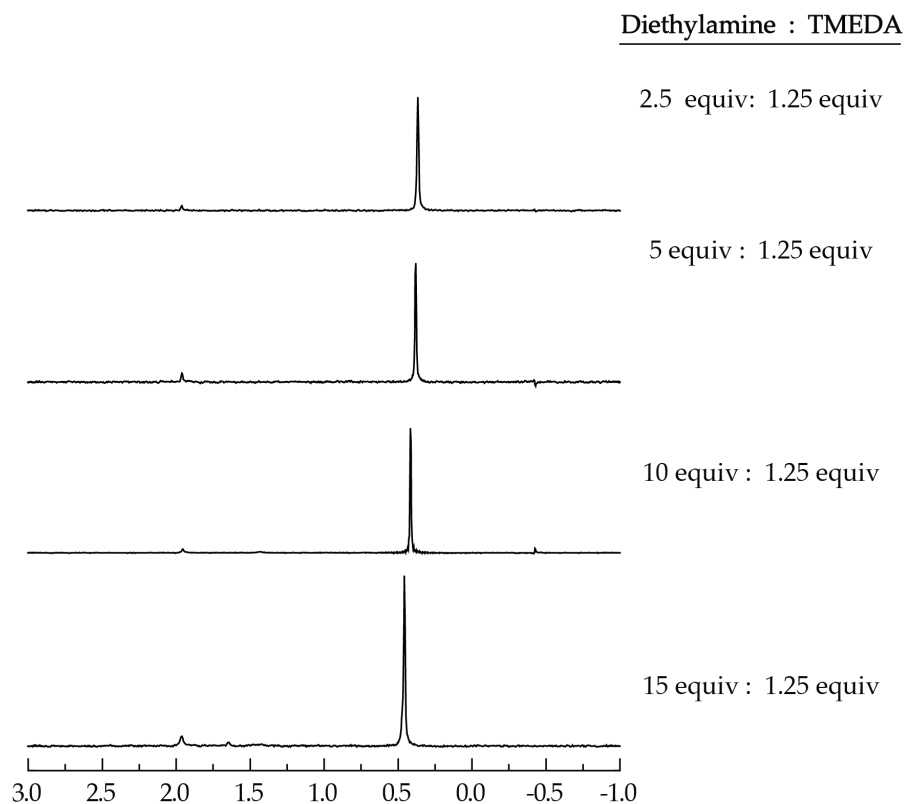


Figure AI.81. Solvent swap on 0.10 M of $[^6\text{Li}]_2$ in various ratios of Et_2NH and TMEDA with toluene as cosolvent at $-40\text{ }^\circ\text{C}$. Addition up to 15 equiv of Et_2NH does not move the naphtholate aggregate from being solely a TMEDA-bound dimer.

Solvent Swap

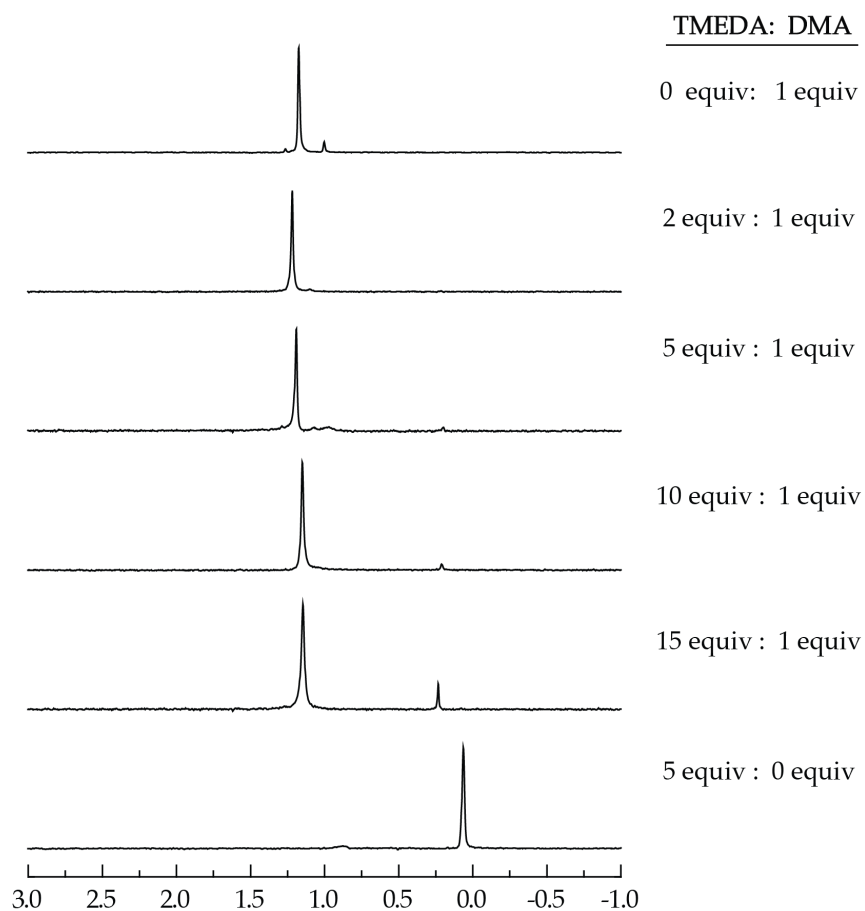


Figure AI.82. Solvent swap on 0.10 M of $[^6\text{Li}]\mathbf{1}$ in 1 equiv dimethylacetamide and various TMEDA concentrations with toluene as cosolvent at $-80\text{ }^\circ\text{C}$. Addition of up to 15 equiv of TMEDA does not affect the chemical shift, indicating that the tetramer is solely DMA-bound. The appearance of a small peak at high TMEDA concentrations may be the concentration-dependent chemical shift of the TMEDA-solvated dimer.

Solvent Swap

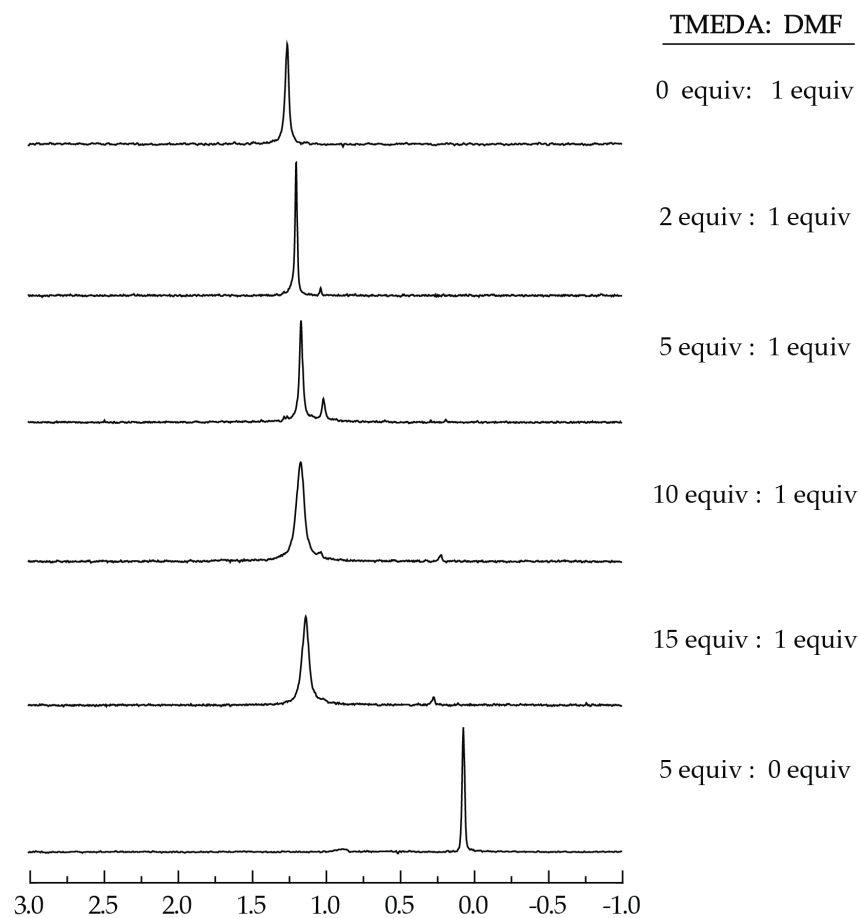


Figure AI.83. Solvent swap on 0.10 M of $[\text{}^6\text{Li}]\mathbf{1}$ in 1 equiv dimethylformamide and various TMEDA concentrations with toluene as cosolvent at $-80\text{ }^\circ\text{C}$. Addition of up to 15 equiv of TMEDA does not affect the chemical shift, indicating the tetramer is solely DMF-bound. The appearance of a small blip at high TMEDA concentrations may be the concentration-dependent chemical shift of the TMEDA-solvated dimer.

Solvent Swap

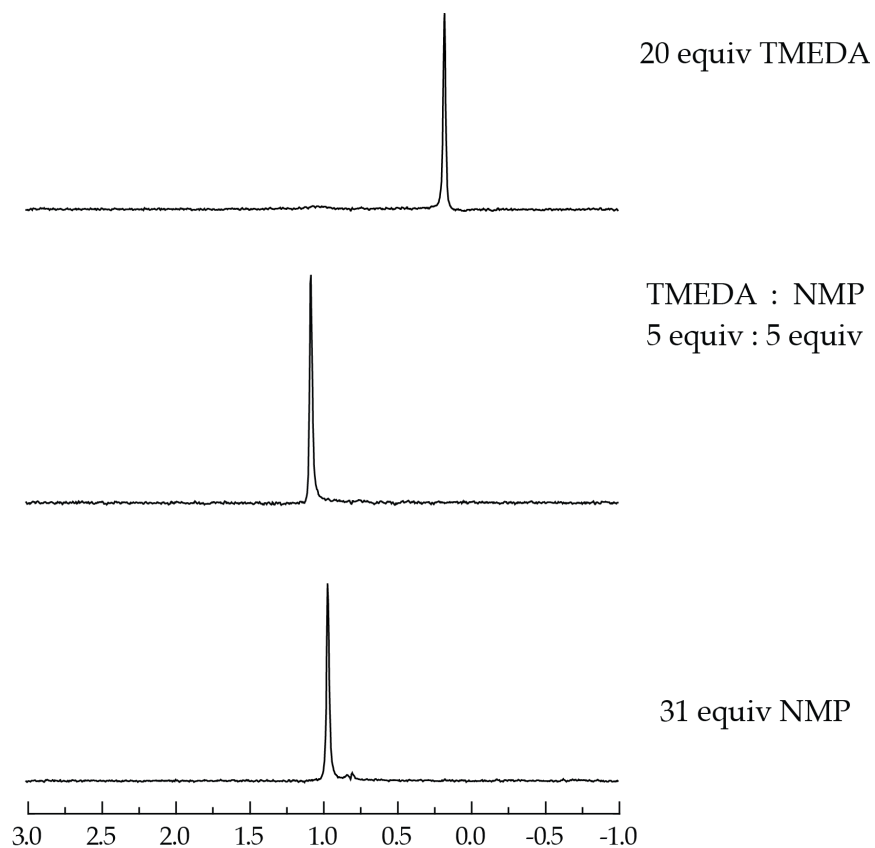


Figure AI.84. Solvent swap on 0.10 M of [⁶Li]**1** in *N*-methylpyrrolidone and TMEDA with toluene as cosolvent at -80 °C. At a 1:1 ligand ratio, the chemical shift closely resembles the chemical shift of NMP, indicating that it is solely a NMP bound tetramer. The slight chemical shift difference is probably due to the difference in ligand concentration (medium effect).

Solvent Swap

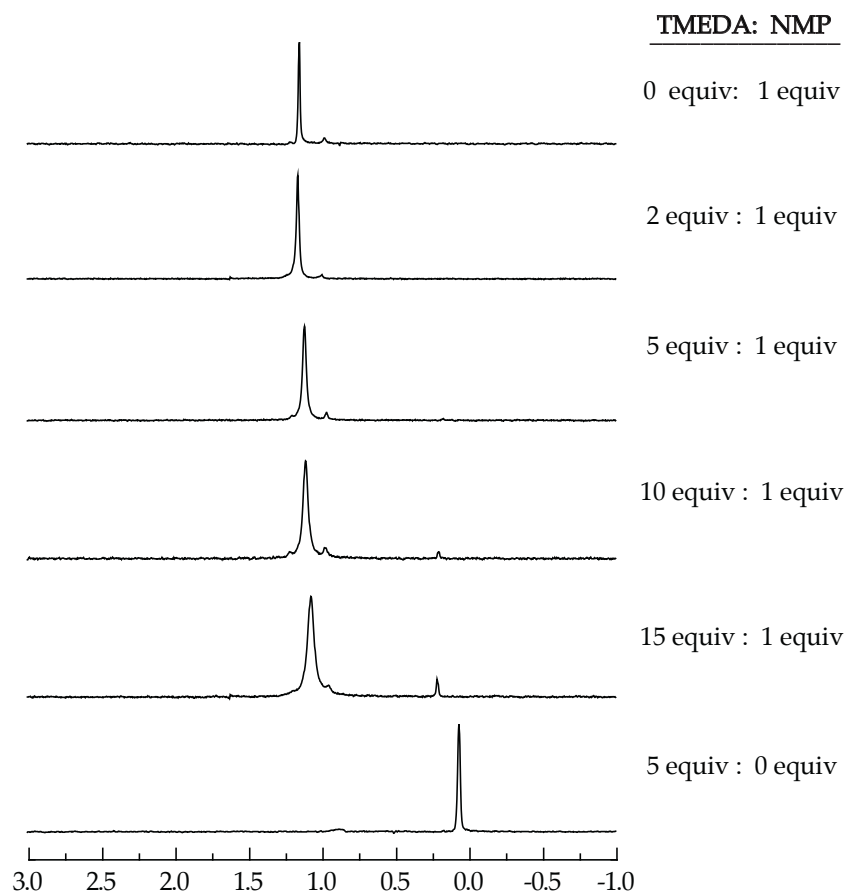


Figure AI.85. Solvent swap on 0.10 M of $[\text{}^6\text{Li}]\mathbf{1}$ in 1 equiv *N*-methylpyrrolidone and various TMEDA concentrations with toluene as cosolvent at $-80\text{ }^\circ\text{C}$. Addition of up to 15 equiv of TMEDA does not affect the chemical shift, indicating the tetramer is solely NMP-bound. The appearance of a small peak at high TMEDA concentrations may be the concentration-dependent chemical shift of the TMEDA-solvated dimer.

Solvent Swap

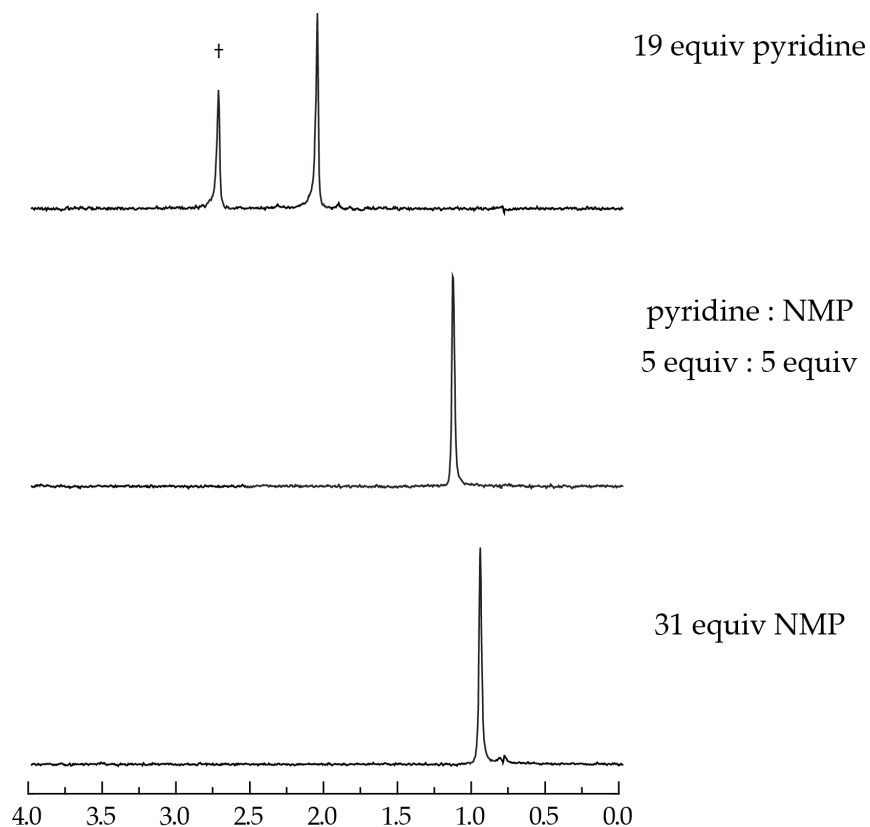


Figure AI.86. Solvent swap on 0.10 M of $[\text{}^6\text{Li}]\mathbf{1}$ in pyridine and *N*-methylpyrrolidone with toluene as cosolvent at $-80\text{ }^\circ\text{C}$. At a 1:1 ligand ratio, the chemical shift closely resembles the chemical shift of NMP, indicating that it is predominantly a NMP bound tetramer. The slight chemical shift difference may be due to minor pyridine binding. † denotes an aggregate present only at high pyridine concentration; it is assumed to be a highly solvated dimer.

Solvent Swap

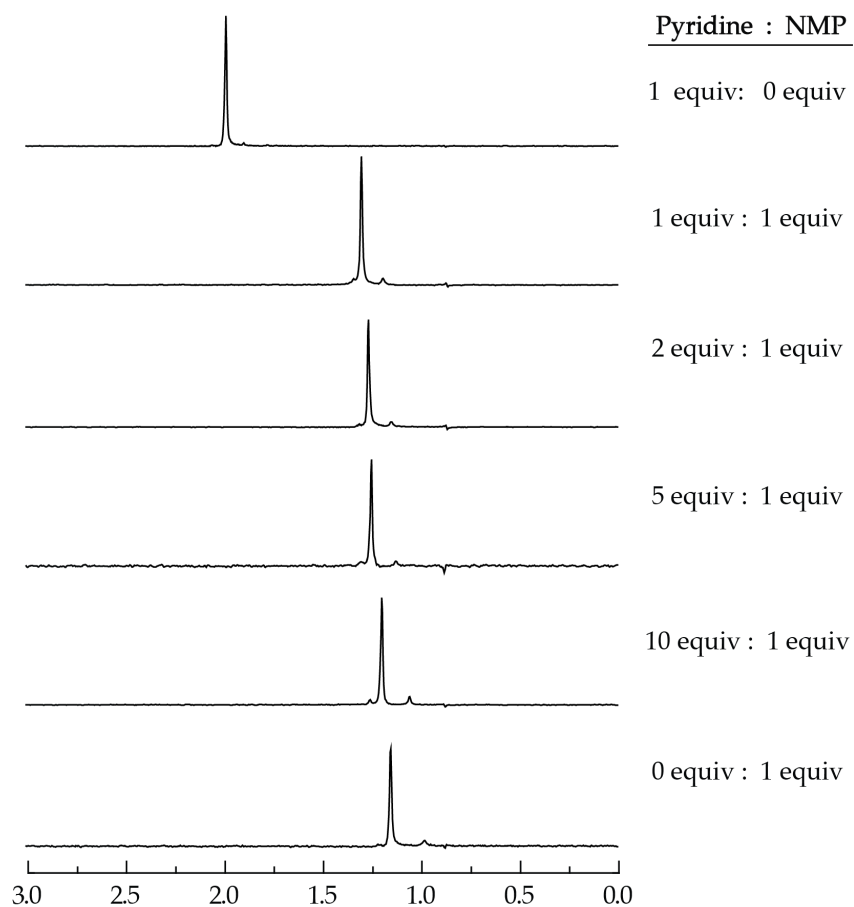


Figure AI.87. Solvent swap on 0.10 M of $[^6\text{Li}]\mathbf{1}$ in 1 equiv *N*-methylpyrrolidone and various pyridine concentrations with toluene as cosolvent at $-80\text{ }^\circ\text{C}$. Addition of up to 10 equiv of pyridine does not affect the chemical shift, indicating the tetramer is solely NMP-bound.

Solvent Swap

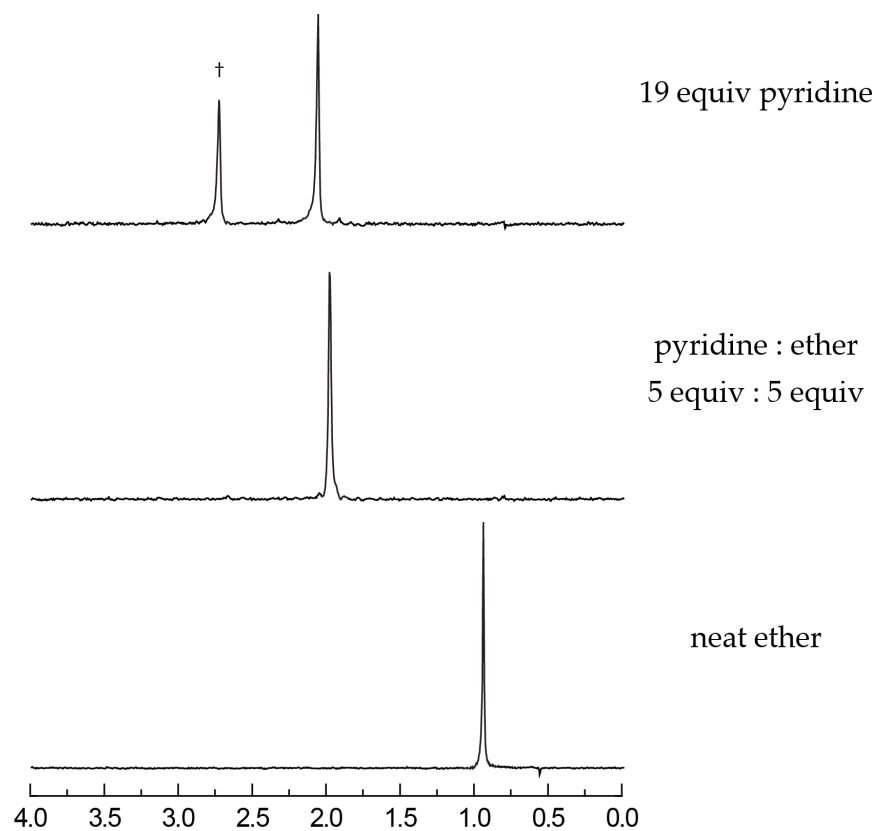


Figure AI.88. Solvent swap on 0.10 M of [^6Li]1 in pyridine and diethyl ether with a toluene cosolvent as needed at -40°C . At a 1:1 ligand ratio, the chemical shift closely resembles the chemical shift of pyridine, indicating that it is predominantly a pyridine bound tetramer. The slight chemical shift difference may be due to minor ether binding. † denotes an aggregate present only at high pyridine concentration; it is assumed to be a highly solvated dimer.

Solvent Swap

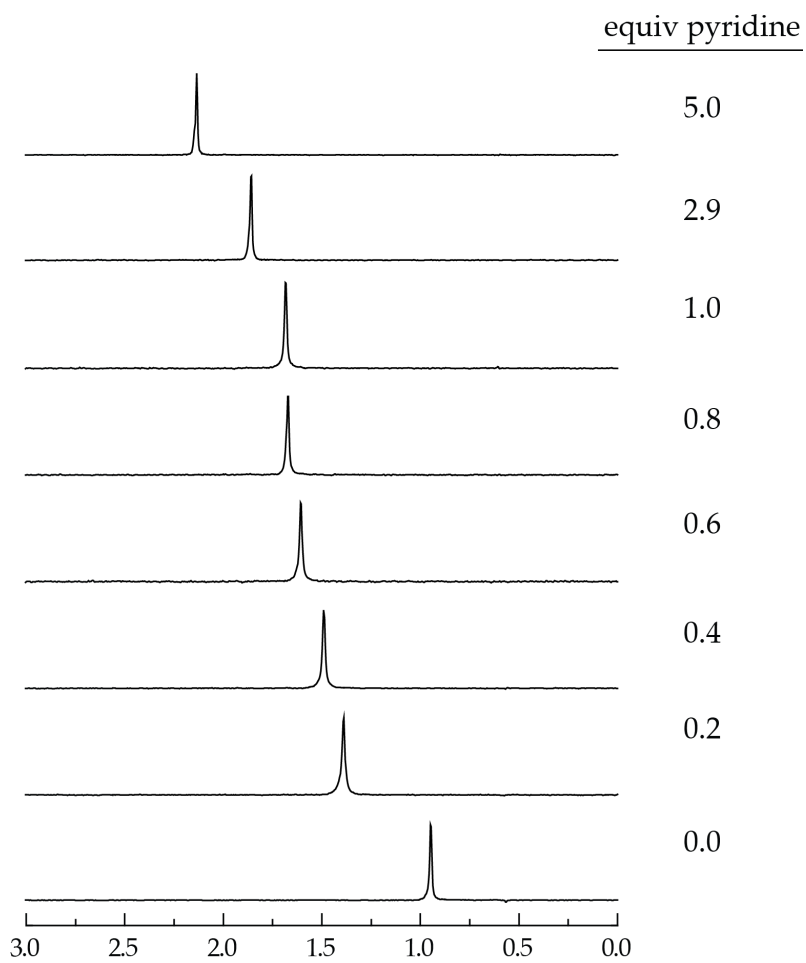


Figure AI.89. Solvent swap on 0.10 M of $[\text{}^6\text{Li}]\mathbf{1}$ in ether with increasing pyridine concentrations at $-40\text{ }^\circ\text{C}$. Using ether as the cosolvent enables ether to compete with pyridine as the ligand for the tetramer.

Solvent Swap

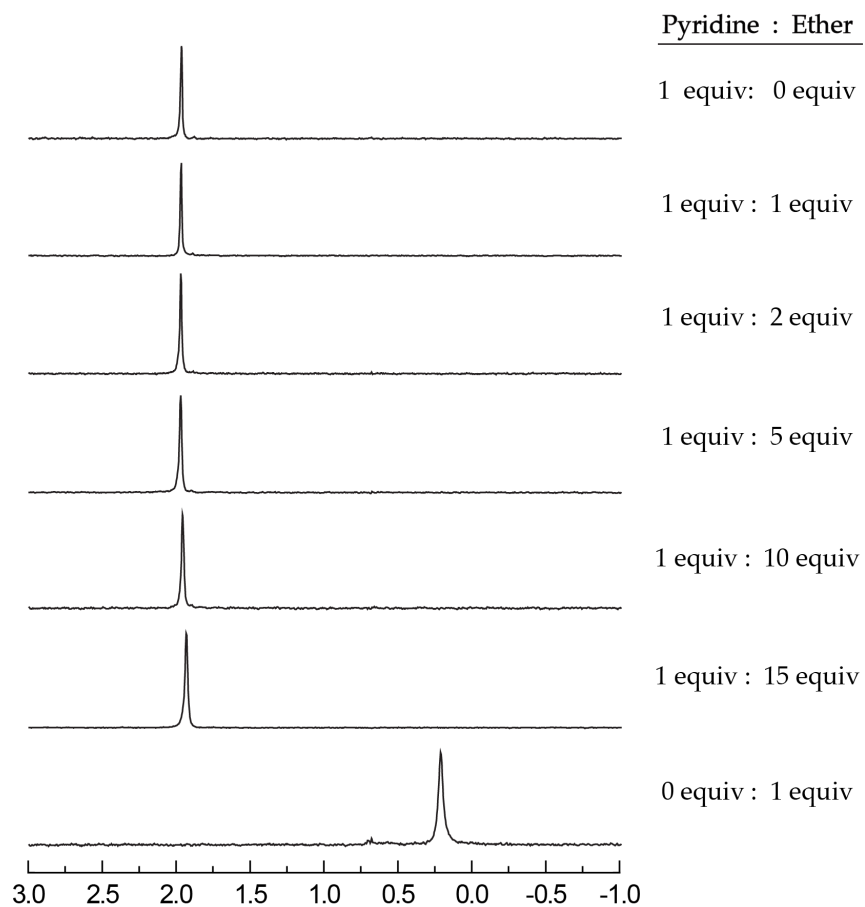


Figure AI.90. Solvent swap on 0.10 M of $[\text{}^6\text{Li}]\mathbf{1}$ in toluene with 1 equiv pyridine and increasing Et_2O concentrations at $-80\text{ }^\circ\text{C}$. Up to 15 equiv of Et_2O yields no impact on the pyridine-solvated tetramer.

Solvent Swap

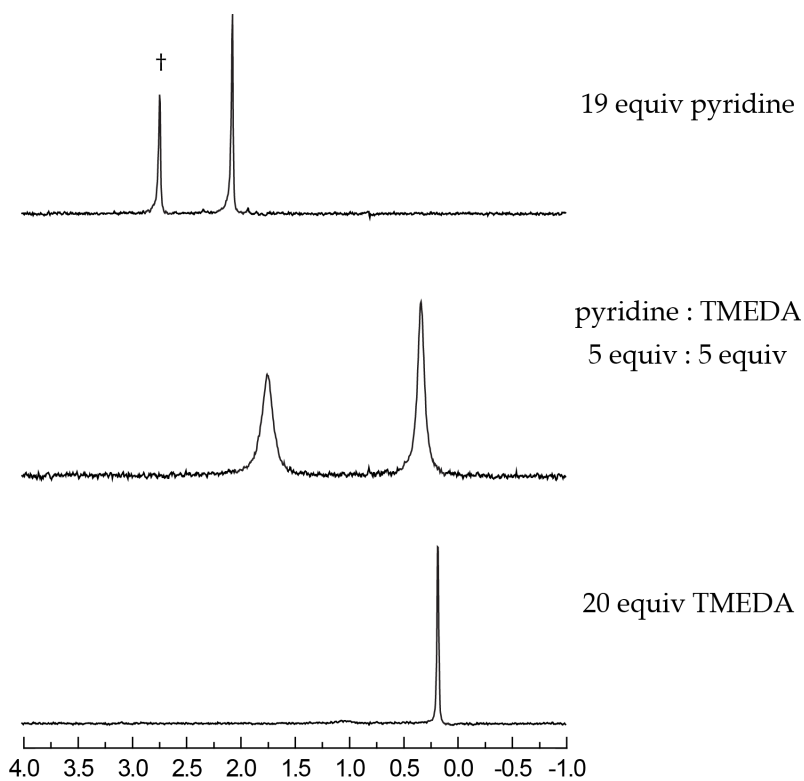


Figure AI.91. Solvent swap on 0.10 M of $[^6\text{Li}]1$ in pyridine and TMEDA with toluene as cosolvent at -40°C . At a 1:1 ligand ratio, there is broadening and minor inward shift of both the pyridine solvated tetramer and the TMEDA solvated dimer. This change indicates the possibility of mixed ligand aggregates. † denotes an aggregate present only at high pyridine concentration; it is assumed to be a highly solvated dimer.

Solvent Swap

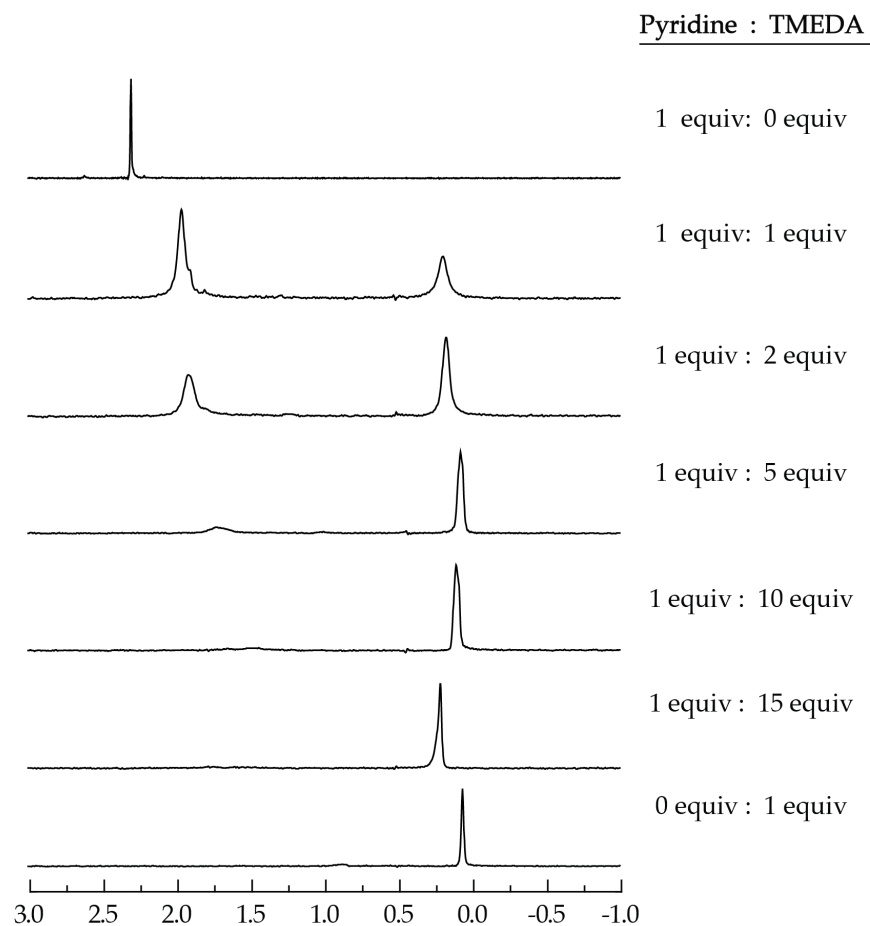


Figure AI.92. Solvent swap on 0.10 M of [^6Li]1 in pyridine and various TMEDA concentrations with toluene as cosolvent at $-80\text{ }^\circ\text{C}$. Addition of TMEDA causes both the appearance of a TMEDA solvated dimer around 0.2 ppm and a slight shift of the pyridine solvated tetramer. The slight shift may be due to incorporation of TMEDA into the tetramer. The chemical shift variation at increasing TMEDA concentration is due to a medium effect.

Solvent Swap

Pyridine : TMEDA

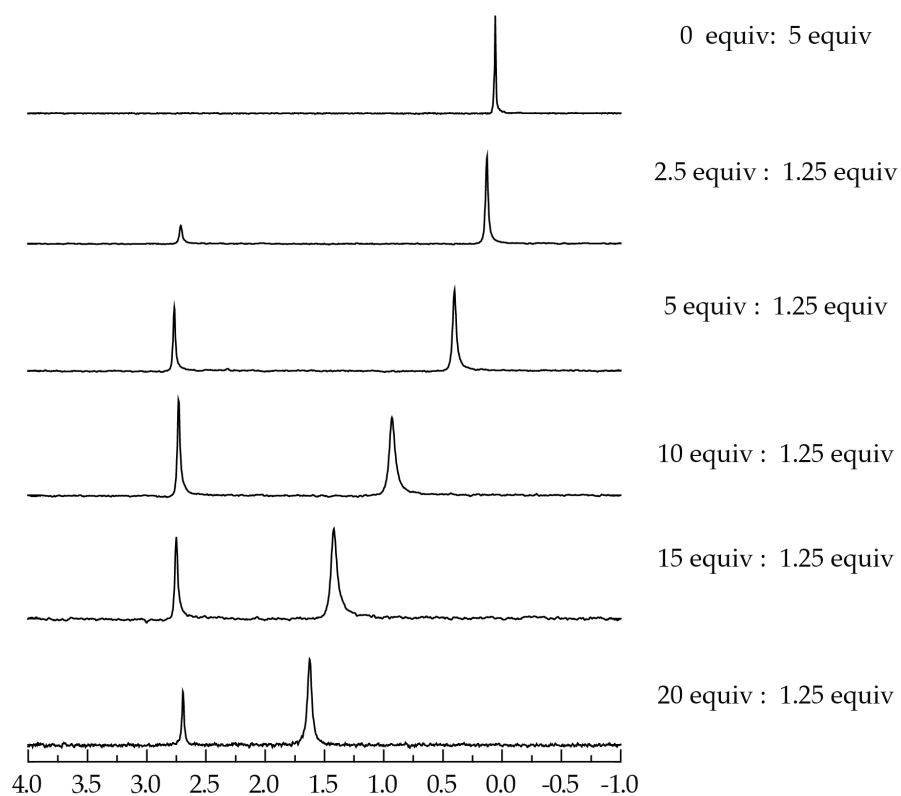


Figure AI.93. Solvent swap on 0.10 M of $[\text{}^6\text{Li}]_2$ in TMEDA and various pyridine concentrations with toluene as cosolvent at $-40\text{ }^\circ\text{C}$. Addition of pyridine causes both the appearance of a pyridine solvated tetramer around 2.75 ppm and the migration of the TMEDA solvated dimer.

Solvent Swap

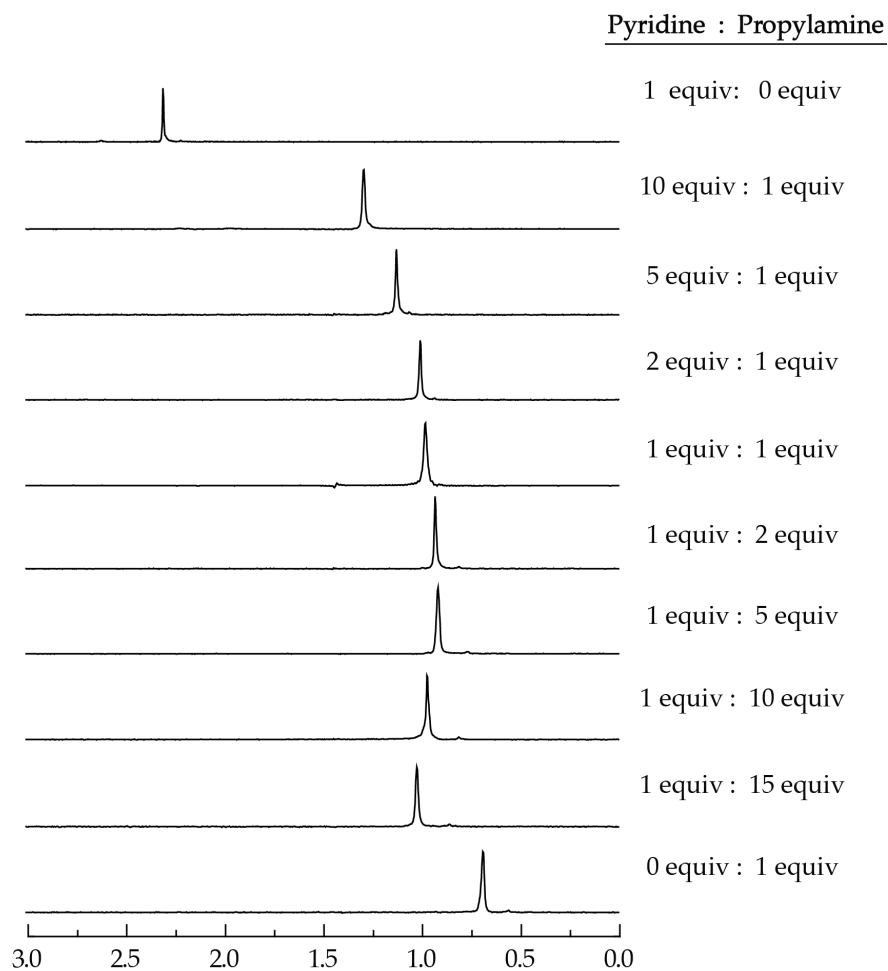


Figure AI.94. Solvent swap on 0.10 M of $[^6\text{Li}]\mathbf{1}$ in various pyridine and *n*-PrNH concentrations with toluene as cosolvent at $-80\text{ }^\circ\text{C}$. The chemical shift more closely resembles *n*-PrNH even at high pyridine concentrations. The medium dependent chemical shift is clearly demonstrated going from 1.0 equiv to 15 equiv of *n*-PrNH.

Solvent Swap

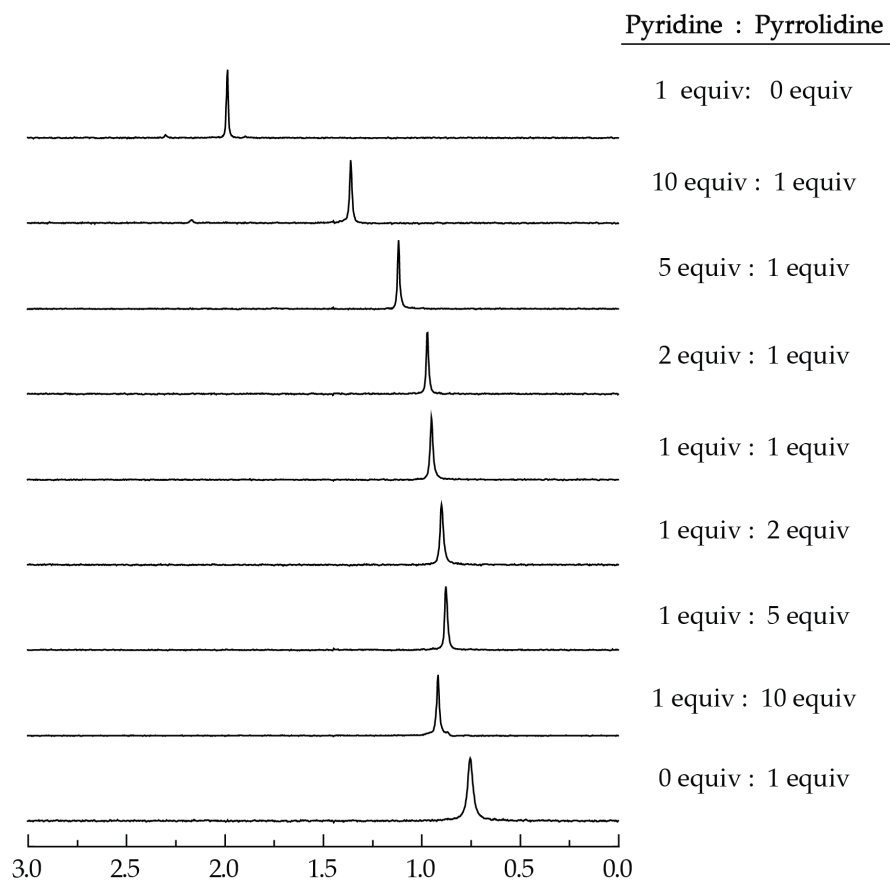


Figure AI.95. Solvent swap on 0.10 M of [^6Li]**1** in various pyridine and pyrrolidine concentrations with toluene as cosolvent at $-80\text{ }^\circ\text{C}$. The chemical shift more closely resembles pyrrolidine even at high pyridine concentrations. The medium dependent chemical shift is clearly demonstrated going from 1.0 equiv to 10 equiv of pyrrolidine.

Solvent Swap

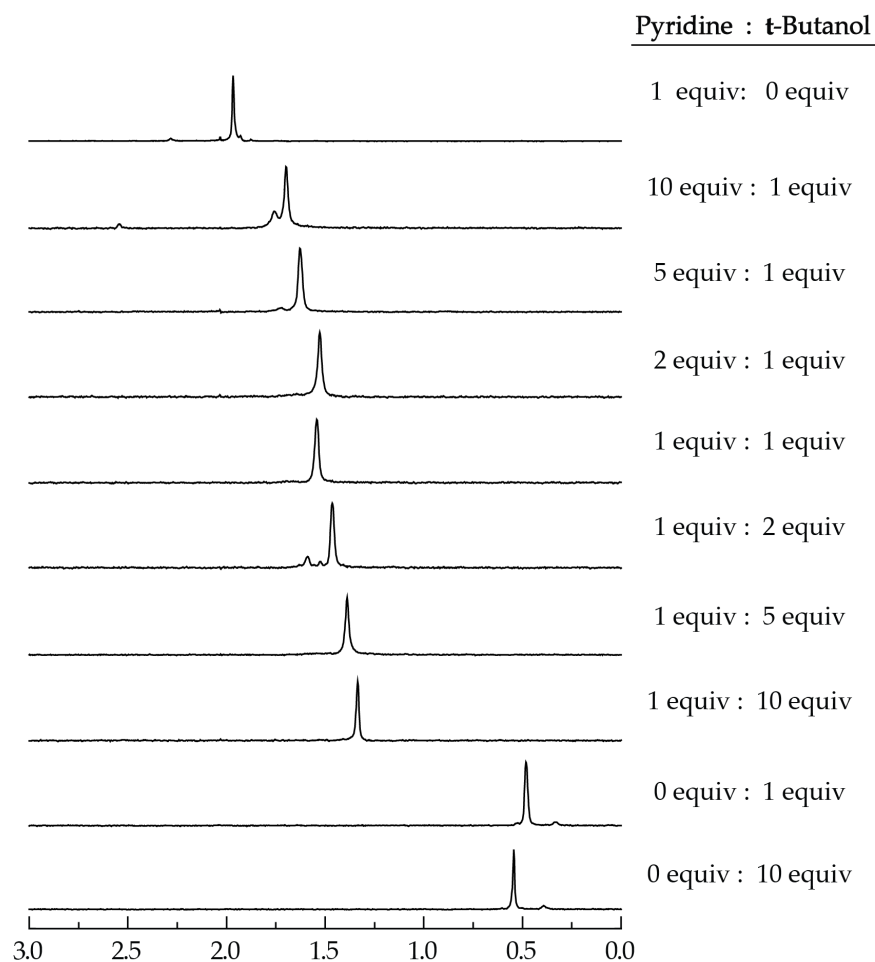


Figure AI.96. Solvent swap on 0.10 M of [⁶Li]1 in various pyridine and *t*-BuOH concentrations with toluene as cosolvent at -80 °C. The chemical shift more closely resembles pyridine even at high *t*-BuOH concentrations. The medium dependent chemical shift is barely present going from 1.0 equiv to 10 equiv of *t*-BuOH.

REFERENCES AND FOOTNOTES I

1. Czekaj, M.; Klein, S. I.; Guertin, K. R.; Gardner, C. J.; Zulli, A. L.; Pauls, H. W.; Spada, A. P.; Cheney, D. L.; Brown, K. D.; Colussi, D. J.; Chu, V.; Leadley, R. J.; Dunwiddie, C. T. *Bioorg. Med. Chem. Lett.* **2002**, *12*, 1667.
2. (a) Green, J. R. In *Science of Synthesis*; Georg Thieme Verlag: New York, 2005; Vol. 8a, pp 427-486. (b) Schetter, B.; Mahrwald, R. *Angew. Chem., Int. Ed.* **2006**, *45*, 7506. (c) Arya, P.; Qin, H. *Tetrahedron* **2000**, *56*, 917. (d) Caine, D. In *Comprehensive Organic Synthesis*; Trost, B. M.; Fleming, I., Eds.; Pergamon: New York, **1989**, Vol. 1, p 1. Martin, S. F. *Ibid.*, Vol. 1, pg. 475. (e) Plaquevent, J.-C.; Cahard, D.; Guillen, F.; Green, J. R. In *Science of Synthesis*; Georg Thieme Verlag: New York, 2005; Vol. 26, pp 463-511. (f) *Comprehensive Organic Functional Group Transformations II*; Katritzky, A. R.; Taylor, R. J. K., Eds.; Elsevier: Oxford, UK, 1995, pp. 834-835. (g) Cativiela, C.; Diaz-de-Villegas, M. D. *Tetrahedron: Asymmetry* **2007**, *18*, 569. (h) Woltermann, C. J.; Hall, R. W.; Rathman, T. *PharmaChem* **2003**, *2*, 4.
3. (a) McNeil, A. J.; Toombes, G. E. S.; Chandramouli, S. V.; Vanasse, B. J.; Ayers, T. A.; O'Brien, M. K.; Lobkovsky, E.; Gruner, S. M.; Marohn, J. A.; Collum, D. B. *J. Am. Chem. Soc.* **2004**, *126*, 5938. (b) McNeil, A. J.; Toombes, G. E. S.; Gruner, S. M.; Lobkovsky, E.; Collum, D. B.; Chandramouli, S. V.; Vanasse, B. J.; Ayers, T. A. *J. Am. Chem. Soc.* **2004**, *126*, 16559.
4. (a) Fraenkel, G.; Hsu, H.; Su, B. P. In *Lithium: Current Applications in Science, Medicine, and Technology*; Bach, R. O., Ed.; Wiley: New York, 1985; Chapter 19. (b) Günther, H. In *Advanced Applications of NMR to Organometallic Chemistry*; Gielen, M.; Willem, R.; Wrackmeyer, B., Eds.; Wiley & Sons: New York, 1996; pp 247-290. (c) Collum, D. B. *Acc. Chem. Res.* **1993**, *26*, 227. (d) Lucht, B. L.; Collum, D. B. *Acc. Chem. Res.* **1999**, *32*, 1035.
5. (a) Jackman, L. M.; Bortiatynski, J. *Adv. Carbanion Chem.* **1992**, *1*, 45.

6. (a) Jackman, L. M.; Lange, B. C. *Tetrahedron* **1977**, *33*, 2737. (b) Jackman, L. M.; DeBrosse, C. W. *J. Am. Chem. Soc.* **1983**, *105*, 4177. (c) Jackman, L. M.; Smith, B. D. *J. Am. Chem. Soc.* **1988**, *110*, 3829. (d) Jackman, L. M.; Chen, X. *J. Am. Chem. Soc.* **1992**, *114*, 403. (e) Jackman, L. M.; Rakiewicz, E. F.; Benesi, A. J. *J. Am. Chem. Soc.* **1991**, *113*, 4101. (f) Jackman, L. M.; Chen, X. *J. Am. Chem. Soc.* **1997**, *119*, 8681. (g) Jackman, L. M.; Petrei, M. M.; Smith, B. D. *J. Am. Chem. Soc.* **1991**, *113*, 3451.

7. (a) Streitwieser, A.; Wang, D. Z. *J. Am. Chem. Soc.* **1999**, *121*, 6213. (b) Leung, S. S.-W.; Streitwieser, A. *J. Org. Chem.* **1999**, *64*, 3390. (c) Wang, D. Z.; Kim, Y.-J.; Streitwieser, A. *J. Am. Chem. Soc.* **2000**, *122*, 10754. (d) Kim, Y.-J.; Streitwieser, A. *Org. Lett.* **2002**, *4*, 573. (e) Kim, Y.-J.; Wang, D. Z. *Org. Lett.* **2001**, *3*, 2599. (f) Streitwieser, A.; Leung, S. S.-W.; Kim, Y.-J. *Org. Lett.* **1999**, *1*, 145. (g) Abbotto, A.; Leung, S. S.-W.; Streitwieser, A.; Kilway, K. V. *J. Am. Chem. Soc.* **1998**, *120*, 10807. (h) Leung, S. S.-W.; Streitwieser, A. *J. Am. Chem. Soc.* **1998**, *120*, 10557. (i) Abu-Hasanayn, F.; Streitwieser, A. *J. Org. Chem.* **1998**, *63*, 2954. (j) Abu-Hasanayn, F.; Streitwieser, A. *J. Am. Chem. Soc.* **1996**, *118*, 8136. (k) Gareyev, R.; Ciula, J. C.; Streitwieser, A. *J. Org. Chem.* **1996**, *61*, 4589. (l) Abu-Hasanayn, F.; Stratakis, M.; Streitwieser, A. *J. Org. Chem.* **1995**, *60*, 4688. (m) Dixon, R. E.; Williams, P. G.; Saljoughian, M.; Long, M. A.; Streitwieser, A. *Magn. Reson. Chem.* **1991**, *29*, 509.

8. Streitwieser, A. *J. Org. Chem.* **2009**, *74*, 4433.

9. Pospisil, P. J.; Wilson, S. R.; Jacobsen, E. N. *J. Am. Chem. Soc.* **1992**, *114*, 7585.

10. (a) Biddle, M. M.; Reich, H. J. *J. Org. Chem.* **2006**, *71*, 4031. (b) Reich, H. J. *J. Org. Chem.* **2012**, *77*, 5471. (c) Kolonko, K. J.; Guzei, I. A.; Reich, H. J. *J. Org. Chem.* **2010**, *75*, 6163.

11. (a) Arnett, E. M.; Moe, K. D. *J. Am. Chem. Soc.* **1991**, *113*, 7288. (b) Arnett, E. M.; Fisher, F. J.; Nichols, M. A.; Ribeiro, A. A. *J. Am. Chem. Soc.* **1990**, *112*, 801. (c) Seebach, D.; Bauer, von W. *Helv. Chim. Acta* **1984**, *67*, 1972. (d) Shobatake, K.; Nakamoto, K. *Inorg. Chim. Acta* **1980**, *4*, 485. (e) den Besten, R.; Harder, S.;

Brandsma, L. J. *Organomet. Chem.* **1990**, 385, 153. (f) Halaska, V.; Lochmann, L. *Collect. Czech. Chem. Commun.* **1973**, 38, 1780. (g) Golovanov, I. B.; Simonov, A. P.; Priskunov, A. K.; Talalseva, T. V.; Tsareva, G. V.; Kocheshkov, K. A. *Dokl. Akad. Nauk. SSSR* **1963**, 149, 835. (h) Simonov, A. P.; Shigorin, D. N.; Talalseva, T. V.; Kocheshkov, K. A. *Bull. Acad. Sci. USSR Div. Chem. Sci.* **1962**, 6, 1056. (i) Armstrong, D. R.; Davies, J. E.; Davies, R. P.; Raithby, P. R.; Snaith, R.; Wheatley, A. E. H. *New J. Chem.* **1999**, 35. (j) Nichols, M. A.; Leposa, C. *Abstracts of Papers*, 38th Central Regional Meeting of the American Chemical Society, Frankenmuth, MI, May 16-20, 2006; American Chemical Society: Washington, D. C. (k) Lochmann, L.; Lim, D. J. *Organomet. Chem.* **1973**, 50, 9. (l) Zune, C.; Jerome, R. *Prog. Polymer Sci.* **1999**, 24, 631. (m) Baskaran, D. *Prog. Polym. Sci.* **2003**, 28, 521. (n) Suzuki, M.; Koyama, H.; Noyori, R. *Bull. Chem. Soc. Jpn.* **2004**, 77, 259. (o) Suzuki, M.; Koyama, H.; Noyori, R. *Tetrahedron* **2004**, 60, 1571.

12. Job, P. *Ann. Chim.* **1928**, 9, 113.

13. (a) Gil, V. M. S.; Oliveira, N. C. *J. Chem. Educ.* **1990**, 67, 473. (b) Huang, C. Y. *Method Enzymol.* **1982**, 87, 509. (c) Hirose, K. *J. Incl. Phenom.* **2001**, 39, 193. (d) Likussar, W.; Boltz, D. F. *Anal. Chem.* **1971**, 43, 1265.

14. Review on Method of Continuous Variation in organometallic chemistry: Renny, J. S.; Tomasevich, L. L.; Tallmadge, E. H.; Collum, D. B. submitted for publication.

15. Weingarten, H.; Van Wazer, J. R. *J. Am. Chem. Soc.* **1965**, 87, 724.

16. Goralski, P.; Legoff, D.; Chabanel, M. *J. Organomet. Chem.* **1993**, 456, 1.

17. Desjardins, S.; Flinois, K.; Oulyadi, H.; Davoust, D.; Giessner-Prettre, C.; Parisel, O.; Maddaluno, J. *Organometallics* **2003**, 22, 4090.

18. Günther, H. *J. Braz. Chem. Soc.* **1999**, 10, 241.

19. Kissling R. M.; Gagne, M. R. *J. Org. Chem.* **2001**, *66*, 9005.
20. (a) Liou, L. R.; McNeil, A. J.; Ramirez, A.; Toombes, G. E. S.; Gruver, J. M.; Collum, D. B. *J. Am. Chem. Soc.* **2008**, *130*, 4859. (b) Gruver, J. M.; Liou, L. R.; McNeil, A. J.; Ramirez, A.; Collum, D. B. *J. Org. Chem.* **2008**, *73*, 7743. (c) McNeil, A. J.; Collum, D. B. *J. Am. Chem. Soc.* **2005**, *127*, 5655. (d) Liou, L. R.; McNeil, A. J.; Toombes, G. E. S.; Collum, D. B., *J. Am. Chem. Soc.* **2008**, *130*, 17334.
21. (a) De Vries, T. S.; Goswami, A.; Liou, L. R.; Gruver, J. M.; Jayne, E.; Collum, D. B. *J. Am. Chem. Soc.* **2009**, *131*, 13142. b) For application of MCV to polyolithiated lithium phenolates, see: H. Nakajima, M. Yasuda, A. Baba, *J. Chem. Soc., Dalton Trans.* **2012**, *41*, 6602.
22. Abbreviations used are as follows: TMEDA = *N,N,N',N'*-tetramethylethylenediamine; DMA = *N,N*-dimethylacetamide; DMF = *N,N*-dimethylformamide; DMSO = dimethylsulfoxide; DMPU = *N,N'*-dimethylpropyleneurea; NMP = *N*-methylpyrrolidone
23. After surveying a subset of the community, we have chosen to refer to $(\text{LiX})_n$ and $(\text{LiX})_m(\text{LiX}')_n$ as a “homoaggregate” and “heteroaggregate”, respectively, and reserve the term “mixed aggregate” for $(\text{LiX})_m(\text{LiY})_n$.
24. Romesberg, F. E.; Bernstein, M. P.; Gilchrist, J. H.; Harrison, A. T.; Fuller, D. J.; Collum, D. B. *J. Am. Chem. Soc.* **1993**, *115*, 3475.
25. (a) Arvidsson, P. I.; Ahlberg, P.; Hilmersson, G. *Chem. Eur. J.* **1999**, *5*, 1348. (b) Bauer, W. *J. Am. Chem. Soc.* **1996**, *118*, 5450. (c) Bauer, W.; Griesinger, C. *J. Am. Chem. Soc.* **1993**, *115*, 10871. (d) DeLong, G. T.; Pannell, D. K.; Clarke, M. T.; Thomas, R. D. *J. Am. Chem. Soc.* **1993**, *115*, 7013. (e) Thomas, R. D.; Clarke, M. T.; Jensen, R. M.; Young, T. C. *Organometallics* **1986**, *5*, 1851. (f) Bates, T. F.; Clarke, M. T.; Thomas, R. D. *J. Am. Chem. Soc.* **1988**, *110*, 5109. (g) Fraenkel, G.; Hsu, H.; Su, B. M. In *Lithium: Current Applications in Science, Medicine, and Technology*;

Bach, R. O., Ed.; Wiley: New York, 1985; pp 273-289. (h) Heinzer, J.; Oth, J. F. M.; Seebach, D. *Helv. Chim. Acta* **1985**, *68*, 1848. (i) Fraenkel, G.; Henrichs, M.; Hewitt, J. M.; Su, B. M.; Geckle, M. J. *J. Am. Chem. Soc.* **1980**, *102*, 3345. (j) Lucht, B. L.; Collum, D. B. *J. Am. Chem. Soc.* **1996**, *118*, 3529. (k) Knorr, R.; Menke, T.; Ferchland, K.; Mahlstäubl, J.; Stephenson, D. S. *J. Am. Chem. Soc.* **2008**, *130*, 14179.

26. Standard ethereal ligands have been observed coordinated to lithium ion in the slow exchange limit only rarely and only at very low temperatures. Leading references: (a) Arvidsson, P. I.; Davidsson, Ö. *Angew. Chem., Int. Ed. Engl.* **2000**, *39*, 1467. (b) Sikorski, W. H.; Reich, H. J. *J. Am. Chem. Soc.* **2001**, *123*, 6527. (c) Lucht, B. L.; Collum, D. B. *J. Am. Chem. Soc.* **1994**, *116*, 6009.

27. Remenar, J. F.; Lucht, B. L.; Collum, D. B. *J. Am. Chem. Soc.* **1997**, *119*, 5567.

28. For discussion and leading reference to the influence of mixed solvation on organolithium structure and reactivity, see: Qu, B.; Collum, D. B. *J. Am. Chem. Soc.* **2006**, *128*, 9355.

29. Cases in which the reactivity of RLi/polyamine mixtures depend on cosolvent may implicate either correlated or competitive solvation. Wu, S.; Lee, S.; Beak, P. *J. Am. Chem. Soc.* **1996**, *118*, 715. Zarges, W.; Marsch, M.; Harms, K.; Boche, G. *Chem. Ber.* **1989**, *122*, 2303. Karsch, H. H.; Appelt, A.; Mueller, G. *Organometallics* **1985**, *4*, 1624. Marsais, F.; Quéguiner, G. *Tetrahedron* **1983**, *39*, 2009. Chadwick, D. J.; Willbe, C. *J. Chem. Soc., Perkin Trans. I* **1977**, 887. Meyers, A. I.; Avila, W. B. *Tetrahedron Lett.* **1980**, *21*, 3335. Cao, J. *Gaodeng Xuexiao Huazue Xuebao* **1989**, *10*, 1246. Ludt, R. E.; Hanger, C. R. *J. Org. Chem.* **1971**, *36*, 1607.

30. Representative examples of crystallographically determined mixed solvation: Zarges, W.; Marsch, M.; Harms, K.; Boche, G. *Chem. Ber.* **1989**, *122*, 2303. Karsch, H. H.; Appelt, A.; Mueller, G. *Organometallics* **1985**, *4*, 1624. Seebach, D.; Hässig, R.; Gabriel, J. *Helv. Chim. Acta* **1983**, *66*, 308. Boche, G.; Marsch, M.; Müller, A.; Harms, K. *Angew. Chem., Int. Ed. Engl.* **1993**, *32*, 1032.

31. (a) Deana, R. K.; Recklinga, A. M.; Chena, H.; Daweab, L. N.; Schneiderac, C. M.; Kozak, C. M. *Dalton Trans.* **2013**, 42, 3504. (b) Reed, D.; Barr, D.; Mulvey, R. E.; Snaith, R. *J Chem. Soc., Dalton Trans.* **1986**, 557.

32. (a) Jackman and coworkers described extensive studies of phenolate **3** in pyridine (ref 6b,f,g). Studies of electronic effects on phenolate aggregation include some pyridine solvates: (b) MacDougall, D. J.; Noll, B. C.; Kennedy, A. R.; Henderson, K. W. *J. Chem. Soc. Dalton Trans.* (2006), (15), 1875. (c) Also, see: Boyle, T. J.; Pedrotty, D. M.; Alam, T. M.; Vick, S. C.; Rodriguez, M. A. *Inorg. Chem.* **2000**, 39, 5133.

33. Reich, H. J.; Kulicke, K. J. *J. Am. Chem. Soc.* **1996**, 118, 273.

34. Some clarification is in order. We use “mixed solvation” to designate any species with two or more different coordination ligands and “cooperative solvation” to suggest a beneficial effect beyond statistical. We have reserved “correlated solvation” to more neutrally denote deviations from statistical without specific notation of antagonistic or protagonistic interactions: Rutherford, J. L.; Hoffmann, D.; Collum, D. B. *J. Am. Chem. Soc.* **2002**, 124, 264.

35. (a) Hoffmann, D.; Collum, D. B. *J. Am. Chem. Soc.* **1998**, 120, 5810. (b) Rutherford, J. L.; Hoffmann, D.; Collum, D. B. *J. Am. Chem. Soc.* **2002**, 124, 264.

36. (a) Bauer, W.; Klusener, P. A. A.; Harder, S.; Kanters, J. A.; Duisenberg, A. J. M.; Brandsma, L.; Schleyer, P. v. R. *Organometallics* **1988**, 7, 552. (b) Köster, H.; Thoennes, D.; Weiss, E. *J. Organomet. Chem.* **1978**, 160, 1. (c) Teclé, B.; Ilsley, W. H.; Oliver, J. P. *Organometallics* **1982**, 1, 875. (d) Harder, S.; Boersma, J.; Brandsma, L.; Kanters, J. A. *J. Organomet. Chem.* **1988**, 339, 7. (e) Sekiguchi, A.; Tanaka, M. *J. Am. Chem. Soc.* **2003**, 125, 12684. (f) Linnert, M.; Bruhn, C.; Ruffer, T.; Schmidt, H.; Steinborn, D. *Organometallics* **2004**, 23, 3668. (g) Fraenkel, G.; Stier, M. *Prepr. Am. Chem. Soc., Div. Pet. Chem.* **1985**, 30, 586. (h) Ball, S. C.; Cragg-Hine, I.; Davidson, M. G.; Davies, R. P.; Lopez-Solera, M. I.; Raithby, P. R.; Reed, D.; Snaith, R.; Vogl,

E. M. *J. Chem. Soc., Chem. Commun.* **1995**, 2147. (i) Wehman, E.; Jastrzebski, J. T. B. H.; Ernsting, J.-M.; Grove, J. M.; van Koten, G. *J. Organomet. Chem.* **1988**, 353, 145. (j) Becker, J.; Grimme, S.; Fröhlich, R.; Hoppe, D. *Angew. Chem., Int. Ed.* **2007**, 46, 1645. (k) Bernstein, M. P.; Romesberg, F. E.; Fuller, D. J.; Harrison, A. T.; Williard, P. G.; Liu, Q. Y.; Collum, D. B. *J. Am. Chem. Soc.* **1992**, 114, 5100.

37. Lucht, B. L.; Collum, D. B. *J. Am. Chem. Soc.* **1995**, 117, 9863 and references cited therein.

38. (a) Burgess, J. *Metal Ions in Solution*, Wiley: New York, 1978. (b) Ohtaki, H.; Wada, H. *J. Soln. Chem.* **1966**, 70, 1502. (c) Ohtaki, H. *Pure Appl. Chem.* **1987**, 59, 1143. Ohtaki, H.; Radnai, T. *Chem. Rev.* **1993**, 93, 1157.

39. We briefly explored possible competitive binding of dipolar ligands (including acetonitrile) using IR spectroscopy^{35a} but found the resolution inadequate for our needs.

40. For representative IR spectroscopic studies of lithium ion solvation, see: (a) Xuan, X.; Zhang, H.; Wang, J.; Wang, H. *J. Phys. Chem. A* **2004**, 108, 7513; (b) Ala, J. M.; Edwards, H. G. M. *Vibrational Spectr.* **2000**, 24, 185. (c) Rouviere, J.; Dimon, B.; Brun, B.; Salvinien, J. *Comptes Rendus des Seances de l'Academie des Sciences, Serie C: Sciences Chimiques* **1972**, 274, 458. (d) Kloss, A. A.; Fawcett, W. R. *J. Chem. Soc., Faraday Trans.* **1998**, 94, 1587.

41. Arvidsson, P. I.; Hilmersson, G.; Ahlberg, P. *J. Am. Chem. Soc.* **1999**, 121, 1883.

42. Aubrecht, K. B.; Lucht, B. L.; Collum, D. B. *Organometallics* **1999**, 18, 2981.

43. Lucht, B. L.; Collum, D. B. *J. Am. Chem. Soc.* **1996**, 118, 2217.

44. Trimeric lithium phenolates have occasionally been observed in the solid state bearing pendant amine ligands. See, for example: (a) van der Schaaf, P. A.; Jastrzebski, J. T. B. H.; Hogerheide, M. P.; Smeets, W. J. J.; Spek, A. L.; Boersma, J.;

van Koten, G. *Inorg. Chem.* **1993**, *32*, 4111. (b) Boyle, T. J.; Pedrotty, D. M.; Alam, T. M.; Vick, S. C.; Rodriguez, M. A. *Inorg. Chem.* **2000**, *39*, 5133.

45. In previous manuscripts we examined the efficacy of parametric fits to distinguish the all-dimer A_2-AB-B_2 model from the A_2-AB-B_4 or A_2-AB-B models as well as the all tetramer $A_4-A_3B-A_2B_2-A_1B_3-B_4$ model from the $A_4-A_3B-A_2B_2-A_1B_3-B_2$ model with one homodimer (ref 3b and 20a).

46. For early discussions of steric effects on solvation and aggregation, see: Settle, F. A.; Haggerty, M.; Eastham, J. F. *J. Am. Chem. Soc.* **1964**, *86*, 2076. Lewis, H. L.; Brown, T. L. *J. Am. Chem. Soc.* **1970**, *92*, 4664. Brown, T. L.; Gerteis, R. L.; Rafus, D. A.; Ladd, J. A. *J. Am. Chem. Soc.* **1964**, *86*, 2135. For a discussion and more recent leading references, see: Zhao, P.; Collum, D. B. *J. Am. Chem. Soc.* **2003**, *125*, 14411.

47. (a) Reichardt, C. *Org. Process Res. Dev.* **2007**, *11*, 105. (b) Reichardt, C. *Chem. Rev.* **1994**, *94*, 2319. (c) Marcus, Y. *The Properties of Solvents*; Wiley: Chichester, New York, 1998.

48. Romesberg, F. E.; Gilchrist, J. H.; Harrison, A. T.; Fuller, D. J.; Collum, D. B. *J. Am. Chem. Soc.* **1991**, *113*, 5751.

49. (a) Seebach, D.; Laube, T.; Dunitz, J. D. *Helv. Chim. Acta* **1985**, *68*, 1373. For additional evidence of secondary amine participation in reactions of lithium dialkylamides: (b) Strazewski, P.; Tamm, C. *Helv. Chim. Acta* **1986**, *69*, 1041. (c) Seebach, D.; Aebi, J. D. *Helv. Chim. Acta* **1985**, *68*, 1507. (d) Seebach, D.; Miller, D. D.; Maller, S.; Weber, T. *Helv. Chim. Acta* **1985**, *68*, 949. (e) Duhamel, L.; Fouquay, S.; Plaquevent, J.-C. *Tetrahedron Lett.* **1986**, *27*, 4975. (f) Narita, T.; Imai, N.; Tsurata, T. *Bull. Soc. Chem. Japan* **1973**, *46*, 1242. (g) Creger, P. L. *J. Am. Chem. Soc.* **1970**, *92*, 1396. (h) Pfeffer, P. E.; Silbert, L. S.; Chirinko, J. M., Jr. *J. Org. Chem.* **1972**, *37*, 451. (i) Regan, A. C.; Staunton, J. J. *Chem. Soc., Chem. Commun.* **1983**, 764. (j) Barr, D.; Clegg, W.; Mulvey, R. E.; Snaith, R. J. *Chem. Soc., Chem. Commun.* **1984**, 469. (k) Fehr, C. *Angew. Chem., Int. Ed. Engl.* **1996**, *35*, 2567.

50. "Pharmaceuticals & Intermediates 1986-1997 Update"; Becker, A., Ed.; Becker Associates, 1997.

51. Studies of lithium salts of amino alcohols show a marked sensitivity of the exchange rates to the presence of trace alcohol: Bruneau, A. M.; Liou, L.; Collum, D. B. unpublished.

CHAPTER II

Method of Continuous Variation:

Characterization of Alkali Metal Enolates Using ^1H and ^{19}F NMR

Spectroscopies

Method of Continuous Variation:

Characterization of Alkali Metal Enolates Using ^1H and ^{19}F NMR Spectroscopies

Abstract

The method of continuous variation (MCV) in conjunction with ^1H and ^{19}F NMR spectroscopies was used to characterize lithium and sodium enolates solvated by *N,N,N',N'*-tetramethylethyldiamine (TMEDA) and tetrahydrofuran (THF). A strategy developed using lithium enolates was then applied to the more challenging sodium enolates. A number of sodium enolates solvated by TMEDA or THF afford exclusively tetramers. Evidence suggests that TMEDA chelates sodium on the cubic tetramers.

Introduction

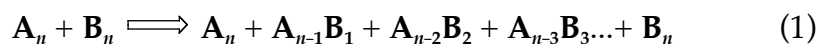
Carbon–carbon bond formations using metal enolates are ubiquitous. A recent survey of large scale procedures carried out over several decades at Pfizer revealed that 44% of these C–C bond formations involved metal enolates.¹ Although lithium enolates dominate the field, metal enolates bearing a wide range of counter ions proliferate.² Sodium enolates, for example, are suggested to be decidedly more reactive than their lithium counterparts.^{2f} However, they are less commonly used in synthesis for several reasons. The lower stability and solubility of *n*-butylsodium (*n*-BuNa)³ and sodium amides⁴ when compared with *n*-butyllithium (*n*-BuLi) and lithium amides make sodium enolates less accessible. Only weakly basic sodium hexamethyldisilazide,⁵ sodium alkoxides,⁶

and sodium hydride are used routinely. Moreover, empirical studies have suggested that, with few exceptions,⁷ the putative greater reactivity imparted by sodium relative to lithium frequently comes at the cost of lower selectivities. Nonetheless, sodium enolates maintain an important niche.^{8,9}

We became interested in studying the influence of aggregation and solvation on the reactivity of sodium enolates with the aim of providing structural and mechanistic support to synthetic applications. Although few sodium enolates have been characterized crystallographically,¹⁰ there is no reason to doubt that further progress could be made. X-ray structures of sodium phenolates (isostructural analogues of enolates) reveals a dominance of cubic tetramers,¹¹ although other forms have occasionally appeared.¹² The challenge of determining solution structures is acute, however. The absence of detectable M–O scalar coupling that plagues all NMR spectroscopic studies of metal enolates is exacerbated by the highly quadrupolar ²³Na nucleus,¹³ rendering the broad sodium resonances of little or no diagnostic value.^{14,15} In what were ambitious and pioneering studies by Zook¹⁶ and Hauser,¹⁷ colligative measurements of relatively stable sodium enolates suggested that they aggregate in solution, but the measured aggregation numbers included non-integer values spanning a wide range. In general, colligative measurements are poorly suited for studying mixtures and can be highly suspect owing to potentially undetectable impurities.^{18,19} Diffusion-ordered NMR spectroscopy (DOSY) explored extensively by Williard²⁰ in organolithium chemistry could be brought to bear on organosodium chemistry, but there are no studies reported to date. Of course, computational chemists have attempted to fill in the experimentally elusive

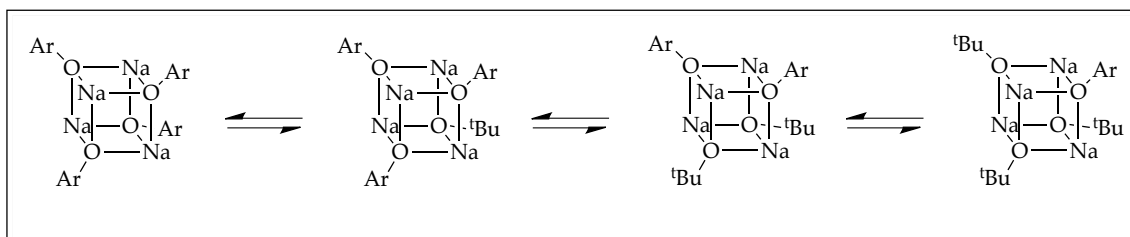
details,²¹ but computational data offers a nice complement to, not a substitute for, experimental data.²²

We wondered whether the method of continuous variation (MCV)²³ could be used to characterize sodium enolates. The idea is simple: mixing two salts of unknown aggregation states denoted as \mathbf{A}_n and \mathbf{B}_n (eq 1) affords an ensemble of homo- and heteroaggregates manifesting spectroscopic fingerprints and concentration dependencies that are highly characteristic of the overall aggregation number, n . We have used such a strategy in conjunction with ^6Li NMR spectroscopy to characterize over 100 enolate-solvent combinations.²⁴

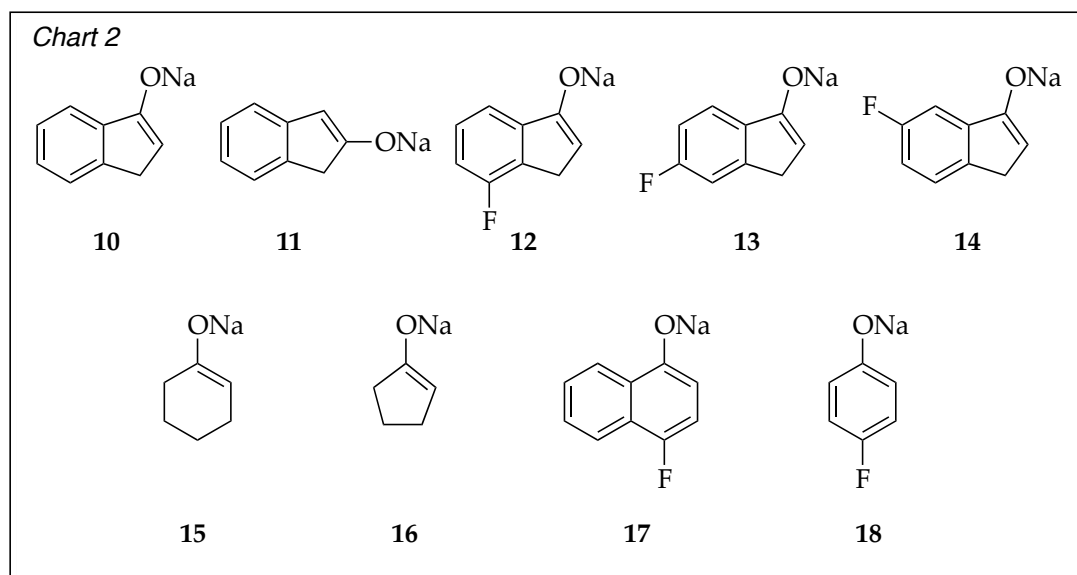
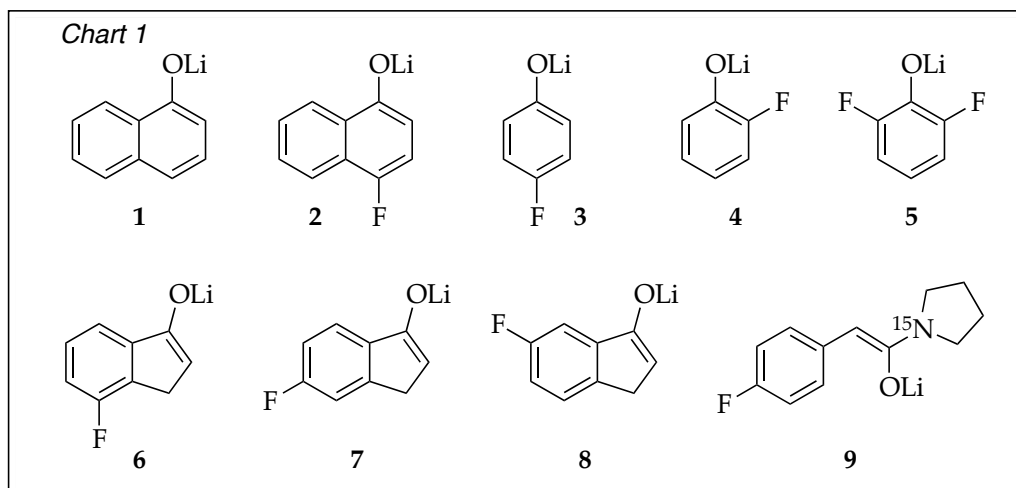


Can this same strategy be used with sodium enolates? Certainly not using ^{23}Na NMR spectroscopy but possibly with a more NMR-friendly nucleus. We took a cue from the seminal study of Gagne and coworkers in which ^1H NMR spectroscopy was used to characterize an ensemble of tetrameric aggregates derived from sodium *tert*-butoxide and sodium phenolates (Scheme 1; Ar = 4-*tert*-butylphenyl).²⁵ This strategy, combined with detailed studies of their concentration dependencies with the application of MCV, could be used to characterize sodium enolates.

Scheme 1



We describe herein using MCV in conjunction with ^1H and ^{19}F NMR spectroscopies to determine the aggregation state of alkali metal enolates. To develop tactics and strategies, we examined lithium enolates (Chart 1) with well-documented solution structures and behaviors demonstrated in previous studies.²⁴ We then applied the methods to characterize the sodium enolates in Chart 2, focusing on synthetically important N,N,N',N' -tetramethylethylenediamine (TMEDA) and tetrahydrofuran (THF) solvates. Several sodium phenolates are included owing to their ease of preparation and convenient tagging with fluoro moieties as well as their central roles in pharmaceutically important O-alkylations.²⁶ ^1H NMR spectroscopy proves more effective than ^{19}F NMR spectroscopy in most instances.²⁷ Despite an emphasis in this study on methods, even the preliminary results revealed that the least stable sodium enolates **15** and **16** are structurally complex in THF, and TMEDA-solvated enolates are quite different for sodium and lithium.²⁸



Results

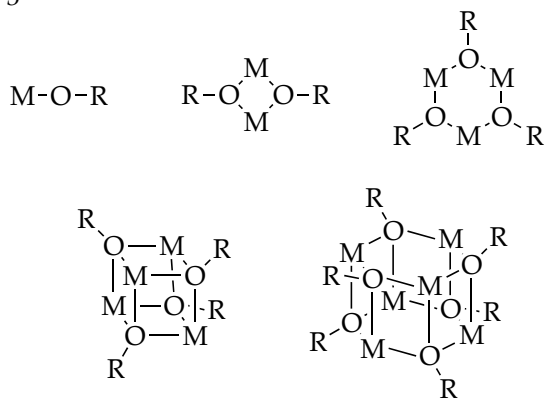
Sodium Bases. We sought sodium bases with optimal solubilities and reactivities. Highly reactive sodium bases such as *n*-BuNa³ and sodium diisopropylamide (NDA)⁴ present challenging technical problems. NDA can be prepared directly from sodium metal²⁹ but is most often prepared from *n*-BuLi/*t*-BuONa metal exchange.^{3b,30} The solubility properties of solvated or ligand-free NDA rendered recrystallization difficult, and the potential complexity arising

from the mixed salt protocol was especially troubling. Sodium tetramethylpiperidide (NaTMP) reported by Mulvey may work well but was not tested.^{4,31} We settled on two bases. The highly soluble sodium hexamethyldisilazide (NaHMDS) is easily prepared and purified.^{2,4} It is often the base of choice, but it is insufficiently basic for all applications (especially cycloalkanone-derived enolates). Sodium isopropylcyclohexylamide (NaICA)^{3b} has been prepared as a crystalline TMEDA solvate³² (which we consider too restrictive). We found, however, that unsolvated NaICA can be prepared as a powder and recrystallized to >90% purity. NMR spectra of NaICA solubilized with TMEDA shows two forms, which we presume to be *cis* and *trans* cyclic dimers based on analogy to lithium isopropylcyclohexylamide.³³ The only contaminant is the protic amine (<5%), which may be generated during NMR sample preparation. The protocols that we used for preparing ligand-free NaICA and NaHMDS as well as an improved procedure to prepare LiHMDS are described in the experimental section.

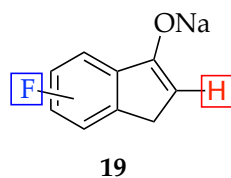
General strategy. Alkali metal enolates are prone to aggregate as illustrated generically in Chart 3.³⁴ The oppressively high symmetry, which causes these structural forms to appear deceptively simple and indistinguishable by NMR spectroscopy, is exacerbated when scalar coupling (such as ¹⁵N-⁶Li and ¹³C-⁶Li) cannot be used to show metal-ligand connectivities. We break the high symmetry by generating ensembles of homo- and heteroaggregates from enolate subunits **A** and **B** as illustrated in eq 1. Monitoring the homo- and heteroaggregates versus mole fraction of subunits **A** and **B** (X_A and X_B) reveals a distribution in which the number, symmetries, and mole fraction dependencies

are characteristic of the aggregation state. Application of MCV affords what is referred to colloquially as a Job Plot.²³ Subsequent examples are illustrative.

Chart 3



The prominent technical challenge is to obtain adequate spectroscopic resolution of the enolate ensembles. ⁶Li NMR spectroscopy suffices for lithium enolates and has been exploited extensively.²⁴ Sodium enolates, by contrast, require the monitoring of resonances emanating from organic fragments using ¹H or ¹⁹F NMR spectroscopies (**19**) rather than the monitoring of a nucleus within the O–M aggregate core. The obvious advantage of monitoring the vinyl proton (**19**; red) is that it requires no explicit tag. We were concerned at the outset (albeit incorrectly) that resolution might be inadequate and, in some cases, that complex splitting by other protons would be problematic. ¹⁹F NMR spectroscopy offered the potential for high resolution but required that at least one enolate contains a fluoro moiety (**19**; blue).



¹⁹F NMR spectroscopy. The methods for determining aggregation states are identical for ¹H or ¹⁹F NMR spectroscopy. We illustrate them with ¹⁹F NMR spectroscopy using an ensemble generated from phenolates **2** and **3** that *both* contain a fluorine tag. Having tags on both enolates is by no means necessary, but this starting point is pedagogically useful. Lithium phenolates **2** and **3** prove to be tetrameric and well behaved. Figure II.1 shows the ¹⁹F NMR spectrum of an approximate 1 : 1 mixture of **2** and **3**. We refer to groups of resonances stemming from a single subunit as envelopes. The two discrete envelopes of four resonances correspond to four of the five tetrameric aggregates containing that particular ¹⁹F tag in each envelope; each envelope is missing the complementary homoaggregate. Accounting for the number of ¹⁹F nuclei per aggregate affords the relative aggregate concentrations and reveals that the aggregate distribution reflected by Figure II.1 is nearly statistical. The slight difference between the two envelopes results in part from a minor deviation from the intended 1 : 1 stoichiometry. Seemingly systematic changes in the chemical shifts in Figure II.1 with the shifting composition are common but somewhat deceptive; the chemical shift orderings of the resonances vary with different enolate pairings.

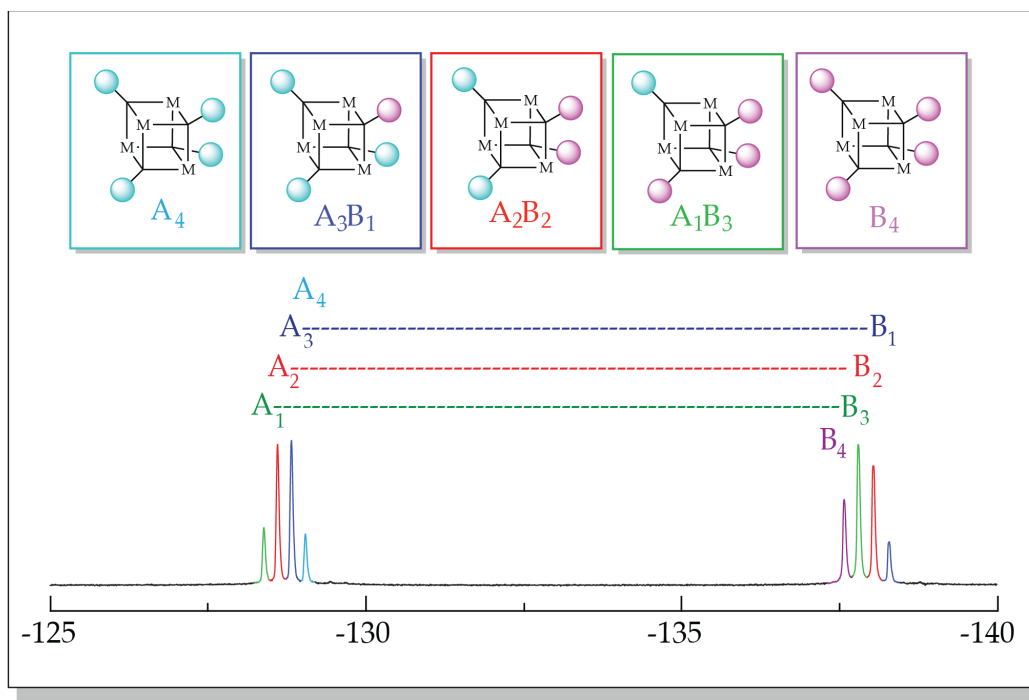


Figure II.1. ^{19}F NMR spectra of 1 : 1 mixture of tetrameric lithium phenolates **2** (**A**) and **3** (**B**) at 0.10 M total phenolate concentration in 0.50 M THF/toluene. The envelope of resonances correspond to subunit **A** (left) and subunit **B** (right). The color code indicates affiliation with the five homo- and heteroaggregates shown above.

Monitoring the ensemble of aggregates represented in Figure II.1 versus enolate mole fractions (X_{A} or X_{B}) at fixed total enolate concentration reveals the changing aggregate proportions (Figure II.2). Plotting the relative aggregate concentrations versus X_{A} affords the Job plot in Figure II.3.³⁵ The relative concentrations are determined by accounting for the differential number of ^{19}F nuclei per aggregate. When, as in this case, both subunits contain visible and well-resolved envelopes of resonances, simply adding the integrations for each aggregate from the two envelopes of resonances is expedient. The parametric fits shown have been described previously.²⁴ The mole fraction, X_{A} , is what we call the *measured* mole fraction—the mole fraction derived from the relative

integrations rather than the intended mole fractions. Ascertaining the mole fraction from the integrations renders the method robust by providing more accurate values for X_A as well as eliminating problems arising from unwanted impurities, standard experimental error, and multiple aggregation states. Using measured mole fraction is optional in this application but becomes imperative when one of the subunits is NMR silent (*vide infra*).

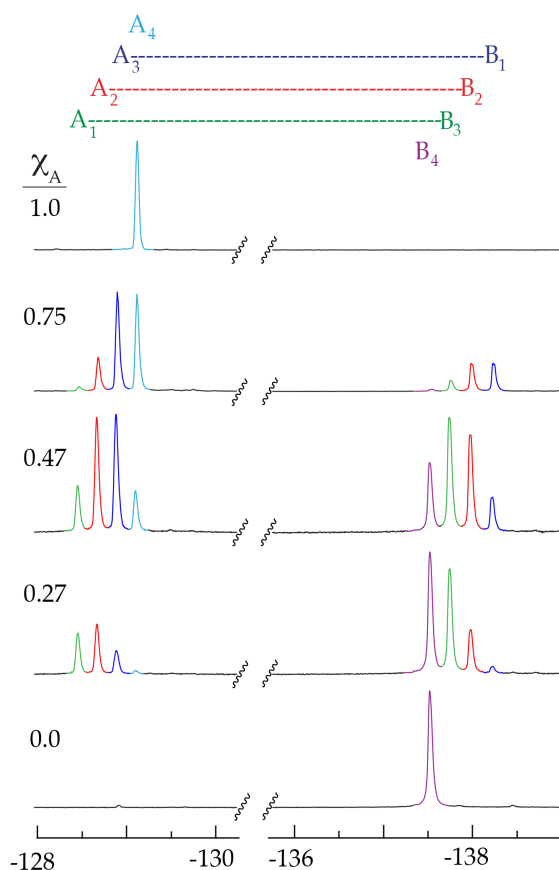


Figure II.2. ^{19}F NMR spectra of mixtures of tetrameric lithium phenolates **2** (**A**) and **3** (**B**) at 0.10 M total phenolate concentration in 0.50 M THF/toluene. The envelopes of resonances correspond to subunit **A** (left) and subunit **B** (right). The color code indicates affiliation with the five homo- and heteroaggregates shown above. The labeled mole fraction X_A corresponds to the measured mole fraction ascertained from the relative integrations.

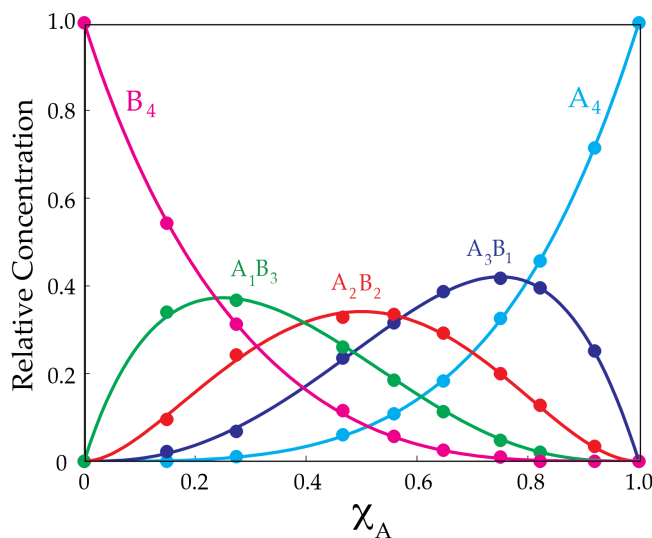


Figure II.3. Job plot showing the relative concentrations of tetrameric homo- and heteroaggregates versus measured mole fractions of **2** (X_A) for 0.10 M mixtures of lithium phenolates **2** (**A**) and **3** (**B**) in 0.50 M THF / toluene at -80 °C. (See Figure II.2.) All aggregates are represented by summing the integrations of each aggregate within the two envelopes of resonances.

The example above exploits two envelopes of resonances to view a *single* ensemble of aggregates, but this degeneracy is neither required nor necessarily desirable. Often only one of two envelopes of resonances is well resolved. More importantly, we envisioned the potential of using ^{19}F NMR spectroscopy to probe the structures of *unfluorinated* enolates. Using a single envelope of resonances, however, markedly impacts how the data are processed in ways that demand careful elaboration. We illustrate the point using a mixture of phenolates **1** and **3** in which only **3** has a fluorine tag. Monitoring the ensemble illustrated in Figure II.4 versus mole fraction affords the Job plot in Figure II.5. The logic is described as follows.

Given any aggregation state, n , there will be a total of $n + 1$ homo- and heteroaggregates but only n of them will be visible owing to the NMR silence of one homoaggregate. The left-hand y -intercept in Figure II.4 corresponds to

measured mole fraction $X_A = 0$ —enolate **A** is absent. In the limit of high **A**, however, the Job plot becomes more abstract. As X_A approaches unity and the spectroscopically silent A_4 homoaggregate becomes dominant, the only remaining *observable* species is the A_3B_1 heteroaggregate. As the real mole fraction of **A** approaches unity—as the added **B** becomes very low—the concentration of A_3B_1 approaches zero in the limit, but the *relative* concentration of A_3B_1 among the *observable* aggregates approaches unity. Moreover, the measured mole fraction X_A in Figure II.4 necessarily approaches only 0.75 because it represents the measured mole fraction of **A** among the *spectroscopically observable* aggregates.

Admittedly, the treatment represented in Figure II.5 has some abstraction. The good news is that the Job plot of a tetrameric enolate missing one homotetramer is visually and mathematically similar to a Job plot corresponding to a trimer,^{24,36} and that pattern holds true for all aggregates: n-mers take on the visual appearance and are mathematically treated as (n-1) -mers. The mathematical treatment for all aggregates is fully developed.²⁴ The asymmetry in Figure II.5 is caused by a minor deviation from statistical behavior. The maxima in Figure II.5 are all found at the appropriate measured mole fraction corresponding to their stoichiometries, consistent with standard Job plots.²³

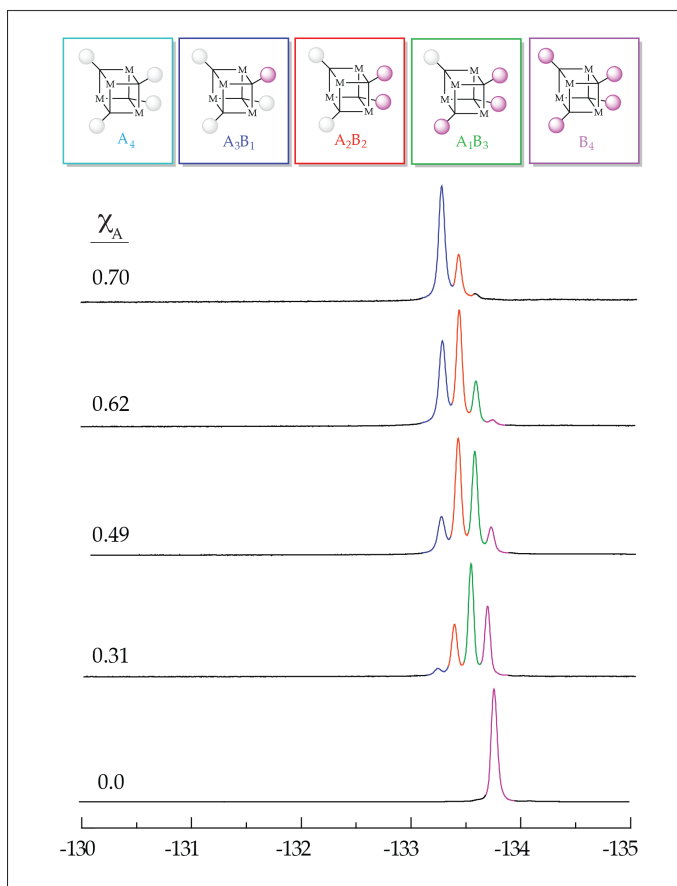


Figure II.4. ^{19}F NMR spectra of lithium phenolates **1** (**A**) and **3** (**B**) at 0.10 M total concentration in 0.50 M propylamine/toluene at $-80\text{ }^\circ\text{C}$. Only **B** contains a fluorine, rendering A_4 spectroscopically invisible.

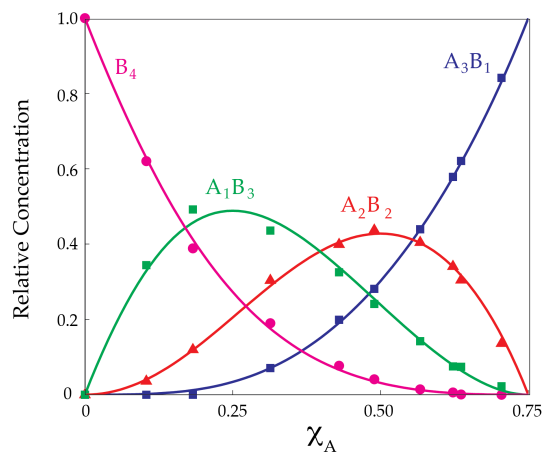


Figure II.5. Job plot showing the relative integrations of tetrameric homo- and heteroaggregates versus measured mole fractions of **1** (χ_{A}) for 0.10 M mixtures of lithium phenolates **1** (**A**) and **3** (**B**) in 0.50 M propylamine/toluene at $-80\text{ }^\circ\text{C}$. (See Figure II.4.) The relative concentrations include corrections for the number of ^{19}F nuclei in each aggregate. The curves result from a parametric fit.

^1H NMR spectroscopy. Ensembles monitored using ^1H NMR spectroscopy are treated as described above. We illustrate the point using sodium enolates, for which ^1H NMR spectroscopy proved especially successful. Figure II.6 shows representative spectra in which envelopes of resonances derived from sodium enolates **10** and **16** are well-resolved. Although unnecessary in this case, single-frequency decoupling is occasionally needed to sharpen the resonances. The representative Job plot derived from the two pairs of sodium enolates is shown in Figure II.7.

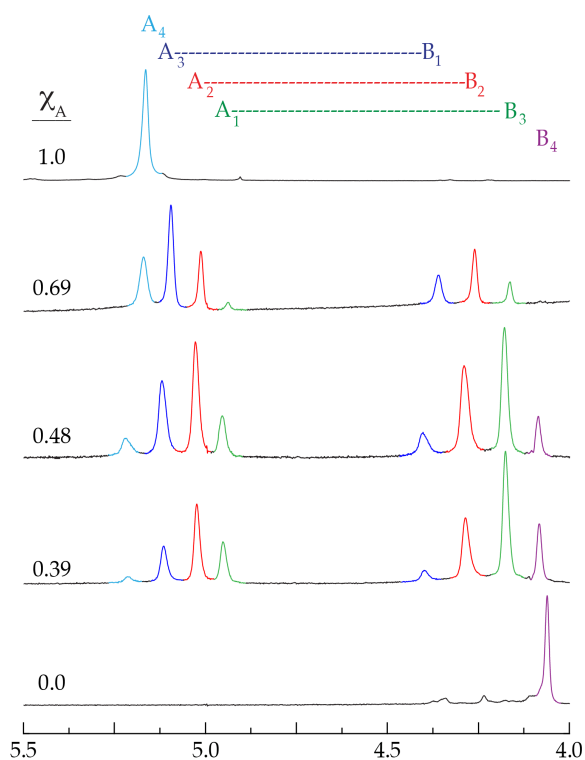


Figure II.6. ^1H NMR spectra of sodium enolates **10** (A) and **16** (B) at 0.10 M total concentration in 0.50 M TMEDA/toluene- d_8 at varying X_A recorded at $-80\text{ }^\circ\text{C}$.

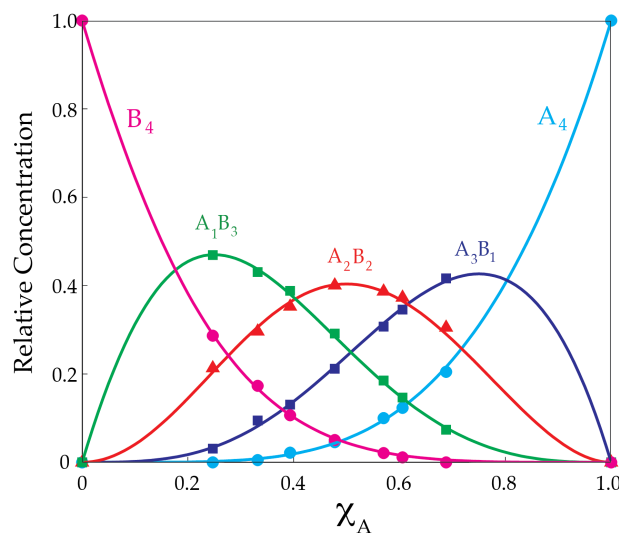
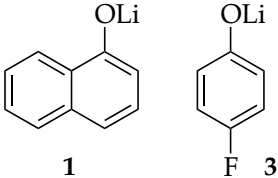


Figure II.7. Job plot showing the relative concentrations of tetrameric homo- and heteroaggregates versus measured mole fractions of **10** (χ_A) for 0.10 M mixtures of sodium enolates **10** (**A**) and **16** (**B**) in 0.50 M TMEDA/toluene- d_8 at -80 °C. The relative concentrations are obtained by simply summing the integrations of each aggregate represented in the two envelopes of resonances. (See Figure II.6.)

Lithium enolates and phenolates. The results for the lithium enolates and phenolates used to develop the protocols are listed in Table II.1. The spectra and affiliated Job plots are archived in supporting information. Previous studies using ^6Li NMR spectroscopy in conjunction with MCV have revealed the structures of the enolates in Chart 1 (except **6** and **9**). In several instances, the high sensitivity of ^{19}F NMR spectroscopy allowed us to detect minor concentrations of a previously undetected ensemble. Despite the large chemical shift window, the ^{19}F resonances broaden at low temperature owing in part to fast T_2 relaxation. For those cases in which one of two envelopes of resonances did not resolve, the unresolved envelope can be integrated and the contribution from the second homoaggregate extracted to provide a standard Job plot showing all species. In practice, this works in the case of dimers but is challenging for tetramers.

Table II.1. Characterization of lithium phenolates and enolates in solution using ^{19}F and ^1H NMR spectroscopies.

Substrates A_n/B_n	Ligand ^a	Structure	Nucleus
 1 3	<i>N</i> -methylpyrrolidone	tetramer ^b	^{19}F
	dimethylformamide		
	dimethylsulfoxide		
	<i>N,N'</i> -dimethylpropylene urea (DMPU)		
	<i>n</i> -PrNH ₂		
	Et ₂ NH		
	<i>n</i> -Pr ₂ NH		
	piperidine		
	<i>t</i> -butanol		
3/4	TMEDA	dimer	
3/5			
2/3			
6/8	THF	tetramer	^1H
	TMEDA	dimer	^1H and ^{19}F
7/8	THF	tetramer	^1H
	TMEDA	dimer	^1H and ^{19}F
7/9	TMEDA	dimer	^1H

^aTypically recorded using 5.0 equiv of ligand in toluene as the bulk solvent.

^bOnly **3** was visible by ^{19}F NMR, resulting in singly-tagged Job plots. In all other instances, both substrates are visible, affording Job plots showing all aggregates.

Sodium enolates and phenolates. We used exclusively ^1H NMR spectroscopy to characterize sodium enolates solvated by TMEDA and THF

(Table II.2) owing to the surprisingly poor resolution using ^{19}F NMR spectroscopy. A representative example is shown in Figures II.6 and II.7 above.

Table II.2. Sodium enolate tetramers characterized using the method of continuous variation and ^1H NMR spectroscopy.

Substrate pairs A_n/B_n	Ligand	Structure
10/16	TMEDA	tetramer
11/13		
12/15		
13/14		
10/11	THF	
11/12		
11/13		
11/14		
17/18		

TMEDA-solvated enolates showed a penchant for forming tetramers rather than the anticipated dimers (although in some cases an additional aggregate could be detected.³⁷) We demonstrated that TMEDA was bound as an η^2 (chelated) rather than η^1 (unchelated) ligand by showing that Me_2NEt and $\text{Me}_2\text{N-}n\text{-Bu}$, which are non-chelating TMEDA surrogates, failed to mimic TMEDA by affording intractable structures. Whether all sodium nuclei are chelated by TMEDA is discussed below.

The results for simple cycloalkanones were confusing at the outset. Enolization of cyclohexanone and cyclopentanone using either NaHMDS/TMEDA or NaICA/TMEDA afforded enolates **15** and **16** (Figure II.8a). By contrast, enolization with NaHMDS/THF afforded no detectable

enolate, and enolization with more basic NaICA/THF afforded broad mounds in the ^1H NMR spectra (Figure II.8b). Treating the cycloalkanones with NaICA/THF and subsequently adding TMEDA, however, afforded the TMEDA solvates cleanly (Figure II.8c), showing that enolizations in THF are adequate but the structural control is poor. The origins of the structural complexity are not known at this point.

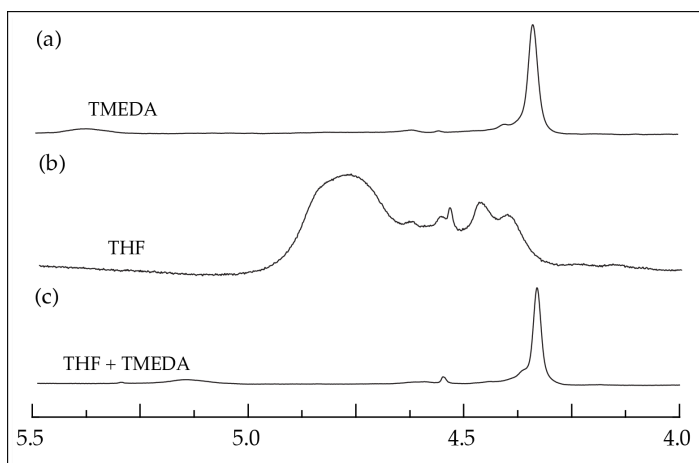


Figure II.8. ^1H NMR spectra recorded on 0.10 M **15** generated from 1.0 equiv NaICA in ligand / toluene- d_8 solution. The ligands are as follows: (a) 5.0 equiv TMEDA, (b) 5.0 equiv THF, and (c) 5.0 equiv THF with addition of 5.0 equiv TMEDA subsequent to enolization.

Discussion

Summary. We described a series of structural studies of alkali metal enolates using the method of continuous variation (MCV) in conjunction with ^1H and ^{19}F NMR spectroscopies. Lithium enolates known from previous studies to give high structural control were used to develop the methods (Chart 1) and to distinguish failed strategies from failed chemistry. We then directed our attention to the more challenging sodium enolates (Chart 2), which are

emblematic of metal salts bearing metal nuclei that resist NMR spectroscopic examination.

By example, a 1 : 1 mixture of two fluorine-tagged enolates afford two envelopes of ^{19}F resonances highly characteristic of an ensemble of enolate tetramers (Figure II.1). Each envelope shows four of the five homo- and heteroaggregates; the fifth is not observable because it lacks that particular tag. Monitoring the relative aggregate concentrations versus mole fraction (X) affords a series of spectra (Figure II.2) and an affiliated Job plot showing the relative concentrations of all five tetrameric forms (Figure II.3). Using ^1H NMR spectroscopy to monitor the enolate vinyl resonance affords analogous envelopes of resonances (Figure II.6) and Job plots (Figure II.7). The implicit assumption in all studies is that the formation of a near-statistical distribution of homo- and heteroaggregates reflects the structures of the homoaggregates from which the ensemble derives. Previous studies of lithium enolates show that two homoaggregated enolates of *differing* aggregation (dimer and tetramer, for example) either resist forming heteroaggregates altogether or form heteroaggregates non-statistically, which lead to the maxim "like aggregates with like."

Although the clearest examples stem from enolate pairs in which *both* subunits can be monitored spectroscopically, this is neither required nor our intent. Our long-term goal is to develop a library of enolates that are either tagged with fluoro moieties or have vinyl proton resonances that afford well-resolved envelopes of vinyl resonances when paired with *any* enolate regardless of how spectroscopically unfriendly it might be. Indeed, monitoring one envelope of resonances showing four of the five tetrameric aggregates—one

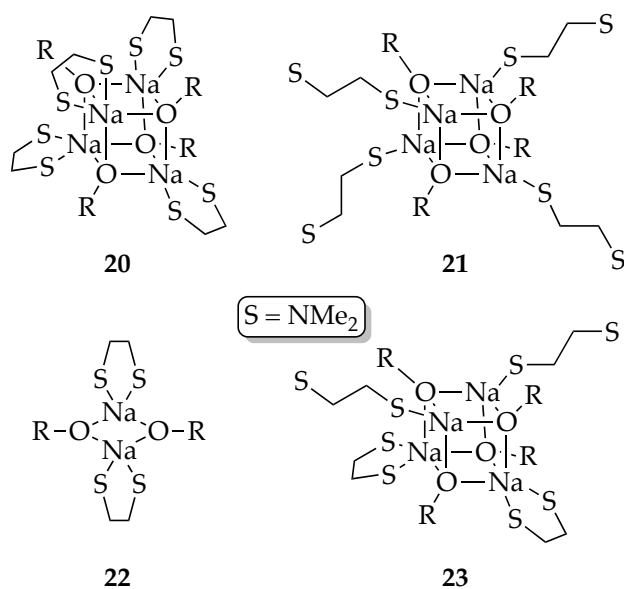
homoaggregate is spectroscopically invisible—affords an accompanying Job plot showing the dependencies of the four visible forms on mole fraction (Figure II.5). Although the Job plot in Figure II.5 is that of a tetrameric ensemble of lithium phenolates **1** and **3**, the missing aggregate renders it visually comparable to an ensemble of trimers and is treated as such mathematically. The nuances of the analysis are described in the results section.

¹H versus ¹⁹F NMR spectroscopy. We examined ¹⁹F NMR spectroscopy assuming that we might achieve superior spectroscopic resolution. ¹H NMR spectroscopy, by contrast, requires no explicit tagging of the substrates and ironically offered superior resolution to that of ¹⁹F NMR spectroscopy. In fact, sodium enolates could only be characterized using ¹H NMR spectroscopy. Although the comparisons of the enolates herein are by no means comprehensive, the fluorine tags, admittedly in relatively remote locations, have offered few advantages so far.

TMEDA-solvated sodium enolates. In contrast to lithium enolates in which TMEDA *invariably* affords chelated dimers from a wide range of enolates,^{24,38} the corresponding sodium enolates in Chart 2 proved to be tetrameric without exception. Putative unchelated (η^1) and chelated (η^2) enolates are illustrated in Chart 4. The small lithium nucleus forces the choice of η^2 -solvated dimers (akin to **22**) over the only sterically accessible tetrameric form, η^1 -solvated cubic Li–X tetramers (akin to **21**).³⁹ By contrast, the much larger sodium nucleus appears to support a chelated TMEDA on cubic Na–X tetramers (**20**) as evidenced in crystal structures.⁴⁰ The chelate is further evidenced by complete failures of Me₂NEt or Me₂N-*n*-Bu—TMEDA analogues lacking the

capacity to chelate—to afford anything tractable. The plot seemed to thicken when *N,N,N',N'*-tetramethylcyclohexanediamine (TMEDA), a TMEDA analog that appears to be incapable of forming η^1 complexes, afforded intractable results. Either TMEDA serves a dual role as an η^1 and η^2 ligand (**23**) or TMEDA suffers from other problems related to bite angle or steric demands.⁴¹

Chart 4



THF-solvated sodium enolates. Characterizations of the sodium indenolates solvated by THF proceeded smoothly. By contrast, the two generic homoaggregates of sodium enolates derived from cyclohexanone (**15**) and cyclopentanone (**16**) afforded broad mounds corresponding to the enolate vinyl protons. Although we initially thought that the enolization by sodium bases in THF had gone afoul, enolizations in THF/toluene with subsequent addition of TMEDA afforded TMEDA-solvated tetramers indistinguishable from samples prepared in TMEDA/toluene. Therefore, the broad mounds attest to structural

complexity—oligomerizations via enolate laddering^{12,42} or cube stacking may be occurring¹²—rather than decomposition during enolization. The consequences in synthesis are not knowable but possibly substantial.⁹ These results also attest to the relative efficacy of TMEDA to coordinate to sodium (albeit only qualitatively).

Conclusions

We have shown that by monitoring NMR-friendly nuclei in the organic fragment, we can use MCV to characterize sodium enolates. Those characterized to date illustrate primarily proof of principle. Nevertheless, the results suggest that putative high reactivities of sodium enolates have structural foundations distinct from their lithium counterparts. After years of studying organolithium chemistry, we have to extrapolate the principles derived from lithium to sodium with caution. Fundamental issues such as rigorously determined solvation numbers have yet to be addressed. Most importantly, we do not have a clue how many principles of structure and reactivity are shared by lithium and sodium salts. Are the synthetically less central sodium salts worth the effort and resources? Can principles of aggregation and solvation unlock potential applications of sodium enolates? We shall see.

Experimental Section

Reagents and Solvents. All substrates are commercially available. TMEDA, THF, and toluene were distilled from blue or purple solutions containing sodium benzophenone ketyl. Owing to the appearance of vinyl ethers from tetraglyme degradation in the ¹H NMR spectra, *no* tetraglyme was added to

dissolve the ketyl in toluene, resulting in a lighter blue color. Liquid substrates were distilled from 4 Å molecular sieves. (Some ketones decompose on exposure to molecular sieves for extended times.) NaHMDS,⁴ NaICA,^{4,32} and [⁶Li]LiHMDS⁴³ were prepared and recrystallized from modified literature procedures as described below. Air- and moisture-sensitive materials were manipulated under argon using standard glove box, vacuum line, and syringe techniques.

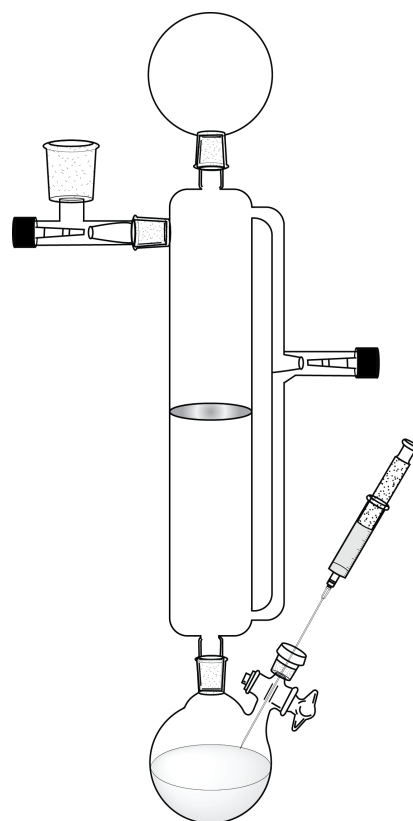
[⁶Li]Lithium hexamethyldisilazide.

Isoprene (8.0 mL, 0.080 mol) was dissolved in 30 mL dry dimethylethylamine (DMEA) and added over 1–2 h via syringe pump to a solution of lithium metal (1.11 g, 0.16 mol) and hexamethyldisilazane (HMDS, 25.8 g, 33.4 mL, 0.16 mol) in 80 mL DMEA at room temperature.

The reaction was run in the bottom of an apparatus with 250 mL round bottom flasks and a fine frit attached directly to a Schlenck line (inset).

The temperature was maintained below 30 °C to avoid darkening. When the solution turned yellow

at low temperature, the HMDS was consumed, and isoprene addition was stopped immediately to avoid further darkening. After the addition of isoprene, the mixture was stirred until the lithium metal was nearly consumed (up to 1 h). The apparatus was inverted to filter the solution, and then the solution was evaporated to dryness under vacuum for 6 h. DMEA had to be removed completely because it provides the LiHMDS with too much added solubility in



the subsequent pentane recrystallization. The white solid was transferred to an analogous coarse frit setup in a glovebox and returned to the Schlenk line. LiHMDS was dissolved in a minimum amount of pentane, crystallized slowly at $-78\text{ }^{\circ}\text{C}$, and filtered to remove the residual liquid. This procedure was repeated 3 times or until the solid was completely white. The solid was spectroscopically pure as described previously.⁴³

Sodium hexamethyldisilazide. Isoprene (8.0 mL, 80 mmol) was dissolved in 30 mL of dry DMEA and added over 1–2 h via syringe pump to a solution of sliced sodium metal (3.7 g, 160 mmol) and HMDS (25.8 g, 33.4 mL, 160 mmol) in 80 mL DMEA at room temperature. The reaction was run in the bottom of a swivel fine frit apparatus with 250 mL round bottom flasks, attached directly to a Schlenk line (picture). The temperature was maintained below $30\text{ }^{\circ}\text{C}$ to avoid darkening. If the cold solution turned yellow HMDS had been consumed, and the addition of isoprene addition was stopped immediately to avoid further darkening. After addition of isoprene a significant amount of sodium remained; the reaction was stirred for an additional 2–3 h. The frit was flipped, the solution was slowly filtered, and the solution was evaporated to dryness under vacuum for 6 h. The white solid was transferred to a coarse frit setup under inert atmosphere. NaHMDS was recrystallized from a minimum amount of DMEA (~30–50 mL), crystallized by cooling slowly in a dry ice/acetone bath, and filtered to remove the residual liquid. This procedure was repeated three times or until the solid was completely white and spectroscopically pure.⁵

Sodium isopropylcyclohexylamide (NaICA). Isoprene (16 mL, 160 mmol) was dissolved in 30 mL dry DMEA and added over 1–2 h via syringe pump to a solution of finely sliced sodium metal (7.36 g, 320 mmol) and cyclohexylisopropylamine (45.2 g, 320 mmol) in 80 mL DMEA at room temperature. Sodium dispersion is reportedly necessary to acquire a reasonable yield;⁴ we sliced the sodium thinly under inert atmosphere and obtained an acceptable amount of NaICA. The reaction was run in a 250 mL round bottom flask attached directly to a Schlenck line. Addition of isoprene resulted in a yellow solution and precipitation of the product. After the addition of isoprene was complete, the reaction was stirred for an additional 6–8 h and evaporated to dryness. A portion of the solid was transferred under inert atmosphere to a fine-frit swivel apparatus (see LiHMDS synthesis figure) and dissolved in DMEA. The frit was flipped and the solution was slowly filtered, then the solution was evaporated to dryness. In a glove box, approximately 3 g of the off-white solid was added to each of two centrifuge tubes (inset) for eventual compaction of a very fine powder. (Substantial crude solid remained for future crystallization.) Under continuous argon flow, the solid was dissolved in DMEA and concentrated to the point of turbidity. Cyclopentane (25 mL) was added, and the vessel cooled with a dry ice/acetone bath. The resulting suspension was centrifuged until a white cake formed, and the solution was removed via syringe. This procedure was repeated until the solution was colorless. The resulting white solid was dried under vacuum. Full NMR spectroscopic characterization included COSY, TOCSY, HSQC, HMBC and ROESY spectroscopies (supporting information). ¹³C (125 MHz, 0.50 M TMEDA / toluene-*d*₈) δ (isomer 1) 23.36, 27.08, 28.33, 39.04,



49.08, 80.92; (isomer 2) 25.73, 26.52, 28.05, 34.13, 43.72, 52.81 ppm.

NMR sample preparation. Individual stock solutions of substrates and base were prepared at room temperature. An NMR tube under vacuum was flame dried on a Schlenck line and allowed to return to room temperature. It was then backfilled with argon and placed in a $-78\text{ }^{\circ}\text{C}$ dry ice/acetone bath. The appropriate amounts of base and substrate were added sequentially via syringe. The tube was sealed under partial vacuum, stored in a $-86\text{ }^{\circ}\text{C}$ freezer, and carefully mixed prior to placement into the spectrometer. Each NMR sample contained 0.10 M total phenol and 0.10 M base.

NMR Spectroscopy. ^1H and ^{19}F NMR spectra were typically recorded at $-80\text{ }^{\circ}\text{C}$ (unless stated otherwise) on a 500 MHz spectrometer with the delay between scans set to $>5 \times T_1$ to ensure accurate integrations. Chemical shifts are reported relative to toluene (^1H) and fluorobenzene (^{19}F). The resonances were integrated using the standard software accompanying the spectrometers. After weighted Fourier transform with 64,000 points and phasing, line broadening was set between 0 and 0.30, and a baseline correction was applied when appropriate. Deconvolution was performed in the absolute intensity mode, with application of a drift correction using default parameters for contributions from Lorentzian and Gaussian line shapes. The mathematics underlying the parametric fits have been described in detail,²⁴ with minor modifications appearing in the supporting information of this paper.

Acknowledgments. We thank the National Institutes of Health (GM077167) and Sanofi–Aventis for direct support of this work.

APPENDIX II

Dimer Job Plots in TMEDA

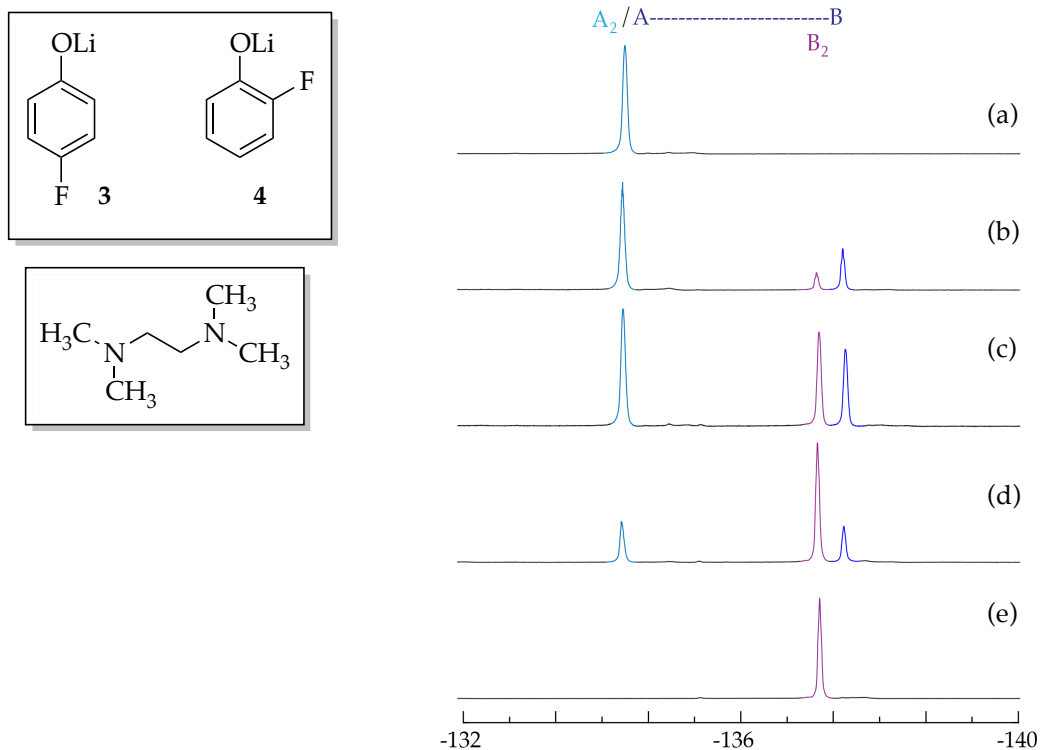


Figure AII.1. ^{19}F NMR spectra of 0.10 M solutions of $[^6\text{Li}]\mathbf{3}$ (**A**) and $[^6\text{Li}]\mathbf{4}$ (**B**) in 0.50 M TMEDA/toluene at $-80\text{ }^\circ\text{C}$. The measured mole fractions of **A** in (a)-(e) are 1.00, 0.62, 0.42, 0.19, and 0.00, respectively.

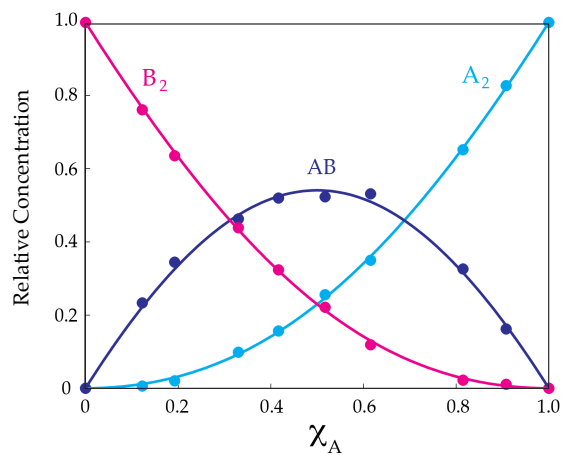


Figure AII.2. Job plot showing the relative integrations versus the measured mole fractions of **A** for 0.10 M mixtures of $[^6\text{Li}]\mathbf{3}$ (**A**) and $[^6\text{Li}]\mathbf{4}$ (**B**) in 0.50 M TMEDA/toluene at $-80\text{ }^\circ\text{C}$.

Dimer Job Plots in TMEDA

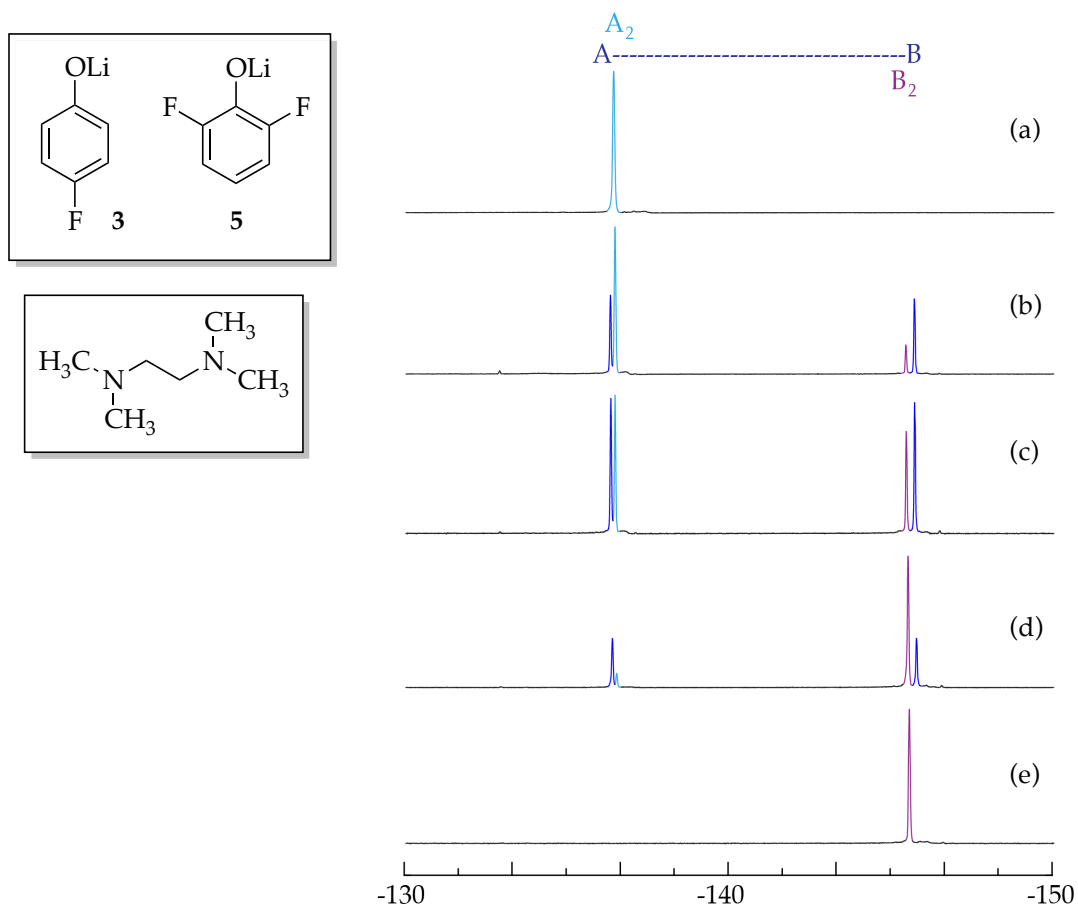


Figure AII.3. ^{19}F NMR spectra of 0.10 M solutions of $[\text{}^6\text{Li}]\mathbf{3}$ (A) and $[\text{}^6\text{Li}]\mathbf{5}$ (B) in 0.50 M TMEDA/toluene at $-80\text{ }^\circ\text{C}$. The measured mole fractions of A in (a)-(e) are 1.00, 0.75, 0.57, 0.40, and 0.00, respectively.

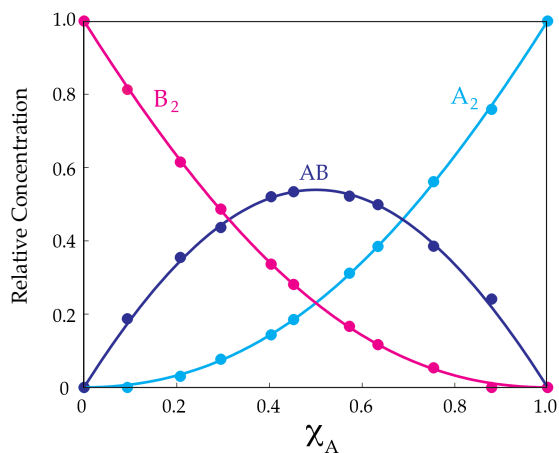


Figure AII.4. Job plot showing the relative integrations versus the measured mole fractions of A for 0.10 M mixtures of $[\text{}^6\text{Li}]\mathbf{3}$ (A) and $[\text{}^6\text{Li}]\mathbf{5}$ (B) in 0.50 M TMEDA/toluene at $-80\text{ }^\circ\text{C}$.

Dimer Job Plots in TMEDA

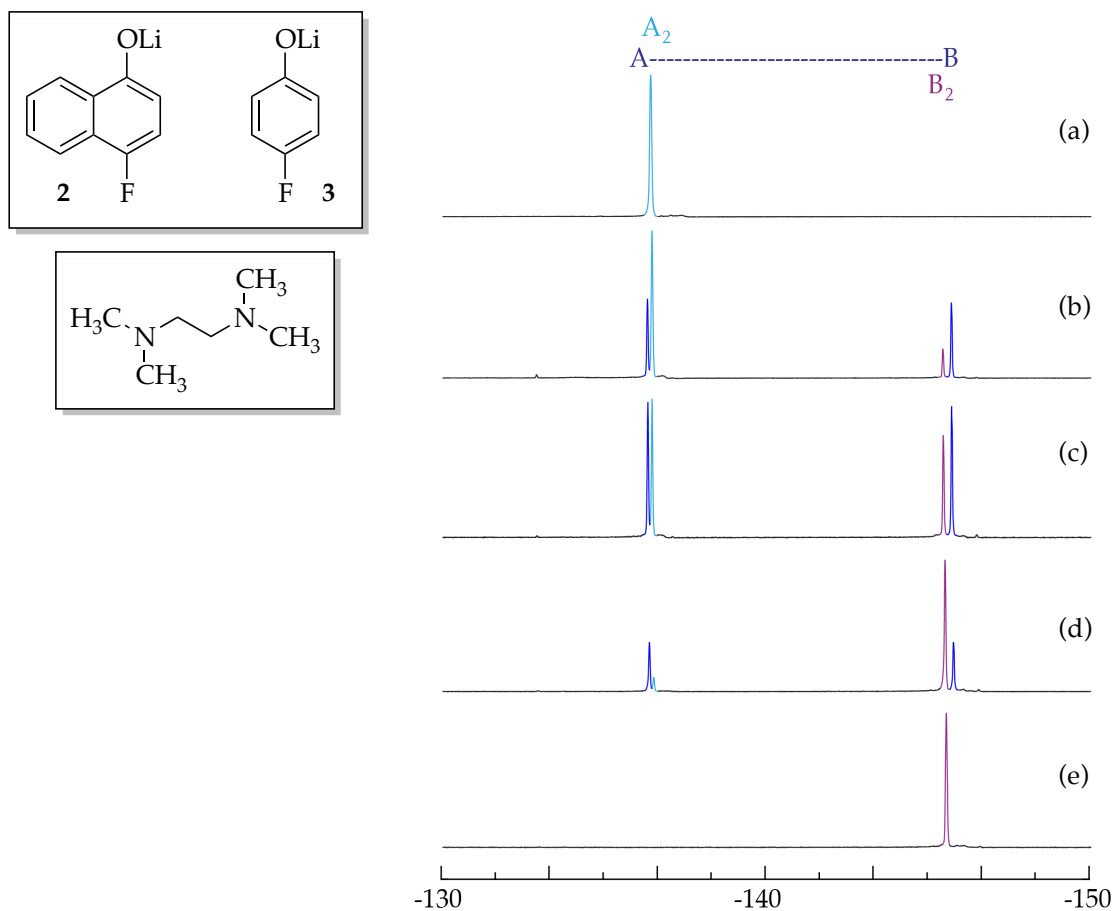


Figure AII.5. ^{19}F NMR spectra of 0.10 M solutions of $[^6\text{Li}]2$ (**A**) and $[^6\text{Li}]3$ (**B**) in 0.50 M TMEDA/toluene at $-80\text{ }^\circ\text{C}$. The measured mole fractions of **A** in (a)-(e) are 1.00, 0.70, 0.41, 0.24, and 0.00, respectively.

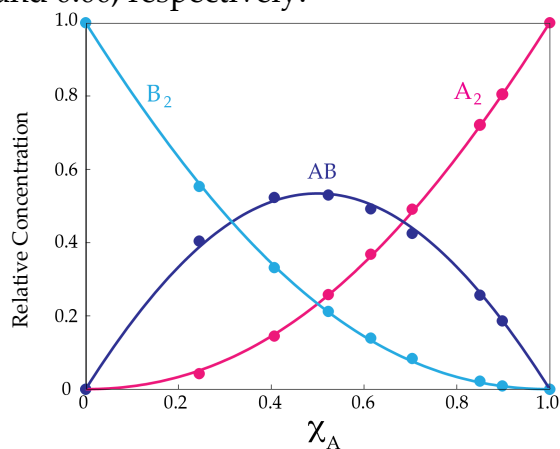


Figure AII.6. Job plot showing the relative integrations versus the measured mole fractions of **A** for 0.10 M mixtures of $[^6\text{Li}]2$ (**A**) and $[^6\text{Li}]3$ (**B**) in 0.50 M TMEDA/toluene at $-80\text{ }^\circ\text{C}$.

Tetramer Job Plots in THF

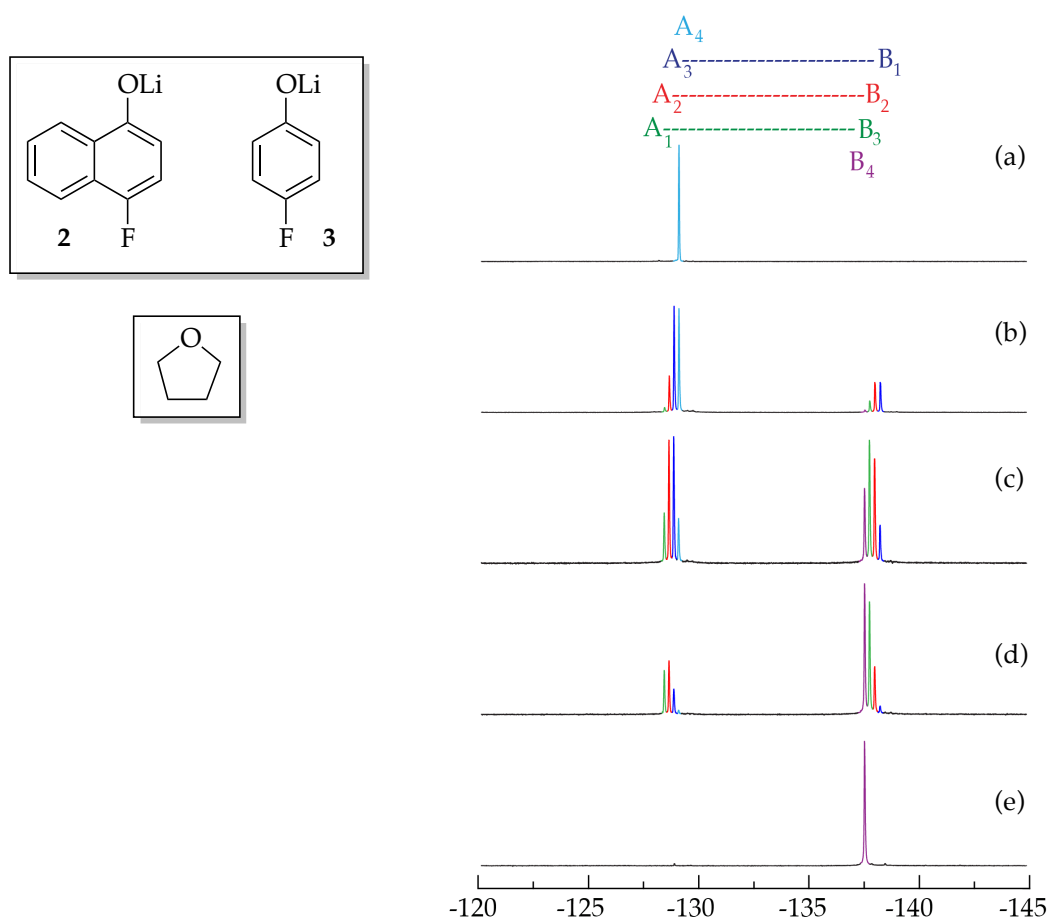


Figure AII.7. ^{19}F NMR spectra of 0.10 M solutions of $[\text{}^6\text{Li}]\mathbf{2}$ (**A**) and $[\text{}^6\text{Li}]\mathbf{3}$ (**B**) in 0.50 M TMEDA/toluene at $-80\text{ }^\circ\text{C}$. The measured mole fractions of **A** in (a)-(e) are 1.00, 0.75, 0.47, 0.27, and 0.00, respectively.

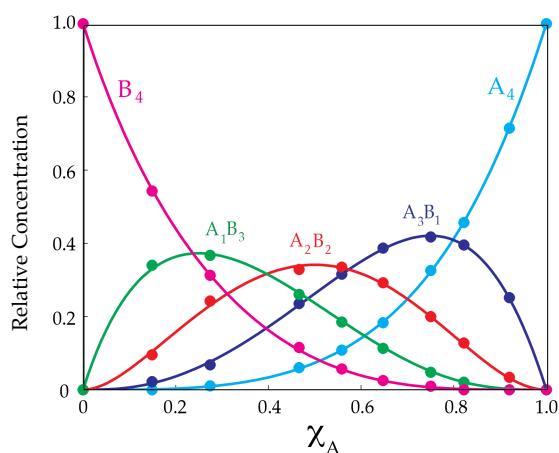


Figure AII.8. Job plot showing the relative integrations versus the measured mole fractions of **A** for 0.10 M mixtures of $[\text{}^6\text{Li}]\mathbf{2}$ (**A**) and $[\text{}^6\text{Li}]\mathbf{3}$ (**B**) in 0.50 M TMEDA/toluene at $-80\text{ }^\circ\text{C}$.

Tetramer Job Plots in *N*-methylpyrrolidone

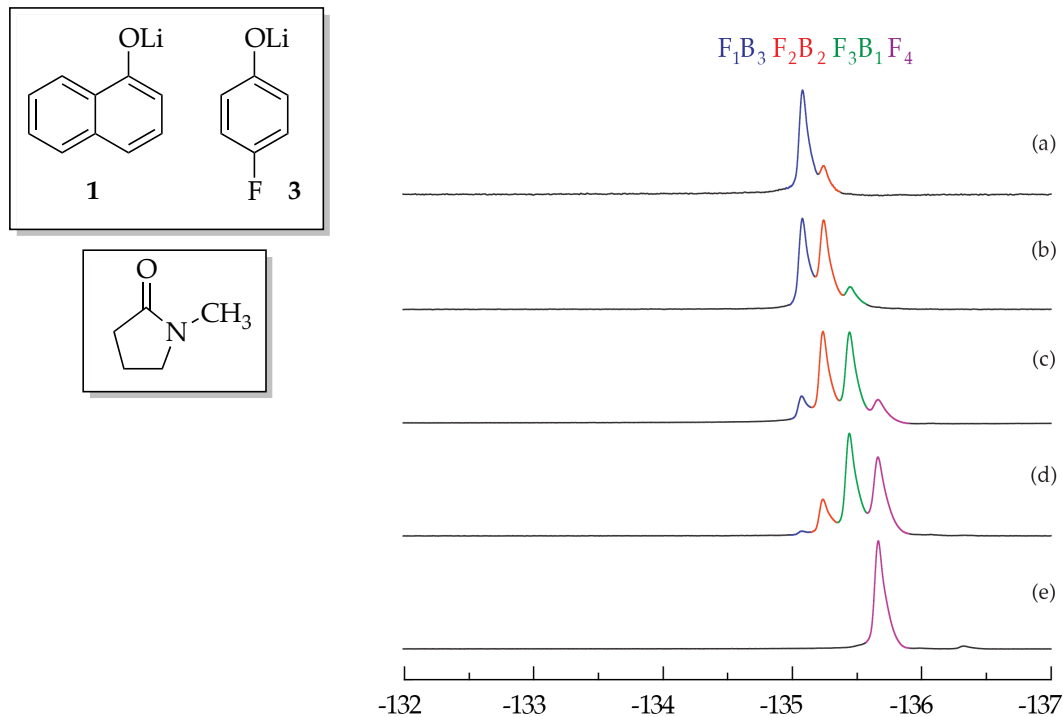


Figure AII.9. ^{19}F NMR spectra of 0.10 M solutions of $[\text{}^6\text{Li}]\mathbf{3}$ (F) and $[\text{}^6\text{Li}]\mathbf{1}$ (B) in 0.50 M NMP/toluene at $-80\text{ }^\circ\text{C}$. The measured mole fractions of F in (a)-(e) are 0.28, 0.37, 0.42, 0.78, and 1.00, respectively. The 1-naphtholate homoaggregate is invisible by fluorine NMR.

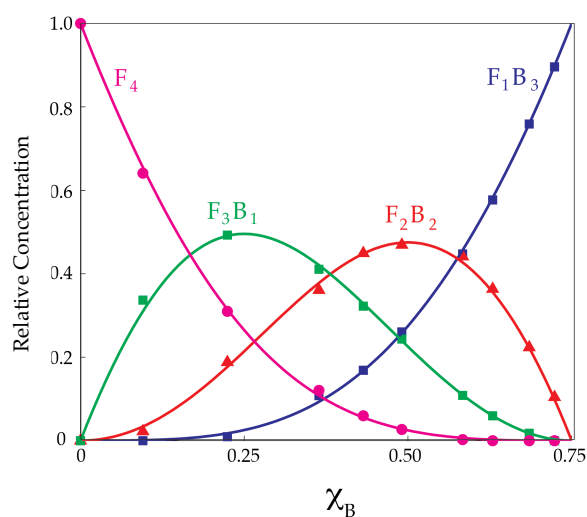


Figure AII.10. Job plot showing the relative integrations versus the measured mole fractions of B for 0.10 M mixtures of $[\text{}^6\text{Li}]\mathbf{3}$ (F) and $[\text{}^6\text{Li}]\mathbf{1}$ (B) in 0.50 M NMP/toluene at $-80\text{ }^\circ\text{C}$.

Tetramer Job Plots in Dimethylformamide

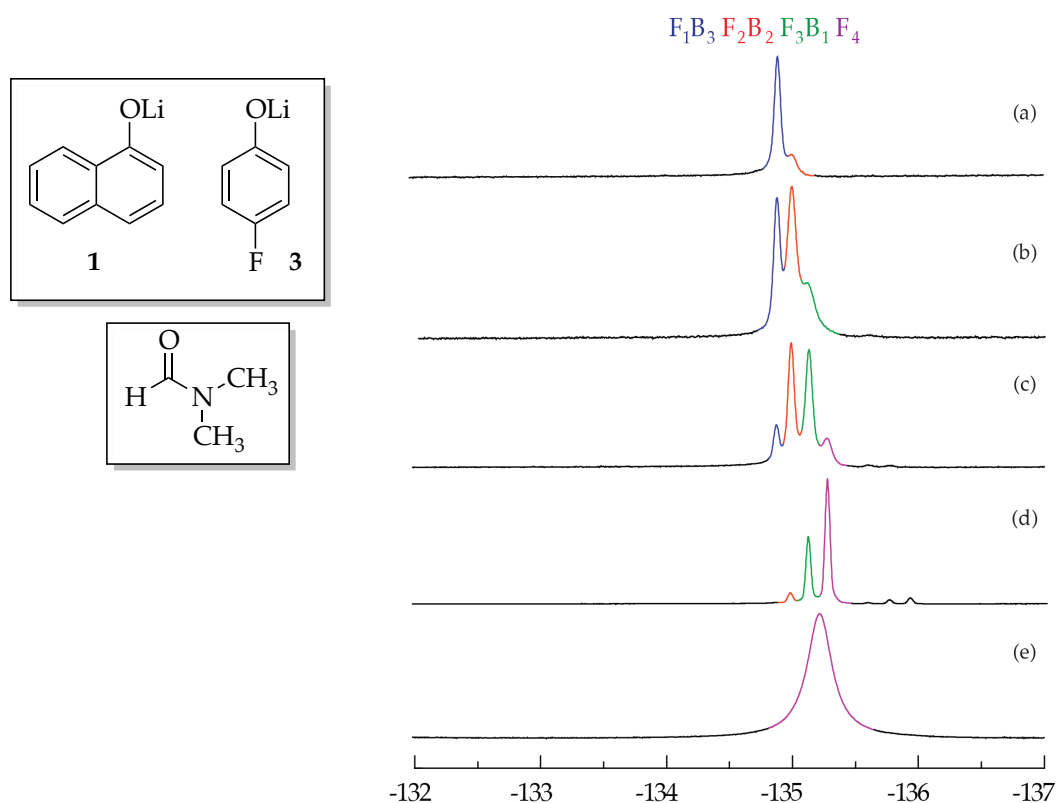


Figure AII.11. ^{19}F NMR spectra of 0.10 M solutions of $[^6\text{Li}]\mathbf{3}$ (**F**) and $[^6\text{Li}]\mathbf{1}$ (**B**) in 0.50 M DMF/toluene at $-80\text{ }^\circ\text{C}$. The measured mole fractions of **F** in (a)-(e) are 0.27, 0.41, 0.55, 0.87, and 1.00, respectively. The 1-naphtholate homoaggregate is invisible by fluorine NMR.

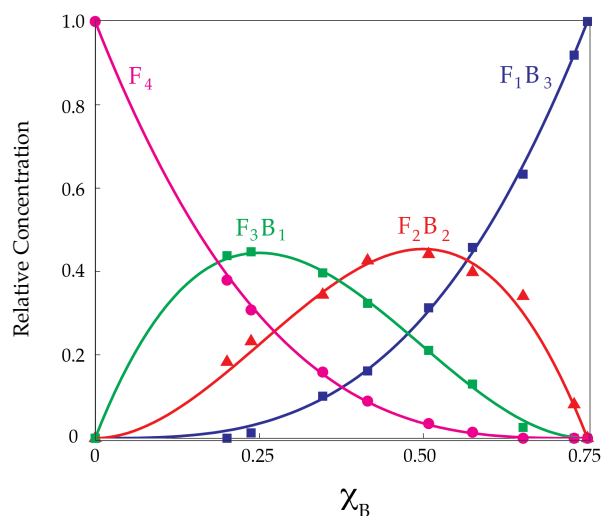


Figure AII.12. Job plot showing the relative integrations versus the measured mole fractions of **B** for 0.10 M mixtures of $[^6\text{Li}]\mathbf{3}$ (**F**) and $[^6\text{Li}]\mathbf{1}$ (**B**) in 0.50 M DMF/toluene at $-80\text{ }^\circ\text{C}$.

Tetramer Job Plots in Dimethylsulfoxide

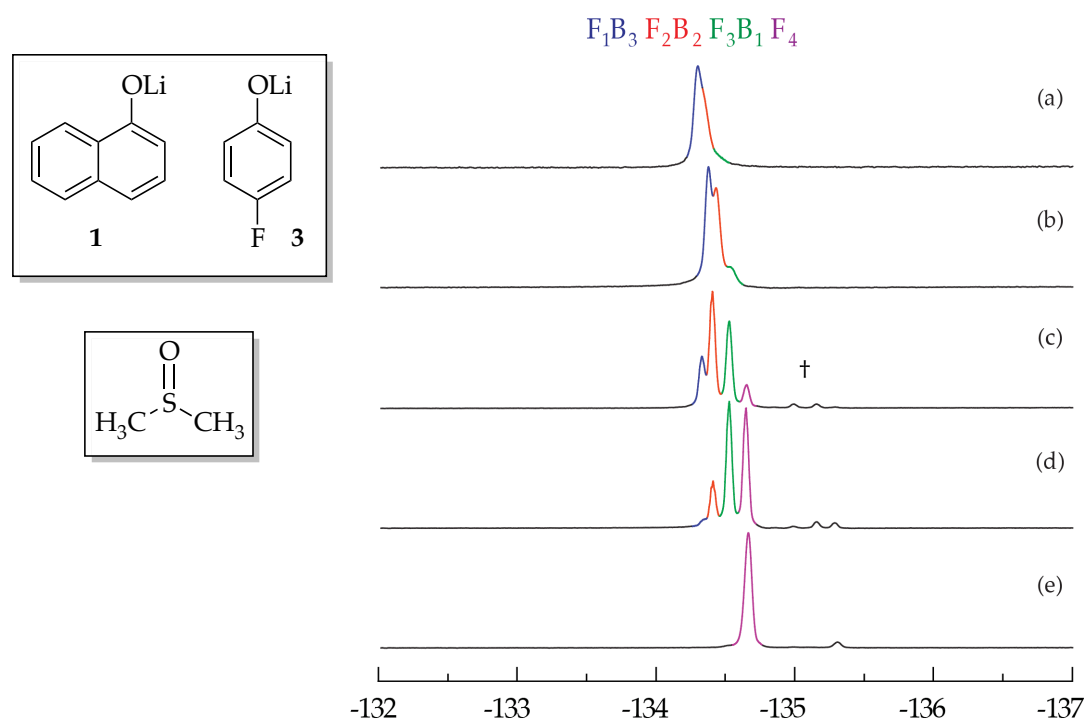


Figure AII.13. ^{19}F NMR spectra of 0.10 M solutions of $[^6\text{Li}]\mathbf{3}$ (**F**) and $[^6\text{Li}]\mathbf{1}$ (**B**) in 0.50 M DMSO/toluene at $-80\text{ }^\circ\text{C}$. The measured mole fractions of **F** in (a)-(e) are 0.27, 0.34, 0.49, 0.65, and 1.00, respectively. The 1-naphtholate homoaggregate is invisible by fluorine NMR. † denotes unknown fluorinated material, possibly minor aggregation states.

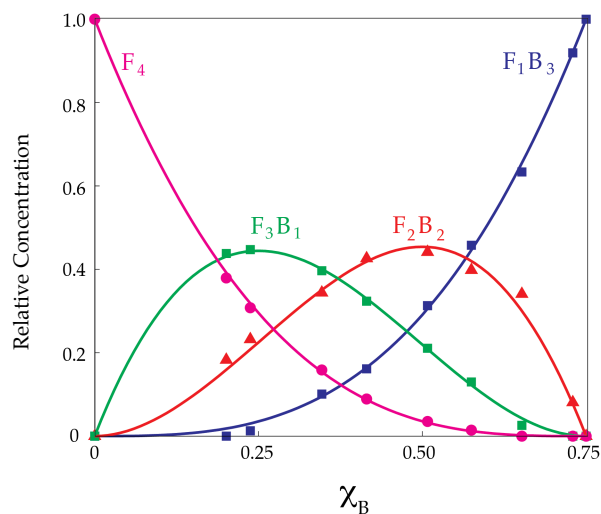


Figure AII.14. Job plot showing the relative integrations versus the measured mole fractions of **B** for 0.10 M mixtures of $[^6\text{Li}]\mathbf{3}$ (**F**) and $[^6\text{Li}]\mathbf{1}$ (**B**) in 0.50 M DMSO/toluene at $-80\text{ }^\circ\text{C}$.

Tetramer Job Plots in Dimethylpropyleneurea

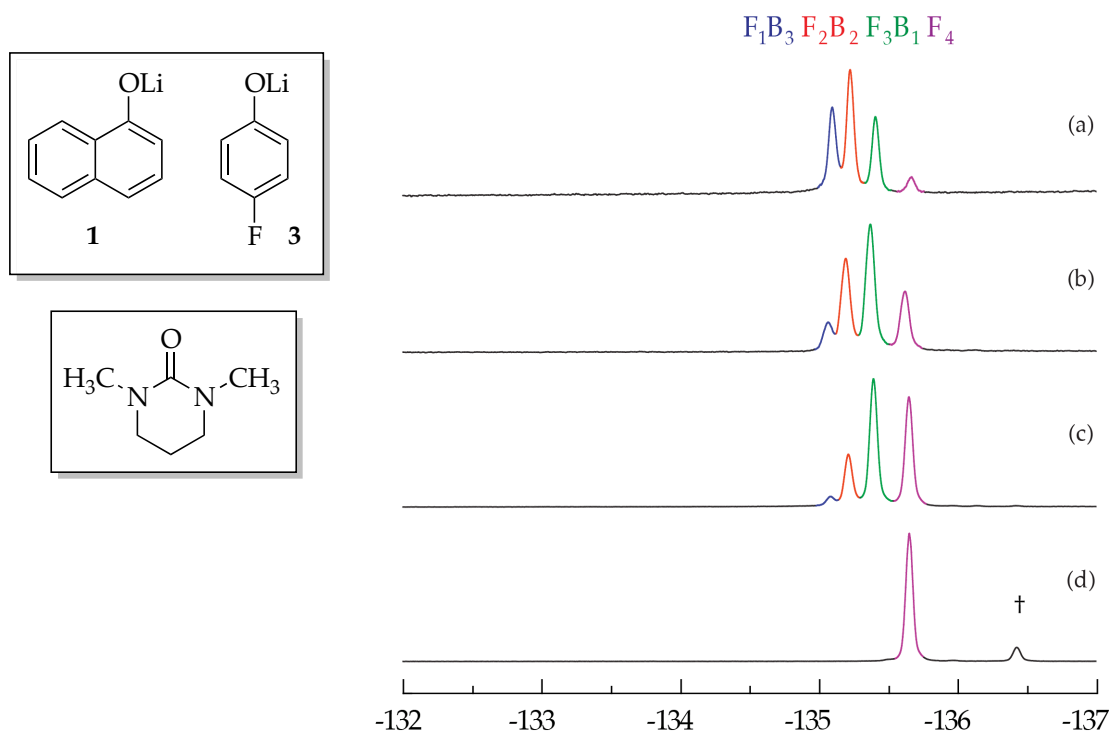


Figure AII.15. ^{19}F NMR spectra of 0.10 M solutions of $[^6\text{Li}]\mathbf{3}$ (**F**) and $[^6\text{Li}]\mathbf{1}$ (**B**) in 0.50 M DMPU/toluene at $-80\text{ }^\circ\text{C}$. The measured mole fractions of **F** in (a)-(e) are 0.43, 0.64, 0.72, and 1.00, respectively. The 1-naphtholate homoaggregate is invisible by fluorine NMR. † denotes unknown fluorinated material, possibly minor aggregation states.

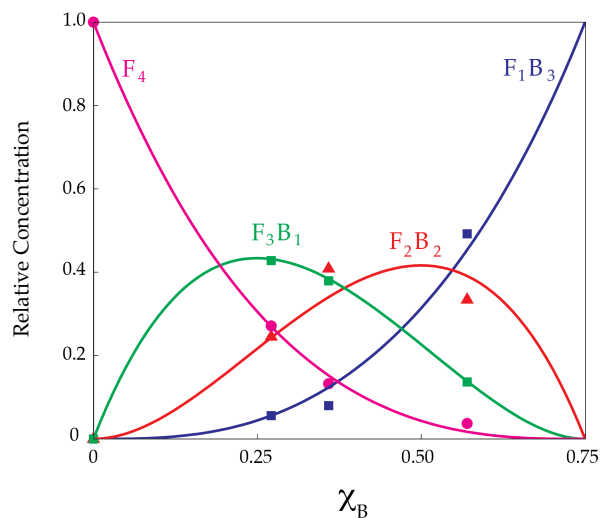


Figure AII.16. Job plot showing the relative integrations versus the measured mole fractions of **B** for 0.10 M mixtures of $[^6\text{Li}]\mathbf{3}$ (**F**) and $[^6\text{Li}]\mathbf{1}$ (**B**) in 0.50 M DMPU/toluene at $-80\text{ }^\circ\text{C}$.

Tetramer Job Plots in *n*-Propylamine

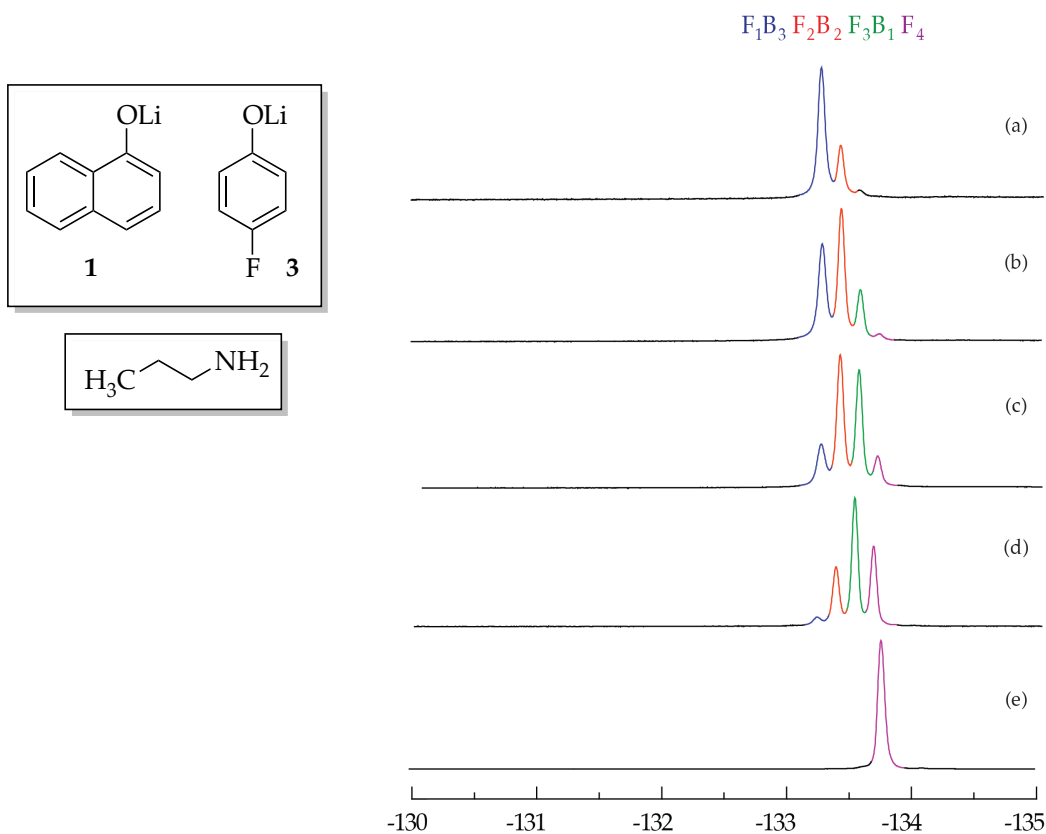


Figure AII.17. ^{19}F NMR spectra of 0.10 M solutions of $[^6Li]3$ (**F**) and $[^6Li]1$ (**B**) in 0.50 M *n*-PrNH₂/toluene at -80 °C. The measured mole fractions of **F** in (a)-(e) are 0.30, 0.38, 0.51, 0.69, and 1.00, respectively. The 1-naphtholate homoaggregate is invisible by fluorine NMR.

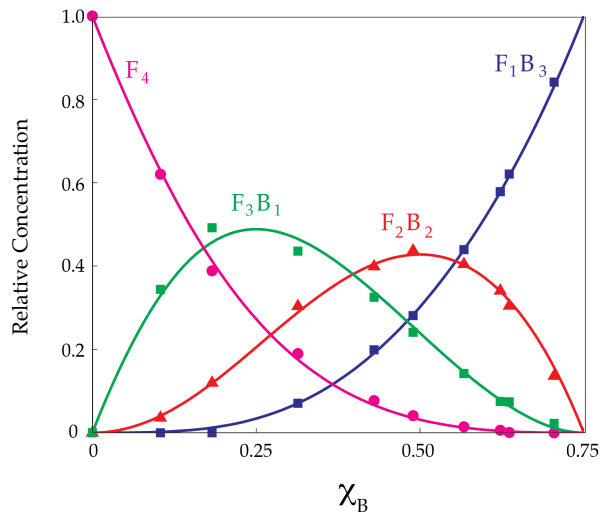


Figure AII.18. Job plot showing the relative integrations versus the measured mole fractions of **B** for 0.10 M mixtures of $[^6Li]3$ (**F**) and $[^6Li]1$ (**B**) in 0.50 M *n*-PrNH₂/toluene at -80 °C.

Tetramer Job Plots in Diethylamine

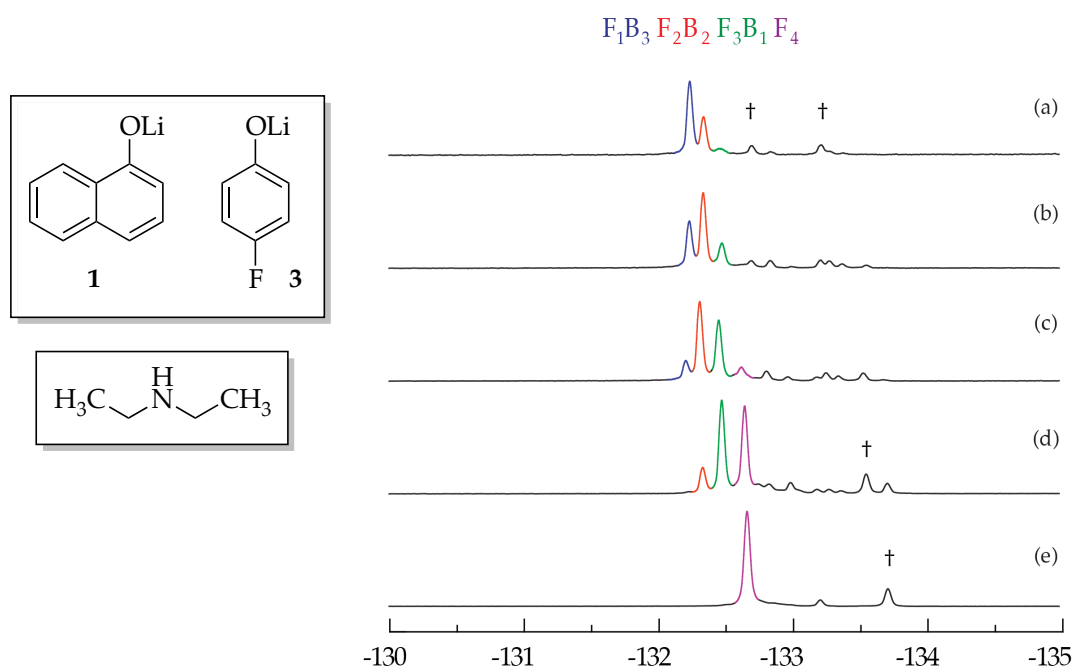


Figure AII.19. ^{19}F NMR spectra of 0.10 M solutions of $[^6\text{Li}]\mathbf{3}$ (**F**) and $[^6\text{Li}]\mathbf{1}$ (**B**) in 0.50 M Et_2NH /toluene at $-80\text{ }^\circ\text{C}$. The measured mole fractions of **F** in (a)–(e) are 0.31, 0.40, 0.55, 0.63, and 1.00, respectively. The 1-naphtholate homoaggregate is invisible by fluorine NMR. † denotes unknown fluorinated material, possibly minor aggregation states.

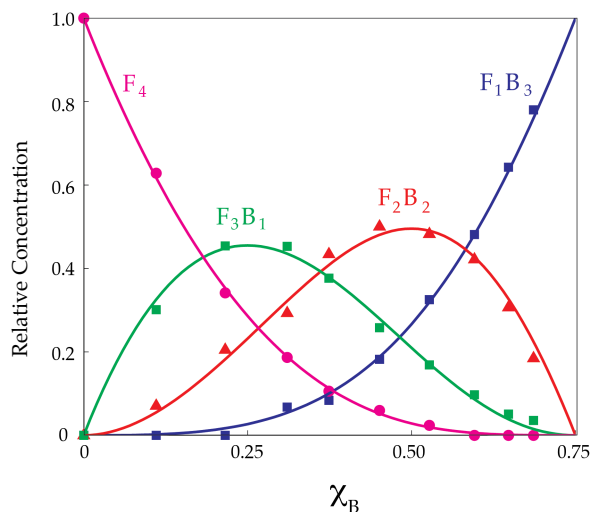


Figure AII.20. Job plot showing the relative integrations versus the measured mole fractions of **B** for 0.10 M mixtures of $[^6\text{Li}]\mathbf{3}$ (**F**) and $[^6\text{Li}]\mathbf{1}$ (**B**) in 0.50 M Et_2NH /toluene at $-80\text{ }^\circ\text{C}$. F_1B_3 is the last ^{19}F NMR visible aggregate, reaching a maximum of 0.75 along the x-axis; B_4 is not visible.

Tetramer Job Plots in Dipropylamine

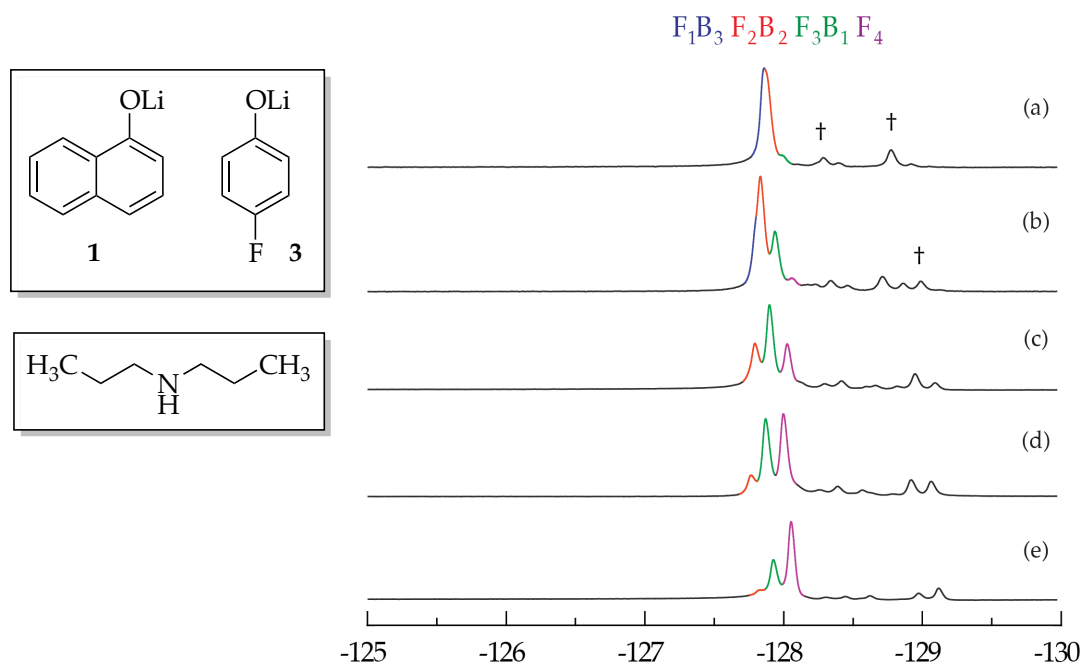


Figure AII.21. ^{19}F NMR spectra of 0.10 M solutions of $[\text{}^6\text{Li}]\mathbf{3}$ (**F**) and $[\text{}^6\text{Li}]\mathbf{1}$ (**B**) in 0.50 M *n*-Pr₂NH/toluene at -90 °C. The measured mole fractions of **F** in (a)-(e) are 0.50, 0.53, 0.69, 0.83, and 0.88, respectively. The 1-naphtholate homoaggregate is invisible by fluorine NMR. † denotes unknown fluorinated material, possibly minor aggregation states.

Tetramer Job Plots in Piperidine

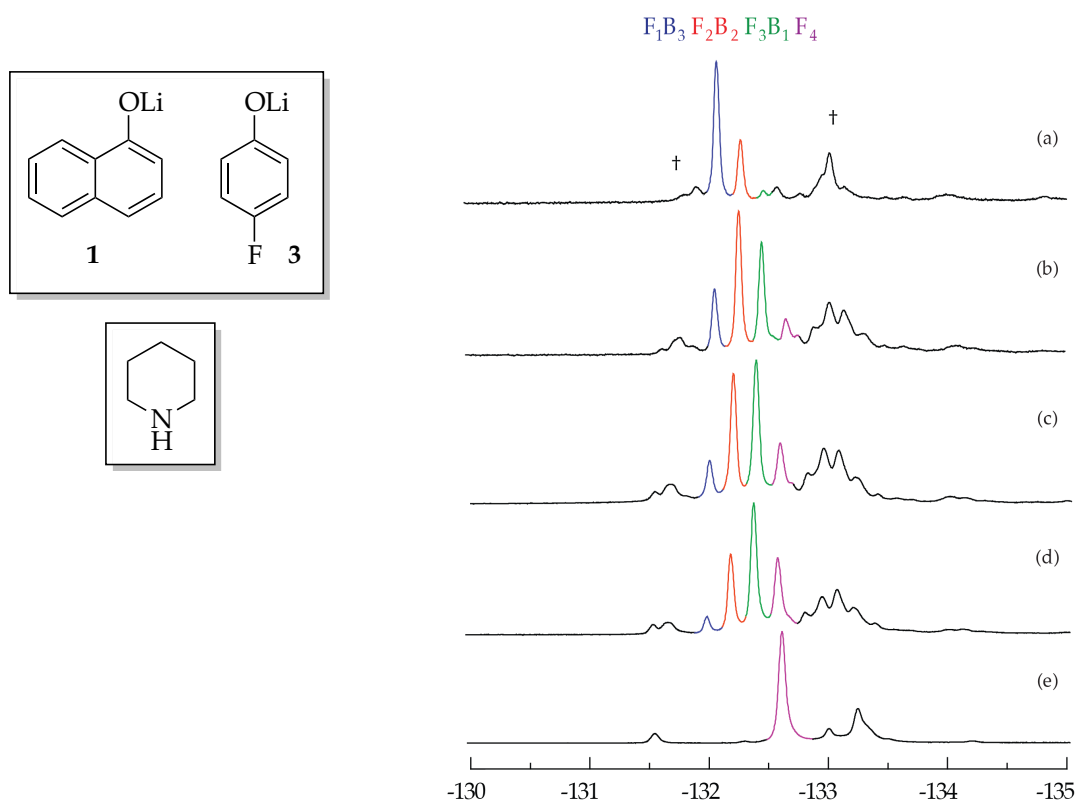


Figure AII.22. ^{19}F NMR spectra of 0.10 M solutions of $[^6\text{Li}]\mathbf{3}$ (**F**) and $[^6\text{Li}]\mathbf{1}$ (**B**) in 0.50 M piperidine/toluene at $-80\text{ }^\circ\text{C}$. The measured mole fractions of **F** in (a)-(e) are 0.31, 0.51, 0.57, 0.67, and 1.00, respectively. The 1-naphtholate homoaggregate is invisible by fluorine NMR. † denotes unknown fluorinated material, possibly minor aggregation states.

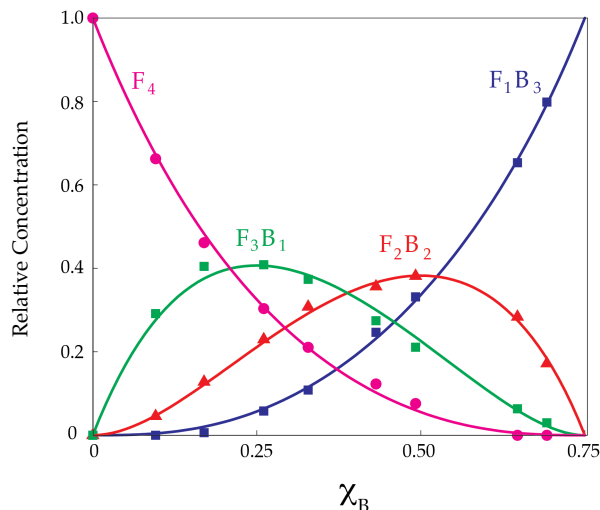


Figure AII.23. Job plot showing the relative integrations versus the measured mole fractions of **B** for 0.10 M mixtures of $[^6\text{Li}]\mathbf{3}$ (**F**) and $[^6\text{Li}]\mathbf{1}$ (**B**) in 0.50 M piperidine/toluene at $-80\text{ }^\circ\text{C}$.

Tetramer Job Plots in *t*-Butanol

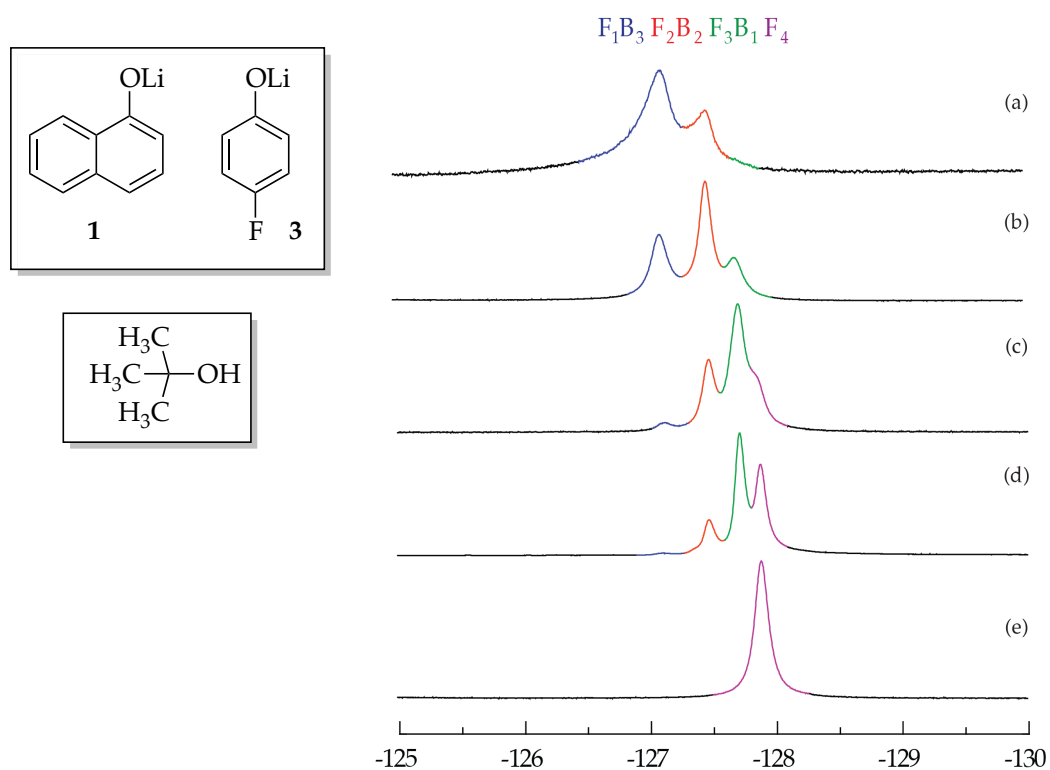


Figure AII.24. ^{19}F NMR spectra of 0.10 M solutions of $[\text{}^6\text{Li}]\mathbf{3}$ (F) and $[\text{}^6\text{Li}]\mathbf{1}$ (B) in $0.50\text{ M } t\text{-BuOH/toluene}$ at $-90\text{ }^\circ\text{C}$. The measured mole fractions of F in (a)-(e) are 0.27, 0.41, 0.66, 0.77, and 1.00, respectively. The 1-naphtholate homoaggregate is invisible by fluorine NMR.

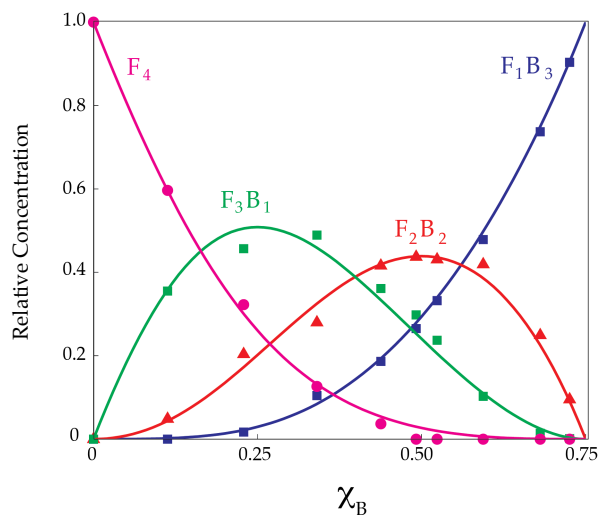


Figure AII.25. Job plot showing the relative integrations versus the measured mole fractions of B for 0.10 M mixtures of $[\text{}^6\text{Li}]\mathbf{3}$ (F) and $[\text{}^6\text{Li}]\mathbf{1}$ (B) in $0.50\text{ M } t\text{-BuOH / toluene}$ at $-90\text{ }^\circ\text{C}$.

Tetramer Job Plots in Tetrahydrofuran

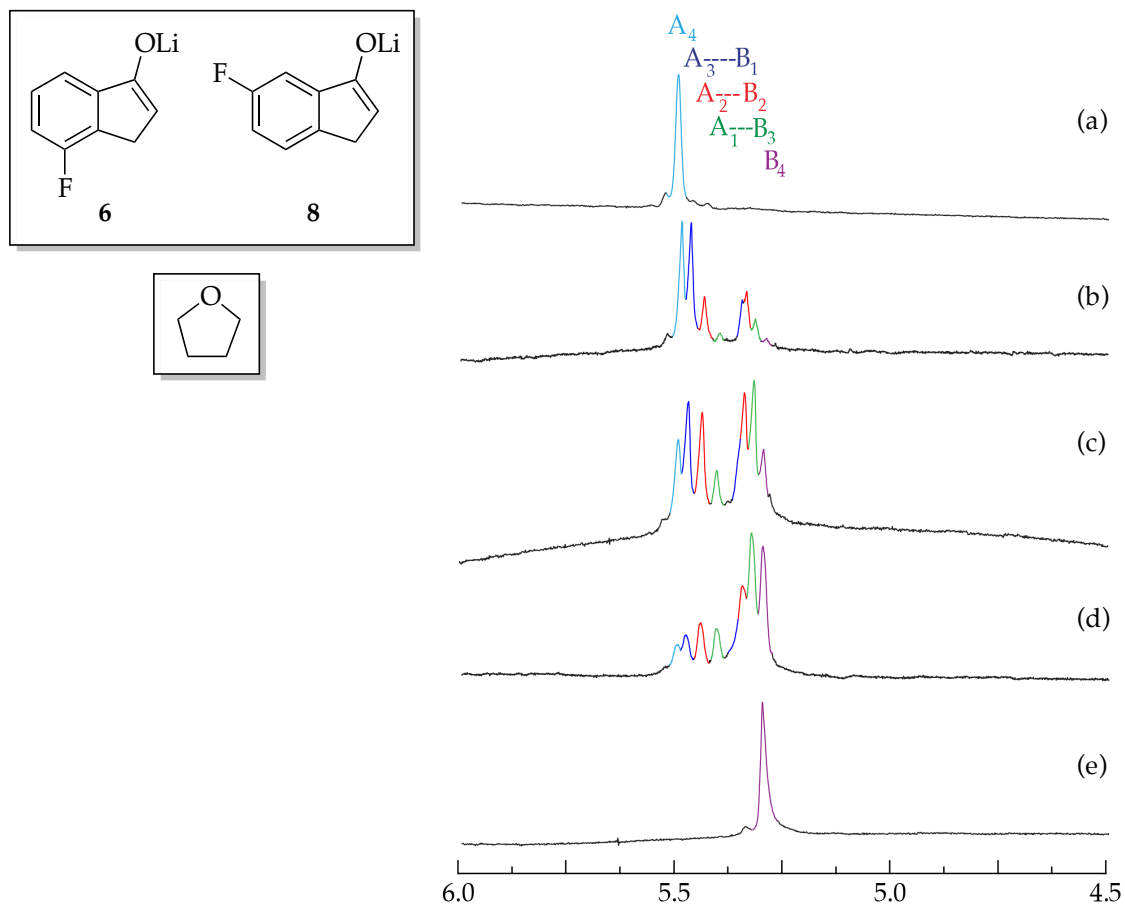


Figure AII.26. ^1H NMR spectra of 0.10 M solutions of $[\text{}^6\text{Li}]\mathbf{8}$ (**A**) and $[\text{}^6\text{Li}]\mathbf{6}$ (**B**) in 0.50 M THF/toluene at $-80\text{ }^\circ\text{C}$. The expected mole fractions of **A** in (a)-(e) are 1.0, 0.8, 0.5, 0.3, and 0.0, respectively.

Dimer Job Plots in TMEDA

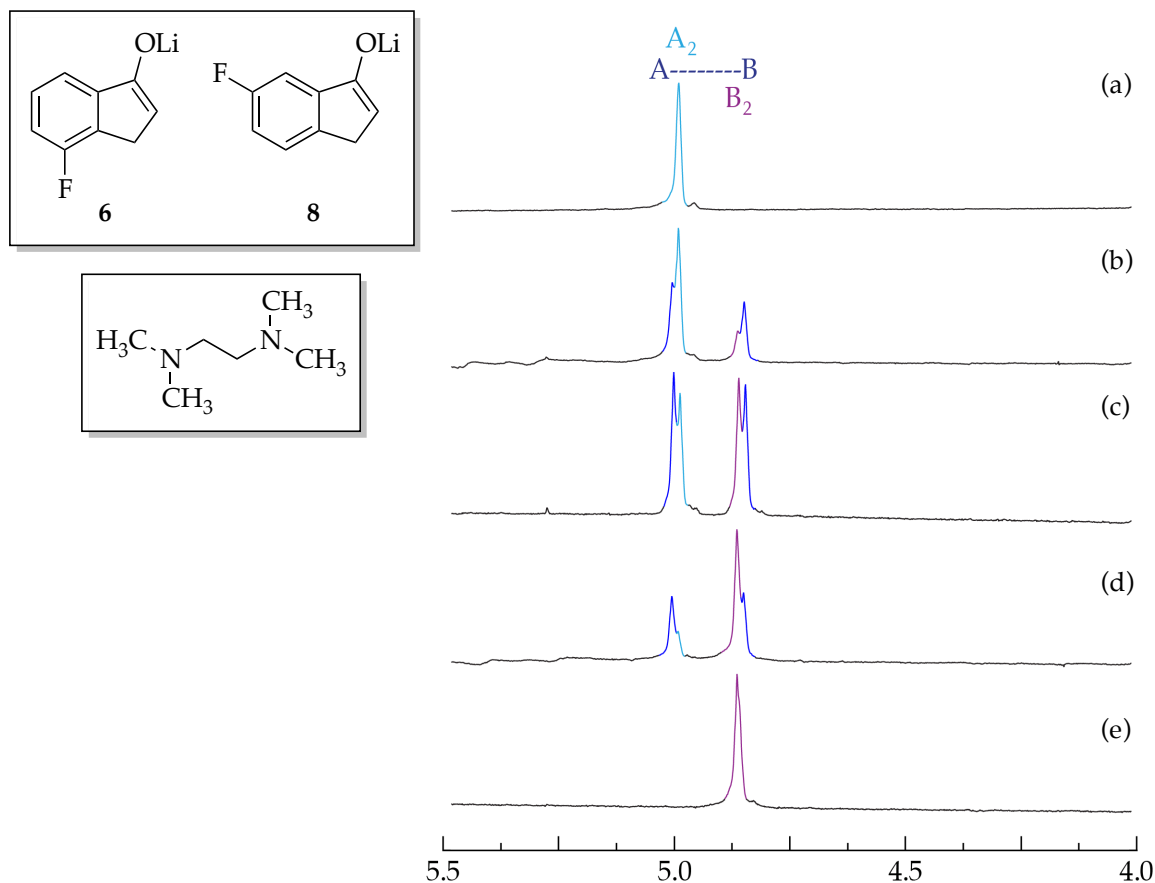


Figure AII.27. ^1H NMR spectra of 0.10 M solutions of $[^6\text{Li}]8$ (A) and $[^6\text{Li}]6$ (B) in 0.50 M TMEDA/toluene at -80°C . The measured mole fractions of A in (a)-(e) are 1.00, 0.65, 0.47, 0.27, and 0.00, respectively.

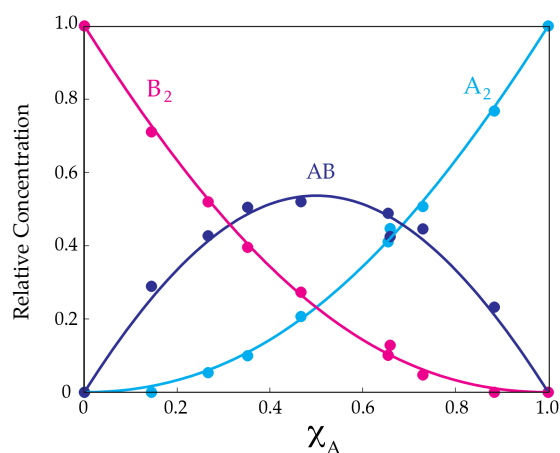


Figure AII.28. Job plot showing the relative integrations versus the measured mole fractions of A for 0.10 M mixtures of $[^6\text{Li}]8$ (A) and $[^6\text{Li}]6$ (B) in 0.50 M TMEDA/toluene at -80°C .

Dimer Job Plots in TMEDA

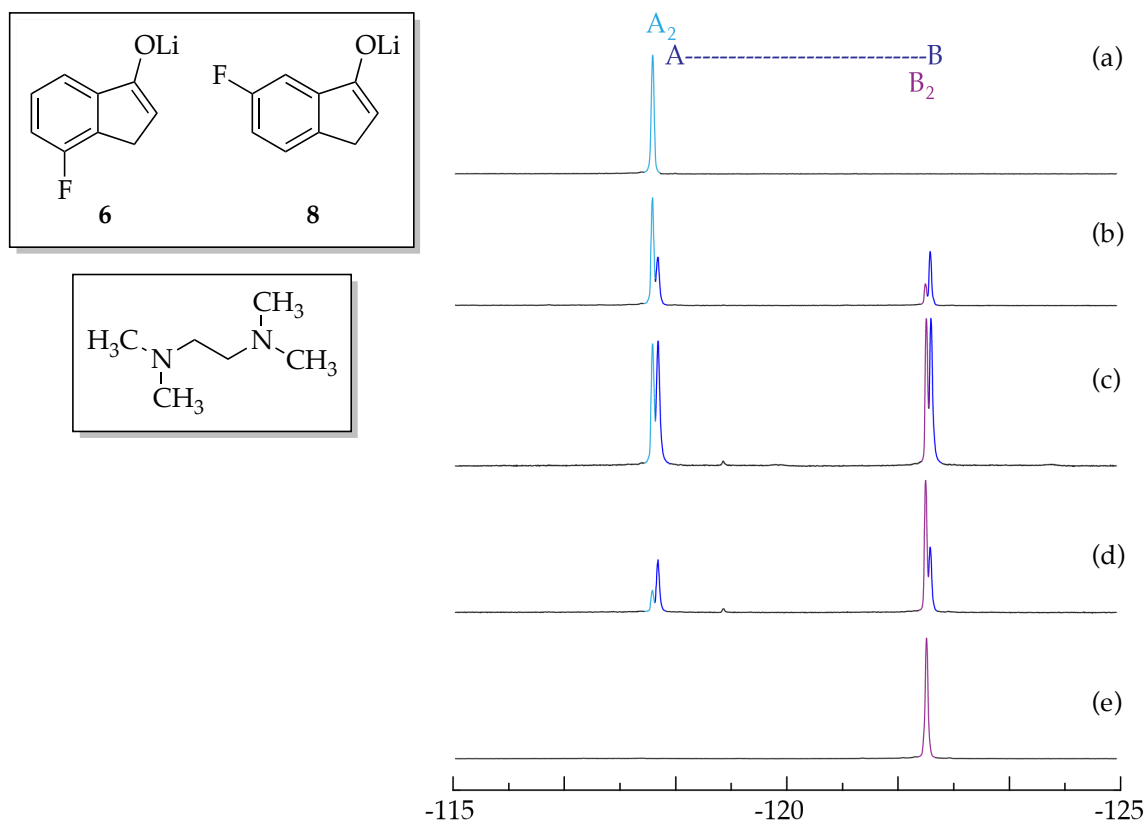


Figure AII.29. ^{19}F NMR spectra of 0.10 M solutions of $[\text{Li}]8$ (**A**) and $[\text{Li}]6$ (**B**) in 0.50 M TMEDA/toluene at $-80\text{ }^\circ\text{C}$. The measured mole fractions of **A** in (a)-(e) are 1.00, 0.72, 0.50, 0.29, and 0.00, respectively. † denotes unknown aggregation states.

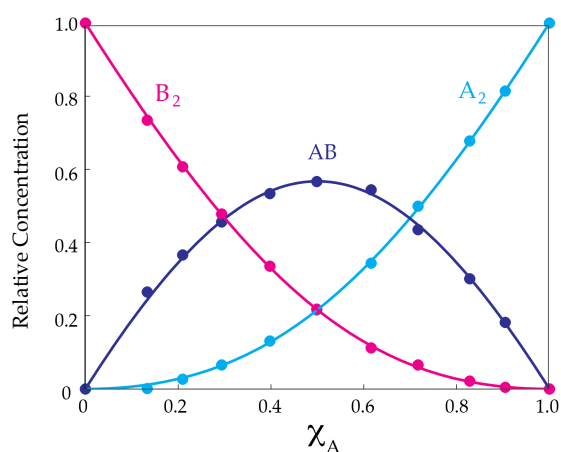


Figure AII.30. Job plot showing the relative integrations versus the measured mole fractions of **A** for 0.10 M mixtures of $[\text{Li}]8$ (**A**) and $[\text{Li}]6$ (**B**) in 0.50 M TMEDA/toluene at $-80\text{ }^\circ\text{C}$.

Tetramer Job Plots in Tetrahydrofuran

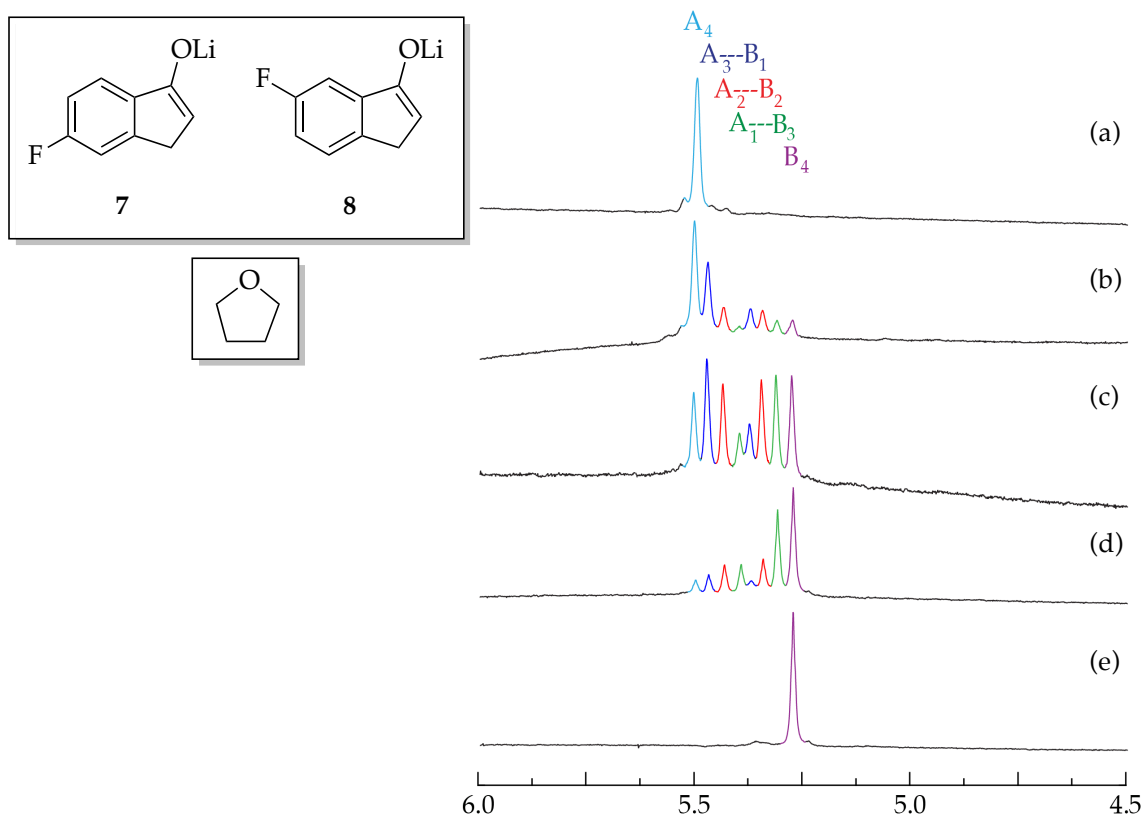


Figure AII.31. ^1H NMR spectra of 0.10 M solutions of $[\text{}^6\text{Li}]\mathbf{8}$ (A) and $[\text{}^6\text{Li}]\mathbf{7}$ (B) in 0.50 M THF/toluene at $-80\text{ }^\circ\text{C}$. The measured mole fractions of A in (a)-(e) are 1.00, 0.69, 0.50, 0.40, and 0.00, respectively. † denotes unknown aggregation states.

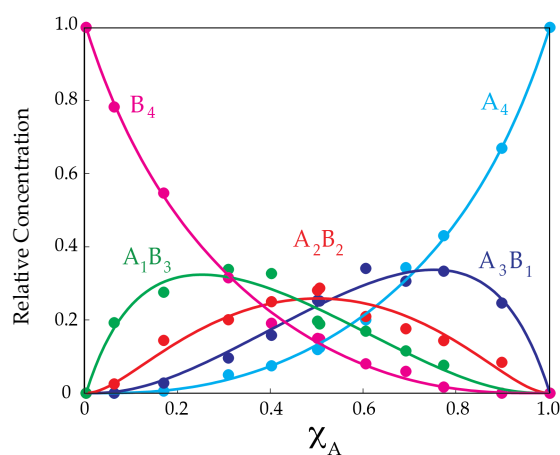


Figure AII.32. Job plot showing the relative integrations versus the measured mole fractions of A for 0.10 M mixtures of $[\text{}^6\text{Li}]\mathbf{8}$ (A) and $[\text{}^6\text{Li}]\mathbf{7}$ (B) in 0.50 M THF/toluene at $-80\text{ }^\circ\text{C}$.

Dimer Job Plots in TMEDA

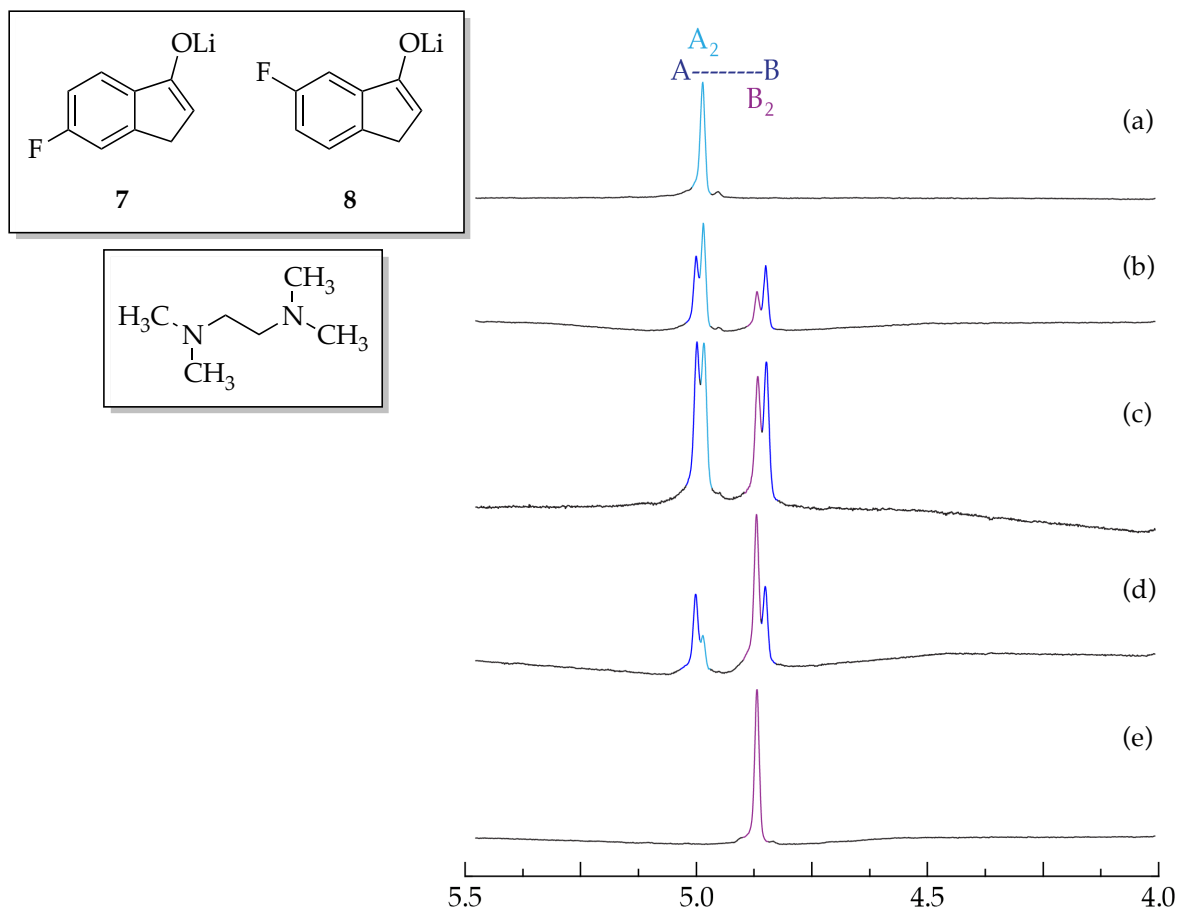


Figure AII.33. ^1H NMR spectra of 0.10 M solutions of $[\text{}^6\text{Li}]\text{8}$ (A) and $[\text{}^6\text{Li}]\text{7}$ (B) in 0.50 M TMEDA/toluene at $-80\text{ }^\circ\text{C}$. The measured mole fractions of A in (a)-(e) are 1.00, 0.58, 0.50, 0.30, and 0.00, respectively.

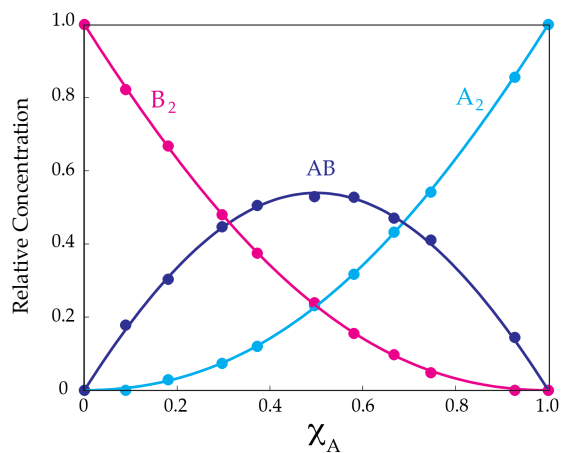


Figure AII.34. Job plot showing the relative integrations versus the measured mole fractions of A for 0.10 M mixtures of $[\text{}^6\text{Li}]\text{8}$ (A) and $[\text{}^6\text{Li}]\text{7}$ (B) in 0.50 M THF/toluene at $-80\text{ }^\circ\text{C}$.

Dimer Job Plots in TMEDA

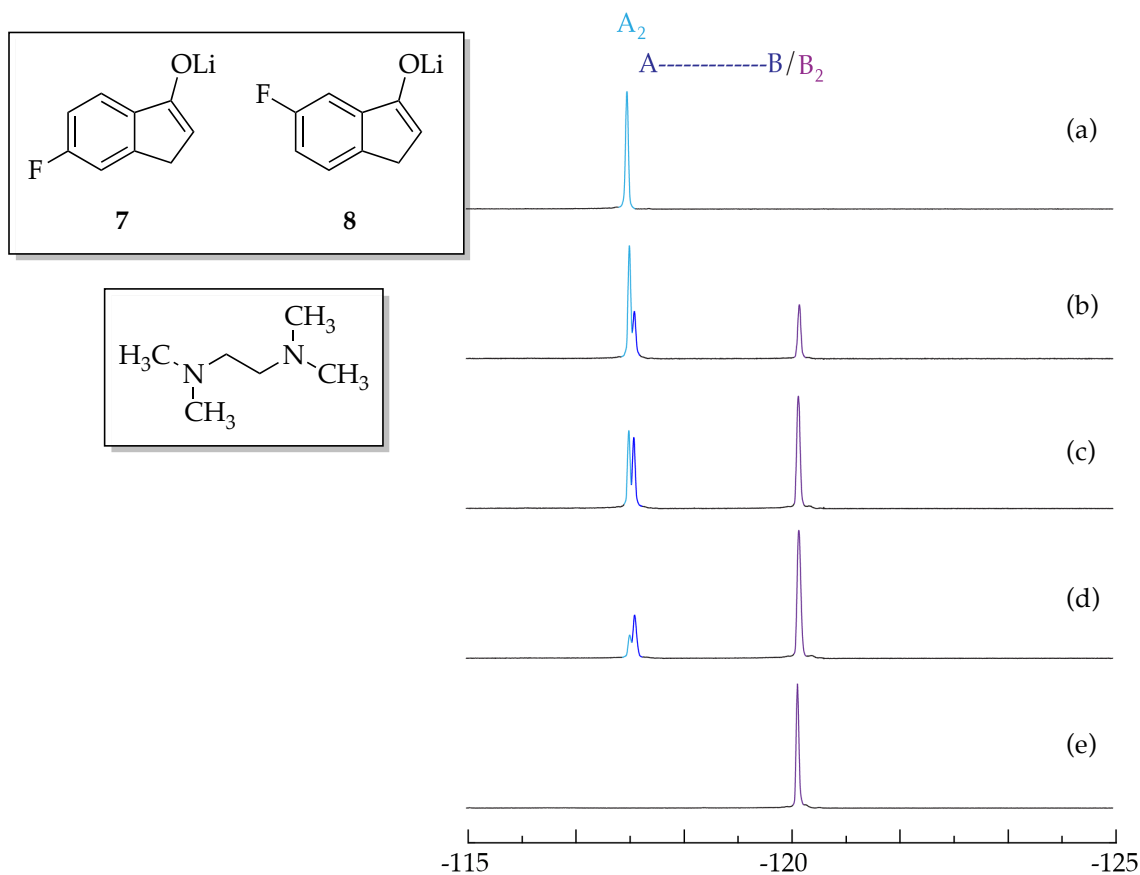


Figure AII.35. ^{19}F NMR spectra of 0.10 M solutions of $[\text{}^6\text{Li}]\mathbf{8}$ (**A**) and $[\text{}^6\text{Li}]\mathbf{7}$ (**B**) in 0.50 M TMEDA/toluene at $-80\text{ }^\circ\text{C}$. The measured mole fractions of **A** in (a)-(e) are 1.00, 0.71, 0.50, 0.31, and 0.00, respectively.

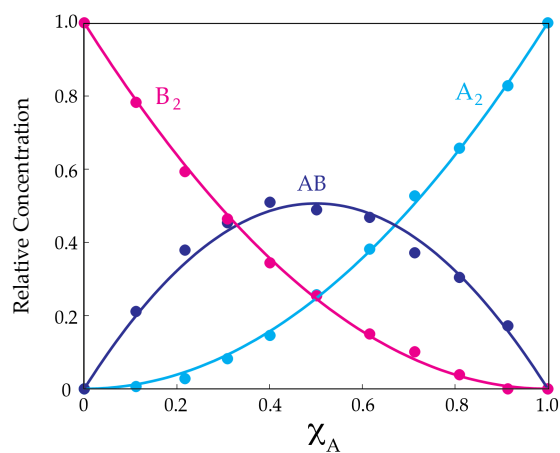


Figure AII.36. Job plot showing the relative integrations versus the measured mole fractions of **A** for 0.10 M mixtures of $[\text{}^6\text{Li}]\mathbf{8}$ (**A**) and $[\text{}^6\text{Li}]\mathbf{7}$ (**B**) in 0.50 M TMEDA/toluene at $-80\text{ }^\circ\text{C}$.

Dimer Job Plots in TMEDA

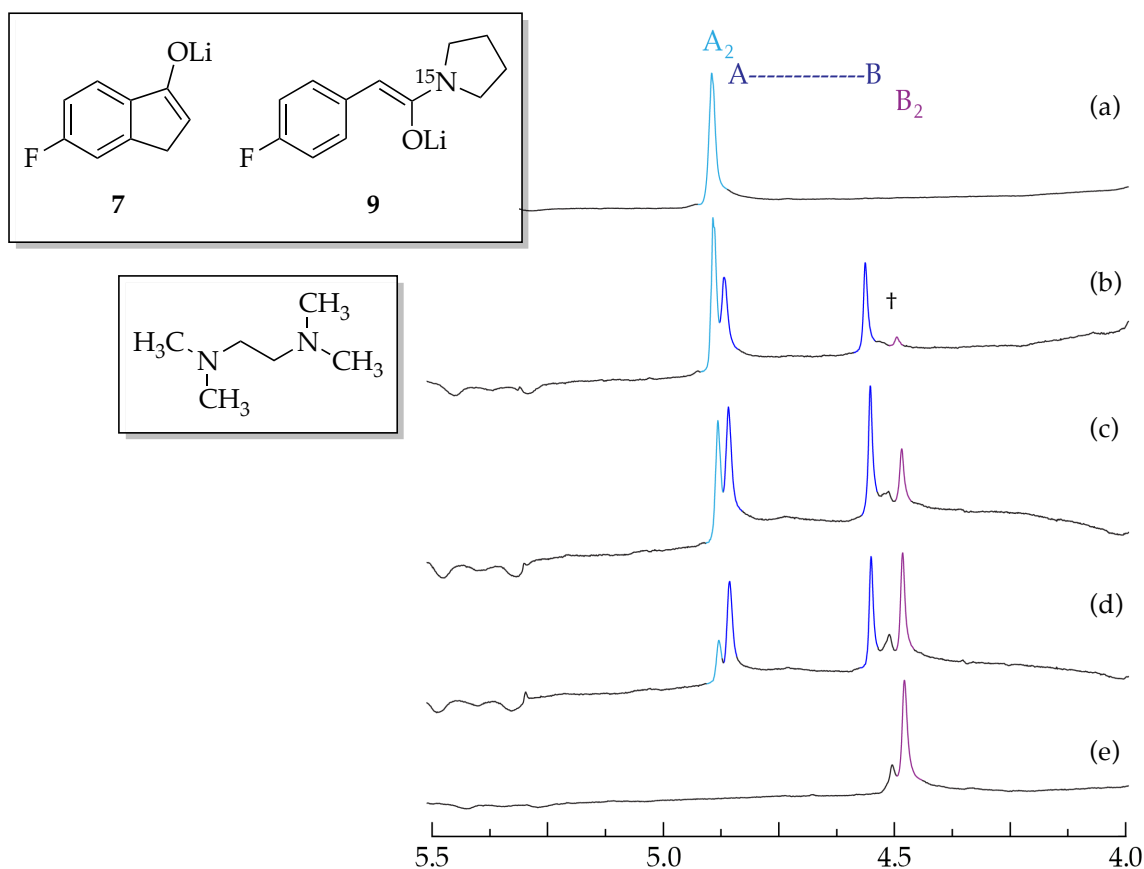


Figure AII.37. ^1H NMR spectra of 0.10 M solutions of $[\text{}^6\text{Li}]\mathbf{7}$ (A) and $[\text{}^6\text{Li}]\mathbf{9}$ (B) in 0.50 M TMEDA/toluene at $-80\text{ }^\circ\text{C}$. The measured mole fractions of A in (a)-(e) are 1.00, 0.59, 0.47, 0.30, and 0.00, respectively. † denotes unknown aggregation states.

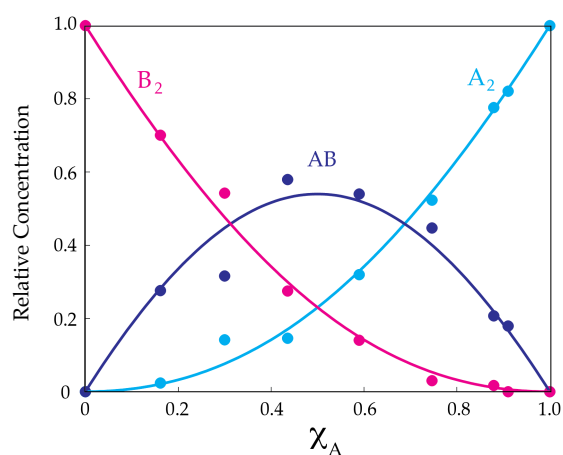


Figure AII.38. Job plot showing the relative integrations versus the measured mole fractions of A for 0.10 M mixtures of $[\text{}^6\text{Li}]\mathbf{7}$ (A) and $[\text{}^6\text{Li}]\mathbf{9}$ (B) in 0.50 M TMEDA/toluene at $-80\text{ }^\circ\text{C}$.

Tetramer Job Plots in TMEDA

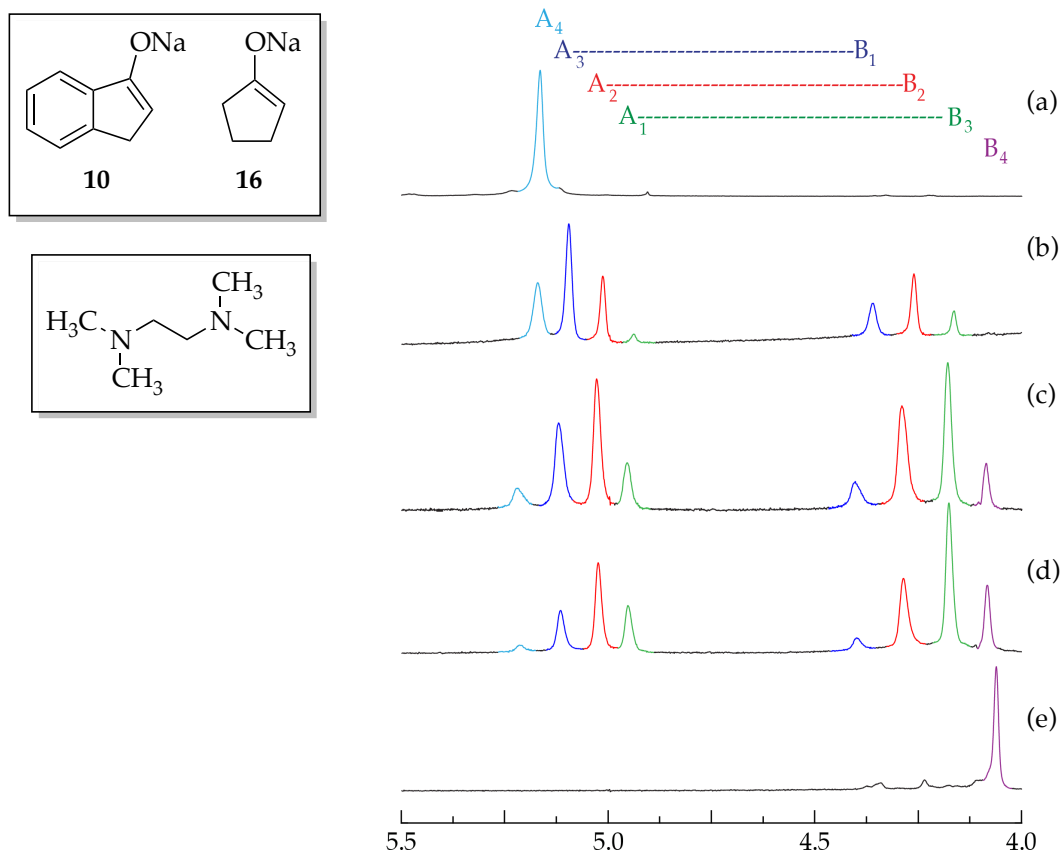


Figure AII.39. ^1H NMR spectra of 0.10 M solutions of [Na]10 (**A**) and [Na]16 (**B**) in 0.50 M TMEDA/toluene- d_8 at $-80\text{ }^\circ\text{C}$. The measured mole fractions of **A** in (a)-(e) are 1.00, 0.69, 0.48, 0.39, and 0.00, respectively.

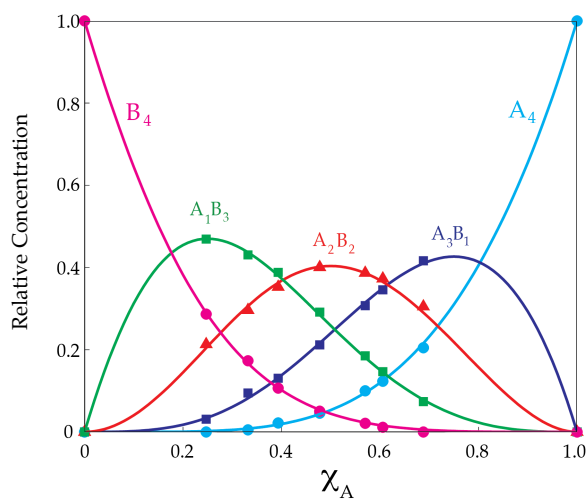


Figure AII.40. Job plot showing the relative integrations versus the measured mole fractions of **A** for 0.10 M mixtures of [Na]10 (**A**) and [Na]16 (**B**) in 0.50 M TMEDA/toluene- d_8 at $-80\text{ }^\circ\text{C}$.

Tetramer Job Plots in TMEDA

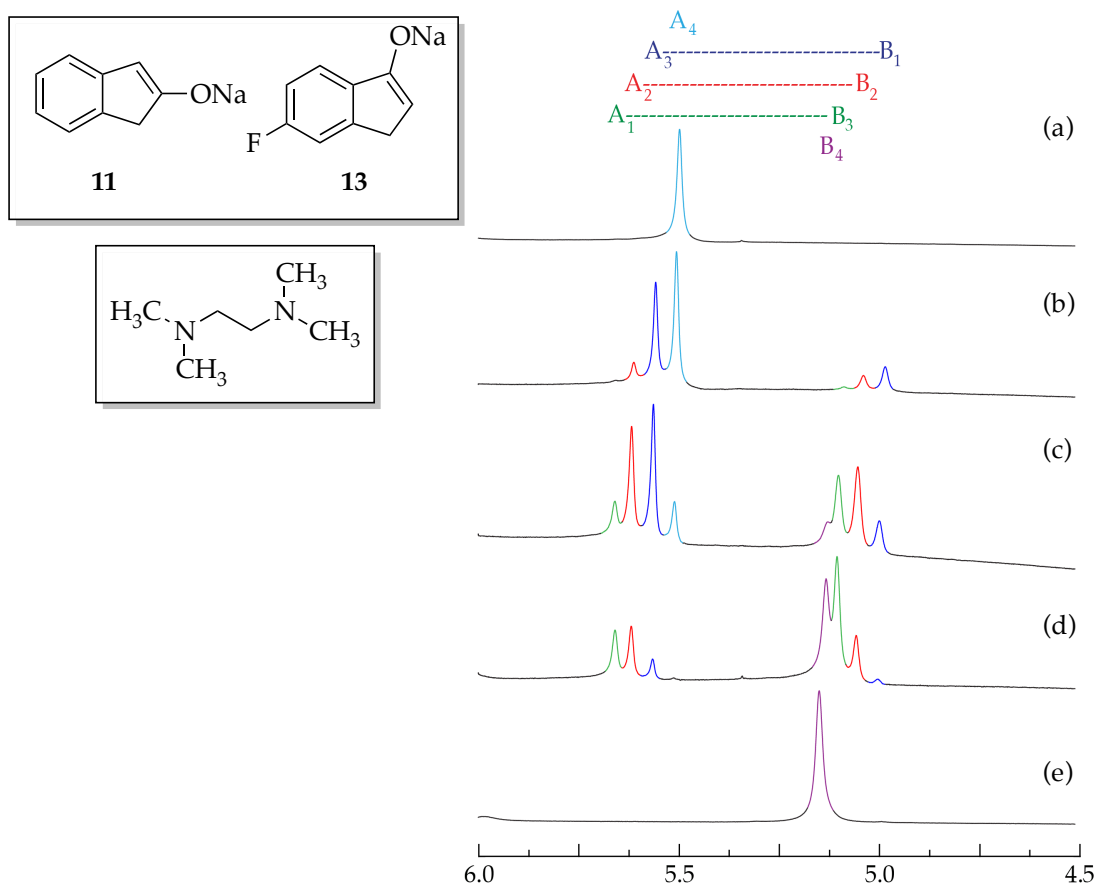


Figure AII.41. ^1H NMR spectra of 0.10 M solutions of [Na]11 (A) and [Na]13 (B) in 0.50 M TMEDA/toluene- d_8 at -80°C . The measured mole fractions of A in (a)-(e) are 1.00, 0.77, 0.50, 0.23, and 0.00, respectively.

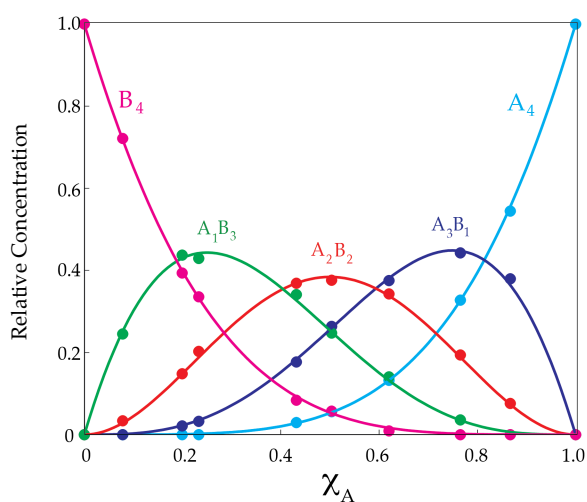


Figure AII.42. Job plot showing the relative integrations versus the measured mole fractions of A for 0.10 M mixtures of [Na]11 (A) and [Na]13 (B) in 0.50 M TMEDA/toluene- d_8 at -80°C .

Tetramer Job Plots in TMEDA

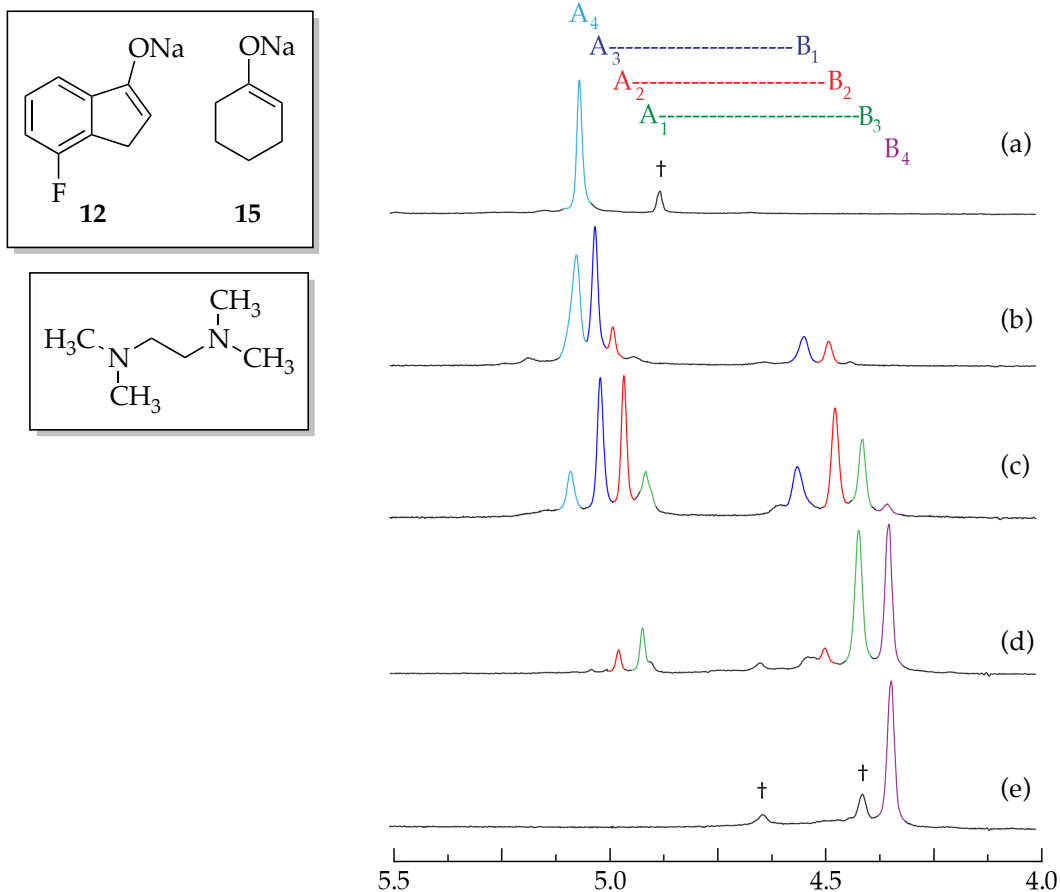


Figure AII.43. ^1H NMR spectra of 0.10 M solutions of [Na]**12** (**A**) and [Na]**15** (**B**) in 0.50 M TMEDA/toluene- d_8 at $-80\text{ }^\circ\text{C}$. The measured mole fractions of **A** in (a)–(e) are 1.00, 0.79, 0.56, 0.21, and 0.00, respectively. † denotes unknown aggregation states.

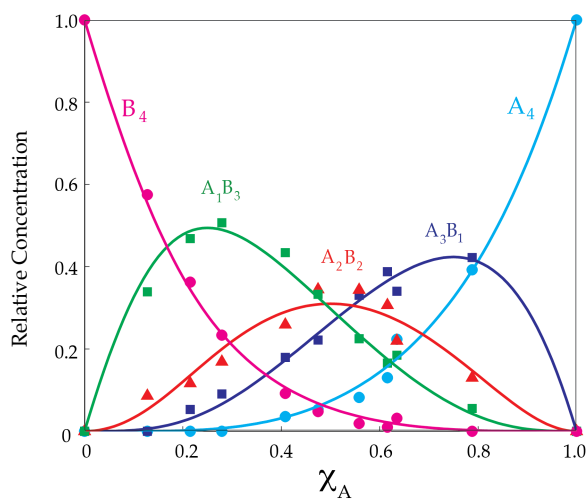


Figure AII.44. Job plot showing the relative integrations versus the measured mole fractions of **A** for 0.10 M mixtures of [Na]**12** (**A**) and [Na]**15** (**B**) in 0.50 M TMEDA/toluene- d_8 at $-80\text{ }^\circ\text{C}$.

Tetramer Job Plots in TMEDA

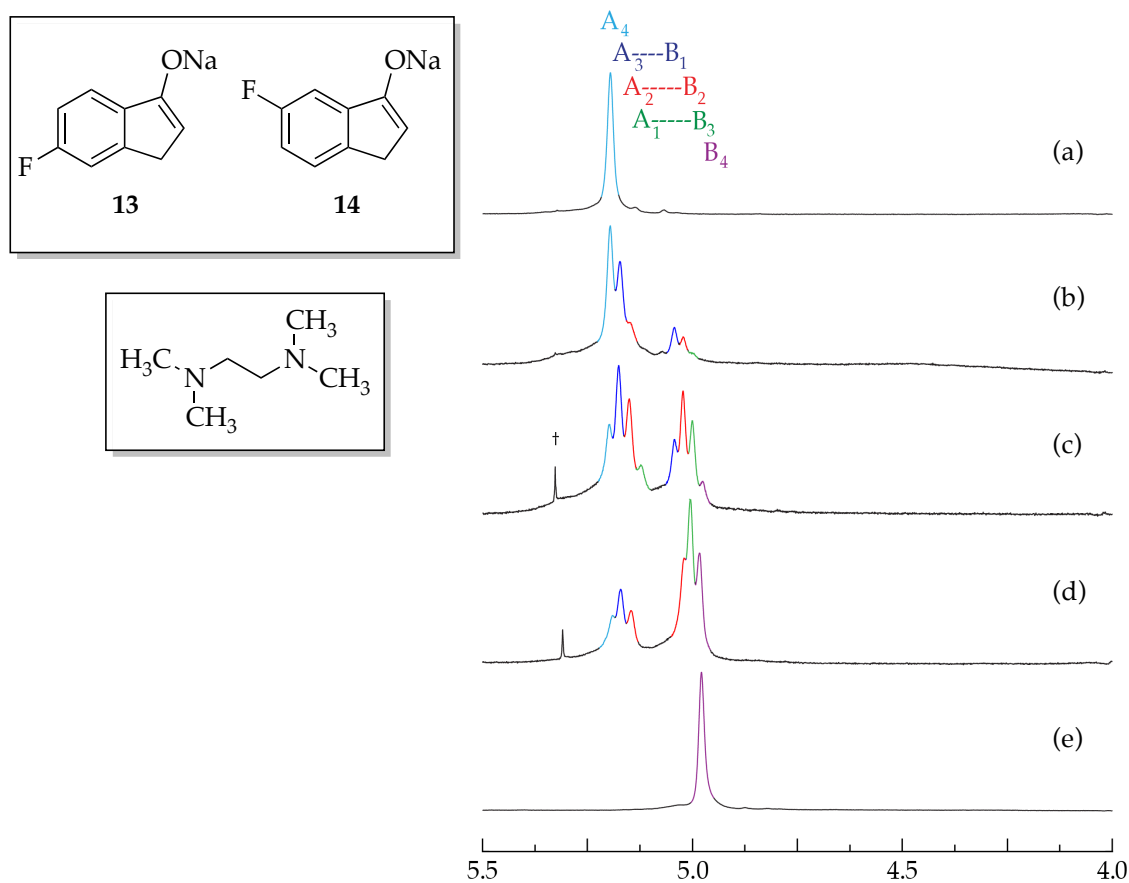


Figure AII.45. ^1H NMR spectra of 0.10 M solutions of [Na]14 (A) and [Na]13 (B) in 0.50 M TMEDA/toluene- d_8 at $-80\text{ }^\circ\text{C}$. The measured mole fractions of A in (a)–(e) are 1.00, 0.80, 0.60, 0.34, and 0.00, respectively. † denotes unknown aggregation states.

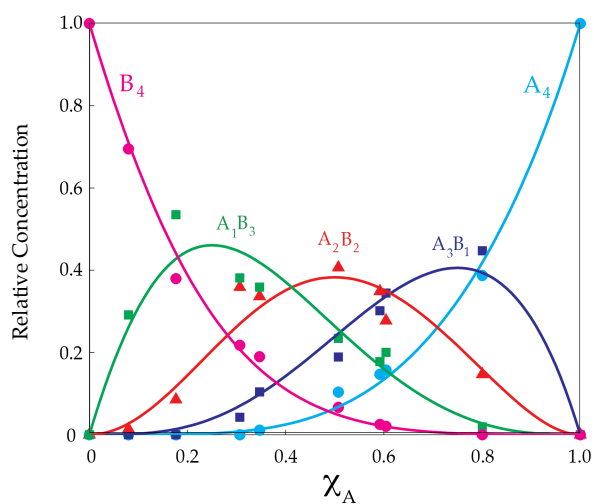


Figure AII.46. Job plot showing the relative integrations versus the measured mole fractions of A for 0.10 M mixtures of [Na]14 (A) and [Na]13 (B) in 0.50 M TMEDA/toluene- d_8 at $-80\text{ }^\circ\text{C}$.

Tetramer Stack Plots in THF

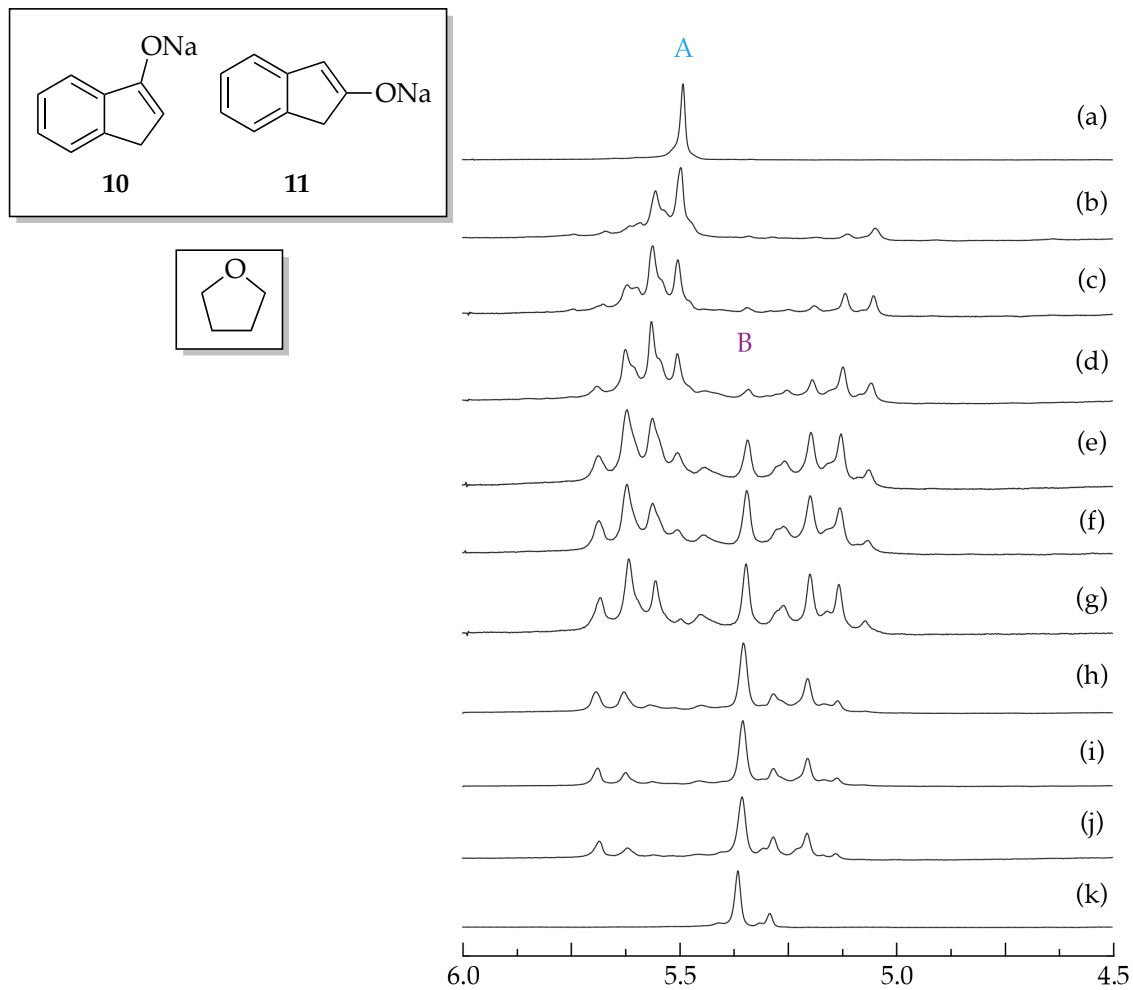


Figure AII.47. ^1H NMR spectra of 0.10 M solutions of $[\text{Na}]11$ (**A**) and $[\text{Na}]10$ (**B**) in 0.50 M THF/toluene- d_8 at -80°C . Spectra (b)-(j) show a superposition of ensembles, though the dominant one appears to be tetramer. The expected mole fractions are in 0.01 increments.

Tetramer Stack Plots in THF

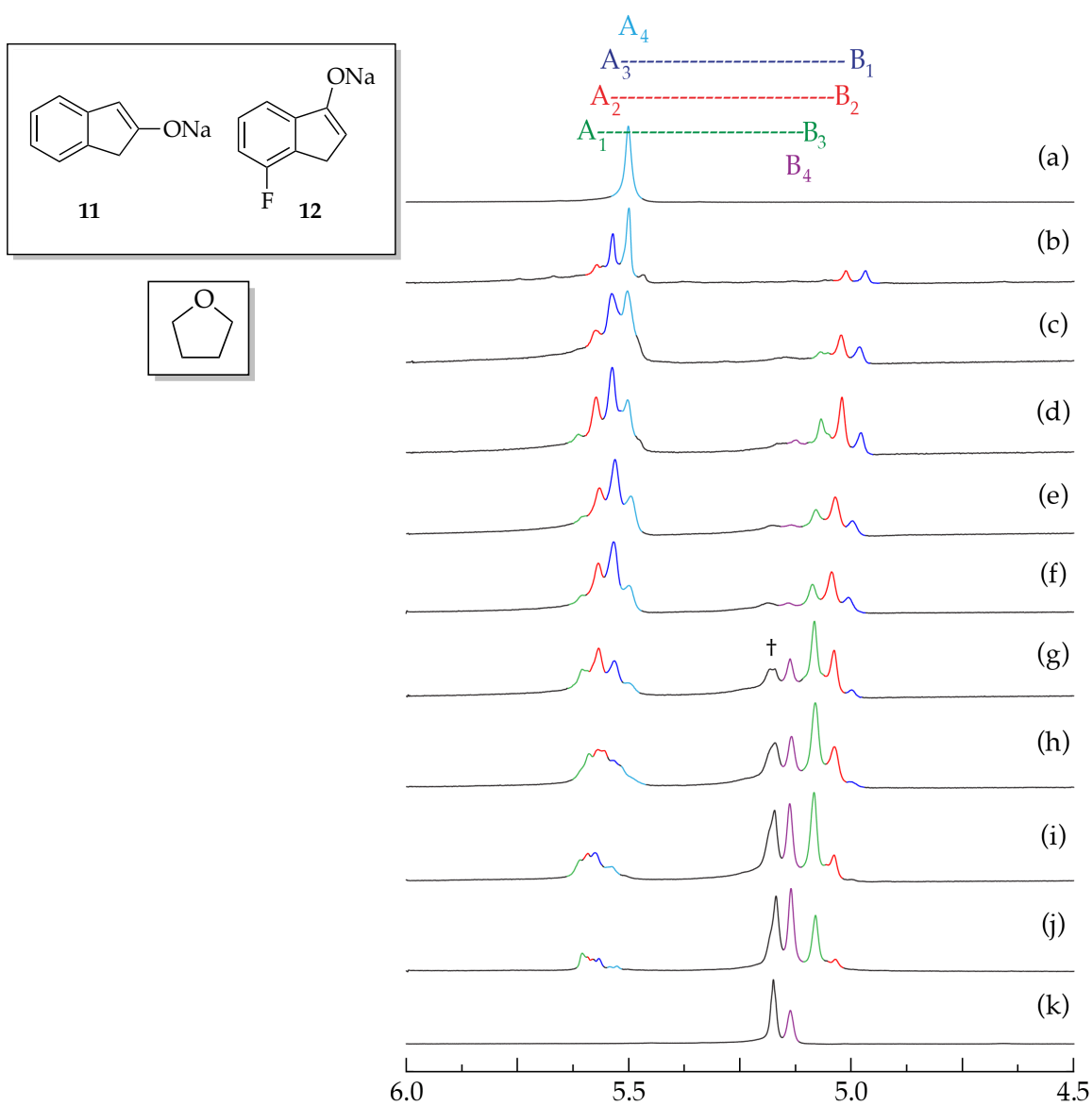


Figure AII.48. ^1H NMR spectra of 0.10 M solutions of [Na]**11** (**A**) and [Na]**12** (**B**) in 0.50 M THF/toluene- d_8 at $-80\text{ }^\circ\text{C}$. At low mole fraction of **11**, the ensemble has poor resolution on the **A** side. The expected mole fractions are in 0.01 increments. † denotes unknown aggregation states.

Tetramer Stack Plots in THF

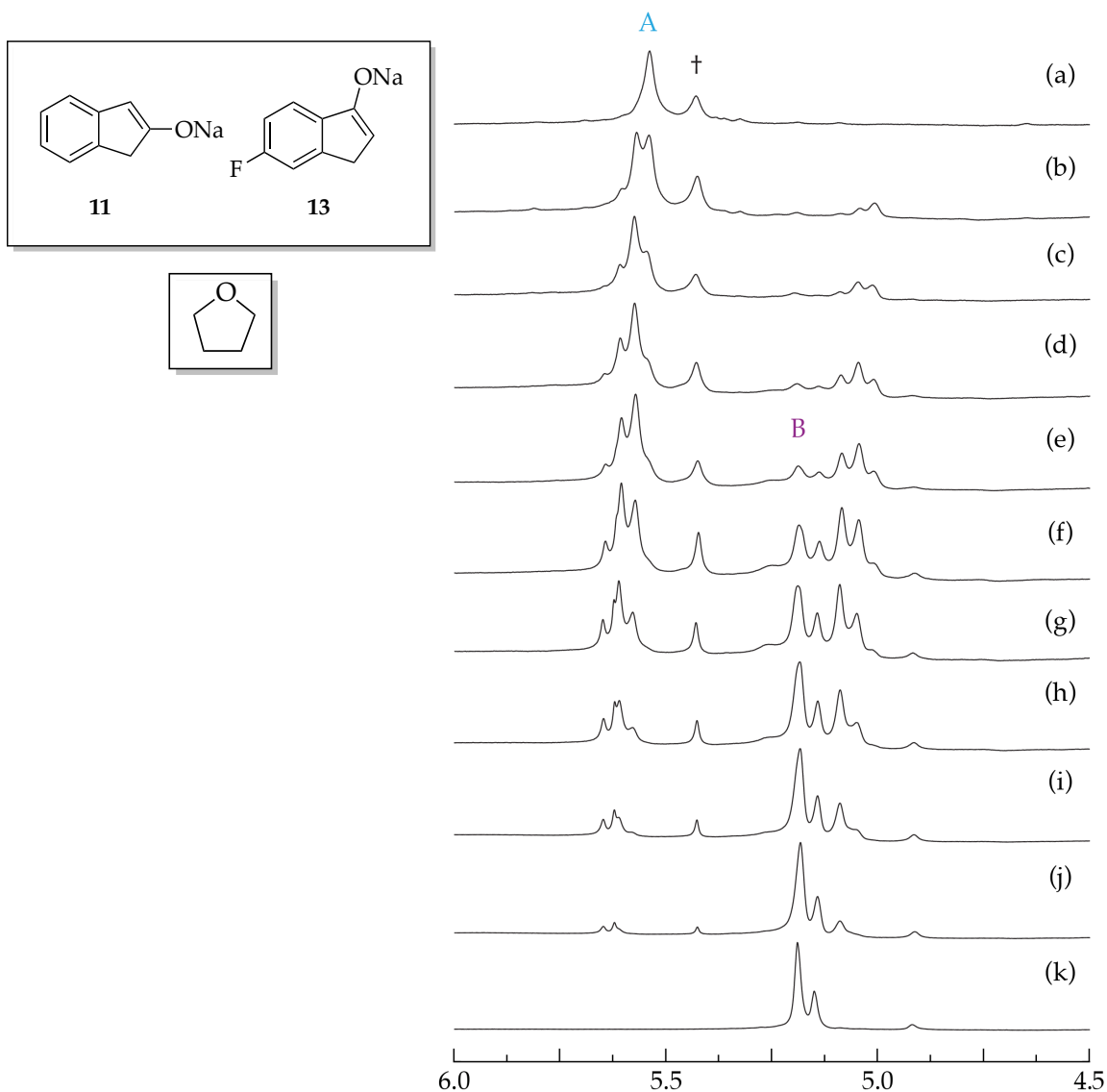


Figure AII.49. ^1H NMR spectra of 0.10 M solutions of $[\text{Na}]11$ (A) and $[\text{Na}]13$ (B) in 0.50 M THF/toluene- d_8 at -80°C . The expected mole fractions are in 0.01 increments. † denotes suspected mixed aggregate with NaHMDS.

Tetramer Job Plots in THF

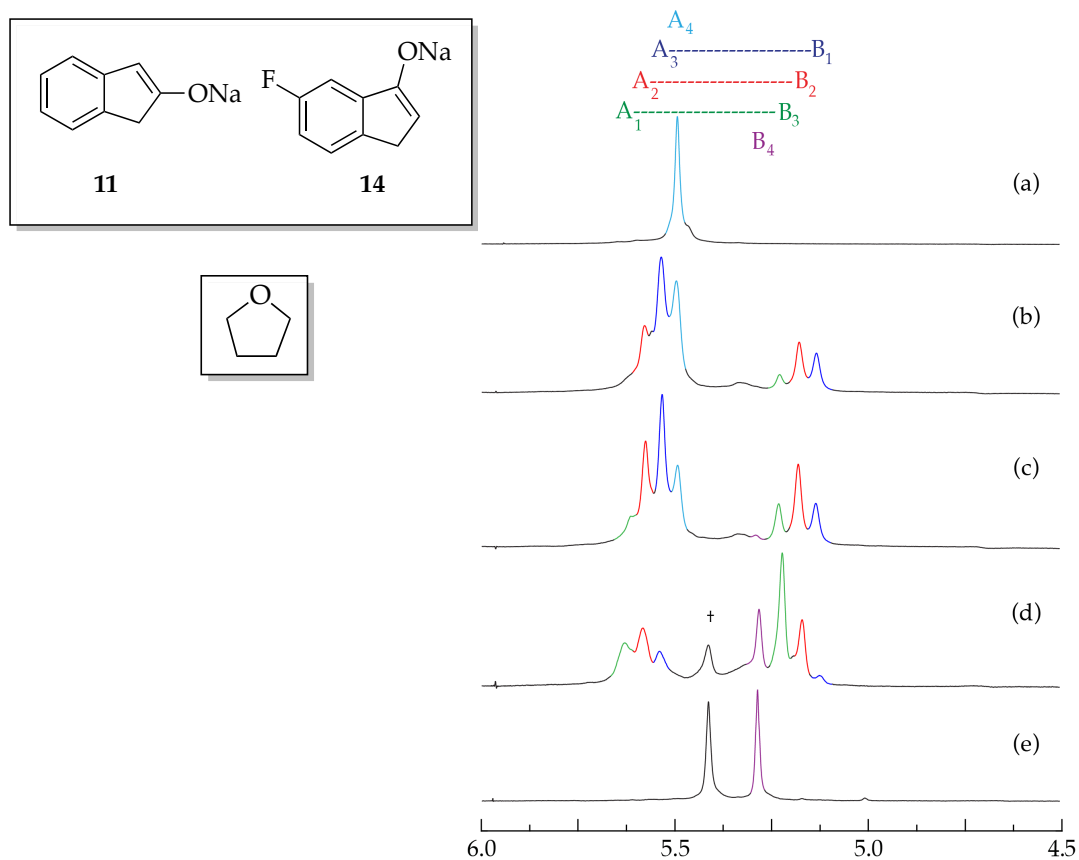


Figure AII.50. ^1H NMR spectra of 0.10 M solutions of [Na]11 (A) and [Na]14 (B) in 0.50 M THF/toluene- d_8 at -80°C . The measured mole fractions of A in (a)-(e) are 1.00, 0.81, 0.63, 0.34, and 0.00, respectively. † denotes unknown aggregation states.

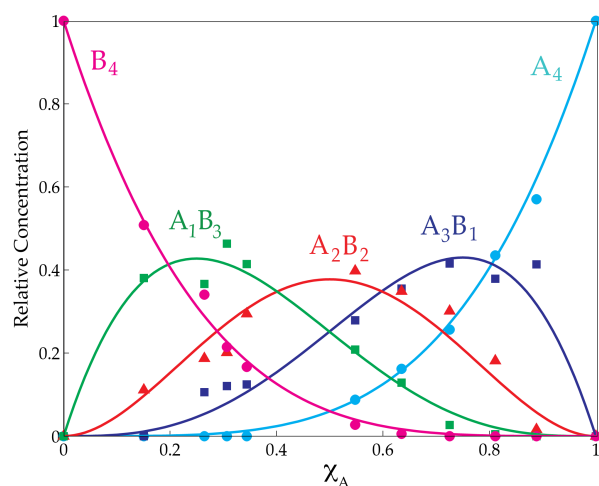


Figure AII.51. Job plot showing the relative integrations versus the measured mole fractions of A for 0.10 M mixtures of [Na]11 (A) and [Na]14 (B) in 0.50 M THF/toluene- d_8 at -80°C .

Tetramer Stack Plots in THF

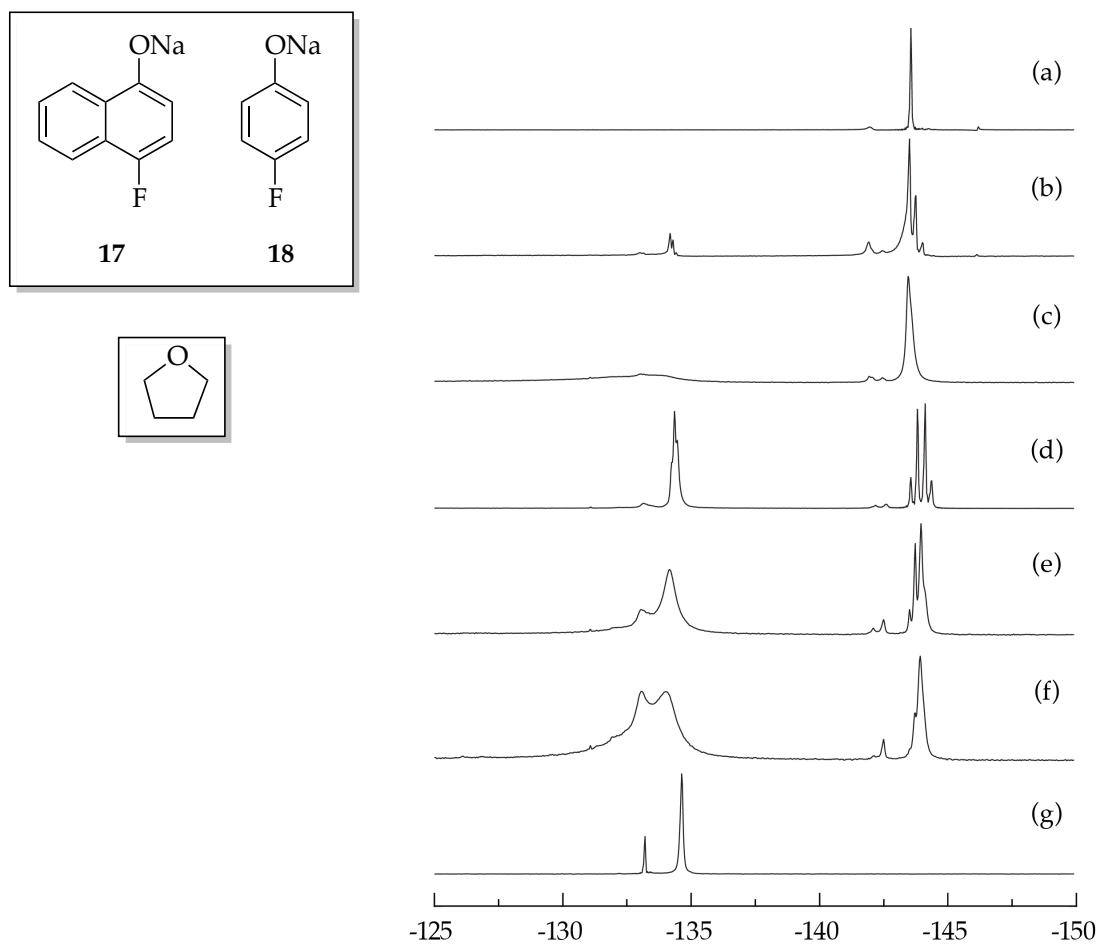


Figure AII.52. ¹H NMR spectra of 0.10 M solutions of [Na]**17** and [Na]**18** in 0.50 M THF/toluene-*d*₈ at -80 °C. The expected mole fractions of **17** in (a)-(g) are 1.0, 0.8, 0.6, 0.5, 0.4, 0.2 and 0.0, respectively.

E. Sodium isopropylcyclohexylamide NMR characterization.

^1H NMR

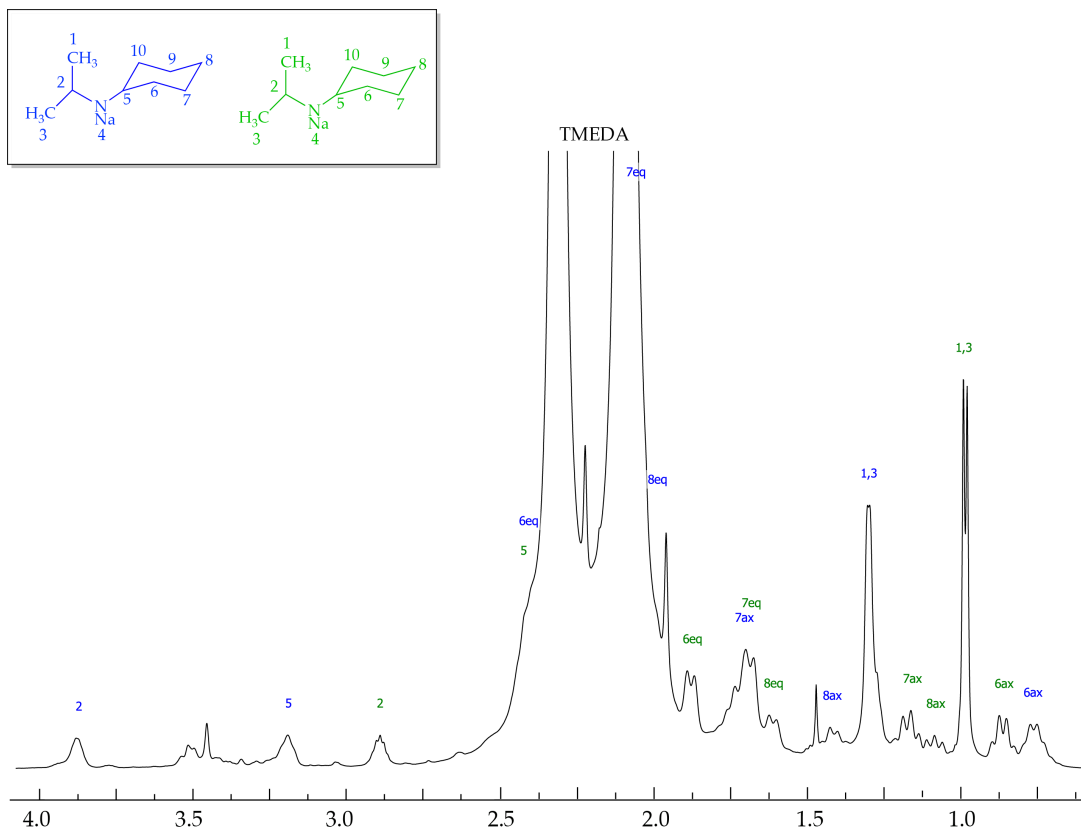


Figure AII.53. ^1H NMR spectrum of NaICA.

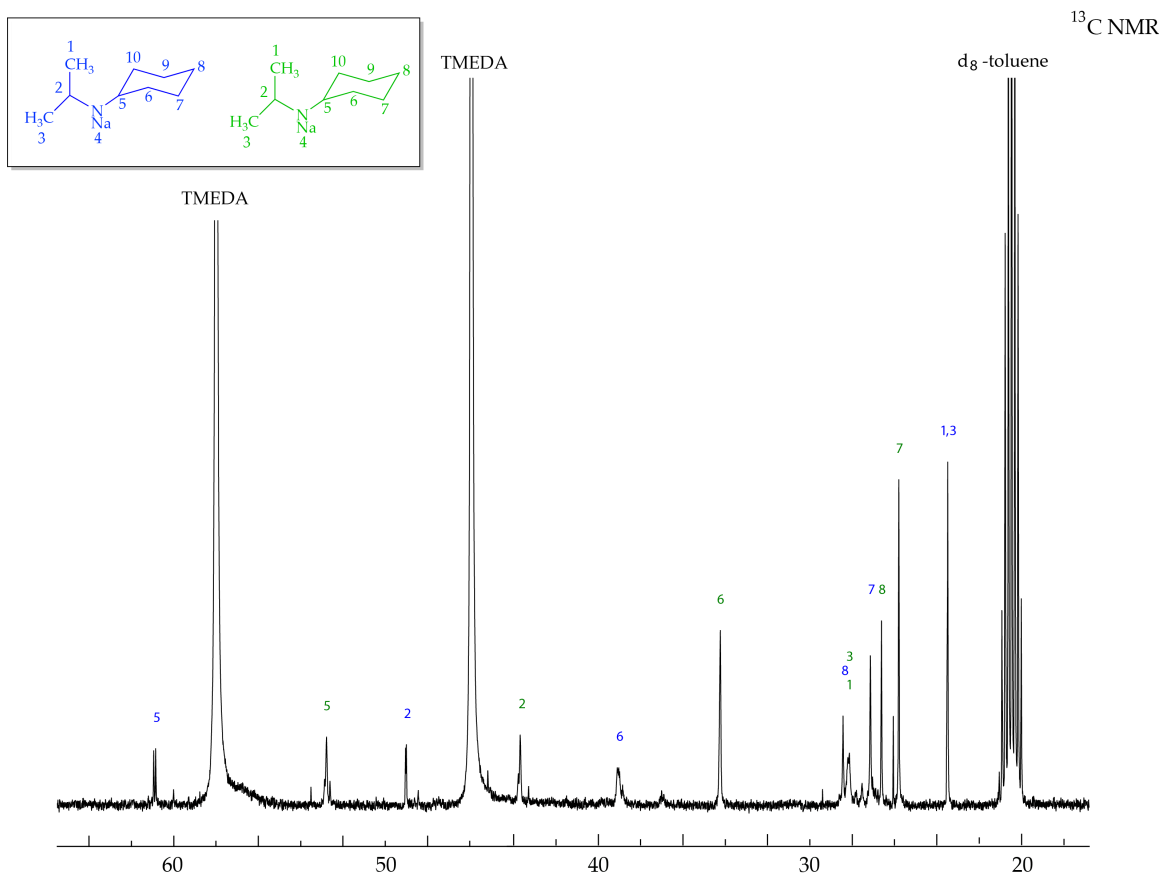


Figure AII.54. ¹³C NMR spectrum of NaICA.

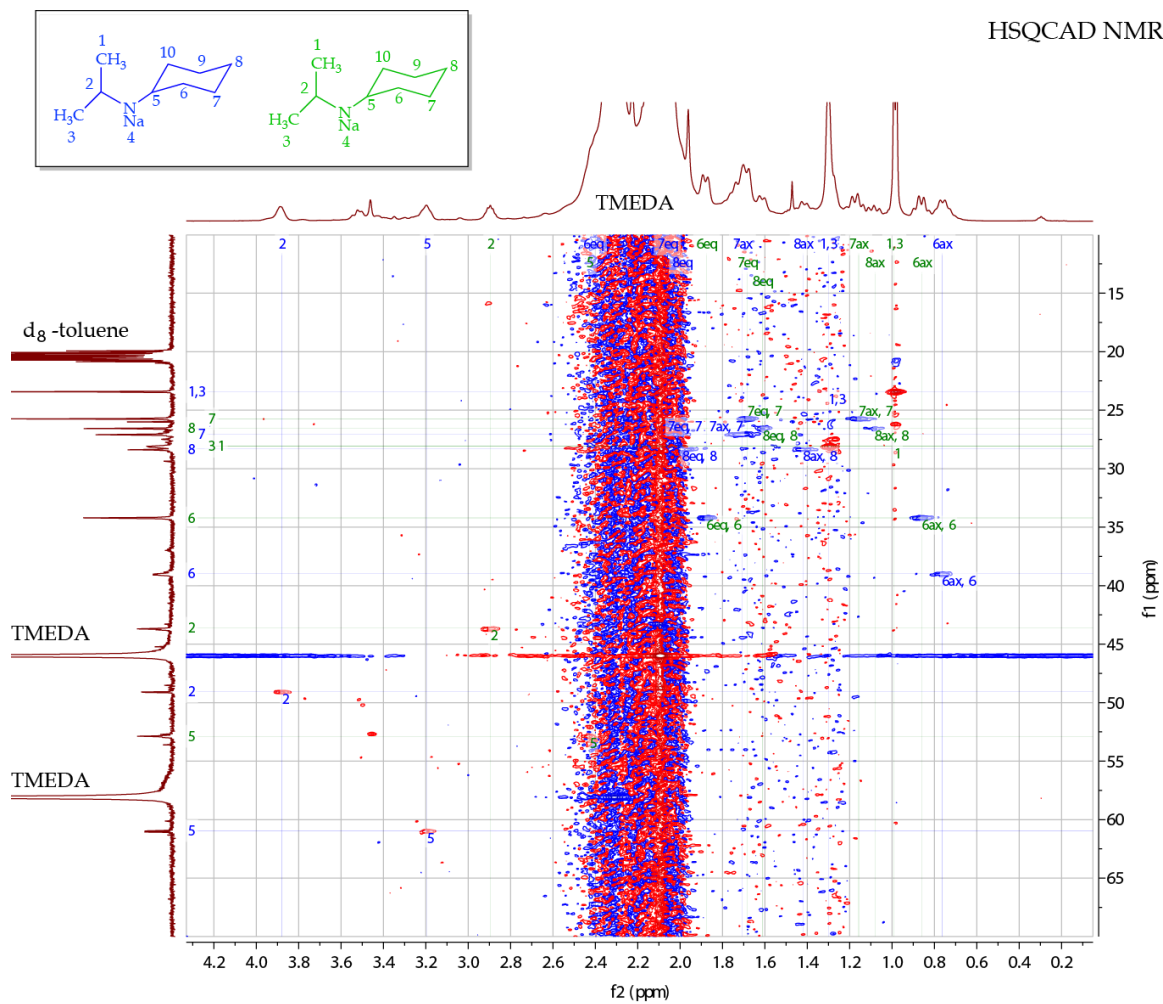


Figure AII.56. HSQCAD NMR spectrum of NaICA.

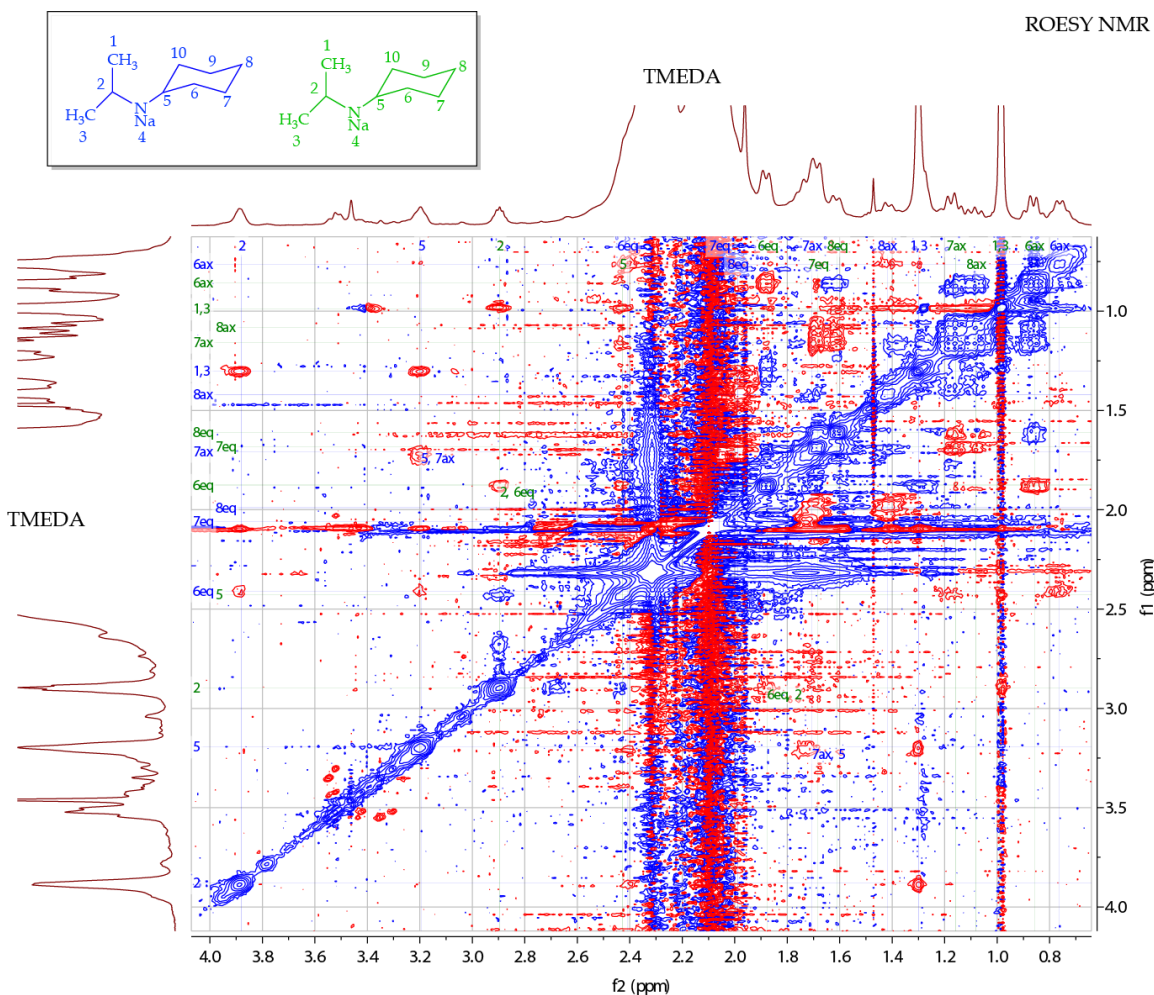


Figure AII.57. ROESY NMR spectrum of NaICA.

Sodium diisopropylamide (NDA). Isoprene (16mL, 0.16 mol) was dissolved in 30 mL dry DMEA and added over 1-2 h via syringe pump to a solution of finely sliced sodium metal (7.36 g, 0.32 mol) and diisopropylamine (32.4 g, 0.32 mol) in 80 mL DMEA at room temperature. The reaction is run in the bottom of a swivel fine frit apparatus with 250 mL round bottom flasks, attached directly to a schlenk line (see picture under LiHMDS synthesis). Addition of isoprene results in a yellow solution. After the addition of isoprene is complete the reaction is stirred for an additional 6-8 h. The frit is flipped and the solution is slowly

filtered, then the solution is evaporated to dryness. Solubility of NDA is high in DMEA yet it is insoluble in diethylmethanamine and triethylamine, making recrystallization difficult. Low amounts can be acquired using the centrifuge method described under the NaICA synthesis with DMEA.

Sodium dicyclohexylamide (NaDCA). Isoprene (16mL, 0.16 mol) was dissolved in 30 mL dry DMEA and added over 1-2 h via syringe pump to a solution of finely sliced sodium metal (7.36 g, 0.32 mol) and dicyclohexylamine (58 g, 0.32 mol) in 80 mL DMEA at room temperature. The reaction is run in a 250 mL round bottom flask attached directly to a schlenk line. Addition of isoprene results in a yellow solution and precipitation of the product. After the addition of isoprene is complete the reaction is stirred for an additional 6-8 h and evaporated to dryness. Solubility of NaDCA is low in DMEA and most amines, though it can be dissolved in *N*-methylpyrrolidine for potential recrystallization.

F. Comparing Lithium and Non-Lithium Ensembles with Underlying Math

For an ensemble formed from two homoaggregates with the same aggregation number (equation 1), the total number of species observed is $n + 1$, where n is the aggregation number



For NMR active nuclei in the center of an ensemble (e.g. lithium), the number of species formed is the same as the NMR peak count, which corresponds to $n + 1$.

Shown in Figure AII.58 is a tetramer example.

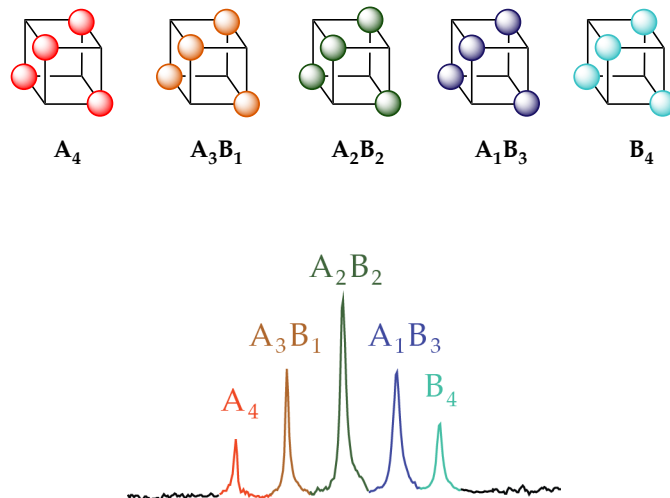


Figure AII.58. A 1 : 1 mixture of A and B, with roughly the expected NMR ratios of 1 : 4 : 6 : 4 : 1.

Using MCV, the statistical Job plots are shown in Figure 59.

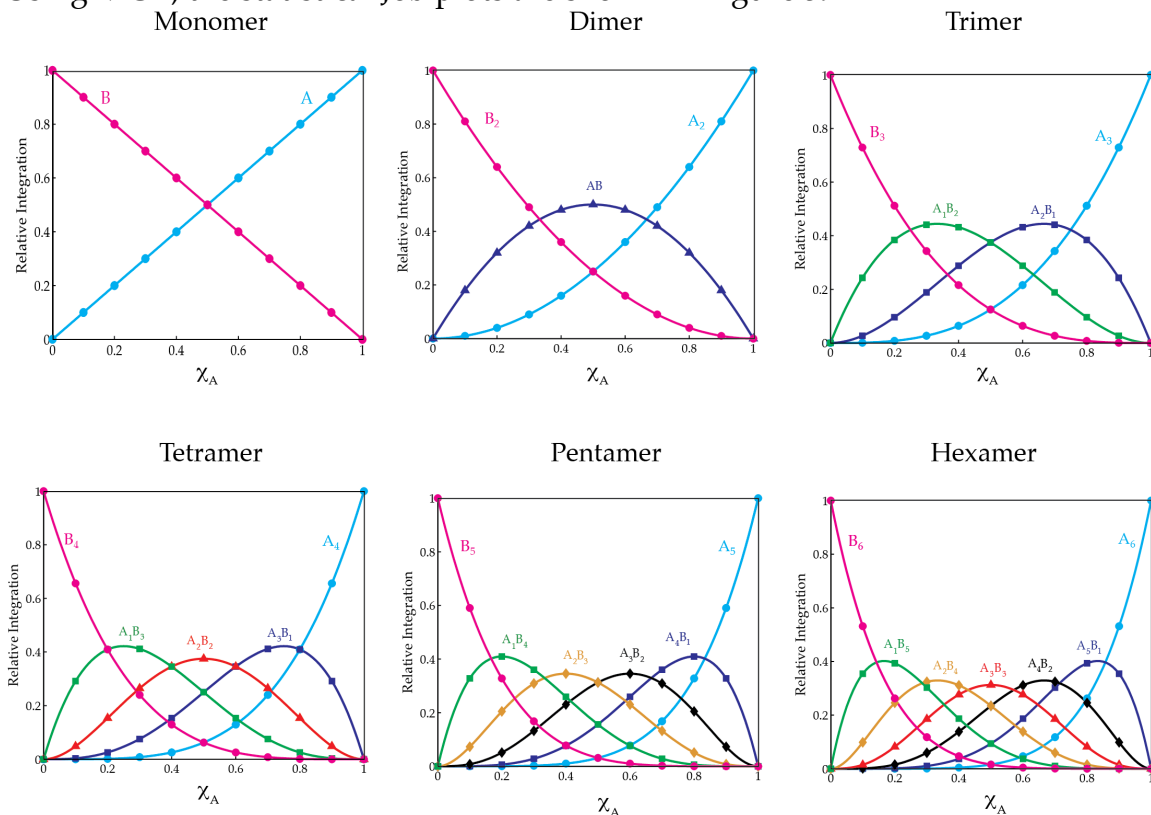


Figure AII.59. For monomer through hexamer, the statistical NMR integrals are shown as points, and the curves are the parametric fits described previously.

When the NMR nuclei used to detect these ensembles is not in the center of the aggregate but rather directly attached to *both* the A *and* B substrate, an A envelope *and* a B envelope are observed, each with n number of peaks (Figure AII.60). Both ^{19}F and ^1H have been used for this purpose.

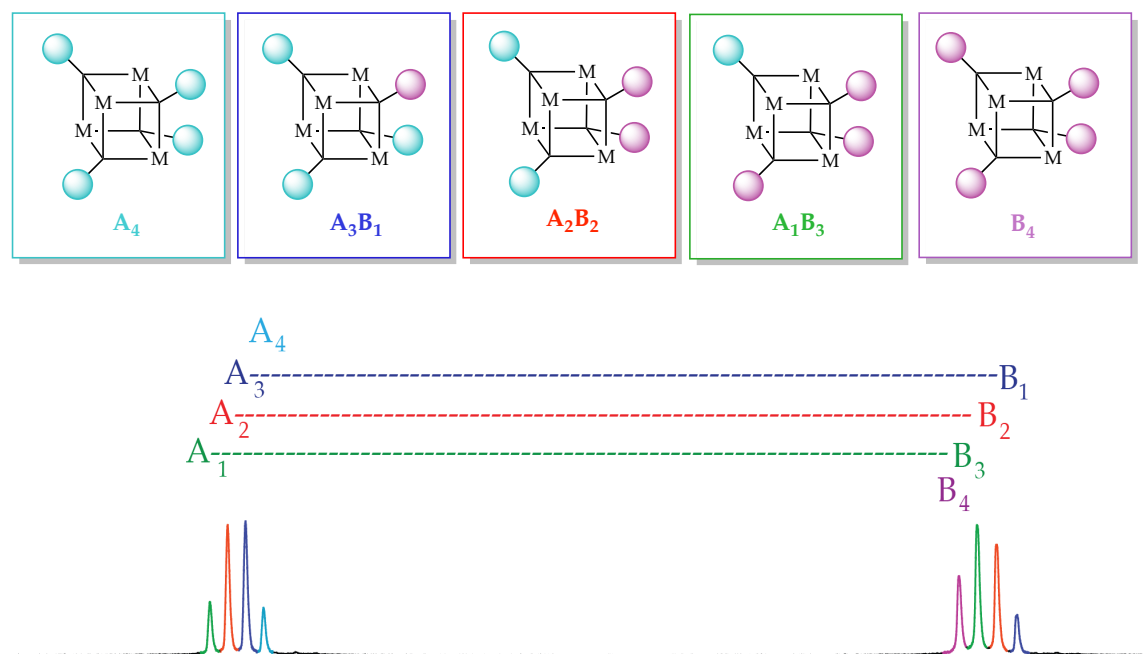


Figure AII.60. A 1 : 1 mixture of A and B, with a distinct A envelope and B envelope.

If both sides are visible and resolved, the heteroaggregate peaks can be summed together to give a standard Job plot. For ^{19}F NMR, it is also important to note that even when both sides are visible, the number of fluorines present should be taken into account (Figure AII.61). The points will shift along the x-axis as the measured mole fraction will change.

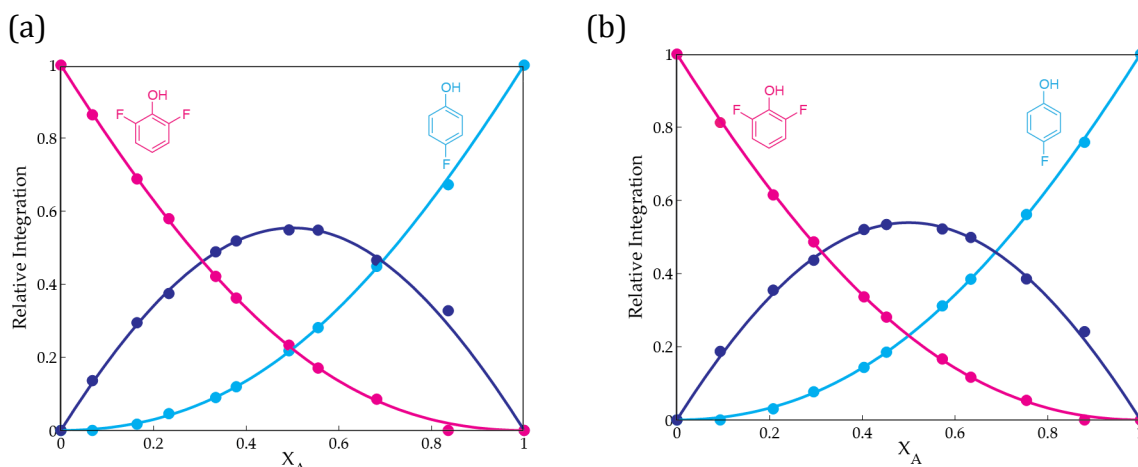


Figure AII.61. Part (a) does not correct for the two fluorines in 2,6-difluorophenol whereas part (b) includes the correction.

When the NMR nuclei used to detect these ensembles is not in the center of the aggregate but rather directly attached to *either* the A or B substrate, *either* an A envelope *or* a B envelope is observed, still with n number of peaks. ^{19}F has most commonly been used where only one substrate has a fluorine attached (Figure AII.62).

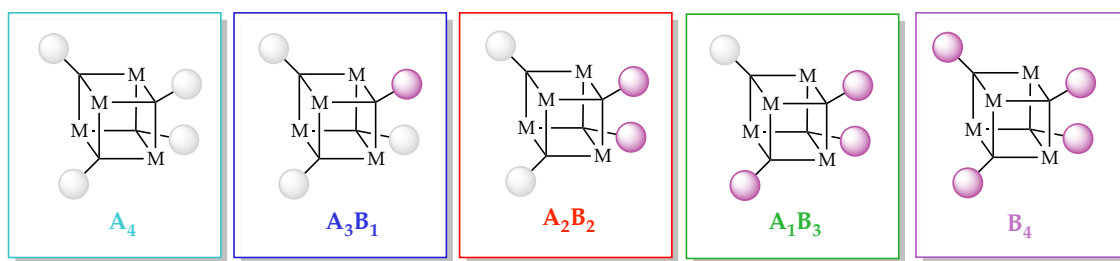


Figure AII.62. The grey spheres in the tetramer ensembles are not visible, resulting in the detection of 4 NMR peaks .

The visibility of only one side results in a different number of visible subunits for each aggregate. Shown in table AII.1 are the predicted NMR ratios based on a statistical distribution for a tetramer.

Aggregation state	Aggregates	Statistical ensemble ratios for 1 : 1 mixture (x # visible subunits)	Statistical singly-tagged ratios for 1 : 1 mixture
Tetramer	$A_4, A_3B_1, A_2B_2, A_1B_3, B_4$	1 (x4) : 4 (x3) : 6 (x2) : 4 (x1) : 1 (x0)	1 : 3 : 3 : 1*

Table AII.1. The statistical ensemble ratios and the statistical singly-tagged NMR ratios for a 1 : 1 tetrameric mixture. The parenthetical numbers indicate the number of visible subunits present per aggregate, which upon multiplication gives the statistical singly-tagged NMR ratios of a 1 : 1 tetramer. *This ratio corresponds exactly to the statistical ensemble ratio of a trimer.

Experimentally, the reverse must occur for the construction of the Job Plot. Each NMR integral must be divided by the number of visible substrates per aggregate, giving a measure of the relative concentration of either substrate A or B. The Job plot is not inherently different, except the last observable species will be either A_1B_{n-1} or $A_{n-1}B_1$. The x-axis limit will now be dependent on the aggregation state following $(n-1)/n$, which corresponds to the maximum of the last observable species (Figure AII.63).

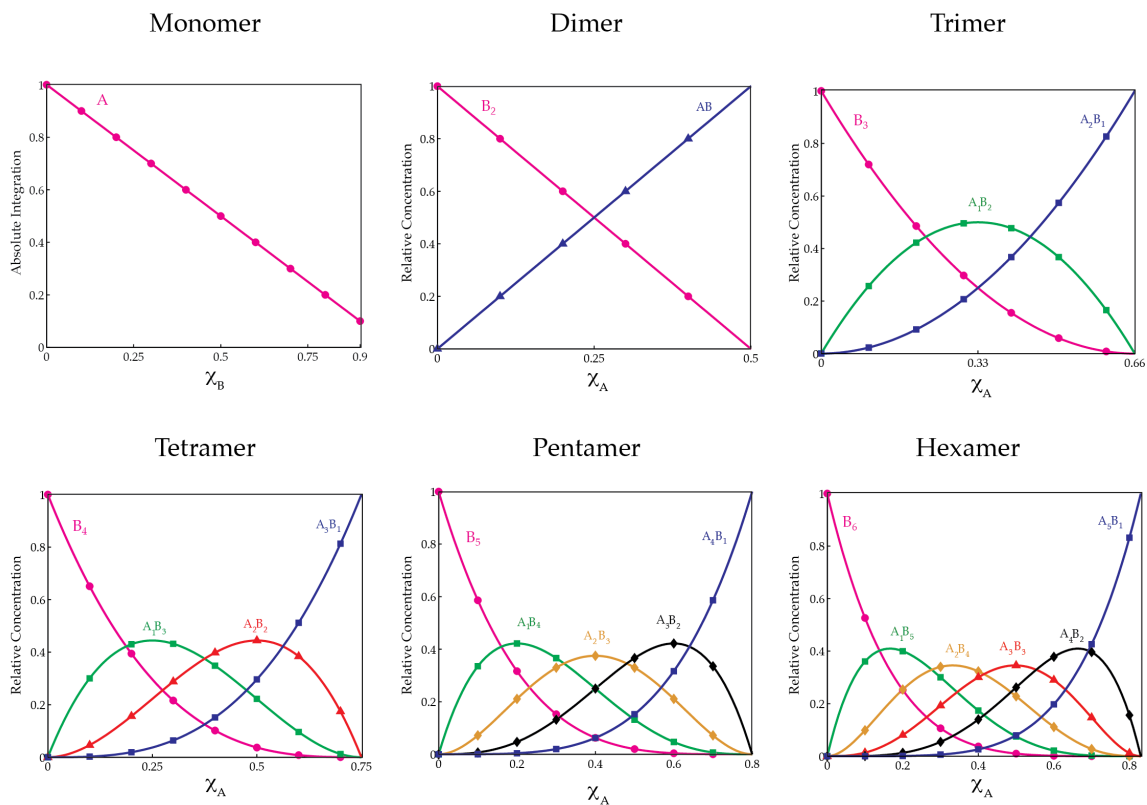


Figure AII.63. For monomer through hexamer, the x-axis will terminate at 0.9, 0.5, 0.67, 0.75, 0.8, and 0.83, respectively. Statistical NMR integrals are shown as points, and the curves are the parametric fits described in the supporting information. The monomer will only have one peak present throughout; shown is a plot of absolute integration instead of relative integration.

G. Matlab Files for a Singly-Tagged Tetramer Ensemble.

The Matlab folders described below in the bold titles are labeled for ^{19}F , though obviously the nuclei does not matter for the parametric fit. To start the process, open **Data1_19F.m** and insert the measured mole fractions and normalized NMR integrals into their appropriate matrix and save the file without changing the file name. Using the Matlab command window, type the following:

```
Data1_19F      % variables will appear in the workspace

try_fit_19F(XA_19F, phi, peak_assignment, Expt_Populations)
% only done to check whether the data is entered correctly; generates a plot

[phi_new, error] = refine_fit_19F(XA_19F, phi, peak_assignment,
Expt_Populations)
% does the curve fitting through an iterative process; gives phi values and errors

phi = phi_new % replaces the old phi values with the new phi values from the fit

try_fit_19F(XA_19F, phi, peak_assignment, Expt_Populations)
% Generates a Job plot with the parametric fit, which can be exported to Adobe
Illustrator
```

Tetramer:

A tetramer will appear like a trimer, and the x-axis will scale to 0.75, corresponding to the stoichiometry of the last visible aggregate, A_3B_1 .

Data1_19F.m:

```
% This script sets up variables for an ensemble of
% aggregates of the same aggregation number.
%
%      XA(j): the measured mole fractions.
%      Expt_Populations(j,k): the normalized NMR integrals
%      peak_assignment: sets the order of NMR peaks.
%      phi: sets the relative energies of each n-mer.

% First, list the mole fractions of A such that it
% correlates with the rows in the Expt_Populations.

%DISCLAIMER: this part is only relevant if your B_n is the
%fluorinated part, but will help align the axis and numbers
%correctly. We are using a tetramer A4 and B4 purely for
%illustrative purposes.
```

```
%If using the same format as with lithium, the
%homoaggregate on the right (B4) will be the curve on the
%left of the Job plot. Usually Mole Fraction is calculated
%with respect to A4. Since B is the fluorinated part, we
%have to calculate it with respect to B4. 1-[MF] is
%necessary if we want the plot to run from 0 to 0.75
%instead of 0.25 to 1.0.
```

```
%Lithium format: L to R
% A4 A3B1 A2B2 A1B3 B4
```

```
%calc MF w.r.t A = A4 + 0.75*A3B1 + 0.5*A2B2 + 0.25*A1B3
```

```
%19F format if B4 is fluorinated: L to R
%A3B1 A2B2 A1B3 B4
```

```
%calc MF w.r.t. B (Fluorine) = 0.25*A3B1 + 0.5*A2B2 +
%0.75*A1B3 + B4
```

```
% pure F (B4) should be at point 0, not 1.
% If following this setup, it will be at MF =1 with
% experimental populations of 0 0 0 1. Hence, 1 -[XA_19F]
```

```
XA_19F = 1-[0.1
0.2
0.3
0.4
0.5
0.6
0.7
0.8
0.9
1];
```

```
% Next, list the experimental populations of the
% aggregates. The number of rows must match XA_19F.
```

```
Expt_Populations =
[0.9    0.09    0.01    0
0.x    0.x     0.x     0.x
0.x    0.x     0.x     0.x
0.x    0.x     0.x     0.x
0.x    0.x     0.x     0.x
0.x    0.x     0.x     0.x
0.x    0.x     0.x     0.x
0.x    0.x     0.x     0.x
0.x    0.x     0.x     0.x
0      0      0      1];
```

```

% following the described format will put it as [4 3 2 1]
% corresponding to A3B1, A2B2, A3B1, B4.
% if peaks overlap, assign them twice. e.g. [3 2 1 1]

```

```

peak_assignment = [4 3 2 1];

```

```

% Assign the "energy" of each n-mer using the computer's
expected ordering.

```

```

phi = [ 1 1 1 1 ];

```

Error_of_Model_19F.m:

```

% The description of this file has been previously
% reported; Please refer to the supporting information in
% J. Am. Chem. Soc. 2008, 130, 4859.

```

```

function [mean_error, pop_error] =
Error_of_Model_19F(XA_19F,phi, peak_assignment,
Expt_Populations, Expt_weights)

    if (nargin<5) % If no info on data given assume all
points equally precise.
        Expt_weights=ones(size(Expt_Populations));
    end

    % Compute values from the model.
Concentrations = multimers_19F(XA_19F,phi);
PP = Populations(Concentrations, peak_assignment);

    % Compute the mean error.
diff = PP - Expt_Populations;
mean_error = sqrt(sum(sum(diff.*diff.*Expt_weights)) /
sum(sum(Expt_weights)));

    % Compute the error for each population independently.
pop_error = sum(diff.*Expt_weights,1) ./
sum(Expt_weights,1);
pop_error(2,:) = sqrt(sum(diff.*diff.*Expt_weights,1)
./ sum(Expt_weights,1));

```

Refine_fit_19F.m:

```

% The description of this file has been previously
% reported; Please refer to the supporting information in
% J. Am. Chem. Soc. 2008, 130, 4859.

```

```

function [phi_new, error] = refine_fit_19F(XA_19F,phi,
peak_assignment, Expt_Populations)

if (nargin<5)
    Expt_weight = ones(size(Expt_Populations));
end

N = length(phi)-1;
param = [ 2:(N+1)];
% We need to select an initial step size of each for trial
improvements 10% is a good starting figure.
step_size = 0.1*phi(param),

% Initialize Search
N_no_progress = 0; % Number of steps since error last
improved.
N_max_trials = 30; % Give up if after 30 steps things have
got no better.
[error_best, temp] = Error_of_Model_19F(XA_19F,phi,
peak_assignment, Expt_Populations) ; % Initial Quality of
Fit
fprintf(1, '\n Initial Error of Fit = %f percent.\n',
error_best * 100);

% Iteratively try to improve fit.
while (N_no_progress < N_max_trials)

    flag = 0;

    for k=1:length(param) % Try tweaking each parameter in
turn.

        % Step to the right
        phi_testr = phi;
        phi_testr(param(k))=abs(phi(param(k)) +
step_size(k));
        [error_testr, temp] =
Error_of_Model_19F(XA_19F,phi_testr, peak_assignment,
Expt_Populations, Expt_weight);

        % Step to the left
        phi_testl = phi;
        phi_testl(param(k))=abs(phi(param(k)) -
step_size(k));
        [error_testl, temp] =
Error_of_Model_19F(XA_19F,phi_testl,
peak_assignment,Expt_Populations, Expt_weight);

```

```

    % Decide if you want to step.
    if (error_testr < error_best)
        % Positive step better so keep going that
way.
        error_best = error_testr; phi = phi_testr;
step_size(k) = step_size(k) * 1.5;
        N_no_progress = 0;
    elseif (error_testl < error_best) % Negative
step better so keep going that way
        error_best = error_testl; phi = phi_testl;
step_size(k) = step_size(k) * 1.5;
        N_no_progress = 0;
    else
        flag = flag + 1; % Failure. Add it to the
list.
    end
end

    if (flag > 2) % Failed to improve by stepping in any
direction
        step_size = step_size * (0.75 + 0.25*rand); %
Reduce step size
        N_no_progress = N_no_progress + 1;
    end

    % After adjust each element of rel_weight, report new
fit.
    fprintf(1, '\nError - %f , Last Good Step - %d , Mean
Step Size - %f \n ', error_best, N_no_progress,
100*mean(step_size./phi(param)));
    fprintf(1, ' Phi - %f', phi);

end

error = error_best;
phi_new = phi;

```

try_fit_19F.m:

```

% The description of this file has been previously
% reported; Please refer to the supporting information in
% J. Am. Chem. Soc. 2008, 130, 4859.

```

```

function try_fit_19F(XA_19F, phi, peak_assignment,
Expt_Populations)

```



```

    % If no experimental errors given, weight all points
    equally.
    if (nargin<5)
        Expt_weights=ones(size(Expt_Populations));
    else
        Expt_weights = 1./ ( Expt_Errors +
mean(mean(Expt_Errors)));
    end

    % Plot the measured values of NMR populations
    % hold on ; cscheme='brgmkcybrgmkcy'; axis([0 0.75 0
1]); xlabel('X_A'); ylabel('Mole Fractions');

    % set(gca,'XTick',[0 0.25 0.50 0.75])

        hold on ; cscheme='brgmbrcbcybrgmkcy'; axis([0.0
0.75 0.0 1.0]);
        set(gca,'XTick',[0.0 0.25 0.50
0.75],'FontSize',14,'FontName','Palatino')
        set(gca,'YTick',[0.0 0.2 0.4 0.6 0.8 1.0])

xlabel('X_B','FontSize',16,'FontName','Palatino');
    %xlabel('X_n_o_
_f_l_u_o_r_i_n_e','FontSize',16,'FontName','Palatino');
    ylabel('Relative
Integration','FontSize',16,'FontName','Palatino');

    for j=1:size(Expt_Populations,2)
        if (nargin<5)
            plot(XA_19F,
Expt_Populations(:,j),sprintf('%so',cscheme(j)), 'MarkerSize
',25,'Marker','.');
        else
            errorbar(XA_19F, Expt_Populations(:,j),
Expt_Errors(:,j),sprintf('%so',cscheme(j)));
        end
    end

    % Plot the model on
    XAc = [0:0.01:0.75];
    TP=Populations(multimers_19F(XAc,phi), peak_assignment);
    for j=1:size(TP,2)
        plot(XAc,TP(:,j), sprintf('%c',cscheme(j)),
'LineWidth',2);
    end

    % Compute how good the model is and AepoAt to the useA.

```

```

    [mean_error, pop_error] =
    Error_of_Model_19F(XA_19F,phi, peak_assignment,
    Expt_Populations, Expt_weights);
    N = length(phi)-1;
        fprintf(1, '\nThe Mean mismatch is %f
peAcent.\n', mean_error*100);
        for j=1:size(pop_error,2)
            fprintf(1, 'Predicted value of species A%dB%d
+A%dB%d exceeds measurement by %f percent and mean square
error of %f percent.\n ', j-1,N-j+1,N-j+1,j-
1,pop_error(1,j)*100,pop_error(2,j)*100);
        end

```

multimers.m and populations.m:

The description and contents of these files have been previously reported; Please refer to the supporting information in *J. Am. Chem. Soc.* **2008**, *130*, 4859.

REFERENCES AND FOOTNOTES II

1. Dugger, R. W.; Ragan, J. A.; Ripin, D. H. B. *Org. Process Res. Dev.* **2005**, *9*, 253.
2. (a) Green, J. R. In *Science of Synthesis*; Georg Thieme Verlag: New York, 2005; Vol. 8a, pp 427-486. (b) Schetter, B.; Mahrwald, R. *Angew. Chem., Int. Ed.* **2006**, *45*, 7506. (c) Arya, P.; Qin, H. *Tetrahedron* **2000**, *56*, 917. (d) Caine, D. In *Comprehensive Organic Synthesis*; Trost, B. M.; Fleming, I., Eds.; Pergamon: New York, **1989**, Vol. 1, p 1. (e) Plaquevent, J.-C.; Cahard, D.; Guillen, F.; Green, J. R. In *Science of Synthesis*; Georg Thieme Verlag: New York, 2005; Vol. 26, pp 463-511. (f) *Comprehensive Organic Functional Group Transformations II*; Katritzky, A. R.; Taylor, R. J. K., Eds.; Elsevier: Oxford, UK, 1995, pp. 834-835. (g) Cativiela, C.; Diaz-de-Villegas, M. D. *Tetrahedron: Asymmetry* **2007**, *18*, 569. (h) Woltermann, C. J.; Hall, R. W.; Rathman, T. *PharmaChem* **2003**, *2*, 4. (i) Seebach, D. *Angew. Chem., Int. Ed. Engl.* **1988**, *27*, 1624. (j) Williard, P. G. In *Comprehensive Organic Synthesis*; Pergamon: New York, 1991; Vol. 1, p 1.
3. (a) Sott, R.; Granander, J.; Williamson, C.; Hilmersson, G. *A Eur. J.* **2005**, *11*, 4785. Owen, D. W.; Puller, P. C. *J. Organometal. Chem.* **1983**, *255*, 173. (b) Lochmann, L.; Trekoval, J. *J. Organometal. Chem.* **1979**, *179*, 123. (c) Lochmann, L.; Pospisil, J.; Lim, D. *Tetrahedron Lett.* **1966**, 257. (d) Schade, C.; Bauer, W.; Schleyer, P.v.R. *J. Organometal. Chem.*, **1985**, *295*, C25.
4. Mulvey, R. E.; Robertson, S. D. *Angew. Chem., Int. Ed.* **2013**, *52*, 11470.
5. Wannagat, U.; Niederprüm, H. *Chem. Ber.* **1961**, *94*, 1540.
6. Msayib, K. J.; Watt, C. I. F. *Chem. Soc. Rev.* **1992**, *21*, 237.
7. (a) Laguf, B. R.; Liotta, D. C. *Tetrahedron Lett.* **1994**, *35*, 4485. (b) Boeckman, R. K., Jr.; Boehmler, D. J.; Musselman, R. A. *Org. Lett.* **2001**, *3*, 3777. (c) Goh, J. B.; Lagu, B. R.; Wurster, J.; Liotta, D. C. *Tetrahedron Lett.* **1994**, *35*, 6029. (d) Davis, F. A.; Sheppard, A. C.; Chen, B.-C.; Haque, M. S. *J. Am. Chem. Soc.* **1990**, *112*, 6679.
8. (a) Khair, N.; Fernandez, I.; Alcudia, A.; Garcia, M. V.; Recio, R. *Carbohydrates: Tools for Stereoselective Synthesis* Boysen, M., Martin K., Eds., 2013, 47-63. (b) De'ne's, F.; Pe'rez-Luna, A.; Chemla, F. *Chem. Rev.* **2010**, *110*, 2366. (c) Alexander, K.; Cook, S.; Gibson, C. L.; Kennedy, A. R. *J. Chem. Soc., Perkin Trans. 1* **2001**, 1538. (d) Evans, D. A.; Wu, L. D.; Wiener, J. J. M.; Johnson, J. S.; Ripin, D. H. B.; Tedrow, J. S. *J. Org. Chem.* **1999**, *64*, 6411. (e) Konigsberger, K.; Prasad, K.; Repic, O.; Blacklock, T. J. *Tetrahedron: Asymm.* **1997**, *8*, 2347. (f) Harwood, L. M.; Houminer, Y.; Manage, A.; Seeman, J. I. *Tetrahedron Lett.* **1994**, *35*, 8027. (g) Cahard, D.; Duhamel, P. *Eur. J. Org. Chem.* **2001**, 1023. (h) Anaya de Parrodi, C.; Clara-Sosa, A.; Pe'rez, L.; Quintero, L.; Maran, V.; Toscano, R. A.; Avin, J. A.; Rojas-Limae, S.; Juaristi, E. *Tetrahedron: Asymm.* **2001**, *12*, 69. (i) Chuna, C. C.; Leea, C.-J.; Kimb, J. N.; Kima, T. H. *Tetrahedron: Asymm.* **2005**, *16*, 2989. (j) Takuwa, T.; Minowa, T.; Onishi, J. Y.; Mukaiyama, T. *Bull. Chem. Soc. Jpn.* **2004**, *77*, 1717. (k) Reyes-Rangel, G.; Jiménez-González, E.; Olivares-Romero,

- J. L.; Juaristi, E. *Tetrahedron: Asymm.* **2008**, *19*, 2839. (l) Reyes-Rangel, G.; Maranon, V.; Avila-Ortiz, C. G.; Anaya de Parrodi, C.; Quintero, L.; Juaristi, E. *Tetrahedron* **2006**, *62*, 8404. (m) Hama, T.; Hartwig, J. F. *Org. Lett.* **2008**, *10*, 1549. (n) Xu, Z. Q.; DesMarteau, D. D.; Gotoh, Y. *J. Fluorine Chem.* **1992**, *58*, 71.
9. (a) Linney, I. D.; Tye, H.; Wills, M.; Butlin, R. J. *Tetrahedron Lett.* **1994**, *35*, 1785. (b) Novikova, Z. S.; Kurkin, A. N.; Lutsenko, I. F. *Z. Obshh Khim.* **1978**, *48*, 305.
10. (a) Fryzuk, M. D.; Gao, X.; Rettig, S. J. *Can. J. Chem.* **1995**, *73*, 1175. (b) Williard, P. G.; Carpenter, G. B. *J. Am. Chem. Soc.* **1986**, *108*, 462. (c) Cambillau, C.; Bram, G.; Corset, J.; Riche, C. *Can. J. Chem.* **1982**, *60*, 2554. (d) Hevia, E.; Henderson, K. W.; Kennedy, A. R.; Mulvey, R. E. *Organometallics* **2006**, *25*, 1778. (e) Henderson, K. W.; Williard, P. G.; Bernstein, P. R. *Angew. Chem., Int. Ed. Engl.* **1995**, *34*, 1117. (f) Chi, Y.; Ranjan, S.; Chung, P.-W.; Liu, C.-S.; Peng, S.-M.; Lee, G.-H. *Dalton Trans.* **2000**, 343. (g) Solladie-Cavallo, A.; Simon-Wermeister, M. C.; Schwarz, J. *Organometallics* **1993**, *12*, 3743. (h) Garden, J. A.; Kennedy, A. R.; Mulvey, R. E.; Robertson, S. D. *Chem. Commun.* **2012**, *48*, 5265. (i) Salmon, L.; Thuery, P.; Ephritikhine, M. *Acta Crystallogr., Section E* **2006**, *62*, m1250-m1251.
11. (a) Boyle, T. J.; Velazquez, A. T.; Yonemoto, D. T.; Alam, T. M.; Moore, C.; Rheingold, A. L. *Inorg. Chim. Acta.* **2013**, *405*, 374. (b) Evans, W. J.; Golden, R. E.; Ziller, J. W. *Inorg. Chem.* **1993**, *32*, 3041. (c) Czado, W.; Muller, U. *Z. Kristallogr.-New Cryst. Struct.* **1999**, *214*, 63. (d) Walther, D.; Ritter, U.; Gessler, S.; Sieler, J.; Kunert, M. *Z. Anorg. Allg. Chem.* **1994**, *620*, 101. (e) Kunert, M.; Dinjus, E.; Nauck, M.; Sieler, J. *Chem. Ber.* **1997**, *130*, 1461. (f) Cole, M. L.; Junk, P. C.; Proctor, K. M.; Scott, J. L.; Strauss, C. R. *Dalton Trans.* **2006**, 3338.
12. (a) Ladder: Hsueh, M.-L.; Ko, B.-T.; Athar, T.; Lin, C.-C.; Wu, T.-M.; Hsu, S.-F. *Organometallics* **2006**, *25*, 4144. (b) stacked cubes: MacDougall, D. J.; Noll, B. C.; Henderson, K. W. *Inorg. Chem.* **2005**, *44*, 1181. (c) TMEDA-solvated cyclic dimer: Clegg, W.; Fleming, B. J.; Garcia-Alvarez, P.; Hogg, L. M.; Kennedy, A. R.; Klett, J.; Martinez-Martinez, A. J.; Mulvey, R. E.; Russo, L.; O'Hara, C. T. *Dalton Trans.* **2013**, *42*, 2512. (d) Cousins, D. M.; Davidson, M. G.; Garcia-Vivo, D. *Chem. Commun.* **2013**, *49*, 11809. (e) Zhang, J.; Wang, C.; Lu, M.; Yao, Y.-M.; Zhang, Y.; Shen, Q. *Polyhedron* **2011**, *30*, 1876. (f) Yuan, F.; Yang, J.; Xiong, L. *J. Organomet. Chem.* **2006**, *691*, 2534.
13. (a) Laszlo, P. *Encyclopedia of NMR* **2012**, *8*, 4581. (b) Kemp-Harper, R.; Brown, S. P.; Hughes, C. E.; Styles, P.; Wimperis, S. *Nuclear Magn. Reson. Spectr.* **1997**, *30*, 157. (c) Laszlo, P. *NMR Spectroscopy: New Methods and Applications*; ACS Symposium Series; American Chemical Society: Washington, DC, 1982.
14. Cornelius, A.; Laszlo, P.; Cambillau, C. *J. Chem. Res. (S)* **1978**, 462.
15. (a) Jackman, L. M.; Lange, B. C. *Tetrahedron* **1977**, *33*, 2737. (b) Vogt, H. H.; Gompper, R. *Chem. Ber.* **1981**, *114*, 2884. (c) Kiyooka, S.; Suzuki, K. *Bull. Chem. Soc. Japan* **1981**, *54*, 623. (d) Kiyooka, S.; Ueda, Y.; Suzuki, K. *Bull. Chem. Soc. Japan* **1980**, *53*, 1656. (e) Howden, M. E. H.; Tyler, M. *Tetrahedron Lett.* **1975**, 1979.

16. (a) Zook, H. D.; Rellahan, W. L. *J. Am. Chem. Soc.* **1957**, *79*, 881. (b) Greene, J. L.; Zook, H. D. *J. Am. Chem. Soc.* **1958**, *80*, 3629. (c) Zook, H. D.; Gumby, W. L. *J. Am. Chem. Soc.* **1960**, *82*, 1386. (d) Zook, H. D.; Russo, T. J. *J. Am. Chem. Soc.* **1960**, *82*, 1258. (e) Zook, H. D.; Russo, T. J.; Ferrand, E. F.; Stotz, D. S. *J. Org. Chem.* **1968**, *33*, 2222. (f) Zook, H. D.; Kelly, W. L.; Posey, I. Y. *J. Org. Chem.* **1968**, *33*, 3477.
17. Hill, D. G.; Burkus, J.; Luck, S. M.; Hauser, C. R. *J. Am. Chem. Soc.* **1959**, *81*, 2787.
18. For examples of colligative measurements on lithium enolates, see: (a) Seebach, D.; Bauer, W. *Helv. Chim. Acta* **1984**, *67*, 1972-1988. (b) Arnett, E. M.; Moe, K. D. *J. Am. Chem. Soc.* **1991**, *113*, 7288-7293. (c) Arnett, E. M.; Fisher, F. J.; Nichols, M. A.; Ribeiro, A. A. *J. Am. Chem. Soc.* **1990**, *112*, 801-808.
19. For examples of colligative measurements on other organolithiums, see: (a) Davidson, M. G.; Snaith, R.; Stalke, D.; Wright, D. S. *J. Org. Chem.* **1993**, *58*, 2810-2816. (b) Kallman, N.; Collum, D. B. *J. Am. Chem. Soc.* **1987**, *109*, 7466-7472. (c) Wanat, R. A.; Collum, D. B.; Van Duyne, G.; Clardy, J.; DePue, R. T. *J. Am. Chem. Soc.* **1986**, *108*, 3415-3422. (d) West, P.; Waack, R. *J. Am. Chem. Soc.* **1967**, *89*, 4395-4399. (e) Davidson, M. G.; Snaith, R.; Stalke, D.; Wright, D. S. *J. Org. Chem.* **1993**, *58*, 2810.
20. Li, D.; Keresztes, I.; Hopson, R.; Williard, P. G. *Acc. Chem. Res.* **2009**, *42*, 270.
21. (a) Sini, G.; Tessier, A.; Pytkowicz, J.; Brigaud, T. *A Eur. J.* **2008**, *14*, 3363. (b) Wang, Y.-G.; Sun, C.-J.; Deng, C.-H. *J. Phys. Chem. A* **1998**, *102*, 5816. (c) Nonella, M.; Suter, H. U. *J. Phys. Chem. A* **1999**, *103*, 7867.
22. Arnett, E. M.; Maroldo, S. G.; Schriver, G. W.; Schilling, S. L.; Troughton, E. B. *J. Am. Chem. Soc.* **1985**, *107*, 2091.
23. (a) Renny, J. S.; Tomasevich, L. L.; Tallmadge, E. H.; Collum, D. B. *Angew. Chem., Int. Ed.* **2013**, *52*, 11998. (b) Huang, C. Y. *Methods Enzymol.* **1982**, *87*, 509. (c) Hubbard, R. D.; Horner, S. R.; Miller, B. L. *J. Am. Chem. Soc.* **2001**, *123*, 5810. (d) Olson, E. J.; Bühlmann, P. *J. Org. Chem.* **2011**, *76*, 8406.
24. (a) Liou, L. R.; McNeil, A. J.; Ramirez, A.; Toombes, G. E. S.; Gruver, J. M.; Collum, D. B. *J. Am. Chem. Soc.* **2008**, *130*, 4859. (b) Gruver, J. M.; Liou, L. R.; McNeil, A. J.; Ramirez, A.; Collum, D. B. *J. Org. Chem.* **2008**, *73*, 7743. (d) Liou, L. R.; McNeil, A. J.; Toombes, G. E. S.; Collum, D. B., *J. Am. Chem. Soc.* **2008**, *130*, 17334. (e) De Vries, T. S.; Goswami, A.; Liou, L. R.; Gruver, J. M.; Jayne, E.; Collum, D. B. *J. Am. Chem. Soc.* **2009**, *131*, 13142. (f) Tomasevich, L. L.; Collum, D. B. *J. Org. Chem.* **2013**, *78*, 7498.
25. Kissling R. M.; Gagne, M. R. *J. Org. Chem.* **2001**, *66*, 9005.
26. "Pharmaceuticals & Intermediates 1986-1997 Update". Becker, A., Ed.; Becker Associates, 1997.

27. Reviews of ^{19}F NMR spectroscopy: (a) Gakh, Y. G.; Gakh, A. A.; Gronenborn, A. M. *Magn. Reson. Chem.* **2000**, *38*, 551. (b) McGill, C. A.; Nordon, A.; Littlejohn, D. J. *Process Anal. Chem.* **2001**, *6*, 36. (c) Espinet, P.; Albeniz, A. C.; Casares, J. A.; Martinez-Ilarduya, J. M. *Coord. Chem. Rev.* **2008**, *252*, 2180.
28. Collum, D. B. *Acc. Chem. Res.* **1992**, *25*, 448.
29. (a) Ward, L.; Barr, D. Brit. UK Pat. Appl. (1995), GB 2280671 A 19950208. (b) Barr, D.; Dawson, A. J.; Wakefield, B. J. *J. Chem. Soc., Chem. Commun.* **1992**, 204.
30. (a) Munguia, T.; Bakir, Z. A.; Cervantes-Lee, F.; Metta-Magana, A.; Pannell, K. H. *Organometallics* **2009**, *28*, 5777. (b) See also ref 3b.
31. (a) NaTMP-TMEDA: Armstrong, D. R.; Graham, D. V.; Kennedy, A. R.; Mulvey, R. E.; O'Hara, C. T. *Chem.-Eur.J.*, **2008**, *14*, 8025. (b) NaTMP-THF: Armstrong, D. R.; Garcia-Alvarez, P.; Kennedy, A. R.; Mulvey, R. E.; Robertson, S. D. *Chem.-Eur.J.* **2011**, *17*, 6725.
32. Andrews, P. C.; Barnett, N. D. R.; Mulvey, R. E.; Clegg, W.; O'Neil, P. A.; Barr, D.; Cowton, L.; Dawson, A. J.; Wakefield, B. J. *J. Organomet. Chem.* **1996**, *518*, 85.
33. Galiano-Roth, A. S.; Michaelides, E. M.; Collum, D. B. *J. Am. Chem. Soc.* **1988**, *110*, 2658.
34. Hsieh, H. L.; Quirk, R. P. *Anionic Polymerization: Principles and Practical Applications*; Marcel Dekker: New York, 1996.
35. Job, P. *Ann. Chim.* **1928**, *9*, 113.
36. By example, a statistical distribution of tetramers missing one homoaggregate will take on the appearance of a 1 : 3 : 3 : 1 trimer.
37. For example, a mixture of **10** and **11** in THF/toluene- d_8 show an additional aggregate, suspected to be dimer.
38. The crystallographic literature of lithium enolates reveals a prevalence of chelated dimers for TMEDA solvates: (a) Nichols, M. A.; Leposa, C. M.; Hunter, A. D.; Zeller, M. J. *Chem. Crystallogr.* **2007**, *37*, 825. (b) Seebach, D.; Amstutz, R.; Laube, T.; Schweizer, W. B.; Dunitz, J. D. *JACS* **1985**, *107*, 5403. (c) Meyers, A. I.; Seefeld, M. A.; Lefker, B. A.; Blake, J. F.; Williard, P. G. *J. Am. Chem. Soc.* **1998**, *120*, 7429. (d) Boche, G.; Langlotz, I.; Marsch, M.; Harms, K. *Chem. Ber.* **1994**, *127*, 2059. (e) Hahn, E.; Maetzke, T.; Plattner, D. A.; Seebach, D. *Chem. Ber.* **1990**, *123*, 2059. (f) Henderson, K. W.; Dorigo, A. E.; Williard, P. G.; Bernstein, P. R. *Angew. Chem., Int. Ed.* **1996**, *35*, 1322.
39. (a) Bauer, W.; Klusener, P. A. A.; Harder, S.; Kanters, J. A.; Duisenberg, A. J. M.; Brandsma, L.; Schleyer, P. v. R. *Organometallics* **1988**, *7*, 552. (b) Köster, H.; Thoennes, D.; Weiss, E. J. *Organomet. Chem.* **1978**, *160*, 1. (c) Harder, S.; Boersma,

J.; Brandsma, L.; Kanters, J. A. J. *Organomet. Chem.* **1988**, 339, 7. (d) Ball, S. C.; Cragg-Hine, I.; Davidson, M. G.; Davies, R. P.; Lopez-Solera, M. I.; Raithby, P. R.; Reed, D.; Snaith, R.; Vogl, E. M. J. *Chem. Soc., Chem. Commun.* **1995**, 2147.

40. (a) Armstrong, D. R.; Clegg, W.; Dale, S. H.; Garcia-Alvarez, J.; Harrington, R. W.; Hevia, E.; Honeyman, G. W.; Kennedy, A. R.; Mulvey, R. E.; O'Hara, C. T. *Chem. Commun.* **2008**, 187. (b) Clegg, W.; Conway, B.; Kennedy, A. R.; Klett, J.; Mulvey, R. E.; Russo, L. *Eur. J. Inorg. Chem.* **2011**, 721. (c) Barker, J.; Barnett, N. D. R.; Barr, D.; Clegg, W.; Mulvey, R. E.; O'Neil, P. A. *Angew. Chem., Int. Ed.* **1993**, 32, 1366.

41. Differences between TMEDA and TMCDA as ligands have also been attributed to the fixed bite-angle of TMCDA: Heuger, G.; Kalsow, S.; Göttlich, R. *Eur. J. Org. Chem.* **2002**, 1848.

42. Mulvey, R. E. *Chem. Soc. Rev.* **1998**, 27, 339.

43. Romesberg, F. E.; Bernstein, M. P.; Gilchrist, J. H.; Harrison, A. T.; Fuller, D. J.; Collum, D. B. *J. Am. Chem. Soc.* **1993**, 115, 3475.